Electrical conduction and discharge processes associated with aluminium oxide

Young, Michael Leonard

ELECTRICAL CONDUCTION AND DISCHARGE PROCESSES ASSOCIATED WITH ALUMINIUM OXIDE

by

Michael Leonard Young

Thesis submitted for the degree of
Doctor of Philosophy in the
University of Durham

Department of Applied Physics and Electronics,

University of Durham

April 1970

ACKNOWLEDGMENTS

The author is grateful to his supervisor, Dr. M.J. Morant, for valuable help and encouragement during this research work. The author is also grateful to the U.K.A.E.A. for financing the work and to Dr. B. Goodings, Mr. K. McMinn and Mr. D. Harrison of the Control and Instrumentation Division, Atomic Energy Establishment, Winfrith, for useful advice. Finally the author would like to thank Mr. A. Wright of the University of London for communicating the results of unpublished work on magnesia and the staff and students of the Department of Applied Physics and Electronics, University of Durham for valuable discussion and technical assistance.

ABSTRACT

At elevated temperatures alumina insulators are a source of small electrical pulses of approximately 10^{-14} coulombs when subjected to an electrical stress. This phenomenon, termed pulse breakdown, has been studied on single crystal and polycrystalline alumina over the temperature range $0^{\circ}C$ to $900^{\circ}C$. The study has been made over a range of ambient gas pressures and at voltages up to 3 kV. The d.c. conductivity of alumina has also been investigated over this range of conditions.

The study has shown that pulse breakdown is dependent on the ambient gas, the electrodes and the alumina surface. The results have been interpreted by means of a surface discharge model, in which discharges occur at both electrodes. The surface discharge at the cathode has been studied in detail and is shown to be produced by a corona discharge which is triggered by the desorption of impurities from the alumina surface. The discharge did not occur once single crystal alumina had been heated to $900^{\circ}C$. The possible explanations for this effect are considered.

The d.c. conductivity of single crystal alumina has been shown to be affected by chemical treatment of the alumina surface. This is due to the surface conduction of the alumina being affected by chemisorption. The activation energy for the surface conduction of alumina has been shown to be 1.7 eV. The very much higher activation energy of 3.9 eV attributed to the bulk conduction shows that alumina is not an ionic conductor below $900^{\circ}C$.

CONTENTS

CHAPTER 1

INTRODUCTION

The work described in this thesis is an investigation of discharges associated with electrical insulation at high temperatures. The work was carried out under a contract, No. CON/WIN/EMR 138, granted by the United Kingdom Atomic Energy Establishment, Winfrith, Dorset, where it forms part of an investigation into the development of nuclear fission neutron counters for use at high temperatures in conditions likely to be found in future nuclear reactors. These studies and other considerations had already shown that the choice of insulating materials for use at about 600^{o}C is extremely limited and that alumina in one form or another is likely to be preferred. The study of the discharge properties of pure alumina in carefully controlled environments provided a rare opportunity of investigating these phenomena in far better conditions than are normally used in the study of insulation, e.g. polymers, technical insulation, etc. where impurity effects may be extensive and where little is known of other properties of the materials. At the same time as obtaining reliable scientific results this work had the possibility of contributing to the development of improved high temperature insulation, which is likely to have extensive application in other branches of technology in the future. To see the origin

of the present work it is first necessary to describe the operation of fission counters.

A nuclear fission counter essentially consists of a pair of electrodes in a gas filled chamber. One of the electrodes, the cathode, is coated with a thin layer of fissile material, normally U235, which is sensitive to neutrons. When a neutron is absorbed by the cathode a radioactive disintegration occurs which produces ionization of the ambient gas. The electrons created in the gas by the fission fragments are swept towards the anode under the influence of a d.c. electric field and collected. Consequently the incidence of a neutron on the cathode causes an electrical impulse in the external circuit. The number of such electrical impulses will therefore be a measure of the neutron flux at the counter. The amplitude of the impulse will be proportional to the number of electrons created by the fission fragments, which will in turn depend on the energy of the incident neutron. Because of α emission from the cathode material the minimum energy particle which can be detected is about 5 MeV (Abson et al[1]). This corresponds to a minimum impulse charge of 3×10^{-14} coulombs.

The efficient operation of a nuclear fission counter depends on the electrical insulation of the counter. This must have a suitably high resistance and breakdown strength at the chosen operating temperature. The temperature at which counters can operate is limited by these insulating properties, since they deteriorate as the temperature is raised. In counters operating at low temperatures glass

insulators have been found to be satisfactory. However above 200°C ceramic insulators are used because of ionic conduction in the glass. Unfortunately the ceramic materials used in the counters, alumina and magnesia, are found to produce spurious electrical pulses at temperatures above 350°C. By suitable treatment of the ceramics it is possible to raise the operating temperature of the counters to 500°C without loss of sensitivity. However above this temperature the ceramics give discharges at a voltage close to the operating voltage of the counter with the result that the impulses produced by the ionizing radiations cannot be distinguished from those produced by 'breakdown' pulses in the ceramic insulators.

In recent years coaxial line counters have been developed to allow the neutron flux to be determined near the reactor core. These consist of a small diameter fission chamber mounted on the end of a long coaxial cable (see reference 1). The electrical leads in the coaxial cable are isolated by small cylindrical ceramic spacers. It is these ceramic spacers in the leads, rather than the ceramic to metal seals in the counter itself, which limit the operating temperature of the counters. The operating voltage of the counter is chosen for the optimum value of electron drift velocity. In a typical coaxial line counter, with a 98°/o argon - 2°/o nitrogen gas mixture, an operating voltage of about 300 volts is used. Consequently the ceramic spacers in these counters must not produce electrical pulses greater than 3×10^{-14} coulombs at an applied voltage of 300 volts while under neutron irradiation.

Apart from an empirical study by Dubois and Goodings,[2] there does not appear to have been any specific study of fast noise pulses in alumina at high temperature. Tucker and Gibbs,[3] and Champion,[4] in low voltage d.c. conductivity work, have reported 'pulsing' effects in single crystal alumina. These 'pulsing' effects are only seen on heating samples after they have been chemically treated. This pulsing coincides with the appearance of a peak in the d.c. conductivity. Both these phenomena have been attributed to the movement of impurities, introduced during chemical cleaning, along dislocation lines in the alumina. Dubois and Goodings studied the production of fast noise pulses in a simulated coaxial cable. They found the 'pulse breakdown' properties of alumina to be affected by surface preparation and ambient gas type. They defined pulse breakdown as the transfer of spurious charge pulses of order of 1×10^{-14} coulombs under a d.c. applied stress. In this work this terminology will also be used to describe the production of fast noise pulses in alumina at elevated temperature.

Although there have been many studies of the d.c. electrical conductivity of single crystal alumina (see Section 7.2), there is no generally accepted theory for the conduction mechanism in this insulator. The relatively recent work of Loup and Antony,[5] and Peters et al[6] challenges the validity of much of the published work on the conductivity of alumina at high temperatures. Loup and Antony showed that the conduction currents at very high temperatures are consistent with thermionic emission from the alumina.

Peters et al found their conductivity measurements to be independent of their samples and suggested that this was due to gas conduction. At low temperatures, i.e. below 900°C, these spurious effects are probably not significant compared with surface conductivity. Surface conductivity does not appear to have been reported on single crystal alumina although it has been reported in sintered material as well as in many other single crystal insulating materials. The dependence of the low temperature conductivity of single crystal alumina (Tucker and Gibbs,[3] and Champion[4]) on chemical preparation indicates that this process may well predominate at low temperatures.

The primary object of the present work was to identify the source of pulse production in alumina. It was also of interest to investigate the effects of pulse breakdown on the d.c. conductivity and to see whether there was any correlation between the integrated pulse charge and the d.c. conduction current. Finally it was hoped to investigate the surface and bulk conductivity of alumina in the temperature range 300 to 900°C. In addition to this work on sapphire the U.K.A.E.A. sponsored an investigation of pulse breakdown in magnesia by Wright[7] at the University of London. Unfortunately the results of this work, which has recently been completed, have not been seen at the time of writing.

CHAPTER 2

DETECTION OF DISCHARGES

2.1 Introduction

There are two principal methods of detecting electrical discharges in insulating materials. Firstly, the individual discharges may be detected directly by measuring the voltage impulses produced across an impedance in series with the sample, or, secondly, the discharges may be detected indirectly by measuring the loss tangent of the material. The latter method is relatively insensitive to single discharges, for example the smallest discharge which can be detected in a 1000 pF sample is about 1000 pC (Mason[8]), and it is normally used to detect discharges in insulation systems where the details of the individual discharges are of secondary importance. Consequently in this work, where it is required to detect single discharges of 0.01 pC, direct detection has been used.

In direct detection the voltage impulse produced across the detection impedance normally has to be amplified before it can be observed. The bandwidth of the amplifier used for this amplification depends on the parameters of the pulse which are of interest. If the shape of the impulse is unimportant the detection impedance can be chosen to concentrate the pulse energy within a narrow frequency band and a narrow band amplifier can be used. However if the pulse

shape is to be observed without undue distortion the amplifier has to have a wide frequency bandpass. Since the shape of the pulses were of interest in this work wideband amplifiers were used.

Wideband detection systems are extremely sensitive to high frequency interference. It is this interference rather than the noise generated by the circuit which limits the sensitivity of the detector. To reduce the interference to an acceptable level in wideband detectors the circuit has to be carefully screened or a balanced detection circuit has to be used. With the carefully screened wideband detector described in this chapter it has been possible to detect single impulses of 2×10^{-14} coulombs and less than 300 nanoseconds duration.

2.2 The Direct Detection of Discharges

The circuit used for the direct detection of pulse breakdown in alumina is shown in Fig 2.1. Discharges in the test sample produce an instantaneous change in voltage across the detection impedance Z in the external circuit. The impulse appearing across Z is displayed on an oscilloscope after being amplified by a wideband head amplifier. After pre-amplification the impulses are processed by a main amplifier. They are then transmitted to a scaler where they are counted. A discriminator is included between the main amplifier and scaler to allow both the amplitude and polarity of the pulses to be varied.

The height of the impulse produced across the detection impedance by an instantaneous discharge in the test sample

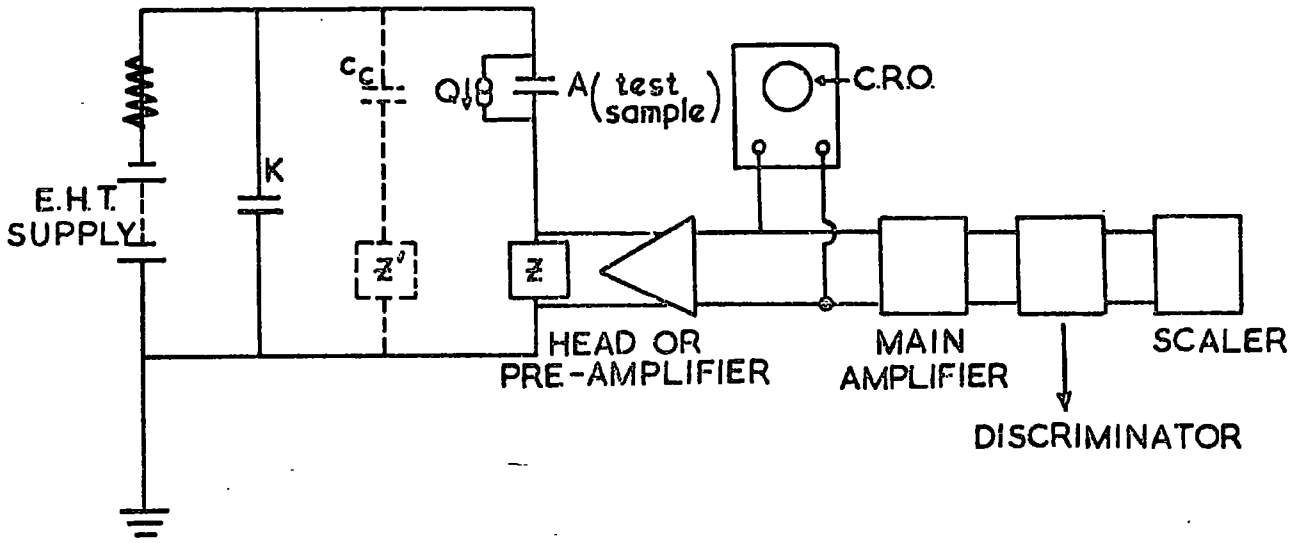

FIG. 2·1 CIRCUIT FOR DIRECT DETECTION OF DISCHARGES

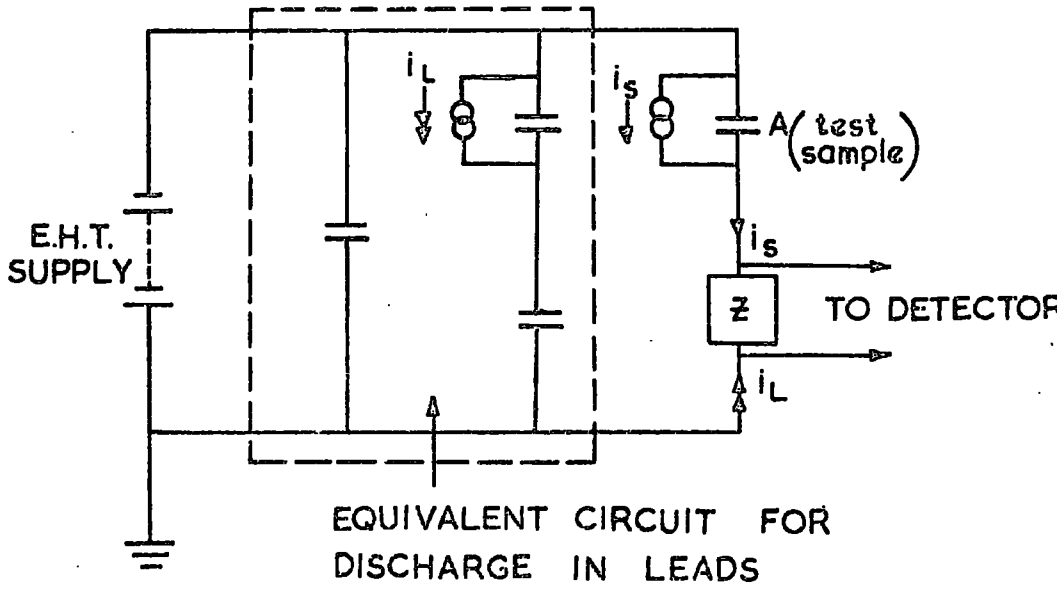

FIG. 2·2 CIRCUIT SHOWING THE EFFECT OF POSITION OF DISCHARGE SOURCE ON POLARITY OF DETECTED IMPULSE.

will be determined by the effective high frequency capacitance of the circuit elements. If the detection impedance is connected in series with the test sample, a discharge of Q coulombs in the sample produces a voltage change across the detection impedance of

$$V = Q/\left(A + K.C/K + C\right) \qquad \text{Eqn 2.1}$$

where C is the capacitive component of Z.
In the case of the detection impedance being an RC circuit, this impulse decays with the time constant $R.(C + A.K/A + K)$.
In practice the capacitance across the high voltage supply, K, is made very much greater than C or A to reduce the impulse equation to

$$V = (Q/A + C) \exp\left(- t/R.(C + A)\right). \qquad \text{Eqn 2.2}$$

If the test sample has a high capacitance it is desirable to connect it directly across the high voltage supply to ground. In this case the detection impedance is connected in series with a large high voltage coupling capacitor C_c. The impulse equation in this case is

$$V = (Q/A + K + C) \exp\left(- t/R.(A + K + C)\right) \qquad \text{Eqn 2.3}$$

$$\text{for } C_c \gg C.$$

With this arrangement it is necessary to keep the capacitance across the high voltage supply, K, as small as possible since it appears in parallel with the sample.

The polarity of the impulse will depend on the position of the detection impedance in the circuit. If the impedance

is in series with the sample the polarity of the impulse will be of the same sign as the high voltage supply whereas if it is in parallel it will be of the opposite sign. Discharges in the leads of the circuit will produce impulses of opposite polarity to those produced by discharges in the sample (Hashimoto[9]), irrespective of the position of the detection impedance (see Fig 2.2). Hence by incorporating a polarity discriminator in the circuit only the impulses produced in the test sample are recorded. Alternative methods of eliminating spurious discharges in the leads, by filter circuits or balanced detection, are well reviewed by Kreuger.[10]

2.3 The Detection Circuit

2.3.1 The detection impedance

The impedance most commonly used in discharge detection is a resistor R shunted by its parasitic capacitance C or an oscillatory LCR circuit. In the CR circuit, the voltage impulse appearing across the impedance decays exponentially with the circuit time constant while in the LCR case the impulse appears as a highly damped oscillation of frequency $(1/LC - 1/4\ R^2\ C^2)/2\pi$. An analysis of the frequency spectrum of these impulses shows that, in the CR case, the spectrum is essentially constant up to $f = 1/2\pi CR$ whereas in the LCR case the spectrum is a normal distribution about $(1/LC - 1/4\ R^2\ C^2)/2\pi$. This means that the LCR circuit concentrates the pulse energy within a narrow frequency band and has the advantage of allowing narrow band amplifiers to be used in the detector. The CR circuit on the other

hand requires wideband amplifiers. If the lower frequency limit of the amplifier pass band is neglected the bandwidth of the amplifier can be related to the decay time constant of the impulse by $f = 1/2\pi CR \tan \pi F/2$, where F = the fraction of the total energy of the impulse transmitted by the amplifier (Dakin and Lim[11]). For 90°/o transmission the amplifier bandwidth requires to be 1.05/CR. Therefore in choosing the detection impedance the amplifier bandwidth has to be considered.

The detection impedance used in this work was an RC circuit. Its capacitive component was composed of the stray capacitance of the leads. This latter, which is about 30 pF, consists of two components, the capacitance of the coaxial cable connecting the low voltage lead of the sample holder to the amplifier input (8 pF) and the capacitance of the low voltage lead itself (21 pF). The measuring resistance normally used was a 10^3 ohms. With this value of resistance the time constant of the detection circuit is 30 nanoseconds and the minimum undistorted risetime 66 nanoseconds. Experimentally the pulse risetimes rarely exceeded these values while the fastest decay times observed have been 200 nanoseconds. Consequently the 10^3 ohms detection resistance is adequate for all but the fastest pulses. To detect the smaller current impulses observed in pure argon ambients a resistance of 10^4 ohms had to be used. With this resistance the risetime of the detection circuit is 660 ns. Fortunately the risetime of the pulses in pure argon ambients was generally greater than this, so that excessive distortion of the pulse shapes did not occur in these conditions.

2.3.2 The amplifiers

Broad band amplifiers are used in the detector circuit. Such amplifiers reduce pulse distortion but make the detector sensitive to interference. As already mentioned the width of the pass band can be related to the time constant of the detection impedance and the fraction of the total pulse energy transmitted by the amplifier, F. For most practical purposes 10°/o distortion of the pulse is considered acceptable. This gives F, the amplifier bandwidth, equal to $\frac{1}{CR}$: so that for an impulse of risetime 100 ns we require a bandwidth of 25 MHz and for a 66 ns impulse (the risetime of the detection impedance) a 33 MHz amplifier.

The impulse appearing across the detection impedance is pre-amplified before being displayed on the oscilloscope. In the preliminary experiments reported in Chapter 5 a U.K.A.E.A. Type 1430A pre-amplifier was used. This gives 32.5 db gain for a bandwidth of 2 MHz. Because of this low bandwidth the 1430A was subsequently replaced by a Textronix Type 1121 pre-amplifier. This was used in all other experiments. The Textronix has a bandwidth of 17 MHz and a gain of 40 db. Pulses with risetimes of 660 ns suffer 2°/o distortion, those with 130 ns risetimes 10°/o distortion and the very fastest pulses, i.e. those of 66 ns risetimes, 20°/o distortion. Hence the distortion introduced by the amplifier can be neglected for all but the fastest pulses.

After pre-amplification the pulses are processed by the main amplifier. A U.K.A.E.A. Type 2057 amplifier was used for this. The amplifier has a wide pass band, 25 MHz,

and a high gain of 52 db. Incorporated in the amplifier are differentiating and integrating circuits for pulse shaping. These circuits control the effective bandwidth of the amplifier and allow the upper frequency limit to be lowered for long risetimes. The amplifier is also capable of inverting the polarity of the impulse.

2.3.3 The measuring instruments

(a) The Oscilloscope

Individual pulses are observed with a Textronix Type 581 Oscilloscope with Type 82 plug-in unit. The risetime of the oscilloscope amplifier is 2.2 ns and in consequence can be neglected. A Polaroid camera records individual traces.

(b) The Counter

The U.K.A.E.A. 2000 Series counting equipment was used in this work. This consists of a main amplifier, Type 2057, a pulse height discriminator, Type 2011, a scaler unit, Type 2130, and a timer unit, Type 2041A. The discriminator level is variable from 0.1 - 4.5 V. The maximum number of pulses which may be counted is 10^6 which is the upper limit of the scaler. These can be recorded in time intervals of 1 - 10^4 seconds, depending upon the timer setting.

2.3.4 The power supply

The high voltage supplies, used in conjunction with the detector, are a 0.3 - 3.3 Kv Dynatron EMT supply and a 0 - 3 Kv U.K.A.E.A. 2000 series E.H.T. unit. The output

resistance of both these units is 10^7 ohms. The units are used with a 0.5 microfarad capacitor across the output.

2.4 Sensitivity

2.4.1 Introduction

The sensitivity of a detector is expressed in terms of the smallest discharge it can detect. This is normally stated as the smallest discharge in coulombs which can be detected in a sample of a specified capacitance. The smallest impulse which can be discerned at the oscilloscope is governed by the noise voltage of the circuit, since the impulse has to be distinguishable from the noise fluctuations. An arbitrary minimum is when the height of the impulse is twice the height of the noise voltage of the circuit. With wideband amplifiers the interference level normally exceeds the noise voltage so that the actual sensitivity is considerably lower than that calculated from the signal to noise ratio.

2.4.2 Noise

The noise voltage at the oscilloscope comes from two sources, the amplifier and the detection impedance. The amplifier noise is governed by the grid current and shot noise arising in the first valve of the head amplifier. This may be represented by an equivalent noise resistance R_{eg} in the grid circuit of the first valve. With the detection impedance and sample connected, the noise at the amplifier input will be increased by the thermal noise of the

resistive elements, R_s, R_m and R_e (see Fig 2.3) in the circuit. In this work R_s is very much greater than R_e or R_m and C_s is very much less than C_e, so that the circuit noise is mostly generated by R_m. The spectral distribution of the noise voltage generated by the circuit at the amplifier input is then

$$\bar{v}^2/\delta f = 4kTR_n / 1 + \omega^2 R_n^2 (C_s + C_n)^2 \qquad \text{Eqn 2.4}$$

(Gillespie[12])

The total mean square noise amplitude effective throughout the amplifier pass band is

$$\bar{v}^2 = \frac{4kT}{2\pi(C_s+C_n)} \left\{ \tan^{-1} 2\pi f_u R_n (C_s+C_n) - \tan^{-1} 2\pi f_L R_n (C_s+C_n) \right\} \qquad \text{Eqn 2.5}$$

where f_U and f_L are the upper and lower frequency limits of the amplifier. Substituting in known values for C_s, C_m, R_m, f_U and f_L gives a value of 6 μv for the circuit noise at the amplifier input. This is very much smaller than the noise generated by the Textronix Type 1121 amplifier (which is about 50 μv) and so it can be neglected. For a signal to noise ratio of 2 the smallest pulse height which can be detected is therefore about 100 μv. In practice interference causes the minimum detectable signal to be nearer 200 μv. The smallest detectable discharge for a sample capacitance of 10 pF is therefore 8×10^{-15} coulombs.

2.4.3 Interference

Detection circuits which utilise wideband amplifiers are sensitive to external electrical disturbances. These

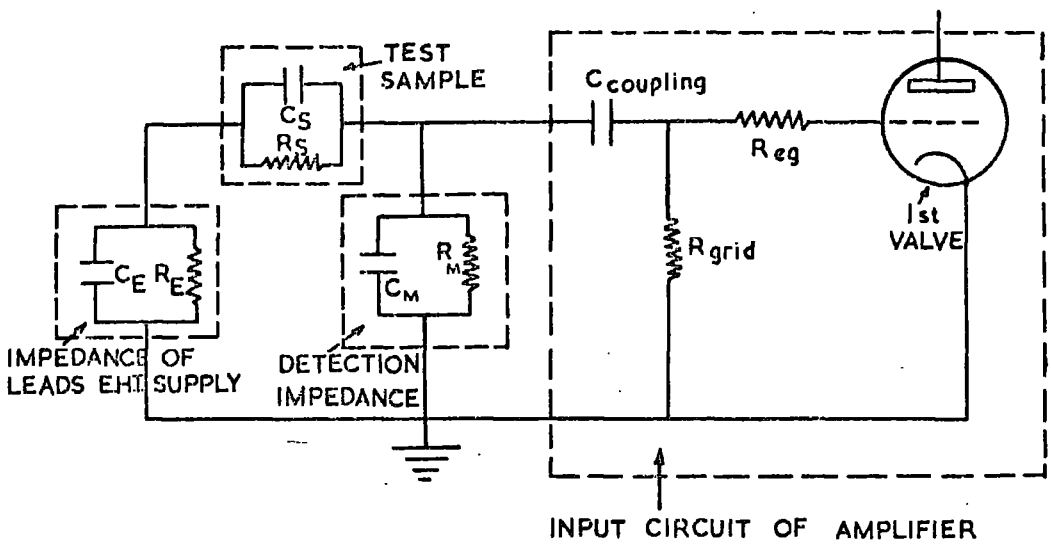

FIG. 2·3 NOISE CIRCUIT FOR DETECTOR.

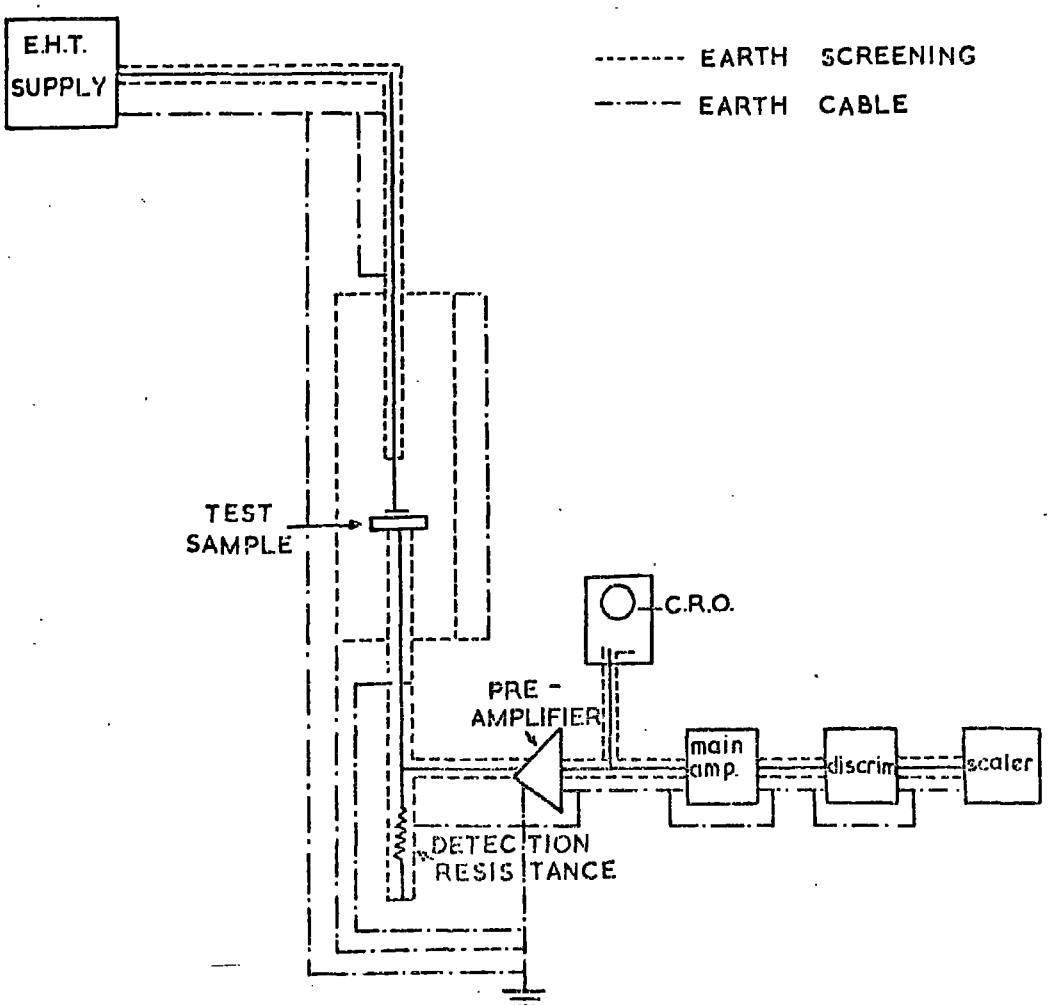

FIG. 2·4 EARTH CIRCUIT OF DETECTOR.

disturbances are transmitted to the detection circuit either directly, by electromagnetic wave coupling, or indirectly via stray coupling components. Direct coupling by e.m. waves is reduced by screening of the disturbing or disturbed circuit. If, as is usual, there are several disturbing sources the detection circuit must be enclosed within a continuous earth screen. Since practical screens are not perfect some penetration will occur and produce disturbances. Indirect coupling, via stray components to earth, produce disturbances in the screen of the detector. The interference in the detector circuit resulting from earth disturbances in the interconnecting cables is a major source of interference. This interference has been analysed by Harrison.[13] The analysis shows that certain practical precautions can be taken to minimize these disturbances. For example, cables should have low screen transfer impedances and be properly terminated. Electrical units should either be isolated or short circuited to avoid passing screen currents through them. In addition single point earthing should be used where possible.

The screen circuit used for the detector in this work is shown in Fig 2.4. With this arrangement interference has been minimized but not eliminated. Unfortunately high frequency interference from switching operations is still troublesome. For this reason the Eurotherm Temperature Controller was replaced by the Correx Saturable Reactor. With a detection resistance of 10^3 ohms the interference level at the input of the pre-amplifier is 90 μv. The

interference level increases with increasing values of measuring resistance, being 120 μv with 10^4 ohms and 300 μv with 10^5 ohms. Hence the sensitivity with the 10^4 ohms is 1.2×10^{-14} coulombs and with the 10^5 ohms is 2.4×10^{-14} coulombs for a sample capacitance of 10 pF.

2.4.4 Calibration of detector

The Types 2057, 1430A and 1121 amplifiers have been calibrated. Pulses from an Advance Type PG 54 pulse generator were used and these were displayed on the Type 581 oscilloscope before and after amplification. For the Type 2057 main amplifier, set to integrating and differentiating time constants of 0.01 and 100 microseconds, a voltage gain of 57 db was obtained for input pulses of between 100 and 1,000 ns duration. The gain with the amplifier decreased to 53 db with integrating and differentiating time constants of 0.1 and 100 microseconds for the 100 ns pulses but remained at 57 db for pulse lengths greater than 300 ns. Throughout this work the main amplifier was used with the integrating time constant less than the time constant of the detection impedance to avoid pulse distortion. The choice of differentiating time constant depends upon the frequency of the pulses and was governed by the resolution of the count.

For the Type 1430A amplifier it is convenient to know the matched charge gain which we define as the ratio of the output charge into a 10^2 ohm terminating resistance to the input charge through a 10^3 ohm measuring resistor. Using input pulses of up to 200 mV it has been found that this

amplifier can handle both positive and negative pulses without undue distortion provided that the input signal is as small as in the sapphire pulse measurements. The distortion depends on the pulse repetition frequency. For pulses below 200 ns duration the upper frequency limit of the amplifier reduces the voltage gain, but the matched charge gain of the amplifier remains constant at about 370. This value has been used in making pulse charge calculations from oscillograms in Chapter 5 only.

The Type 1121 pre-amplifier was calibrated with 70 ns duration pulses. With no input attenuation the gain of the amplifier was 40 db and the bandwidth 17 MHz. Input attenuation slightly reduced the bandwidth, the figures obtained being 16.5, 16.0 and 14.5 MHz for 26, 34 and 40 db of attenuation respectively.

A 'in situ' calibration of the detector has been made by measuring the current impulses produced in the detection impedance by changes in voltage at the high voltage lead of the detector. Pulses of known amplitude were fed through a single crystal sample of low capacitance to the input of the amplifier. The impulses appearing across the detection resistance were then amplified by the Type 1121 and observed on the 581 oscilloscope. To the test waveform the input capacitance is the sample capacitance, 4 pF, in series with a stray capacitance of the low voltage lead, 30 pF. Hence during each abrupt voltage change, V, of the input waveform a current impulse of $3.5 \times 10^{-12} \times V$ coulombs flows through the detection resistance. The calibration curves obtained for

detection resistances of 10^3 and 10^4 ohms are shown in Fig 2.5. These are seen to be linear for pulse charges above 2×10^{-14} coulombs.

2.5 Resolution

The ability of a counting circuit to resolve individual pulses is called the resolution of the circuit. This is specified in terms of the resolving time t_r of the circuit which is defined as the time from the start of the incoming pulse to the time when the trailing edge falls below the threshold level of the discriminator. The resolving time depends upon the threshold level, V_t, the amplifier differentiating and integrating time constants, T_1 and T_2 respectively, and the parameters of the pre-amplified pulse (Fig. 2.6). If the pulse is shaped by the amplifier time constants, T_r and T_d can be neglected and the resolving time can be evaluated from the expression

$$V_t = \frac{V_0 T_1}{T_0 (T_1 - T_2)} \left\{ T_1 \exp\left(-\frac{t_r}{T_1}\right)\left[\exp\frac{T_0}{T_1} - 1\right] - T_2 \exp\left(-\frac{t_r}{T_2}\right)\left[\exp\frac{T_0}{T_2} - 1\right]\right\} \qquad \text{Eqn 2.6}$$

(Gillespie[12])

In most cases the threshold voltage V_t is fixed for maximum sensitivity so that Eqn 2.6 allows the bandwidth of the amplifier to be calculated for a given resolving time. On the other hand the amplifier time constants can be neglected if the amplifier bandwidth is wide. The resolving time is then simply obtained from the input pulse.

The Type 2057 amplifier has differentiating and integrating time circuits for pulse shaping. These allow the

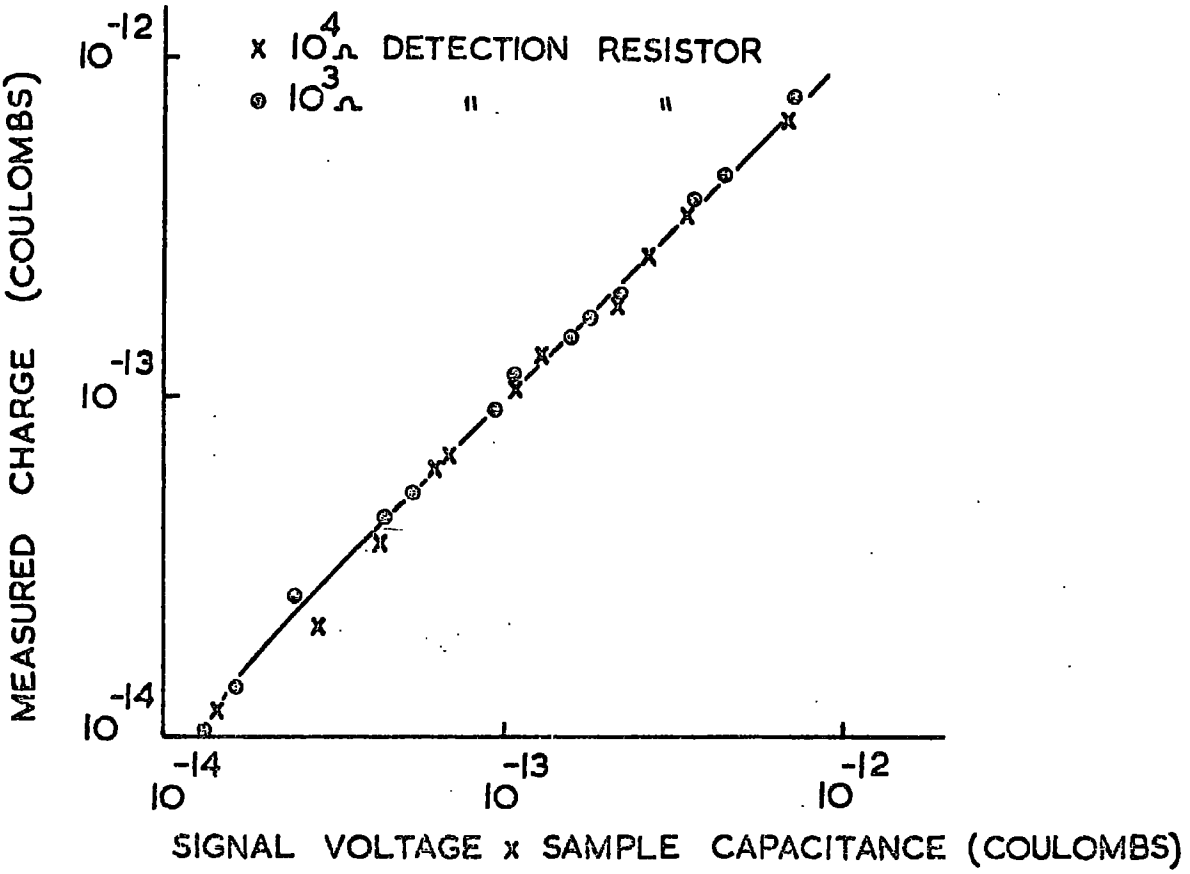

FIG. 2·5 CHARGE CALIBRATION OF DETECTOR.

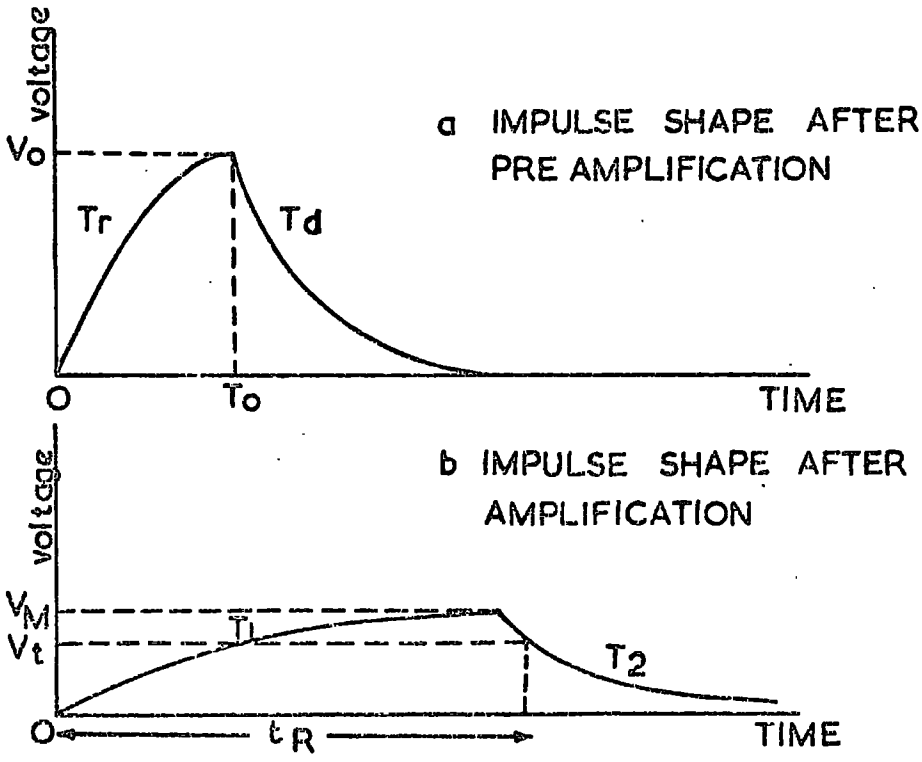

FIG. 2·6 IMPULSE SHAPE BEFORE (a) AND AFTER (b) AMPLIFICATION.

upper frequency limit to be varied from 53 kHz to 16 MHz and the lower frequency limit from 1.6 kHz to 16 MHz. Normally the amplifier is used in the wideband condition and the resolving time calculated from oscillograms of the pulses. The exact settings of T_1 and T_2 used depend upon the rise and decay times of the pulses. For example T_1 and T_2 are set at 0.01 and 10 μs respectively for pulse measurements in air where $T_r \simeq 70$ ns and $T_d \simeq 200$ ns. In pure argon however the pulse rise and decay times are longer, $\approx$ μs, and T_1 and T_2 are accordingly adjusted to 0.1 and 100 μs. When the pulse repetition rate approaches the maximum resolution, $1/t_r$, of the circuit the pulse is differentiated to reduce the resolving time.

The resolving time of the circuit is ultimately controlled by the response of the discriminator. The discriminator is paralysed 25 ns after the start of the incoming pulse for the duration of the dead time. Since the minimum dead time is 100 ns the minimum resolving time is 125 ns and pulses occurring within this time interval will not be resolved. In practice the discriminator resolving time only exceeds the pulse resolving time for the smallest pulses. These occur near the onset voltage where the pulse count rate is low in any case. Typically a pulse of 5×10^{-14} coulombs occurring at 40 volts above the onset voltage has a peak height of 250 microvolts and a resolving time of 100 ns. However the pulse count at this applied voltage was perhaps 200 counts per second, very much less than the limit set by the discriminator. Consequently

even when the pulse resolving time falls below that of the circuit the errors introduced in the count rate can be neglected because of the low count rate.

CHAPTER 3

APPARATUS

3.1 Introduction

Experimental work on aluminium oxide has shown that both the d.c. conductivity and discharge breakdown of this insulator are temperature and voltage dependent. In addition these properties are strongly affected by the condition of the ambient gas. For this reason the experimental apparatus was designed to measure the conductivity and discharge breakdown of aluminium oxide under controlled conditions of temperature, ambient gas pressure and voltage. These measurements may be made up to 1,200^{o}C in gas pressures of between 760 and 10^{-2} torr and at voltages up to 3 kV on disc shaped samples of a few mm thickness and several cm diameter.

Reliable electrical measurements on insulation are best obtained with three-terminal techniques. This appears to be especially important for aluminium oxide where both the ambient gas and the surface are likely to be more conducting than the bulk material. Consequently the apparatus requires a three-terminal electrode arrangement and a high leakage resistance to satisfy the d.c. requirements. For the pulse work, the H.T. lead must be discharge-free to 3 kV and of minimum capacitance. To avoid excessive distortion of the pulse the measuring lead capacitance also has to be small.

These electrical requirements coupled with the need to maintain a vacuum of 10^{-2} torr at 1,200°C determined the design of the apparatus.

A study of single and double ended sample holders suggested that the latter better satisfied the above electrical requirements. In such an arrangement the H.T. and measuring leads enter the apparatus from opposite ends so that they are well separated, and the leakage conductance and capacitive coupling between the leads are minimized. To obtain the necessary electrical insulation the sample requires to be supported solely by the electrodes. This is achieved by mounting the sample holder vertically and applying a small axial force from the electrodes. With a double ended arrangement the length of the electrode support tubes must be twice that of the furnace work tube if the sapphire sample is to be mounted between the electrodes before insertion in the furnace. Once the sample is mounted, either the furnace or the electrode arrangement must be moved. The former is preferred as this allows the sample and electrodes to be examined 'in situ' after every experiment. However this arrangement requires the sample holder to be undisturbed by vertical movement of the furnace. This is achieved by mounting the sample holder and furnace on a rigid framework and aligning the electrodes along the axis of the furnace.

3.2 Description of Apparatus

The apparatus consists of a sample holder mounted in a tubular furnace. The inner work chamber of the furnace is

isolated from the air and may be evacuated.

(a) Sample Holder

The sample is held between Pt-40°/o Rh electrodes mounted on the ends of high purity recrystallised alumina tubes (see Fig 3.1). These tubes are supported by stainless steel end pieces, A and B, secured to the aluminium base plates C and D. The base plates are in turn mounted on the main frame by spring-loaded bolts. By adjusting these bolts the electrodes and support tubes can be accurately aligned with the axis of the furnace. The measuring electrode, E, is fixed in the end piece, A, by a locking screw. The high voltage electrode, F, is spring loaded to maintain the electrodes in contact with the sample at high temperatures. A third alumina tube, also spring loaded, supports a platinum guard ring against the sample. This tube also carries, in a twin bore alumina tube, a Pt-13°/o Rh thermocouple for monitoring the temperature of the sample. The alumina tubes supporting the high voltage and guard electrodes are coated with thick layers of platinum paste to screen the leads from external interference. The high voltage and measuring leads are 25 S.W.G. Pt-40°/o Rh wires. These are attached to coaxial sockets on the alumina tubes. The high voltage lead may be modified to avoid corona discharges by increasing the effective diameter of the conductor. A 4 mm diameter alumina tube coated with platinum paste and bonded to a Pt-40°/o Rh wire replaces the single wire as the high voltage conductor.

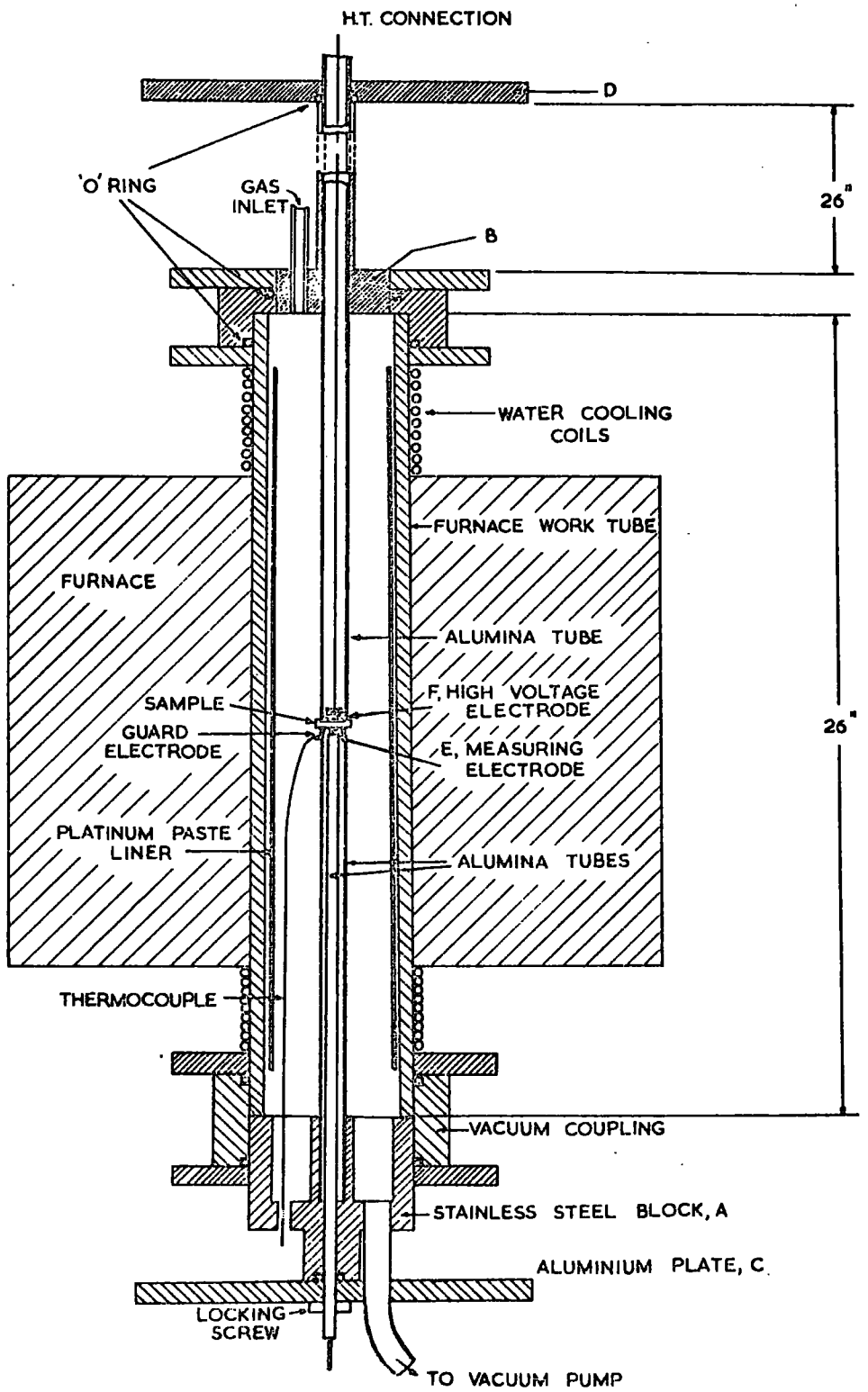

FIG. 3·1 SIMPLIFIED DIAGRAM OF APPARATUS.

The lead is thus a coaxial line of characteristic impedance 22 ohms or 140 ohms depending upon the conductor diameter. This coaxial arrangement extends to within 15 cm of the high voltage electrode. Beyond this the platinum paste screen is not present and the lead is unshielded. The length of the high voltage lead is 100 cm and that of the measuring lead 30 cm.

(b) The Furnace

The furnace consists of a recrystallised alumina work tube, 26 inches long and 50 mm inside diameter, located inside a Morgan Type DM Crusilite heating element. The element and work tube are insulated with fire bricks and the whole arrangement encased in Syndanyo. With an element current of 20 amps, equivalent to $2\frac{1}{2}$ kW, a temperature of 1,400°C is reached in the central portion of the furnace. The furnace moves vertically on wheels attached to the furnace sub-frame. These are kept in contact with a guide rail by pairs of spring loaded wheels (see Fig 3.2). For ease of movement the furnace is counterbalanced. The total movement of the furnace is 26 inches, the length of the work tube, so that when it is raised the sample holder is fully exposed. The temperature of the furnace is controlled by a Correx saturable reactor. This system, while accurately controlling to within 5°C, causes interference in the measuring lead. Consequently the inner wall of the work tube is coated with platinum paste and is earthed.

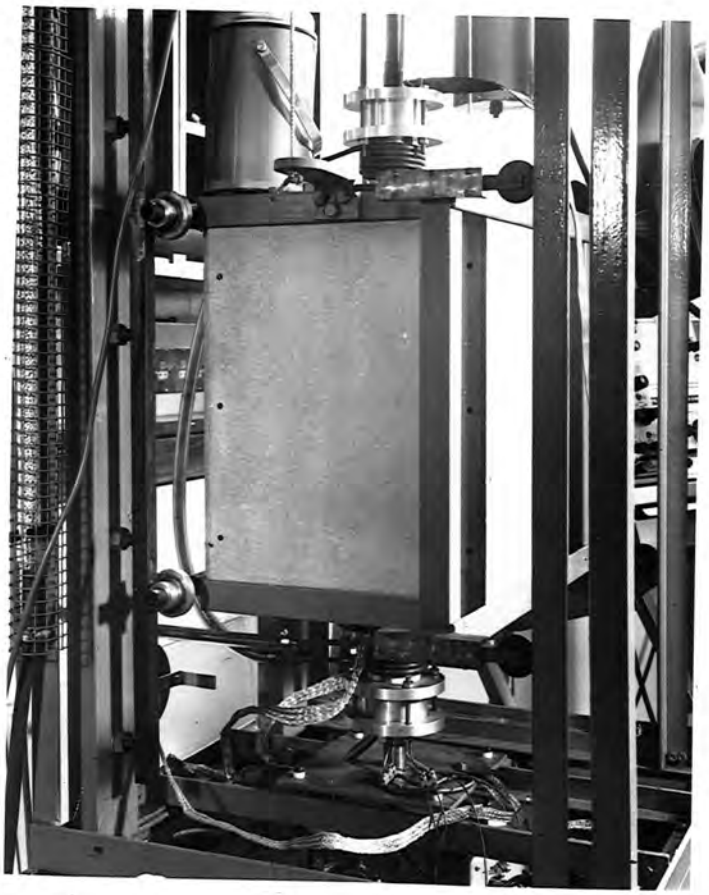

FIG. 3.2. SIDE VIEW OF FURNACE, SHOWING GUIDE RAIL AND LOCATING WHEELS

(c) The Vacuum System

The furnace chamber is evacuated by an Edwards ED 35 two stage rotary pump. This is capable of maintaining a pressure of 10^{-3} torr in the system with a leak rate of 1 lusec. Vapour contamination due to desorption is troublesome up to 600°C. This is reduced by P_2O_5 and solid CO_2 traps near the pump inlet. The ambient gas is dried before being admitted to the furnace by passing it through a molecular sieve and solid CO_2 trap. The gas is admitted via needle valves at either the top or bottom of the chamber. Normally the ambient gas is admitted at the top inlet and impurities at the bottom (see Fig 3.3). The pressure in the system is measured with Pirani, Vacustat and capsule dial gauges over the range 760 to 10^{-3} torr.

The pump is connected to the chamber by ½ inch diameter stainless steel pipe welded into the end piece A. This contains four ceramic to metal vacuum seals (manufactured by 20th Century Electrics Ltd.), which take the thermocouple, guard and screen earth leads from the sample holder. The measuring electrode runs vertically through the end piece and is sealed by an 'O' ring between the end piece and base plate D. The electrical lead in the support tube is sealed by Araldite at the exposed end. A similar arrangement exists at the high voltage end of the sample holder. The seals at the open ends of the work tube are made by compressing Viton 'O' rings between aluminium plates. When clamped the 'O'

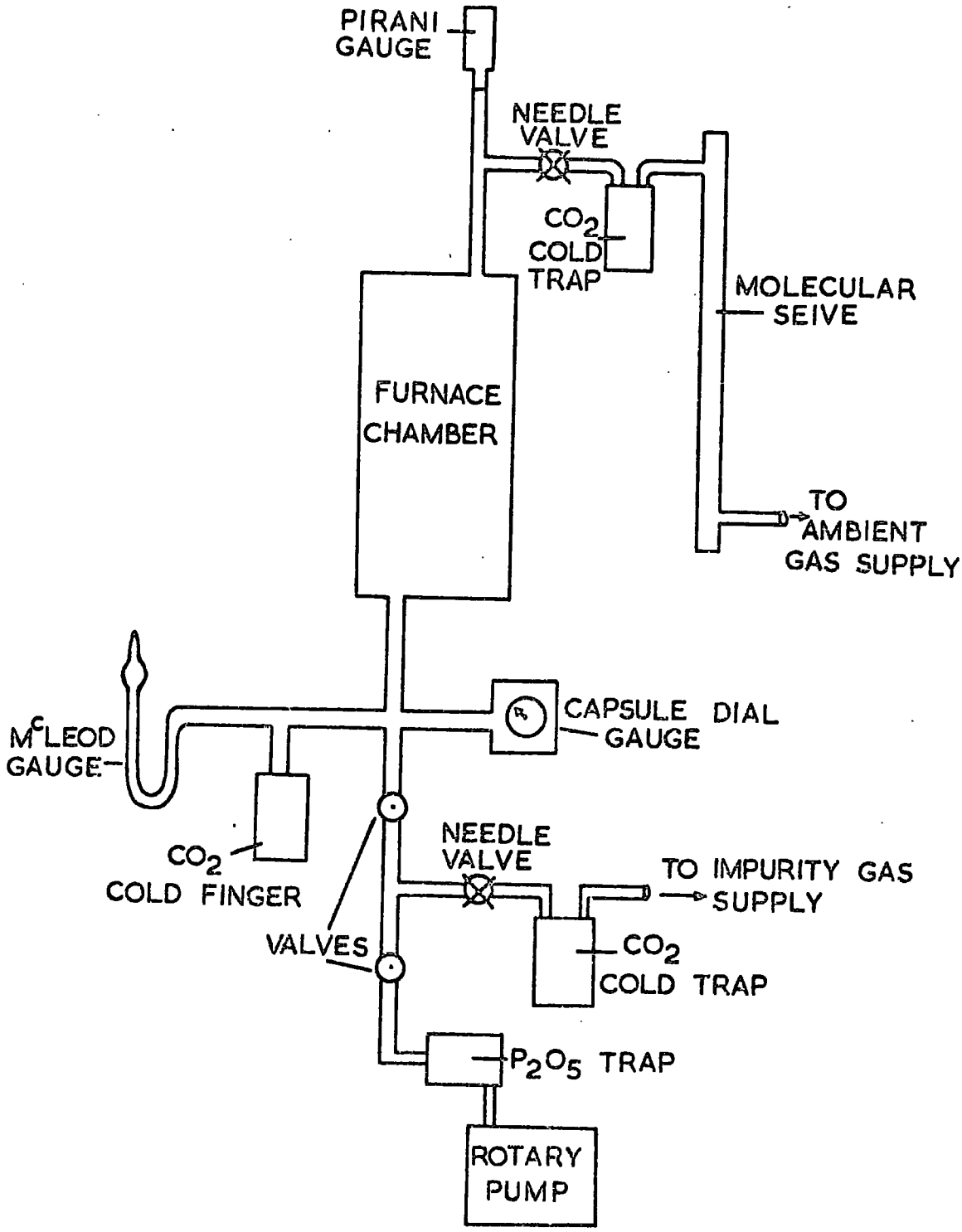

FIG. 3·13 VACUUM SYSTEM OF FURNACE

rings are squeezed against the sides of the work tube and end piece and seal the chamber from the atmosphere.

3.3 Electrode Arrangements

The field distribution at the high voltage electrode has been altered by using electrodes of two different geometries. In all, three high voltage electrodes were constucted, two plane ones of similar geometry and a spherical one. Two of these electrodes, namely the sphere and one plane, were made of stainless steel while the other was of Pt-40°/o Rh. The plane electrode arrangement is shown in Figure 3.4. The high voltage electrode, 10 mm diameter, sits in the alumina support tube. The end of the tube is coated with platinum paste to prevent surface discharges to the tube. The electrode is either stainless steel or Pt-40°/o Rh. The measuring electrode, 4 mm diameter, and guard electrode, 7 mm inside and 10 mm outside diameter, are both Pt-40°/o Rh. The spherical electrode (not shown) is of stainless steel with a $\frac{1}{2}$ inch radius of curvature face. Like the plane electrode it is mounted in an alumina support tube. The same measuring and guard electrodes are used with the spherical electrode as with the plane electrode arrangement shown in Figure 3.4. Unless otherwise stated all pulse breakdown and d.c. conductivity measurements were made with the Pt-40°/o Rh plane parallel electrodes of Figure 3.5.

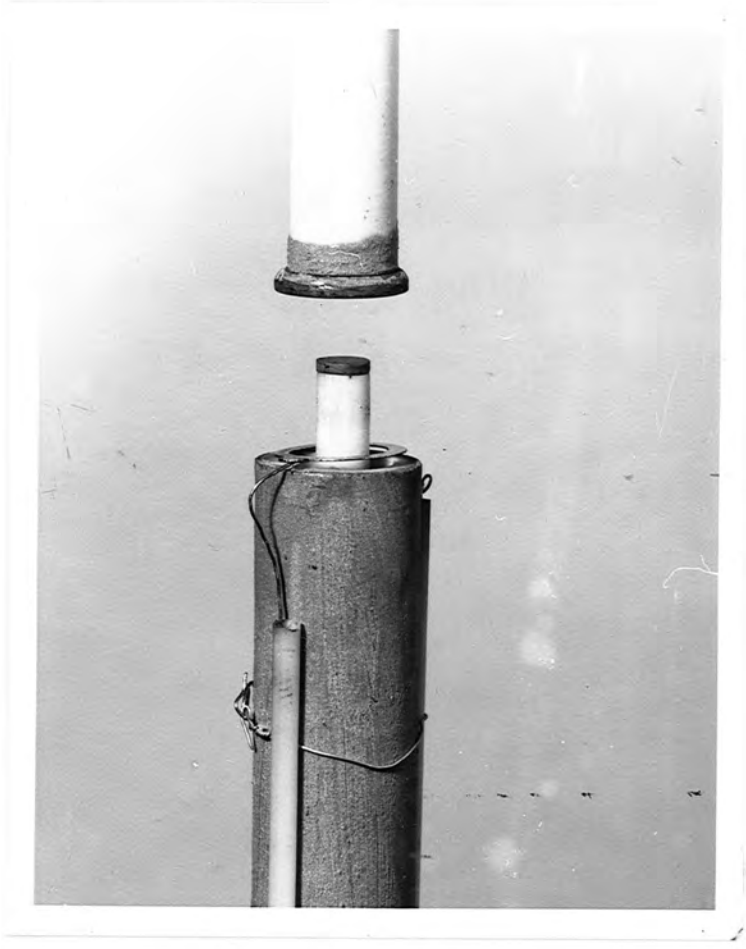

FIG. 3.4. PHOTOGRAPH OF PLANE ELECTRODE ARRANGEMENT

3.4 Development of Apparatus

During the course of the work, modifications were made to the apparatus to improve the performance. For this reason the final apparatus, which is described in Sections 3.2 and 3.3, was different to that originally used. The apparatus was developed in two phases after the preliminary measurement reported in Chapter 5 and during the work on reproducibility with polycrystalline specimens in argon ambients (see Sec 6.2).

(a) Modifications made after preliminary measurements:

Preliminary measurements showed that the response of the head amplifier was slower than the risetime of the pulses and that the pulses were being distorted as a result. To avoid this the Type 1430A head amplifier was replaced by one of greater bandwidth, the Textronix 1121. The increased bandwidth of this amplifier made the detector more sensitive to external interference and modifications had to be made to the earth circuit to improve the electrical screening.

Initial measurements also showed the need for accurate control of the specimen temperature. For this reason the Honeywell high limit temperature indicator originally used was replaced by a proper temperature controller. Unfortunately the first one tried, a Eurotherm stepless proportional controller, caused too much circuit interference and had to be replaced by the Correx saturable reactor. These developments made it necessary to screen the electrodes by adding the

platinum paste screens to the alumina E.H.T. support and work tubes. It also became necessary to isolate the guard electrode from the earth screen surrounding the low voltage electrode. The pressure measurement range was extended from 10^{-1} to 760 torr at this point by adding Vacustat and capsule dial gauges to the rig.

(b) Modifications made during reproducibility studies:

The use of argon ambients in the furnace led to corona discharges in the apparatus at low gas pressures. This was overcome by increasing the diameter of the E.H.T. lead to 4 mm with the platinum coated alumina tube. Modifications were also made to improve the purity of the argon ambient by including a molecular sieve and CO_2 cold trap at the gas inlet and a further cold trap into the system at the pump inlet.

CHAPTER 4

EXPERIMENTAL

4.1 Introduction

In the preliminary measurements reported in Chapter 5 the experimental parameters were inadequately controlled. Large variations in the pulse count rate and onset voltage, which were consistent with the different temperature used for each measurement, were recorded in the same experiment on any one sample. In subsequent work the temperature of the sample was accurately controlled at 400°C with the Correx saturable reactor. However large variations in the pulse count rate were still observed in successive measurements at constant temperature. This inability to obtain reproducible results at constant temperature suggested the need for stricter control of the experimental conditions. Consequently a standard experimental procedure was introduced for cleaning the sample, purifying the ambient gas and measuring the pulse count rate. This procedure is the best that could be achieved in normal laboratory conditions and it was rigorously adhered to in all the later experimental work. It is described here in detail because it is possible that the results are influenced by some particular feature of the technique used even though this was designed to eliminate spurious effects as far as possible. It should be noted that this standard technique was only introduced after the preliminary investigation of pulse breakdown had been made.

4.2 Specimens

Single crystals of alumina, grown by the Verneuil process, were obtained from Salford Electrical Instruments. The precise purity of the individual samples was unknown. According to S.E.I. they should contain about 100 p.p.m. of Fe, and 10 p.p.m. of Pb and Mg, these being the main impurities (see Champion[4] for an analysis of similar samples). The samples used for d.c. conductivity measurements were discs of 1.0, 1.6, 2.0 and 2.6 cm diameters and 0.3 cm thickness. The orientation of the samples was determined by Laue back reflection technique and the results are given in Table 4.1. The back reflection photographs showed no signs of crystallite misorientation, which is a common fault with Verneuil grown material. This means that the mosaic structure of the crystals in the regions examined by the X-ray beam is less than 1^{o} (Curtis[14]). The surface roughness of the polished faces of the discs was 10 microinches, there being little difference between samples. The roughness was determined by measurements made with a Hobson Rank Talleysurf.

Sintered polycrystalline discs a few mm thick and of various diameters were obtained from Degussa Ltd. These are reputed to be 99.95^{o}/o pure, the main impurity being silica, and of low porosity, about 1^{o}/o. The average grain size of the samples was 10 microns. The surface roughness of the samples was 200 microinches, both the faces and sides of the samples having the same finish. There was no significant difference in the grain size and roughness of different samples.

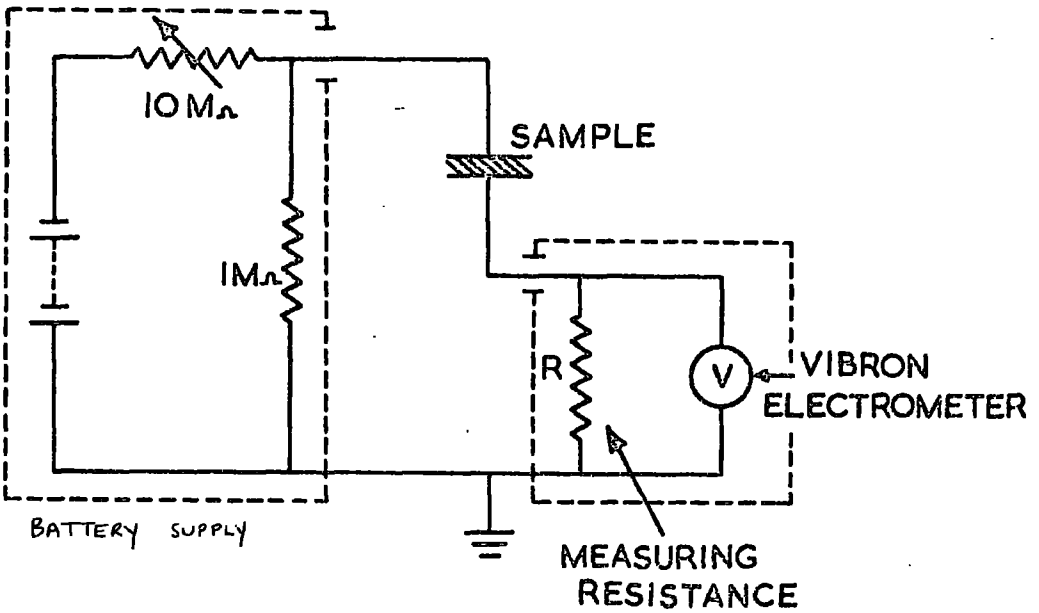

FIG. 4·1 D.C. MEASURING CIRCUIT

TABLE 4·1 ORIENTATION OF SINGLE CRYSTAL SAMPLES.

DIA. OF SAMPLE	ORIENTATION OF C AXIS TO FLATS
1·0 CM	90 ± 1°
1·6 CM	20 ± 1°
2·0 CM	90 ± 1°
2·6 CM	30 ± 1°

All specimens were given a standard cleaning procedure before being placed in the measuring jig. This involved washing in Teepol solution, rinsing in distilled water, boiling in a 7 $\pm$ 1N solution of HCl for 15 minutes to remove excess aluminium, rinsing again in distilled water and finally washing in absolute alcohol. Where samples were deliberately contaminated by boiling in Aqua Regia, the contamination was introduced after this procedure. Contacts of Pt-40°/o Rh were sputtered on the faces of some of the samples after cleaning. The samples were masked and placed in a Type GE3 Edwards High Vacuum Coating Unit. With the pressure in the unit adjusted for the maximum rate of sputtering, about 5 torr of argon, a 2500 $\pm$ 500 Å film of high reflectivity was formed in 15 minutes. The thickness of the film was measured with an interference microscope. The resistance of the films so formed, when measured across the diameter with the two probes of an Avometer, was less than 200 ohms. After the contacts had been sputtered the specimens were thoroughly washed in deionized water and absolute alcohol and were then placed between the electrodes.

4.3 The Ambient Gas

Argon, air, nitrogen and oxygen were used as the ambient gases in this work. With the exception of air the gases were obtained from B.O.C. cylinders of nominally 99.9995°/o A, 99.999°/o N and 99.96°/o O. Gases from these cylinders contain water vapour and must be dried before use. For this reason the gas was passed through a zeolite

molecular sieve (B.D.H. Type) and CO_2 trap before admission to the furnace chamber. A CO_2 cold trap was included at the inlet to the chamber to reduce the vapour pressure of the residual impurities in the chamber to the saturated vapour pressure of the cold trap. During the heating of the sample the chamber was evacuated with the rotary pump on gas ballast to remove the impurities, H_2O and OH, desorbed from the walls of the furnace chamber and other alumina components. When the sample reached the required temperature, the system was flushed with the ambient gas and then re-evacuated to 5×10^{-3} torr. Finally the chamber was filled to the required pressure with freshly dried gas. In experiments where the ambient gas was deliberately contaminated, the system was evacuated and filled with the impurity gas before the ambient was admitted.

In earlier experiments the furnace chamber was filled with the ambient gas several hours before the pulse count rate was measured to allow the system to reach thermal equilibrium. This procedure was later modified because it was found that considerable quantities of air were diffusing into the chamber in the time interval between filling the chamber and the start of the measurements. Hence in the later experimental work, the pulse count rate was measured immediately after the furnace chamber was filled with the ambient gas. In pulse breakdown measurements at different pressures the chamber was filled to atmospheric pressure and measurements were made at progressively reduced pressures to ensure that the same ambient gas existed in each consecutive measurement.

4.4 Electrode Deterioration

After long periods at high temperatures the Pt-40°/o Rh electrodes have been found to deteriorate with the formation of surface films. This effect has been attributed to the oxidation of the rhodium since Rh_2O_3 is produced by heating the metal in air to 800°C. The electrodes have been restored to their original condition by heating the electrodes to white heat in an oxy-gas flame and reducing the oxide to the metal. In addition the electrodes have been periodically polished to remove any transparent films.

4.5 Circuit for D.C. Conductivity Measurements

The circuit used for determining the sample resistance is shown in Fig 4.1. An Electronic Instruments Vibron Electrometer Model 33C was used to measure the voltage across the resistance R, which is contained in an Electrometer B33C head unit, the output of which was fed to a potentiometric pen recorder. The head unit provided resistors of 10^9, 10^{10}, and 10^{11} ohms, lower values being clipped in parallel with these resistors when required. The voltage to the sample was supplied by 120 V H.T. batteries or the Dynatron unit, thus allowing the voltage range 1 - 3,000 volts to be covered. The voltage output of the supplies were checked before each experiment with a Sweeney valve voltmeter. The resistors were calibrated by substituting standard resistances of 10^9, 10^{10} and 10^{11} ohms for the sample and determining the voltage developed across R for various applied voltages. All the resistors were

found to be within 10°/o of the quoted values. The resistances were also found to be independent of the temperature of the low voltage lead which was connected in parallel with the measuring resistances during the calibration.

4.6 Measurement Technique

4.6.1 Standard procedure for pulse breakdown measurements

The specimen was cleaned, placed between the electrodes and heated in vacuum to 400°C. The rate of heating was not controlled and varied in each experiment, although in most cases the specimen reached the required temperature within 4 hours. Finally the ambient gas was admitted to the required pressure. With the discriminator level set above the noise level of the circuit, the time constants of the amplifier were adjusted for minimum interference and maximum bandwidth. The E.H.T. unit was switched on and the voltage across the specimen slowly increased until pulses were just observed on the oscilloscope. The voltage was then lowered slightly and the pulse count determined by measuring the number of pulses in 10 seconds. The pulse count was measured several times and the mean calculated. The voltage was increased in small steps of 20 - 40 volts in the onset voltage region, i.e. up to 200 volts above the onset voltage, and thereafter in larger increments of 100 - 250 volts. At each voltage the pulse count rate was determined and some half dozen individual pulses were photographed with

the Polaroid camera. The final voltage across the specimen was 3.0 kV unless spark breakdown occurred at a lower voltage. When the final voltage was reached the E.H.T. lead was earthed and the specimen examined for pulse activity with no applied field. The voltage was increased at the rate of 100 volts every 5 minutes in the onset region and at twice this rate over the remaining range. All measurements were made two minutes after the application of each new voltage increment.

In addition to standard measurements of pulse charge and count rate, the onset voltage and the distribution of the pulse heights have been examined at constant temperature. The latter was measured by altering the discriminator and attenuation levels and counting the number of pulses above various threshold levels. The difference in pulse count rate between two levels then gives the number of pulses whose heights lie between these two voltage levels. The voltage at which pulses first appear is called the onset voltage. This is defined as the voltage at which the pulse count rate reaches a constant value of 1 count per 10 seconds as the voltage across the sample is raised. In experiments where the onset voltage has been investigated, the pulse activity was kept to a minimum by not applying more than 20 volts above the onset voltage to the specimen. In this way reproducible measurements have been obtained.

4.6.2 Temperature measurement of pulse breakdown

The variation of pulse activity with temperature has been investigated with two experimental procedures. In the

first procedure, where only the pulse activity of the sample was determined, the specimen was cleaned before and after each temperature measurement. For example, most of the polycrystalline sample results presented in Section 6.7.2. were obtained by cleaning the sample between successive temperature measurements. This procedure was not used where pulse measurements were combined with d.c. measurements. In these experiments the sample was cleaned only once, at the beginning of the experiment, and not in between temperature measurements as previously. Apart from the cleaning procedure, the measurement procedures were also different in the two types of experiment. The pulse activity was determined at only one pressure, i.e. one atmosphere of argon, in the case of the pulse measurements and at two pressures, 10^{-2} torr and atmospheric, in the case of combined d.c. and pulse measurement. Direct current and pulse measurements were made simultaneously every 100°C in combined measurements.

4.6.3 D.C. conductivity measurements

Before any measurements were made the leakage resistance of the sample holder was determined by measuring the resistance between the electrodes with an air gap of 5 mm. The results are shown in Fig 4.2. The leakage resistance was independent of the ambient gas pressure and the applied voltage. The large scatter is due to fluctuations in the electrometer readings, presumably due to the build-up of static charge on the electrodes.

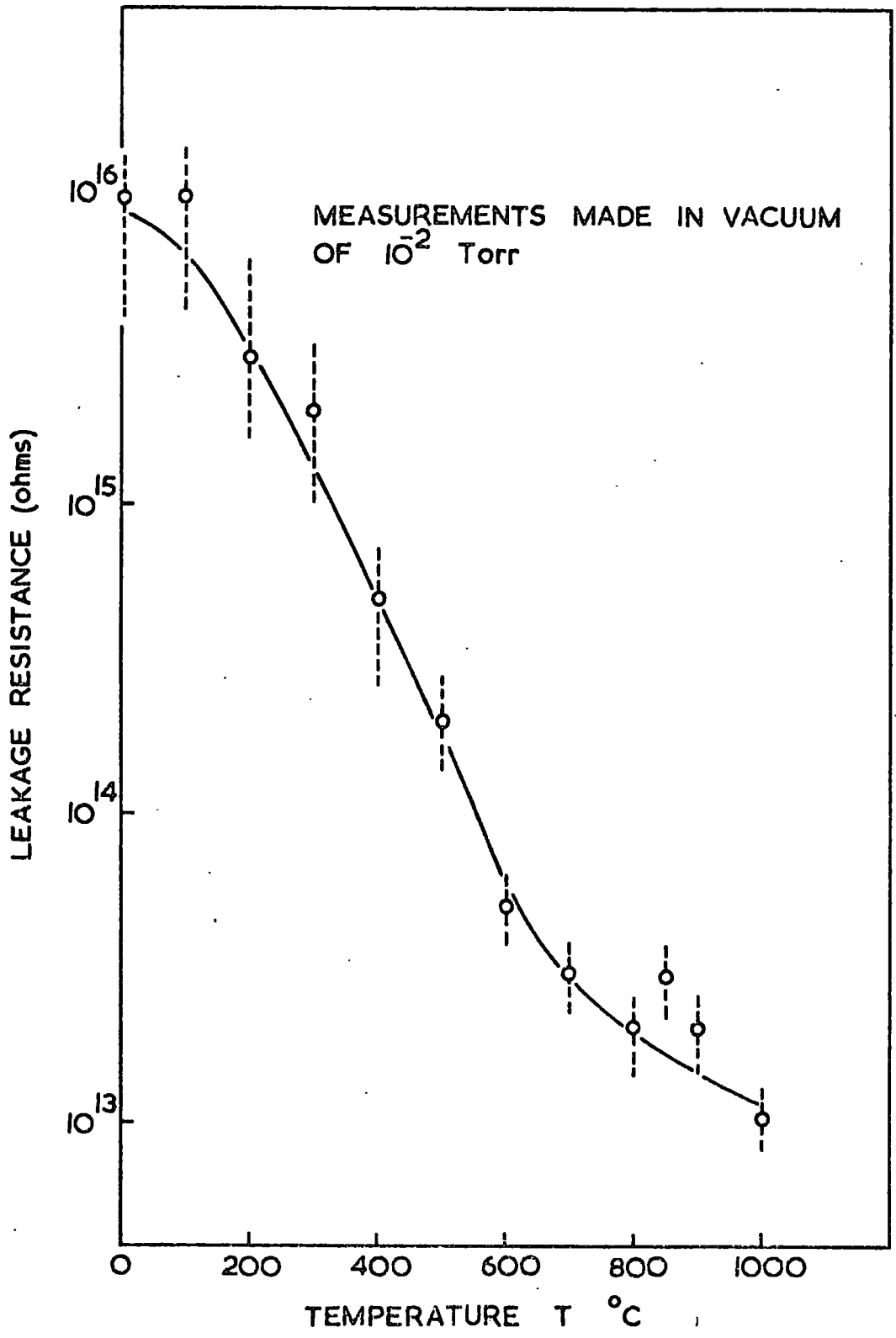

FIG. 4·2 LEAKAGE RESISTANCE OF SAMPLE HOLDER

Two-terminal measurements were made with the electrodes 5 mm above the guard ring upon which was mounted the thermocouple. This arrangement eliminates electrical leakage due to the thermocouple insulation but has the disadvantage that the thermocouple is not in contact with the sample. The temperature error introduced as a result of the arrangement was estimated by embedding a thermocouple in a polycrystalline sample, 3 mm thick by 15 mm diameter, and measuring the two temperatures over the range 0 to 900°C. The guard temperature was found to be within 1.5°/o of the sample temperature in °C over the total temperature range. The thermocouple e.m.f. was measured with a Pye Portable Potentiometer. This was supplemented with a Honeywell Electronik 15 temperature recorder when available.

The d.c. conductivity was obtained from the resistance of the sample which was measured from the slope of the I-V curves taken at every 100°C at gas pressures of 760 and 10^{-2} torr. In between these temperatures the resistance of the sample was measured at 10^{-2} torr with 100 volts applied. The sample was examined for pulse breakdown every 100°C as the d.c. measurements were being made. Polarisation currents were exhibited by all samples. Although these sometimes persisted for several hours, the current normally reached 10°/o of the equilibrium value within 5 minutes of the stress being applied. Consequently all measurements were made after at least 5 minutes.

4.7 Analysis of Pulse Breakdown Results

4.7.1 Measurements from oscillograms

The peak height, transit time and charge of the pulses has been determined from oscillograms. The pulse charge has been determined by measuring the area under the oscillograms. The transit time, i.e. the time taken by the current to reach the maximum value (termed peak height), and the peak height have all been measured directly. In calculating the size of the various pulse parameters from the oscillograms it was assumed that the head amplifier did not significantly distort the pulse, i.e. no allowance was made for the limited bandwidth of the head amplifier. This assumption is probably only justified for the slower pulses in argon (see Chapter 2).

The oscillograms were analysed by computer. The computer programme is given in Appendix A. To use this programme the pulse shape must be expressed in cartesian coordinates and a digital plotter was used to measure these off the oscillograms. In addition to the charge, transit time and peak height of the pulses the rise and decay times of the pulses were calculated by the computer programme.

4.7.2 Tests of significance

The large scatter in the pulse breakdown measurements made it necessary to compare results using statistical tests. The most satisfactory test of significance for a limited amount of data is the Student's T-test (Brownlee[15]), which was used in this work taking a 10°/o level of

significance. The significance test was used to compare the variation of pulse count rate and pulse shape with voltage in different experiments. The technique used was to compare the results obtained at each applied voltage under the different experimental conditions and to see whether these were significantly different. If in comparing two pulse count curves, for example, the pulse count rate was found to be significantly different at only one or two values of the applied voltage the results were not considered significantly different. However if there was a systematic difference between three or four measurements at consecutive voltages then the two results were taken as being significantly different. Where there have been several measurements of pulse breakdown under one set of experimental conditions the data from all the measurements was combined and considered as being drawn from the same population. The results in the new experimental conditions were then compared with the total data from all the measurements under the original conditions.

CHAPTER 5

PRELIMINARY EXPERIMENTS ON POSSIBLE PULSE BREAKDOWN SOURCES

5.1 Possible Sources of Pulse Breakdown

Since very little was known about the origin of pulse breakdown in sapphire, some preliminary measurements were made to find out which of the possible sources of discharges in gases and solids appeared to be operative in this case. On a macroscopic scale there appear to be five possible types of discharge source in any insulation system containing a mixture of solid and gaseous dielectrics. These are:-

(a) Sources in the bulk of the solid dielectric.

(b) Sources in voids or cavities inside the solid.

(c) Sources entirely due to gas discharge and the electrodes.

(d) Sources in voids or cavities between the electrodes and the surface of the dielectric.

(e) Sources associated with the surface of the solid and its interface with the gas.

To establish which of these sources is responsible for pulse breakdown some preliminary experiments were conducted over a range of temperatures and ambient air pressures on single crystal and sintered polycrystalline samples. The results show conclusively that source (e) is primarily responsible for pulse breakdown in sapphire in these experimental conditions.

5.2 Experiments to Determine the Breakdown Source

5.2.1 Pulse production as a function of gas pressure

If pulse breakdown is caused by either source (a) or (b) (sources in the bulk of the dielectric or in internal cavities), pulse breakdown should be independent of the ambient gas pressure. This has not been found to be the case. Figure 5.1 shows the results of early three-terminal measurements on a single crystal sample at 400°C. This shows that pulse breakdown is not observed at any applied voltage below 3.0 kV when the ambient air pressure is less than 0.4 torr. This result was found to be independent of the polarity of the voltage and of the measuring resistance used. Similar results were obtained on a sintered polycrystalline specimen.

Experiments were conducted to determine the minimum pressure at which pulse breakdown may be observed by allowing the ambient gas pressure to rise from 0.005 torr to atmospheric, while constant voltages of a range of magnitudes were applied continuously. Below pressures of 1 torr pulses were not observed at all. Between 1 and 20 torr there was severe pulse activity due to gas sputtering at the cathode and this was confirmed by the obvious transfer of cathode material seen on opening the system. The exact pressure at which this occurred could not be determined in these preliminary measurements. Subsequent measurements, reported in Chapter 6, show that the pulses first appear at pressures between 10 and 40 torr in argon and nitrogen ambients,

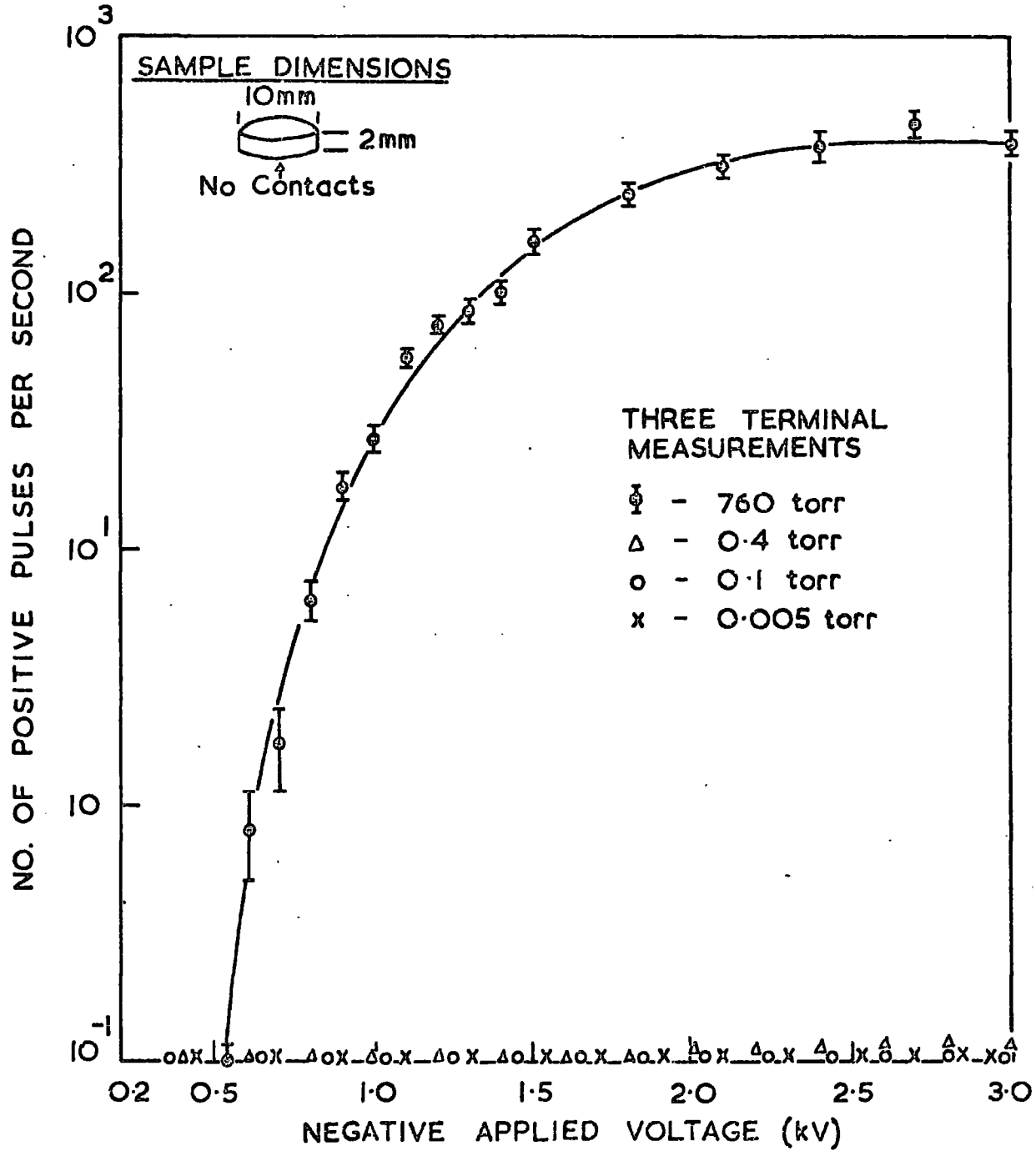

FIG. 5·1. EFFECT OF AMBIENT AIR PRESSURE ON THE POSITIVE PULSE COUNT RATE OF SINGLE CRYSTAL ALUMINA AT 400°C.

depending on the voltage. In all the preliminary experiments pulse breakdown was immediately observed on increasing the ambient air pressure to 1 atmosphere. The pulse count rate at 1 atmosphere of air immediately after evacuation of the furnace chamber was not significantly different from the pulse count rate recorded before the evacuation. There was also no detectable variation of pulse count rate with time either before or after evacuation of the chamber. These experiments show the very large effect of ambient gas pressure on pulse breakdown. From this it is clear that the bulk sources (a) and (b) cannot be the main source of pulse breakdown in these conditions.

5.2.2 The influence of the alumina on pulse breakdown

The dependence of pulse breakdown on ambient gas pressure suggests that the pulses are associated with gas discharges. If these discharges are entirely in the gas or associated with the electrodes, i.e. source (c), they will be independent of the type of dielectric sample. To find whether this type of gas discharge was responsible for pulse breakdown the following experiments were conducted:-

(i) A sintered polycrystalline sample in the form of an annular ring was inserted between the guard and high voltage electrode. With the detection resistance in series with the guard electrode, pulse breakdown was observed in the temperature range 400°C to 600°C at various applied voltages. Pulse breakdown was not seen, however, with the detection resistance in the lead from the low voltage electrode.

(ii) A sintered polycrystalline disc of the same diameter as the low voltage electrode was placed between the high and low voltage electrodes, with the guard electrode in the same position as previously. Pulse breakdown was now only seen when the detection resistance was in the lead from the low voltage electrode, and was not seen when the resistance was in the lead from the guard electrode.

(iii) The rig was examined for pulse breakdown with an air gap between the electrodes instead of a sample. Under these conditions no pulse breakdown was detected at 600°C with up to 3.0 kV applied with the detection resistance connected either in series or parallel with the electrodes, i.e. positions Z and Z^1 in Figure 2.1 respectively.

These experiments show conclusively that pulse breakdown is associated with the presence of the sapphire sample in addition to the ambient gas.

5.2.3 The influence of contacts on pulse breakdown

Sources associated with the gas and the sample are of Types (d) and (e) listed in Section 5.1. Source (d) is due to discharges in cavities between the electrode or contact and the underlying surface of the sapphire. This would be expected to depend on the type of contact used if it were the major source of pulse breakdown.

The effect of contacts on pulse breakdown was examined on single crystal material. Figure 5.2 shows the result of

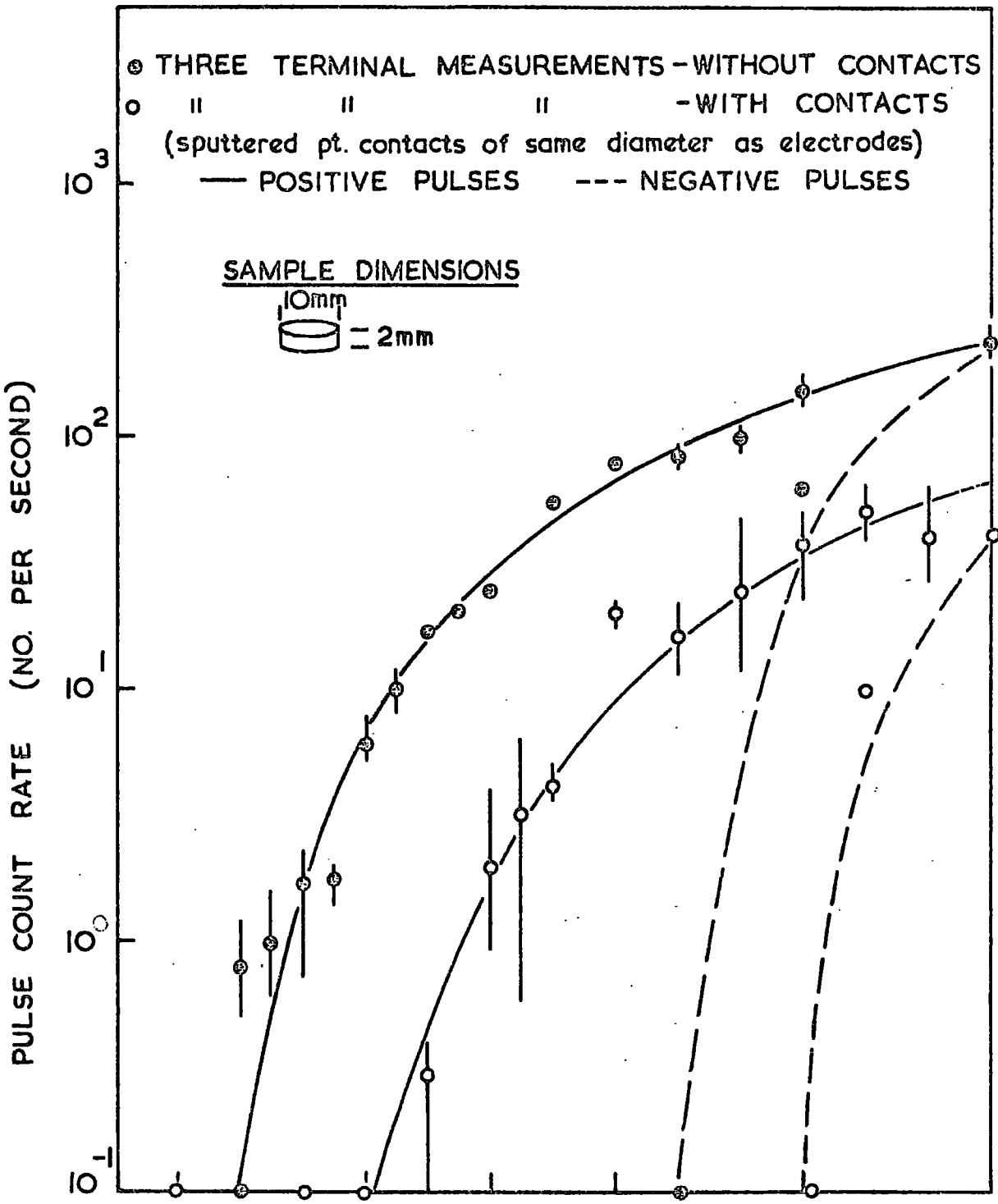

FIG. 5·2. EFFECT OF SPUTTERED CONTACTS ON THE PULSE COUNT RATE OF SINGLE CRYSTAL ALUMINA IN AN ATMOSPHERE OF AIR AT 400 °C.

three-terminal measurements on a single crystal before and after the sputtering of contacts. Although the pulse count rate appears to be lower after the deposition of contacts, this result cannot be considered to be significant in view of the fact that similar results were obtained in successive measurements on an identical sample on which there were no contacts. Hence it can be concluded that contacts do not significantly affect the pulse count rate. Figure 5.3 shows the variation of the measured pulse charge with applied voltage for this experiment. From this it can be seen that the general shapes of the two curves are similar. The shapes of the pulses themselves were also very similar in the two measurements as can be seen from the typical oscillograms shown in Figure 5.4. However, since the impulse shape in these preliminary experiments was limited by the circuit response (see Sec 2.4) these results may not be of much significance. Figure 5.5 shows the results of two-terminal measurements on an etched single crystal before and after the sputtering of contacts. From this it can be seen that the pulse count rate is not significantly reduced by the deposition of contacts on the alumina surface. This confirms the results of the three-terminal measurements, namely that the pulse breakdown of single crystal samples is not significantly affected by the existence of contacts under the electrodes.

Similar results were obtained in two- and three-terminal measurements on polycrystalline samples. Figure 5.6 shows the results of three-terminal measurements on a

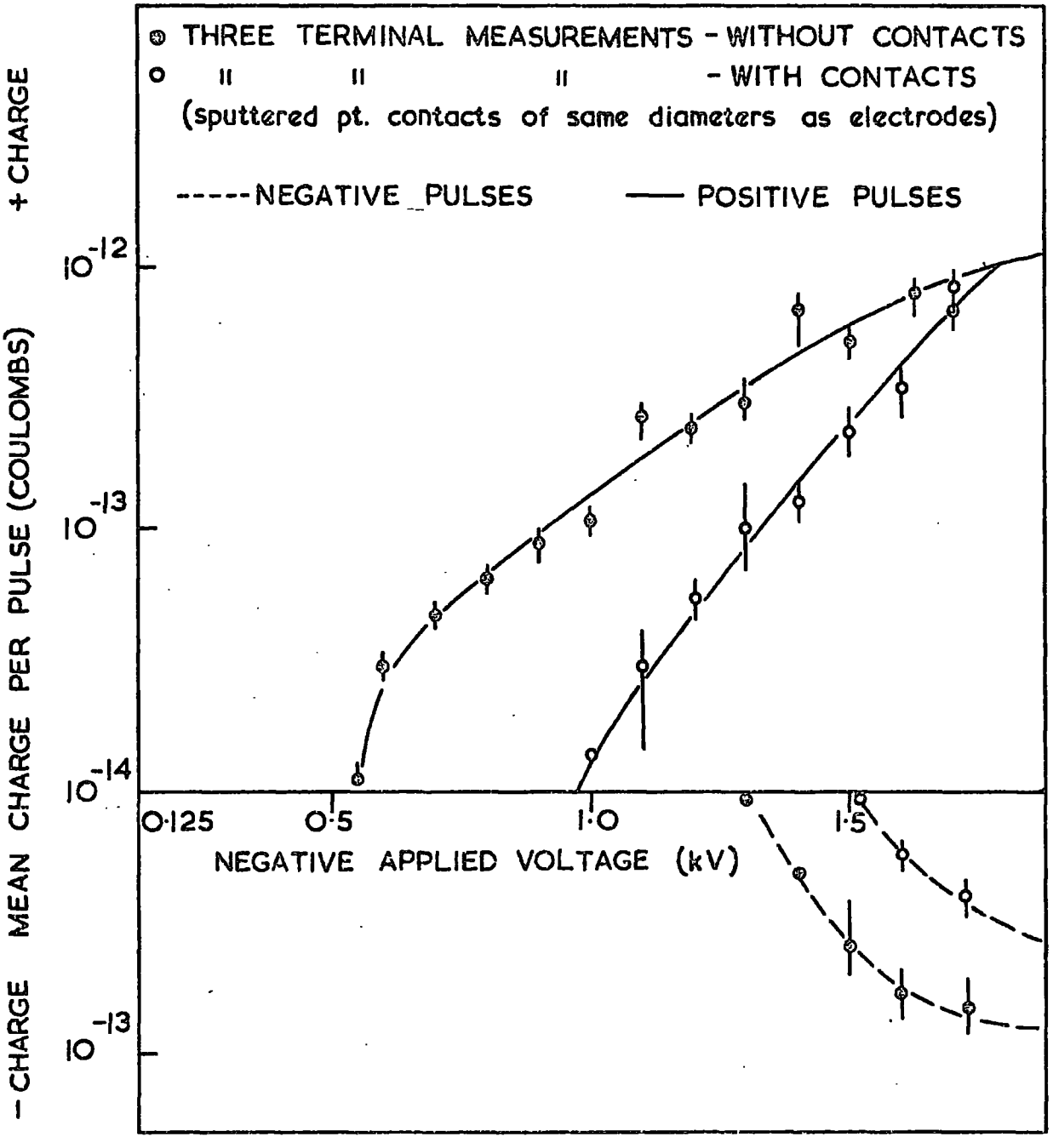

FIG. 5·3. EFFECT OF SPUTTERED CONTACTS ON THE MEAN PULSE CHARGE OF SINGLE CRYSTAL ALUMINA IN AN ATMOSPHERE OF AIR AT 400°C.

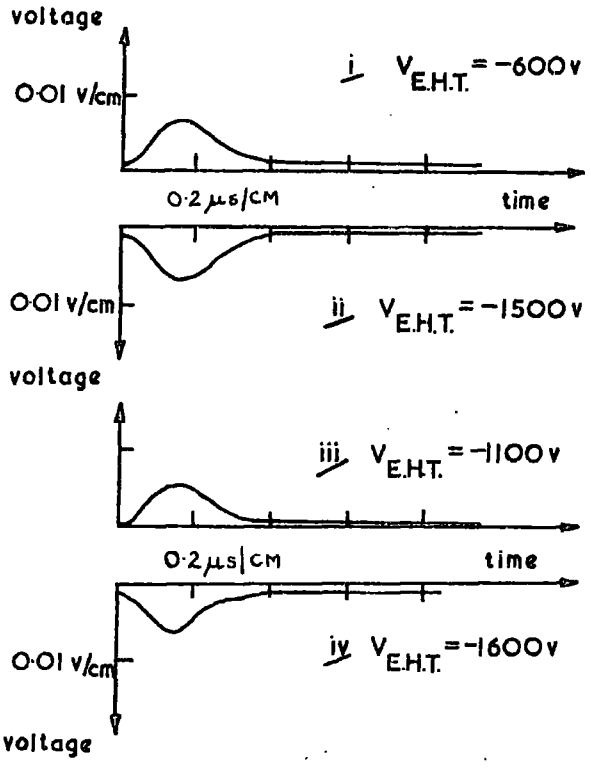

FIG. 5·4 TYPICAL PULSES IN THREE TERMINAL MEASUREMENTS ON SINGLE CRYSTAL IN AIR AT 400°C. (i & ii-no contacts, iii & iv-sputtered contacts)

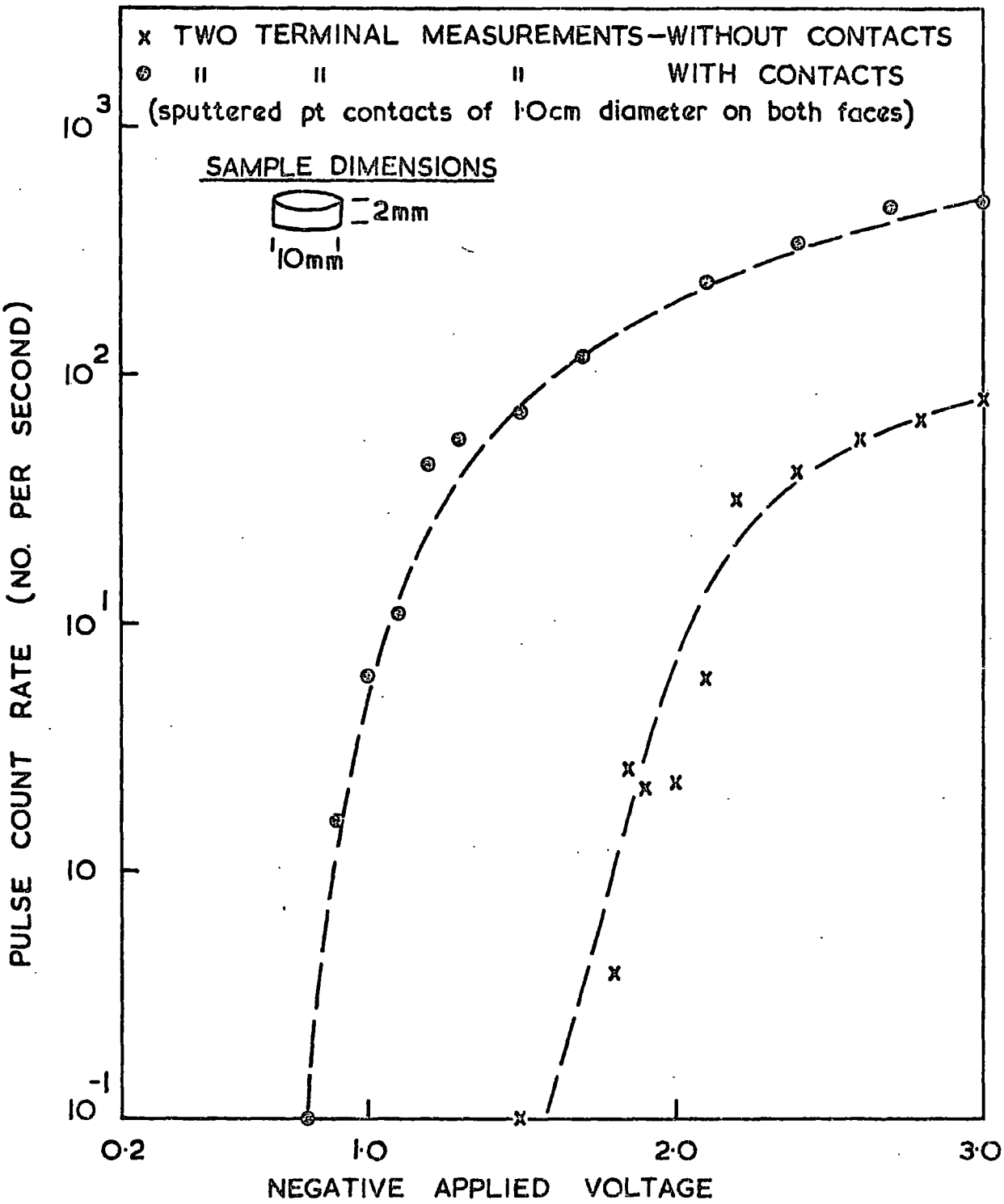

FIG. 5·5 EFFECT OF SPUTTERED CONTACTS ON THE PULSE COUNT RATE OF AN ETCHED SINGLE CRYSTAL IN AN ATMOSPHERE OF AIR AT 480°C.

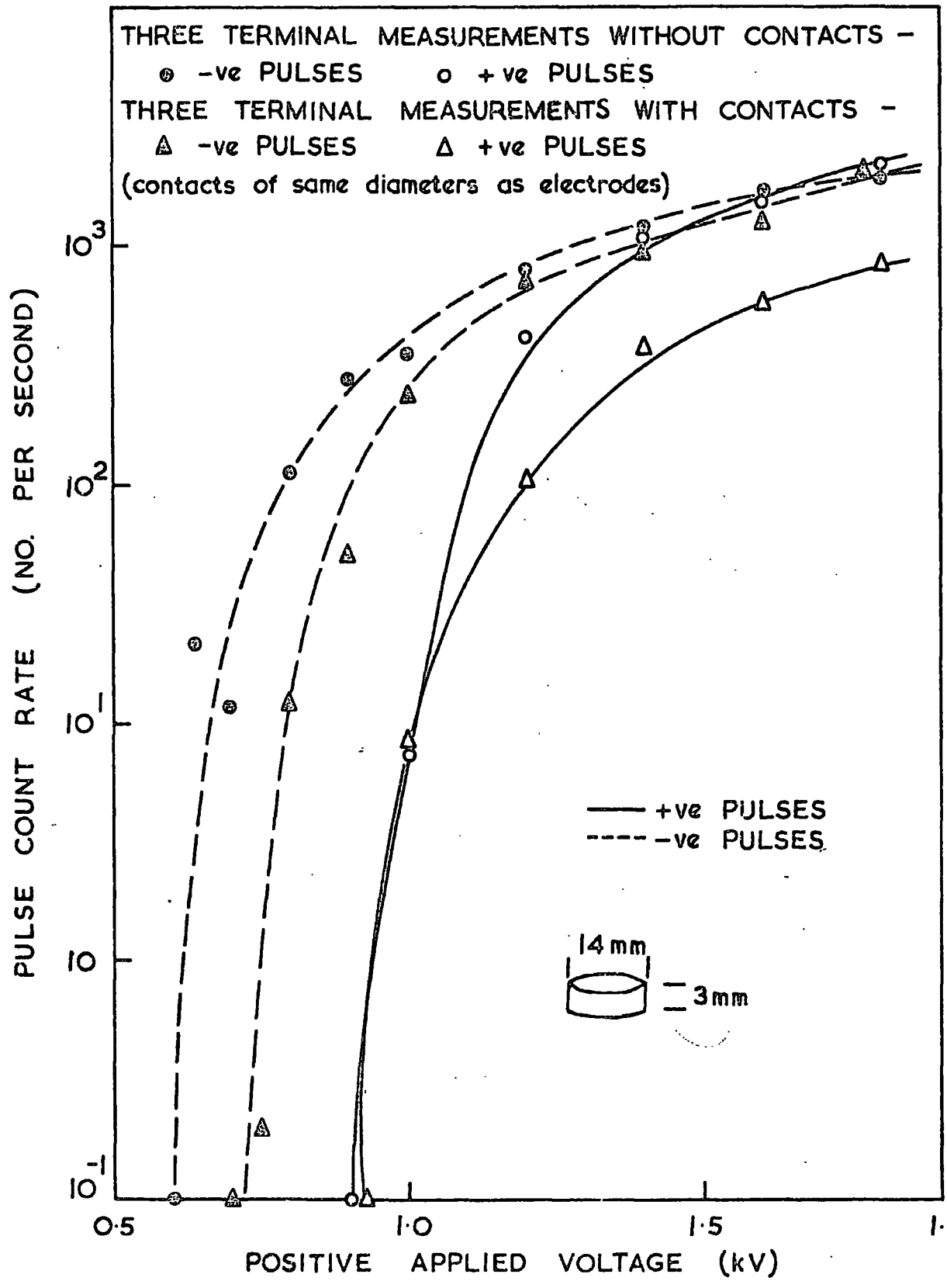

FIG. 5·6 EFFECT OF SPUTTERED CONTACTS ON THE PULSE COUNT RATE OF SINTERED POLYCRYSTALLINE ALUMINA IN AIR AT 400°C

sintered sample in dry air. The difference in the two pulse count rates is not significant in view of the experimental scatter in successive measurements under constant experimental conditions. The sizes and shapes of the pulses before and after the sputtering of contacts were also very similar. Two-terminal measurements on sintered samples were also not found to be significantly affected by contacts (see Sec 6.6). Hence from these experiments it is concluded that pulse breakdown on both single crystal and sintered polycrystalline alumina is not significantly affected by the presence of contacts under the electrodes. This must eliminate source (d) as a major source of pulse breakdown.

5.3 Discussion

The experiments described in Section 5.2 appear to show that pulse breakdown is a phenomenon involving both the ambient gas and the dielectric surface. This conclusion is reached largely by eliminating sources entirely in the dielectric and entirely in the gas. The conclusion was of great importance for the further development of the work since it limited the whole field of investigation. Before proceeding it is therefore worthwhile to discuss these experiments in more detail to ensure that the conclusion is valid.

The failure to observe pulse breakdown at ambient air pressures below 20 torr shows the importance of the ambient gas on pulse breakdown. This fact must eliminate intrinsic

processes in the bulk of the alumina as the source but extrinsic processes in the bulk could be pressure dependent if changes in the ambient conditions caused corresponding changes in the bulk stoichiometry. In ionic crystals significant changes in bulk stoichiometry only occur at temperatures above the Tammann temperature, since at lower temperatures the ions do not have sufficient thermal energy for diffusion (Rees[16]). Since the Tammann temperature of alumina is 890°C, changes in pressure are unlikely to significantly affect the bulk stoichiometry of alumina at temperatures below 600°C. Consequently extrinisic processes in the bulk would also appear to be eliminated as the source of pulse breakdown.

Pulse breakdown could also result from gas discharges in cavities within the dielectric. If this is the case, all the cavities in the alumina would have to be connected to the ambient gas to account for the pressure dependence of pulse breakdown. In addition, the conductance of the paths connecting the cavities to the ambient gas would have to be high to account for the immediate response of pulse breakdown to changes in the ambient conditions. These requirements would appear to eliminate this type of source unless all the cavities are localised at the surface. In view of the similarity in the pulse breakdown characteristics of single crystal and polycrystalline alumina it seems reasonable to assume that the pulses are produced by the same source in the two types of sample. X-ray examination of the single crystals used in these experiments did not show

any sign of crystallite misorientation. This means that in the surface regions examined with the X-ray beam there is less than 1^{o} misorientation between crystallites. Since surface cavities would produce a detectable misorientation of the crystallites, their existence is unlikely in single crystal material. This conclusion was also supported by optical examination of the samples. Consequently surface cavities are unlikely to be the source of pulse breakdown in either single crystal or polycrystalline alumina.

The measurement of pulse breakdown on samples with and without contacts shows that gas discharges under the electrodes are not a major source of pulse breakdown. The results also indicate that there is no significant contribution to the pulse count rate from this source. While this might have been expected from the single crystal, it is a surprising result at first sight for the polycrystalline material in view of the surface topography shown by the Talleysurf measurements. From these measurements a simple estimate can be made of the electric stress in an air gap under the electrodes. The Talleysurf measurements show that the maximum air gap which can exist under the electrodes is approximately 4×10^{-3} cm deep if irregularities in the surface of the electrode are neglected. If the field in the dielectric is assumed to be uniform and the boundary between the dielectrics is parallel to the electrode faces, the lines of flux pass normally through the dielectric surface as shown in the diagram (Fig 5.7). Under these conditions, the field in a small cavity under the electrode

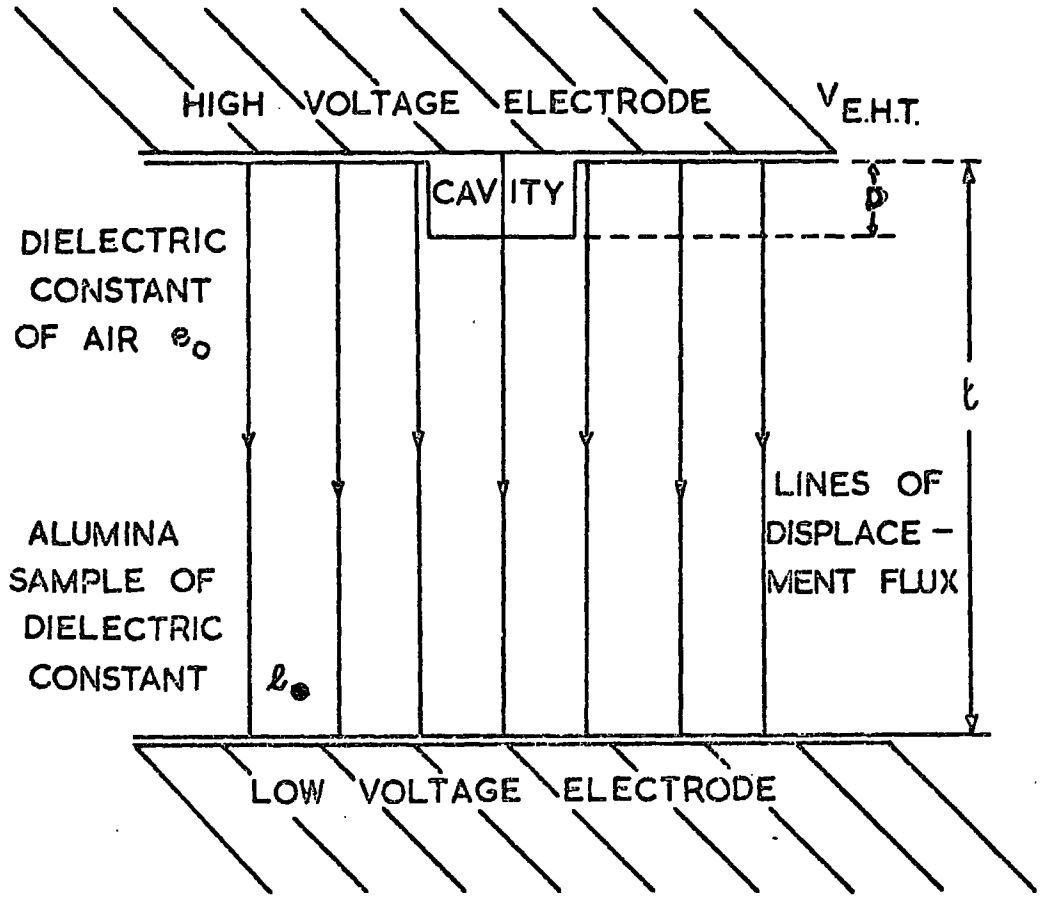

FIG. 5-7 SIMPLE CAVITY MODEL FOR DISCHARGES UNDER ELECTRODE.

is given by

$$E = V_{E.H.T.} \left(\frac{1}{K} - 1\right) \Big/ D \left(\frac{1}{K} + \frac{e_o}{e-1}\right) \qquad \text{Eqn 5.1}$$

where $k = (t - D)/t$, and e_o and e are the dielectric constants of air and alumina respectively. Substituting known values of D, t, e_o and e into Eqn 5.1 and applying the maximum voltage to the electrodes, i.e. $V_{E.H.T.} = 3.0$ kV, gives values for the field in the cavity of 90 kV cm^{-1} and the voltage across the cavity of 360 volts. The pd value for a gap of 4×10^{-3} cm in an atmosphere of air corrected to room temperature is 1.2 torr cm. The Paschen breakdown voltage for this pd product is approximately 400 volts (Meek and Craggs[17a]). Consequently the voltage across the cavity only approaches the breakdown voltage of air at the highest applied voltages. On the basis of this estimate, it is unlikely that Paschen breakdown occurs under the electrodes at applied voltages less than 3.0 kV, even though allowance has not been made for the irregular shape of the cavities. Although the field is too low for Paschen breakdown, single or multiple avalanches of a few generations could occur in the gas cavity provided there are sufficient primary electrons to initiate the avalanches. With 1.0 kV applied to the electrodes, the field in the cavity is approximately 30 kV cm^{-1}. At 400°C and an atmosphere of air, the E/p ratio in the gas is about 100 volts cm^{-1} $torr^{-1}$. The ionization coefficient at this E/p ratio for air is 200 cm^{-1} (Meek and Craggs[17b]).

Consequently the multiplication factor of a single avalanche in the cavity is very small, expαd being about 2. It therefore seems that contributions to pulse breakdown from avalanches under the electrodes are unlikely unless the number of primary electrons is very large or the series exceedingly long, in which case Paschen breakdown would be occurring.

Pulse breakdown is only observed when an alumina sample is present between the electrodes. This fact must eliminate purely gas processes as the source of pulse breakdown because otherwise there should be no effect of removing the sample. In fact, removing the sample increases the sensitivity of the detector, because of the lower capacitance between the electrodes, and it should make the detection of pulse breakdown possible at lower onset voltages. This is not found and it must be concluded that the sample is essential to pulse production.

The results of these pulse breakdown measurements eliminate four out of the five sources outlines in Section 5.1 and leave only source (e), i.e. mechanisms associated with the interface between the alumina and the ambient gas, as the possible source of pulse breakdown. Although there could be numerous mechanisms associated with this type of source, the critical dependence of pulse breakdown on ambient gas pressure suggests that gas discharges are responsible. If this supposition should be confirmed, the gas discharges are most likely to be occurring in the high stress regions near the electrodes in view of the relatively high dielectric

constant of alumina. This could explain why pulses of both polarity are seen in three-terminal measurements as described in the following Section 5.4.

5.4 Pulse Polarity and Equivalent Circuit

Two- and three-terminal measurements on single crystal and sintered alumina samples show that the polarity of the detected impulses is affected by the electrode arrangement used in the measurements. In two-terminal measurements it was found that the polarity of the impulses was the same as that of the E.H.T. supply. However in three-terminal measurements both positive and negative going pulses were observed in the same experiments as shown, for example, in Figure 5.6. The onset voltages of the pulses of each polarity varied from measurement to measurement. However the pulse of opposite polarity to the high voltage supply was always found to have a lower onset voltage than that of the pulse of the same sign as the supply.

Figure 5.4 shows typical oscillograms of the positive and negative pulses seen in three-terminal measurements. From these it can be seen that the shapes of the two pulses are very similar. Figure 5.8 shows the results of pulse charge measurements on a sintered sample with a three-terminal arrangement. From this it can be seen that the charge of both the negative and positive pulses varies with voltage in a similar manner. Hence it can be concluded that the only significant difference between the two pulses, apart from the obvious one of polarity, is in the observed onset voltages.

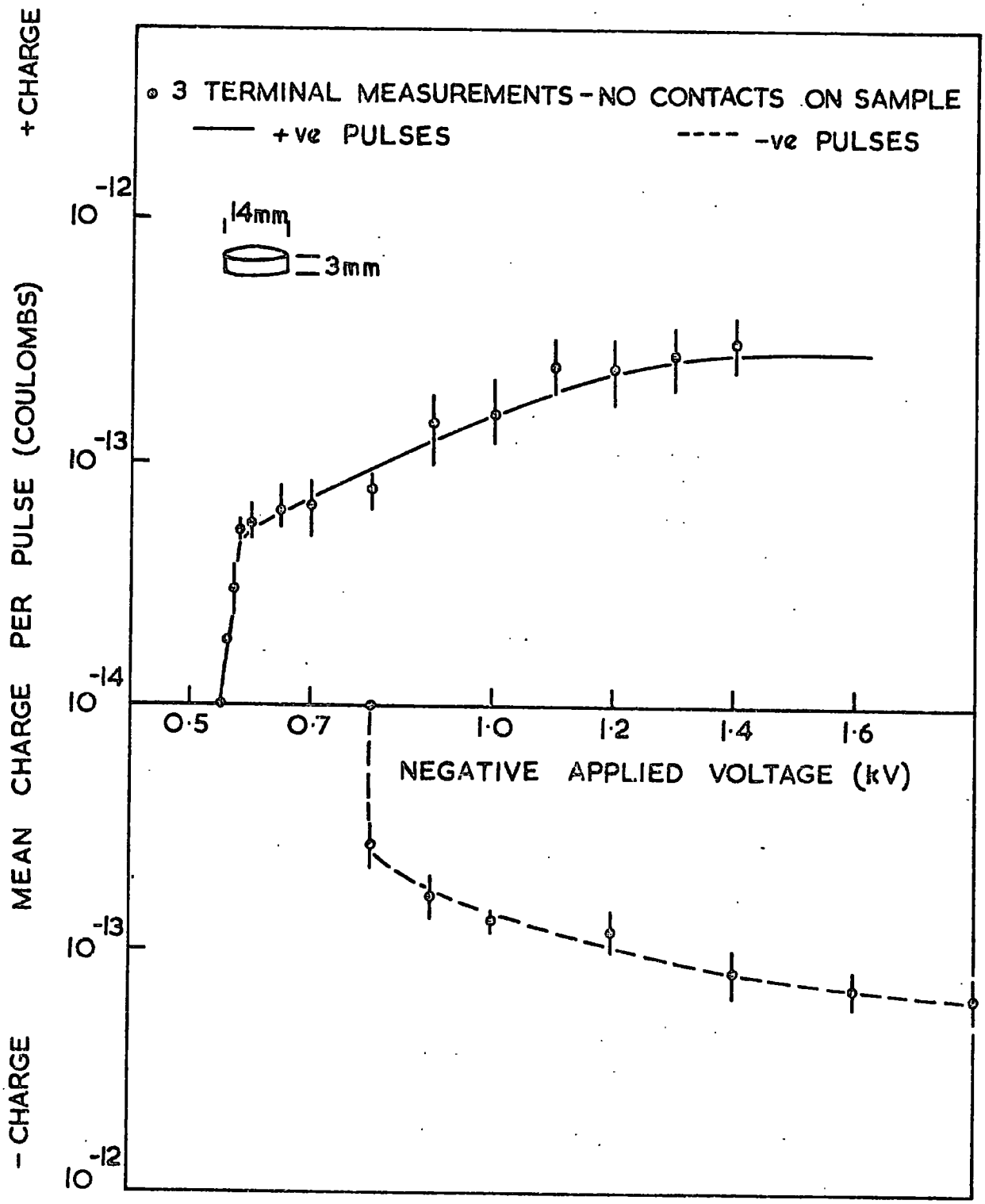

FIG. 5·8 MEAN PULSE CHARGE – v – APPLIED VOLTAGE OF SINTERED POLYCRYSTALLINE SAMPLE IN AIR AT 460 °C.

These pulse polarity effects can be explained by an equivalent circuit model in which there are two different sources of pulse breakdown. In deriving this model two basic assumptions have been made. Firstly it has been assumed that the sources of pulse breakdown can be represented in the equivalent circuit by current generators in parallel with resistances. These resistances represent the internal resistances of the sources when they are conducting. Secondly it has been assumed that the sample can be represented by slightly different equivalent circuits in two- and in three-terminal measurements. This is because it is necessary to take account, in the three-terminal case, of the capacitive coupling between the low voltage and guard electrodes through the sample.

Figure 5.9 shows the equivalent circuit for the sample and associated leads in the two-terminal case. The sample is represented by the circuit within the dashed lines. R_bC_b and R_sC_s represent the discharge free regions of the bulk and surface of the sample while $R_b'C_b'$, $R_s'C_s'$ and $R_b''C_b''$, $R_s''C_s''$ represent the bulk and surface regions of the sample in parallel and series with the discharge source. Let us suppose that pulse breakdown is caused by a discharge between a point A on one of the electrodes and a point B on the alumina surface. If the discharge is between the high voltage electrode and the surface, $R_s'C_s'$ and $R_b'C_b'$ represent the capacitance and resistance of the surface and bulk of the sample between the point B and the high voltage electrode respectively, while $R_s''C_s''$ and $R_b''C_b''$ represent

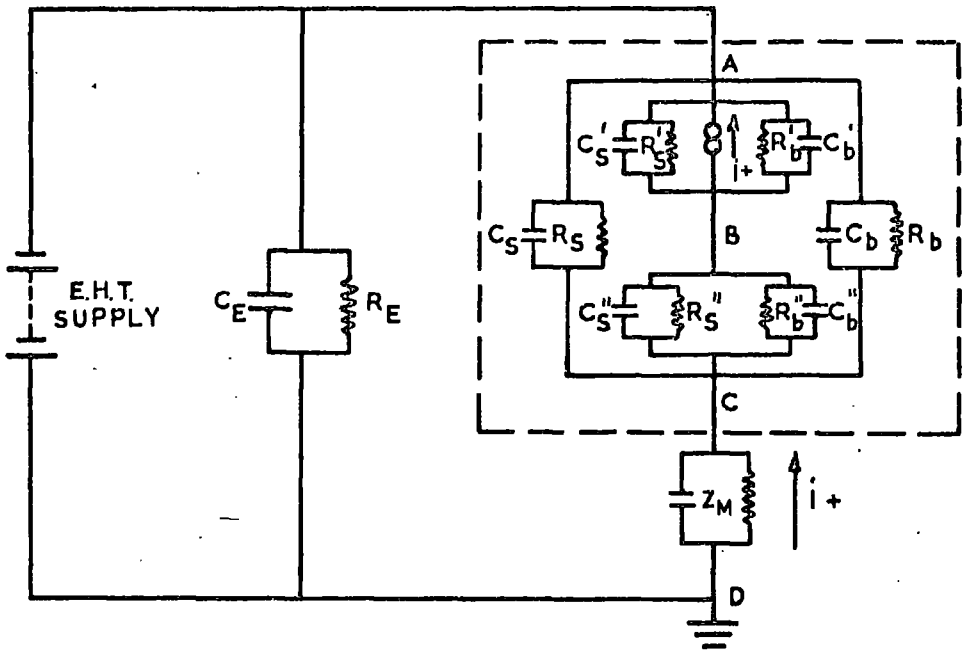

FIG. 5·9 EQUIVALENT CIRCUIT FOR SAMPLE AND LEADS IN TWO TERMINAL MEASUREMENTS

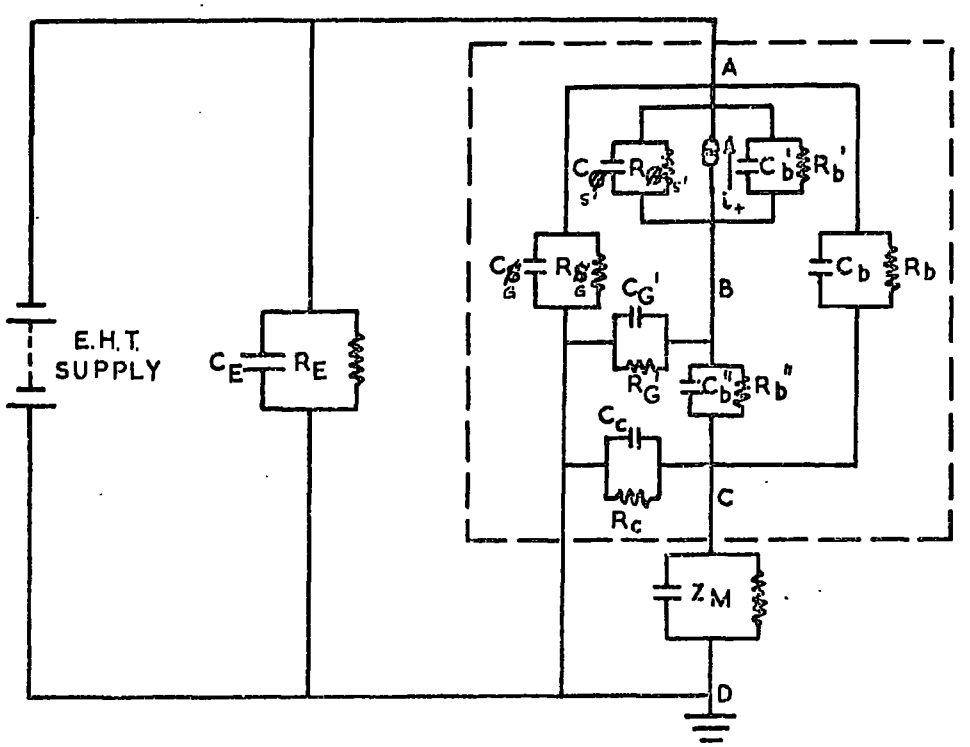

FIG. 5·10 EQUIVALENT CIRCUIT FOR SAMPLE AND LEADS IN THREE TERMINAL MEASUREMENTS

the capacitance and resistance of the surface and bulk of the sample between the point B and the low voltage electrode. It can be seen from Figure 5.9 that when A is at a negative voltage with respect to C, the current impulse produced by the pulse source across AB will flow through the external circuit in the direction ADC. Hence the voltage impulse produced across the detection impedance Z_m will be negative, i.e. C will be negative with respect to D. The same result is obtained when the pulse source is across CB, i.e. when the discharge occurs between the low voltage electrode and the surface of the alumina, since the current impulse also flows round the external circuit in the direction ADC in this case. Hence in two-terminal measurements the polarity of the detected impulse is independent of the position of the pulse breakdown source.

Figure 5.10 shows the equivalent circuit for the sample and associated leads in the three-terminal case. With the exception of R_cC_c, which represents the electrical coupling between the low voltage electrode and the guard through the sample, the circuit components in Figure 5.10 are similar to those shown in Figure 5.9. R_bC_b, $R_b'C_b'$, $R_b''C_b''$ and $R_s'C_s'$ represent the bulk and surface of the sample as before. However R_gC_g now represents the discharge free region of the sample between the high voltage electrodes and the guard rather than just the discharge free region of the surface as previously, and $R_g'C_g'$ the capacitance and resistance of the sample between the guard electrode and the point B. Discharges between the high voltage

electrode and the surface of the alumina are still represented by a current generator, across the points A and B, in parallel with $R_b'C_b'$ and R_gC_g. Discharges between the low voltage electrode and the surface of the sample do not now occur, because the tangential stress component of the electric field between the guard and low voltage electrode will be small with the guard circuit earthed. Hence the discharges which occurred in the two-terminal case between the low voltage electrode and the alumina surface now occur at the guard electrode. Consequently the current generator representing the low voltage discharge is connected in parallel with $R_g'C_g'$, i.e. between BD. This causes the low voltage source to produce pulses of <u>opposite</u> polarity to the high voltage source.

The pulse polarity effects are best explained by reference to the diagrams in Figure 5.11. These show the capacitive components of the circuit as they appear to the breakdown sources, the resistive components of the circuit being omitted since they do not affect the polarity of the impulses. When the breakdown source is across AB, Figure 5.11a, the detection impedance is in the balance arm of the bridge network, C_b C_b'' C_g'; $C_e + C_s$. Hence if $V_{AC} > V_{AD}$, which is justified because C_e is large compared to C_b, C is negative with respect to D for current discharges across AB as shown. Thus with the pulse source across AB the external impulses are of the same sign as the E.H.T. supply. When the source is across DB, Figure 11b, the detection impedance is in one of the arms of the bridge circuit. In

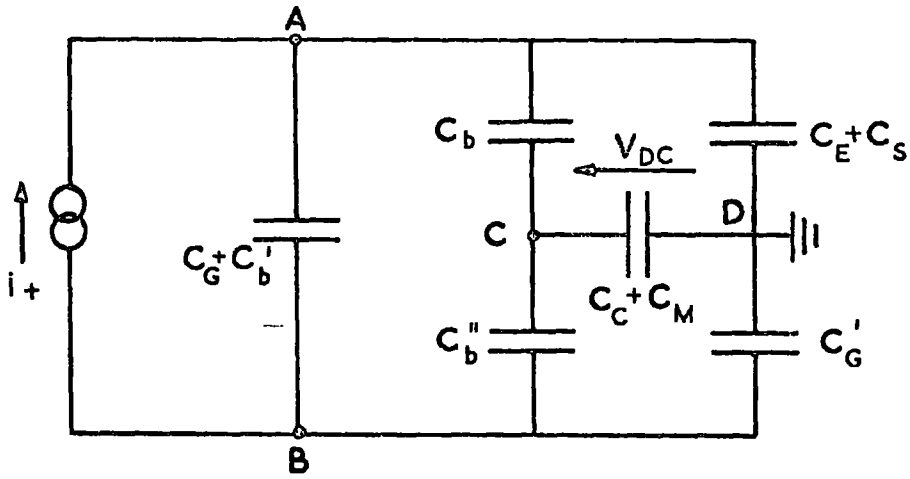

FIG. 5·11a HIGH VOLTAGE DISCHARGE

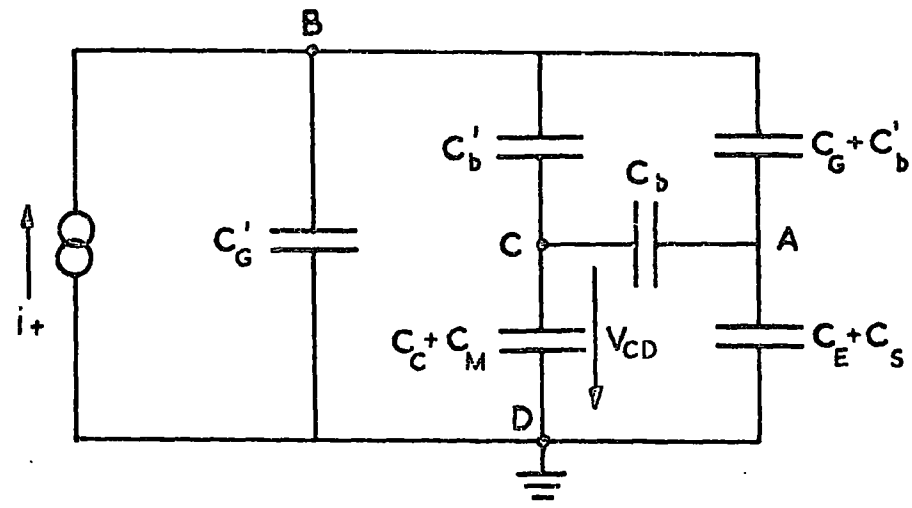

FIG. 5·11b LOW VOLTAGE DISCHARGE

FIG. 5·11 CAPACATIVE COMPONENT OF EQUIVALENT CIRCUIT OF FIG. 5·10, SHOWING EFFECT OF DISCHARGES AT THE HIGH (a) and LOW (b) VOLTAGE ELECTRODES ON POLARITY OF DETECTED IMPULSES.

this case the impulses across the detection impedance are positive since C is at a higher potential than D when the current flow is as shown in the diagram.

Although the observed pulse polarity effects can be explained by the above model, a single pulse source model could equally explain the results if it is assumed that the introduction of the guard circuit causes differentiation of the pulse shape. Since some gas discharges will produce current impulses of the square wave type, e.g. Hornbeck,[18] the possibility of two opposite polarity pulses being produced by a single source cannot be excluded if the source of pulse breakdown is a gas discharge.

5.5 Conclusion

The process of elimination described in this chapter leads to the conclusion that pulse production in alumina at high temperatures is associated with the interface between the sample and the ambient gas. While there are many electrical processes that may occur at the surface of such an insulator, discharges at the edges of the electrodes appear to be a likely source. Equivalent circuits for the discharge currents are derived and these can explain the different pulse polarities found with two- and three-terminal electrode arrangements.

CHAPTER 6

PULSE BREAKDOWN ON ALUMINA

6.1 Introduction

The preliminary studies of pulse breakdown eliminated all sources except those associated with the surface of the sample. On the basis of the pressure dependence of the pulse activity, the work described in Chapter 5 suggested that surface discharges were a likely source of the pulses. A more detailed study of the dependence of pulse breakdown on the ambient gas was then undertaken and the results are presented in this chapter. These showed that the shape of the pulses depended on both the pressure and purity of the ambient gas. In argon ambients two pulses of different shapes were observed. This was not seen in air. The effect of different electrode and contact configurations on pulse breakdown was also studied and the results indicated a dependence on the contacts but not on the electrodes. A quantitative comparison of results is difficult because of the lack of reproducibility between successive measurements. Consequently statistical tests have had to be applied to the results to determine the significance of various parameters. The analysis of the results was further complicated by the wide distribution in the pulse sizes. This is believed to be due to fundamental fluctuations in the gas breakdown mechanism.

The importance of chemical cleaning on pulse breakdown was shown by the temperature dependence of the pulse count rate on single crystal alumina. When single crystal alumina was heated to 900°C after chemical cleaning a peak in the pulse count rate was normally observed. Once the crystal had been heated to 900°C however no significant pulse activity was detected below 900°C either on cooling or on reheating the crystal. If the crystal was chemically cleaned before being reheated the peak in the pulse count rate reappeared, showing that cleaning of the crystal caused the peak in the pulse count rate. Although no comparable study was made on polycrystalline alumina a peak in the pulse count rate was also detected on heating a sintered sample to 900°C after chemical cleaning.

Most of the detailed measurements of pulse breakdown reported in this chapter were made on sintered polycrystalline samples. This was because measurements on this type of sample were found to be more reproducible. Experiments on single crystals were, for the most part, restricted to qualitatively confirming the results of the more important measurements on the sintered sample. In all these experiments the results, which will not be given in any detail, were substantially the same as measurements on polycrystalline samples. In general the sizes of the pulses were greater and the pulse count rate lower on single crystal than on polycrystalline samples.

6.2 Pulse Counting Experiments

The reproducibility of pulse count rate measurements in an atmosphere of argon at 400°C has been studied on two identical sintered polycrystalline alumina samples. These samples were discs of 39 mm diameter and 5.5 mm thickness. The voltage sensitivity of the detector was the same in all experiments irrespective of the value of the detection resistance, the minimum voltage impulse detectable across the resistance being 0.18 mV. All measurements were made on samples without contacts by the two terminal technique and, unless otherwise stated, with a 10^3 ohms detection resistance.

The results of pulse count measurements on one of these samples are shown in Figure 6.1. These measurements were made at 400°C in an atmosphere of argon, the sample being maintained at temperature throughout the measurements. Between measurements 1 and 2 and 3 and 4 the pulse count was determined for other ambient pressures. A similar experiment was then performed on the other sample with the results shown in Figure 6.2. Again the pulse count was determined at other ambient pressures between measurements 1 and 2 and 2 and 3. It can be seen that in this second experiment there is good agreement between successive measurements in comparison to the first. Apart from the use of different samples, the only other difference between the experiments was in the drying of the ambient gas. In experiment 1, the gas was dried by passing it through a molecular sieve while in experiment 2 a CO_2 cold trap and molecular sieve were used. This appears to indicate that

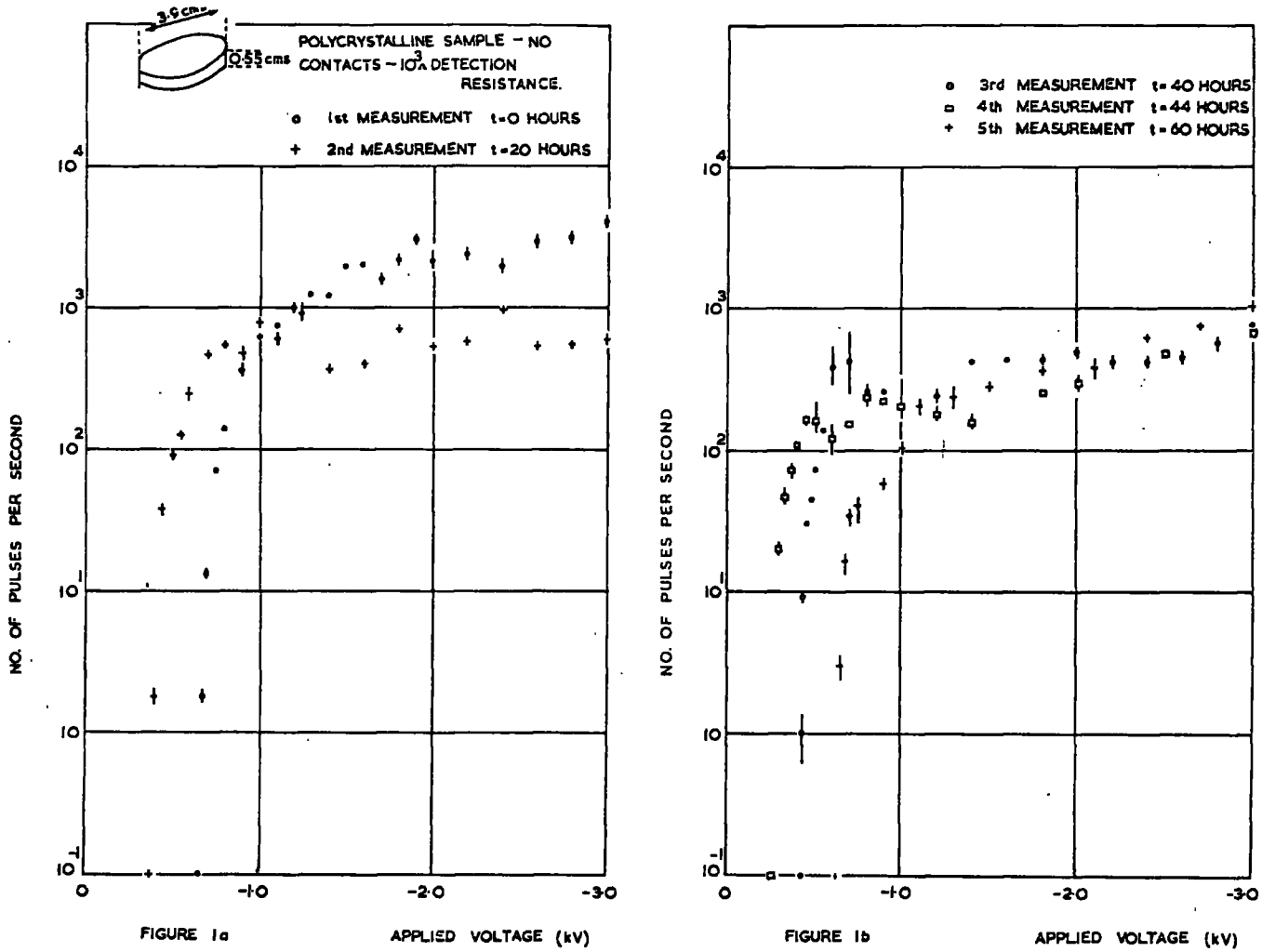

FIGURE 1a

FIGURE 1b

FIG. 6-1. PULSE COUNT RATE — vs — APPLIED VOLTAGE FOR SINTERED ALUMINA IN AN ATMOSPHERE OF ARGON AT 400°C

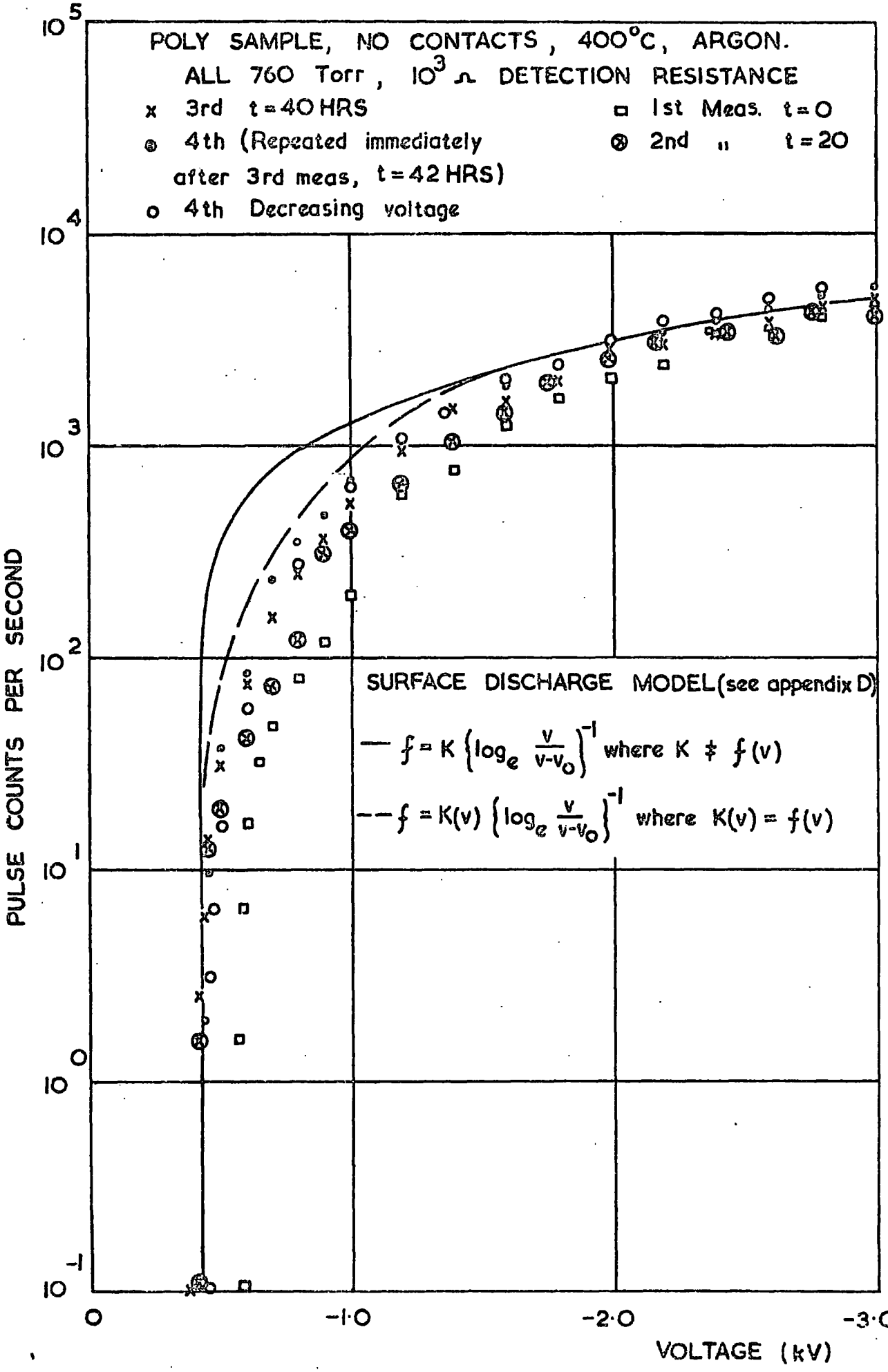

6·2. PULSE COUNT RATE – v – APPLIED VOLTAGE FOR POLYCRYSTALLINE ALUMINA IN AN ATMOSPHERE OF DRY ARGON AT 400°C.

there is good reproducibility of pulse count measurements if the ambient gas is sufficiently dry.

From the preliminary measurements the pulse count rate was known to be very sensitive to temperature. Consequently the temperature variations between measurements were kept to a minimum ($400^{o}C \pm 5^{o}C$) in these two experiments by allowing the sample several hours in which to reach thermal equilibrium after the introduction of the ambient gas into the chamber. As a result of this impurities may have diffused into the chamber from the surrounding air and contaminated the argon. An experiment was conducted to determine the pulse count immediately after the introduction of dry argon (i.e. argon passed through a cold trap) into the chamber. To minimize diffusion in this experiment the leak rate of the chamber was reduced to 3×10^{-4} torr litres per second and the time to record the pulse count curve was reduced to approximately 30 minutes, i.e. time interval between measuring the pulse count rate at each voltage was only a few seconds. Under these conditions no pulses at all were found over the voltage range 0 to 3.0 kV with a 10^{3} ohms detection resistance at $400^{o}C \pm 10^{o}C$. With a 10^{4} ohms resistor the count rate was as shown in Figure 6.3. This indicated that the pulse height must be very dependent on the purity of the ambient gas.

The impurities in the ambient gas, other than those inherent in the gas supply, stem from several sources. The most important of these are:-

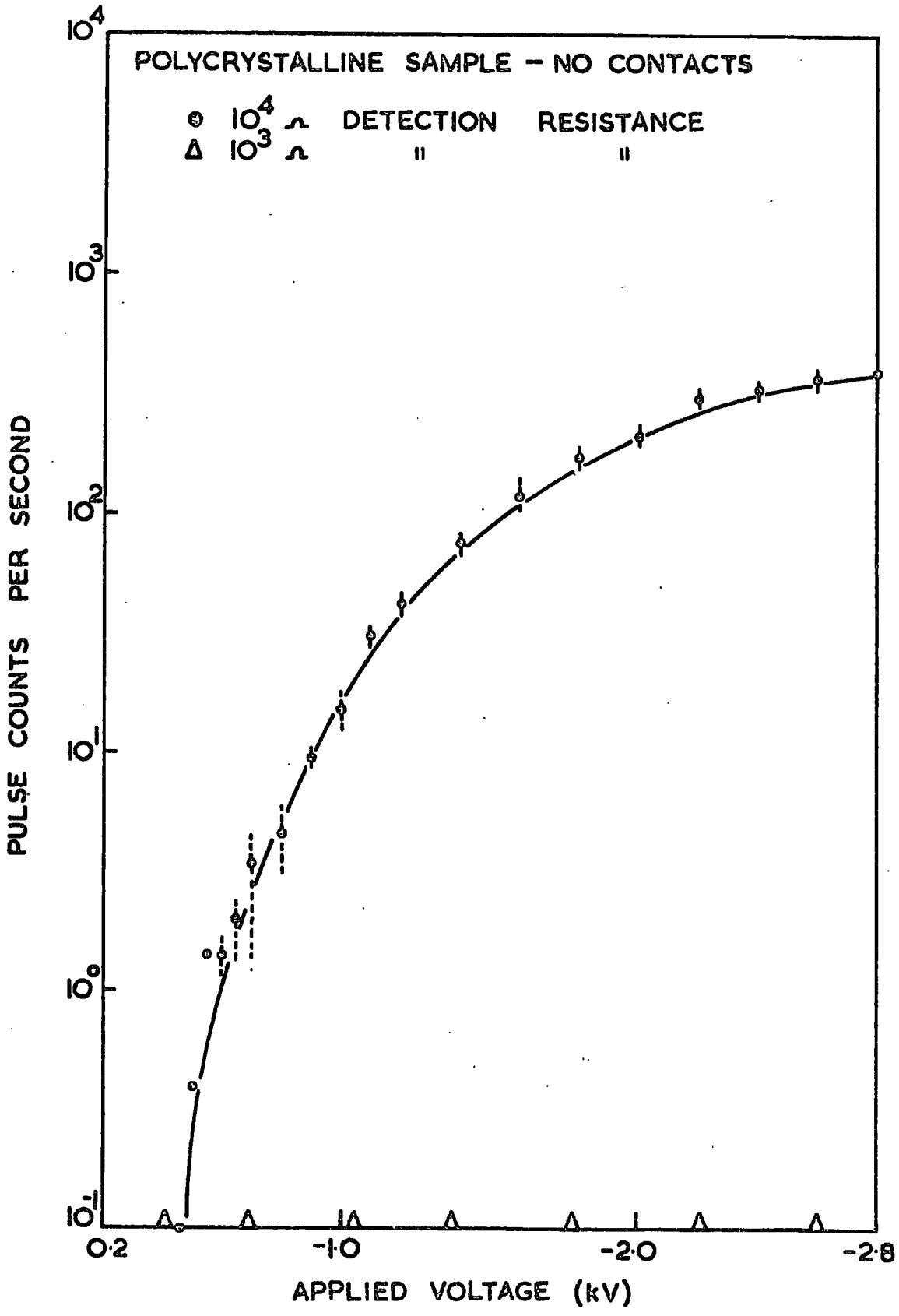

FIG. 6·3. PULSE COUNT RATE - ν - APPLIED VOLTAGE FOR SINTERED ALUMINA IN AN ATMOSPHERE OF NOMINALLY PURE ARGON AT 400 °C.

(i) The impurities in the furnace chamber before it is filled with the ambient gas. Since these are due to incomplete evacuation of the chamber the impurity pressure from this source may be put at 5×10^{-3} torr, the lowest pressure in the furnace chamber during evacuation.

(ii) The leakage of air into the chamber during filling with the ambient gas. The partial pressure of air in the furnace chamber from this source is estimated to be 0.03 torr for a leak rate of 8×10^{-4} torr litre per second (see Appendix B), the leak rate in the earlier pulse count measurements, and 0.01 torr for a leak rate of 3×10^{-4} torr litres per second, the leak rate in the later experiments.

(iii) The diffusion of air into the chamber after admission of the ambient gas. In the experiments where the time interval between filling of the chamber with the ambient gas and making the pulse count measurements is about 2 hours, the air pressure in the chamber from diffusion is estimated to be 4 torr and the pressure due to water vapour 0.1 torr (see Appendix C). Where measurements were made directly after the chamber has been filled the air and water vapour content of the ambient gas was very much less. By the end of the measurement, i.e. after 30 minutes diffusion, it is estimated that the air and water vapour pressure in the system from this source is 0.5 and 0.01 torr respectively (see Appendix C).

From the above the minimum impurities in the ambient gas can be estimated (for experiments where diffusion has been kept to a minimum). In the case of water impurities in the ambient gas, source (i) can be wholly attributed to vapour, source (ii) can be neglected, and a mean value for the water vapour from source (iii) can be put at 0.005 torr. Hence a value of approximately 0.01 torr can be put on the mean partial pressure of water vapour in the ambient gas for these pulse count measurements. In the case of air and oxygen impurities, sources (i) and (ii) can be neglected in comparison to source (iii). This allows mean values to be put on the air and oxygen pressures in the chamber of 0.25 and 0.05 torr, i.e. 20^{o}/o of 0.25 torr, respectively. These are believed to be the impurities in the argon for the previous experiment (results of Fig. 6.3) and for all subsequent experiments in which gas contamination has been minimized, i.e. in experiments in which the ambient gas is described as 'nominally pure'.

An experiment was conducted on one of the sintered samples to investigate the effects of the partial pressure of oxygen on count rate. The results for detection resistance of 10^3 and 10^4 ohms are shown in Figures 6.4 and 6.5 respectively. The pulse count rate is independent of the detection resistance for oxygen partial pressures above 1 torr. At lower partial pressures the pulse count curves obtained with the two detection resistances are significantly different. This shows that the height of the pulses is influenced by the oxygen impurities in the argon. As the

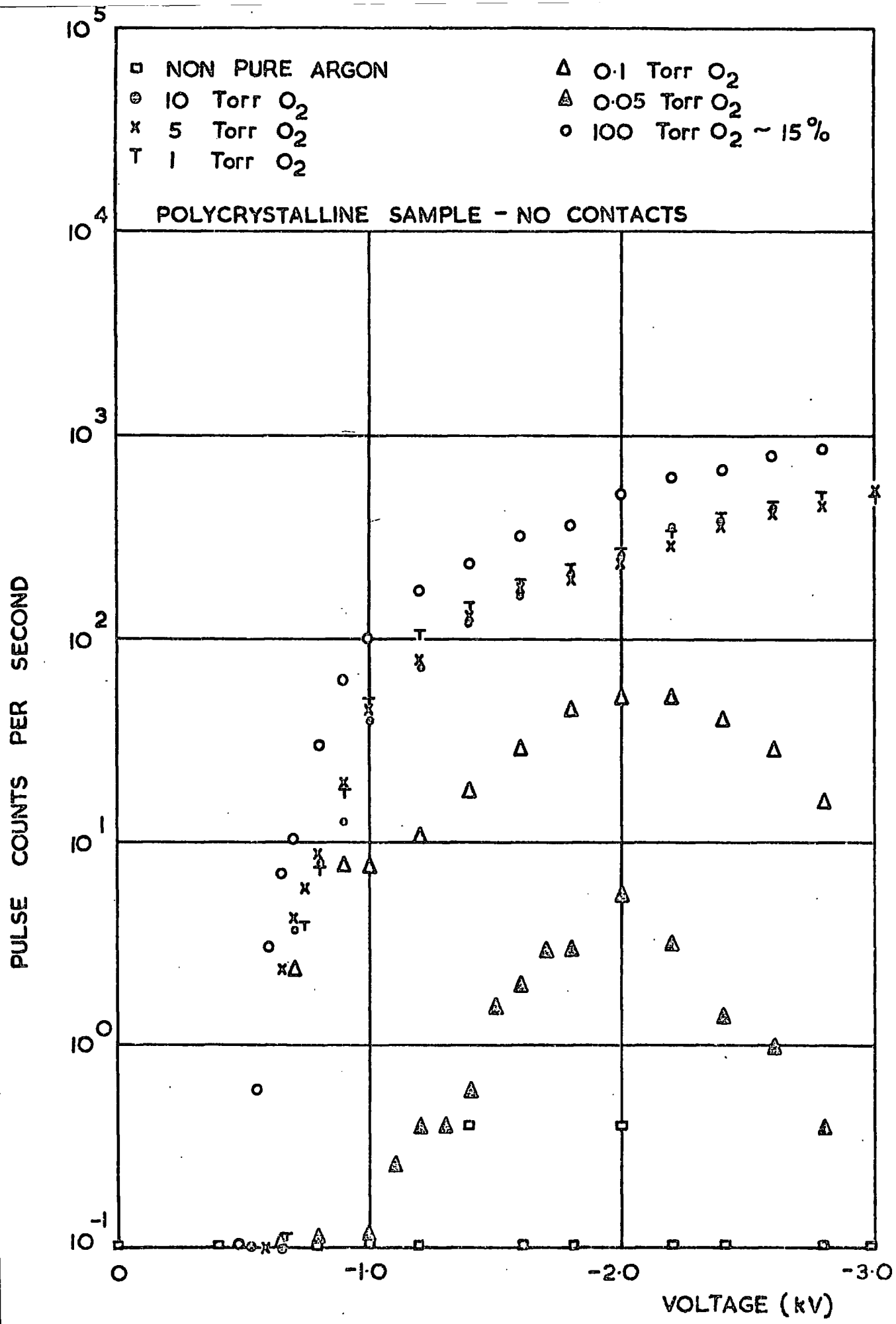

FIG. 6·4. EFFECT OF OXYGEN ON PULSE COUNT RATE OF POLYCRYSTALLINE ALUMINA IN AN ATMOSPHERE OF ARGON AT 400°C (10^3 DETECTION RESISTANCE)

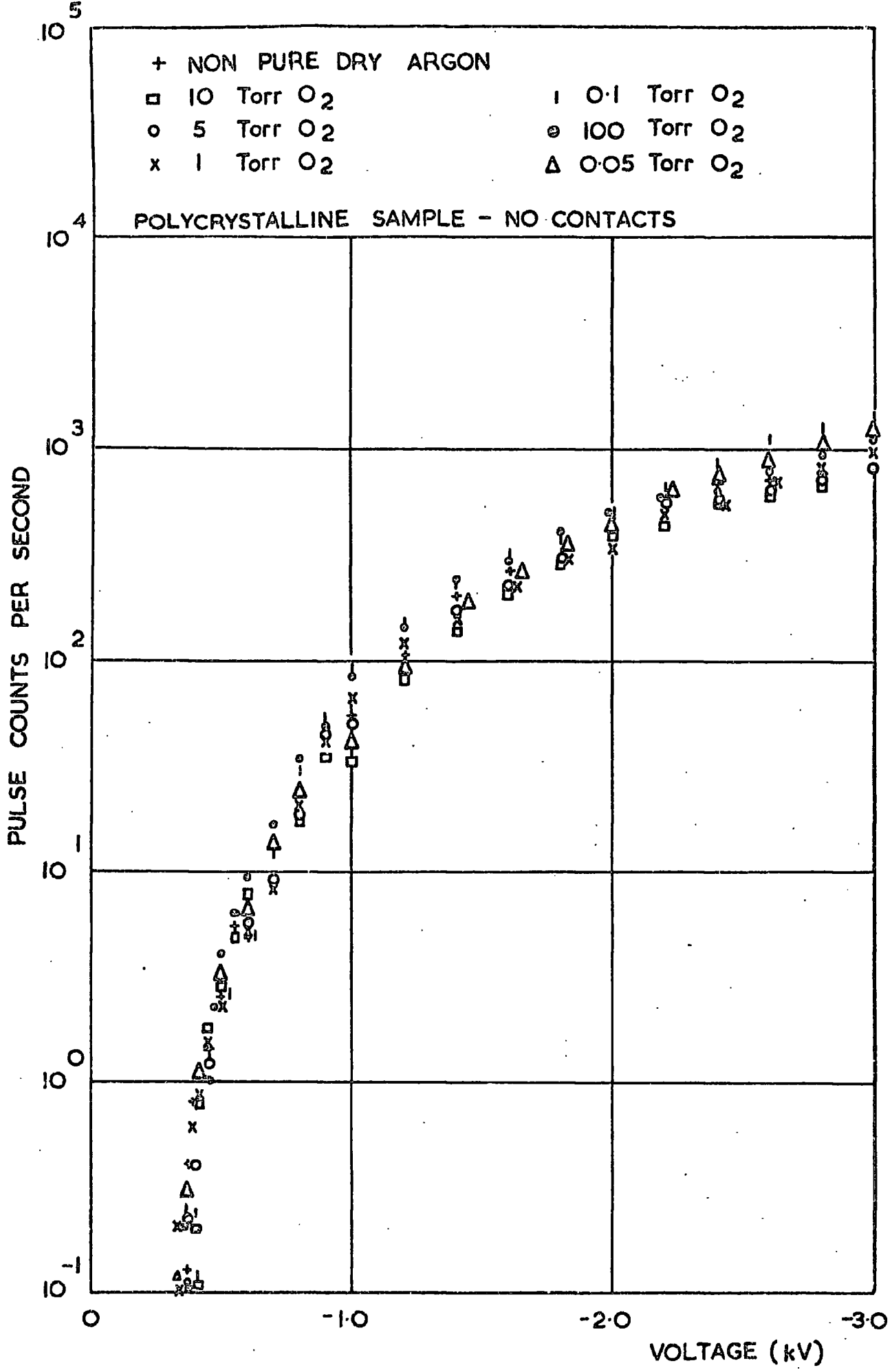

FIG. 6·5. EFFECT OF ADDING OXYGEN ON THE PULSE COUNT RATE OF SINTERED ALUMINA IN ARGON AT 400°C ($10^4\,\Omega$ DETECTION RESISTANCE)

oxygen pressure is increased an increasing proportion of the pulses appear above the 10^3 ohms detection level, i.e. 0.8 microamps, until at 1 torr most of the pulses are above this level. Hence oxygen impurities in argon affect the height of the pulses but do not significantly change the pulse count rate. The curves for pressures of 0.05 and 0.1 torr show maximas at about 2.0 kV, indicating a decrease in the pulse height above this voltage. A similar variation of pulse height with oxygen partial pressure was seen in qualitative measurements on a single crystal sample.

It was not possible to carry out similar experiments with the addition of water vapour because of difficulties in measuring the partial pressure. Instead the effect of rigorously drying the ambient gas was examined. Figure 6.6 shows the results of eight successive pulse count measurements. With the exception of measurements 6 and 8, the gas was dried by passing the argon through the molecular sieve at different flow rates. In curves 6 and 8, CO cold traps were used to dry the gas in addition to the molecular sieve. These results show that water vapour impurities in the argon have a similar effect on the pulse height as oxygen impurities.

The results presented in Figures 6.2-6.6 were all obtained on one sample. This will be called sample 2 to distinguish it from sample 1 which was used in obtaining the results of Figure 6.1. It would appear from the results so far given that on sample 2 successive measurements in any one experiment are quite reproducible even though

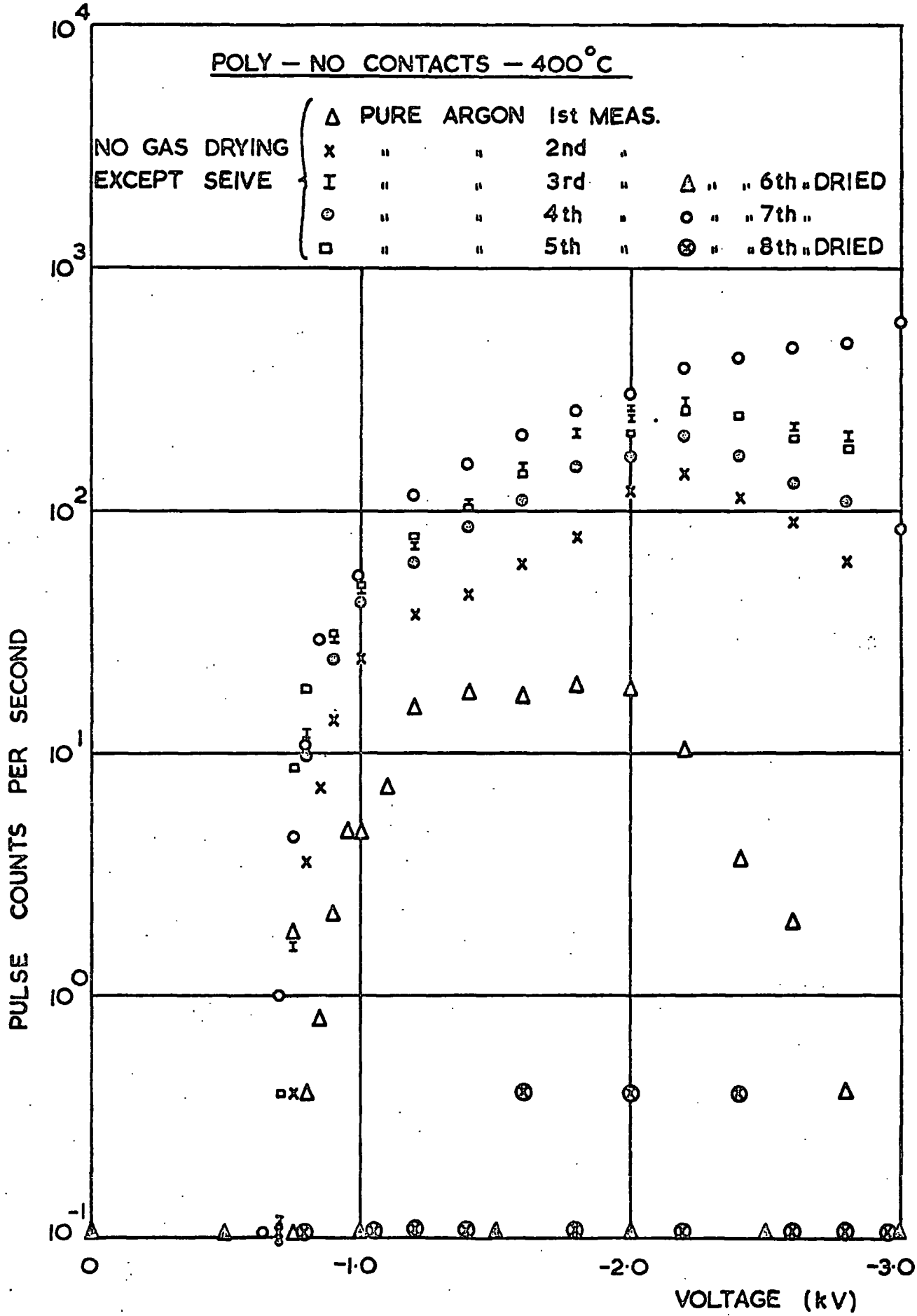

FIG. 6·6. EFFECT OF MOISTURE ON THE PULSE COUNT RATE OF POLYCRYSTALLINE ALUMINA IN AN ATMOSPHERE OF ARGON AT 400°C (10^3 Ω DETECTION RESISTANCE)

measurements in successive experiments are not. For example the pulse count rate in Figure 6.2 is about an order of magnitude greater than those shown in Figures 6.3, 6.4, 6.5 or 6.6. These latter were all obtained on the same heating cycle, i.e. the sample was not cooled to room temperature and cleaned between the experiments whose results are shown in Figures 6.3, 6.4, 6.5 and 6.6. This suggests that the difference between experiments is caused by removing the sample from the holder and cleaning it.

After the gas drying experiment the sample was cooled to room temperature and cleaned by the normal procedure. The sample was then reheated and three successive measurements made of the pulse count. The results of this experiment are shown in Figure 6.7. The gas drying and measurement technique were as used in the previous experiments, i.e. drying of the gas with CO_2 traps and molecular sieve, minimizing water impurities in the chamber with a cold finger, and making measurements within 30 mins of gas admittance. Although there is not the same spread in the onset voltage as in Figure 6.1 there is again a large difference in pulse count rate between successive measurements. This conclusion was confirmed by repeating the experiment with a slightly different cleaning procedure (see Fig. 6.8). Consequently reproducible results are not obtained on sample 2 even when the most stringent precautions are taken to purify the argon.

Upon re-examining Figure 6.1 it can be seen that measurements 2-5 would be in good agreement if there were less scatter in the onset voltage. Since this scatter is

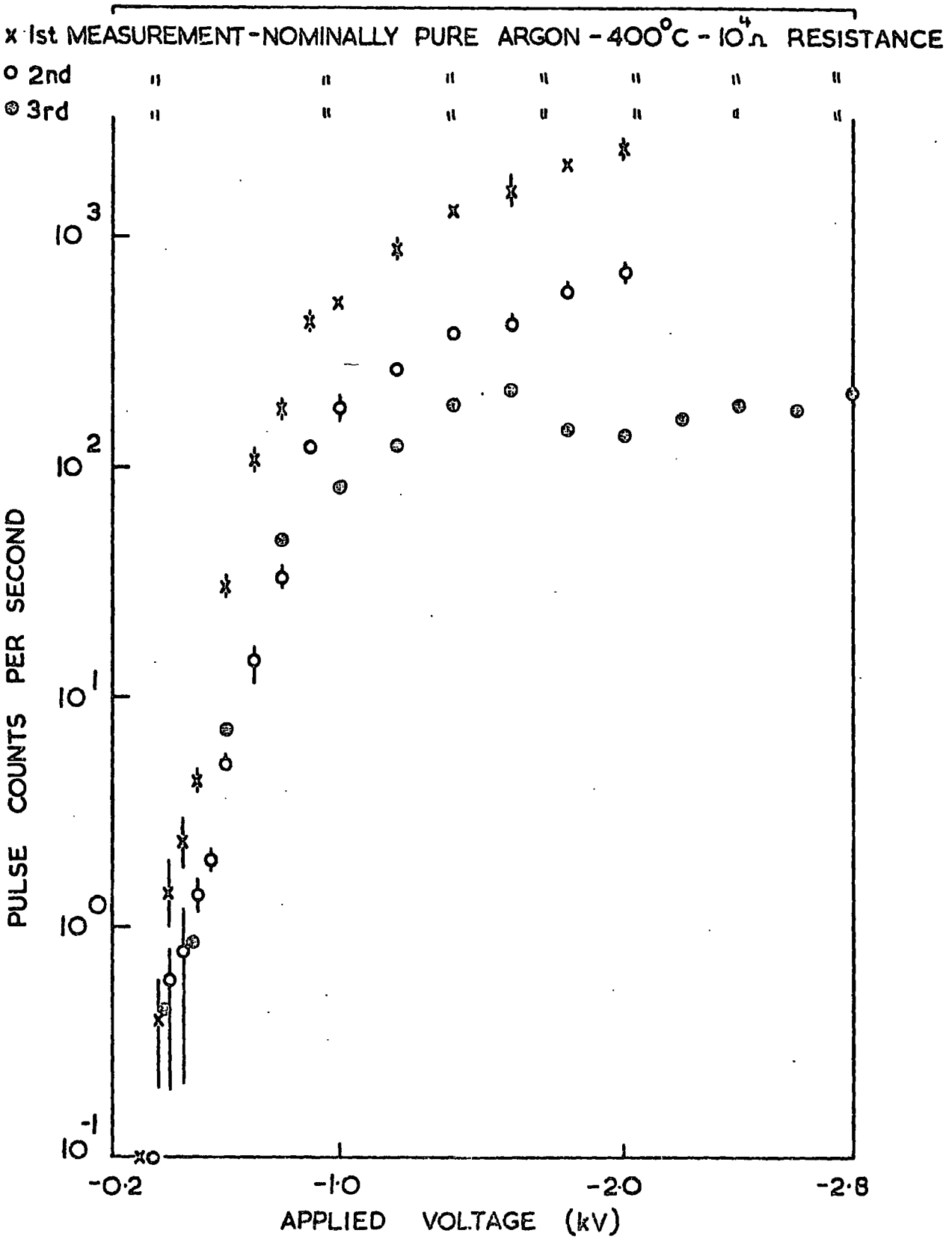

FIG. 6·7 VARIATION IN PULSE COUNT RATE BETWEEN SUCCESSIVE MEASUREMENTS ON A SINTERED SAMPLE CLEANED BY THE NORMAL PROCEEDURE.

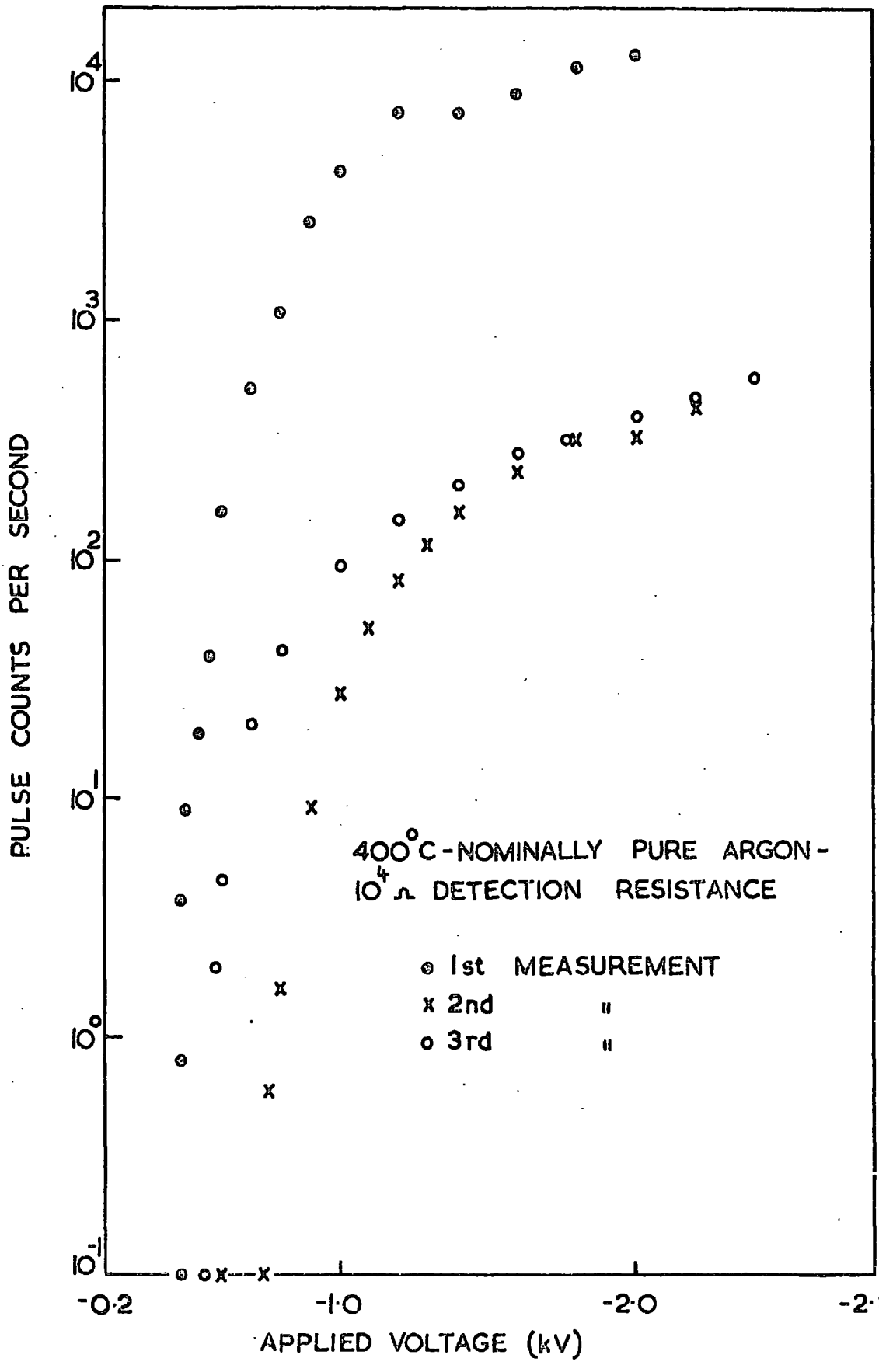

FIG. 6·8 VARIATION IN PULSE COUNT RATE BETWEEN SUCCESSIVE MEASUREMENTS ON A SINTERED SAMPLE WHICH HAD BEEN CONTAMINATED IN AQUA REGIA

not observed in other experiments it seems reasonable to attribute it to varying levels of water vapour in the argon (see Sec 6.3 for the effect of H_2O vapour on onset voltage). The main source of the scatter is now the anomalously high count rate of measurement 1. This also appears to be the case in Figure 6.7. These measurements are compared with four others, also obtained directly after cleaning, in Figure 6.9. Measurements 1, 2 and 3 were obtained on sample 1 and 4, 5 and 6 on sample 2. Apart from measurement 5, where the sample was boiled in Aqua Regia in addition to the normal cleaning, the samples were cleaned identically before each measurement. Thus it appears that measurements on these two samples directly after chemical cleaning by the normal procedure are in good agreement. It is interesting to see that measurements which are not made directly after cleaning, Figures 6.1, 6.3, 6.4, 6.5 and 6.6, are also in fairly good agreement.

In experiments in which measurements were made as the voltage across the sample was both raised and lowered the pulse count rate was observed to be higher immediately after cleaning of the sample. Figure 6.10 shows the results of pulse count measurements on a polycrystalline sample in argon containing a small quantity of air impurities, about 5 torr. From this it can be seen that the pulse count rate, in the first measurement after cleaning of the sample, is higher at voltages above 0.9 kV on raising the voltage than it is on lowering it. These measurements were repeated 8 hours later, the sample being maintained at

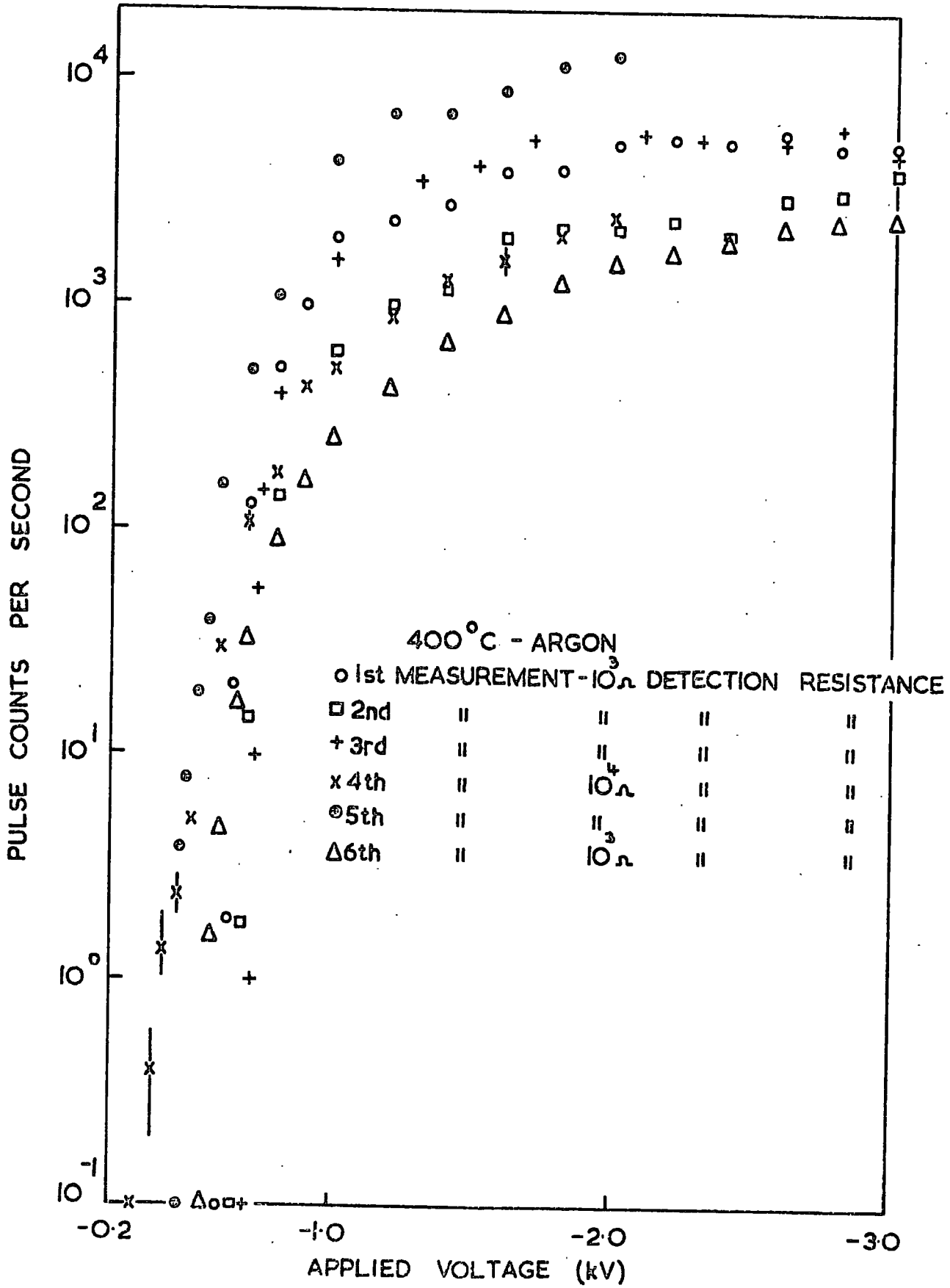

FIG. 6·9 VARIATION IN PULSE COUNT RATE BETWEEN MEASUREMENTS MADE DIRECTLY AFTER CLEANING OF THE SAMPLE.

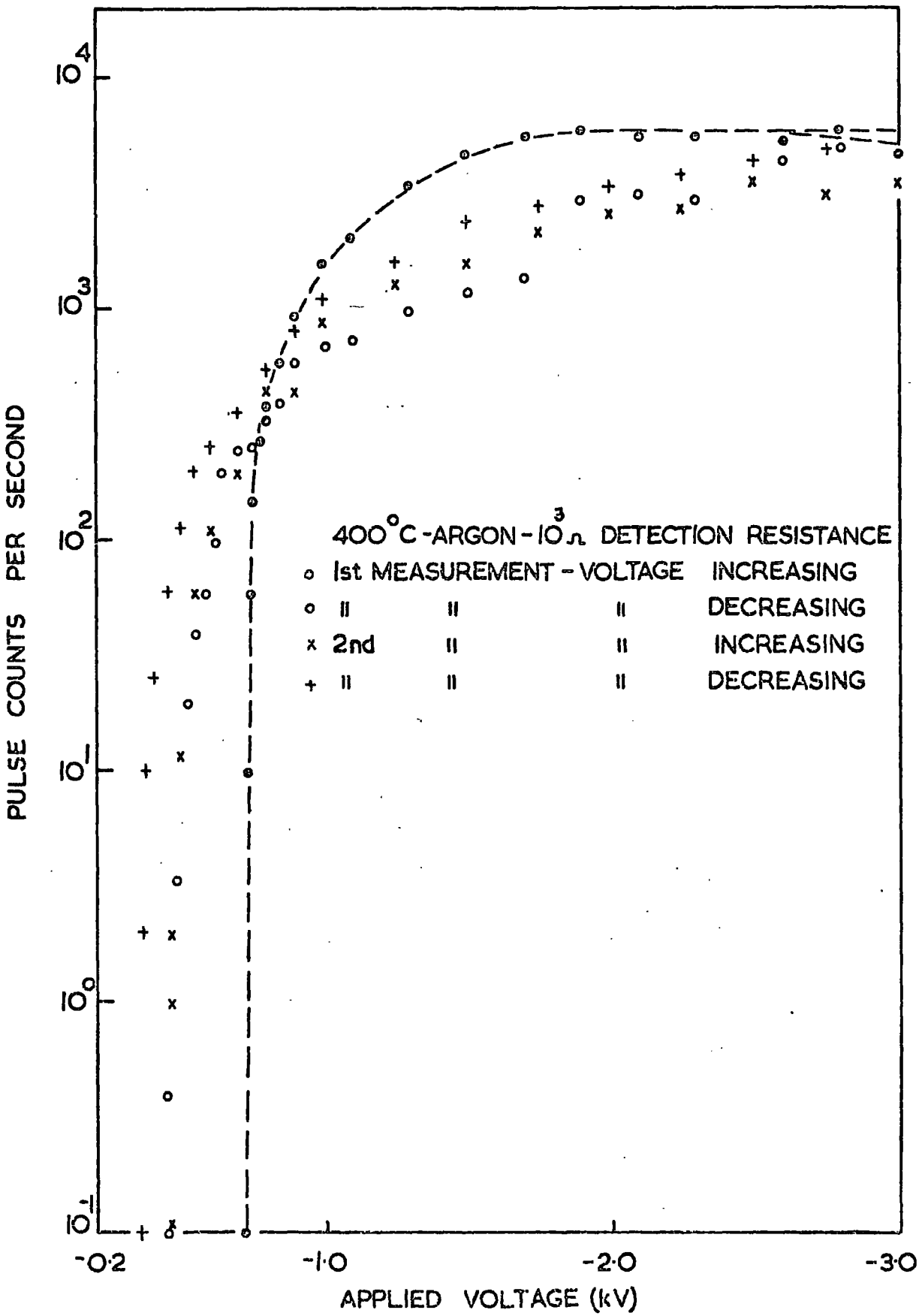

FIG. 6·10 VARIATION OF PULSE COUNT RATE OF SINTERED ALUMINA WITH INCREASING AND DECREASING VOLTAGE.

400°C during the time interval. On remeasurement the pulse count rate above 0.9 kV was not found to be significantly affected by raising or lowering the voltage. In both these measurements it can be seen that the voltage at which the pulses appear as the voltage is raised, termed the onset voltage, is different to that at which they disappear as the voltage is lowered, termed the offset voltage. This phenomenom was observed in all experiments in which the voltage was raised and lowered. Although the onset voltage in Figure 6.10 was greater than the offset voltage this was not found to be the case in all experiments. In several experiments, for example, offset voltages 100°/o greater than onset voltages were recorded. Unfortunately this difference in the two voltages could not be related to purity of the ambient gas or condition of the specimen surface.

The reproducibility studies on these two samples show that the pulse count measurements depend upon the current sensitivity of the detector and the purity of the ambient gas. This is well illustrated on one of the samples for different oxygen partial pressures. However for partial pressures above 1 torr the pulse count rate can be regarded as independent of both air impurities and detection resistance. It is estimated by the method outlined in Appendix C that the partial pressure of air in the experiments of Figures 6.1 and 6.2 was about 4 torr. Consequently variations in the air content about this level are unlikely to cause the observed scatter.

Water impurities in the argon also affect the count rate, as probably do other molecular vapours if present in the small quantities found in B.O.C. cylinders (about 50 p.p.m. [McMinn, Private Communication]). The effect of higher concentrations of H_2O such as might be found in the chamber after two hours diffusion (0.1 torr) on the pulse count are unknown. If pulse breakdown is extremely sensitive to water as an impurity inadequate control might well cause the scatter between measurements observed in Figures 6.1 and 6.7. However the absence of scatter in Figures 6.2 and 6.5 is then slightly surprising, since there is no reason to suppose the control of the water vapour is any better in these experiments than in later ones.

Measurements directly after cleaning of the samples appear to show a higher count rate than measurements which are not made directly after cleaning. This suggests that the pulse count rate is affected by the chemical treatment of the sample. The measurements directly after cleaning are in reasonably good agreement, showing that the position of the sample in the sample holder is not a major source of non-reproducibility between experiments. This is important if the discharges are localised at the electrodes since the pulse count rate may depend on the surface topography in a localised region around the electrodes. Changes in position of the sample as a result of cleaning might then have been a source of non-reproducibility. The results show that an order of magnitude spread in count rate can be expected in measurements on these samples at 400°C. Therefore only parameters which caused major changes in pulse

activity would be observed in pulse count measurements.

6.3 The Effect of Gas Impurities on the Onset Voltage

The variation of onset voltage with partial pressure of oxygen and air in an atmosphere of argon at 400°C is shown in Figure 6.11. The argon used in this experiment was nominally pure with an estimated residual impurity content of 0.05 torr air and 0.01 torr H_2O. The detection resistor used in this experiment was 10^4 ohms and, with a discriminator level of 2.5 volts, the minimum current sensitivity was 1.8 10^{-8} amps. Both the oxygen and the air were dried with liquid nitrogen traps before being admitted to the furnace. The results show that the voltage at which the onset of pulse breakdown occurs depends on the type of ambient gas. The onset voltages, in this experiment, were -350 v, -560 v and -750 v for argon, air and oxygen respectively. The results also show that the onset voltage in argon is relatively unaffected by large percentages of oxygen or air impurities. For example the onset voltage in a 660 torr A - 100 torr Air mixture is only 18°/o greater than the onset voltage in nominally pure argon. Since even the most impure argon used in this work is unlikely to contain 16.5°/o air, the variation of the onset voltage observed in early pulse count measurements, see for example Figure 6.1, would not appear to be due to oxygen or air impurities in the argon.

Although no quantitative study has been made of the effects of water vapour on the onset voltage of pulse breakdown in argon a qualitative examination has been made. An

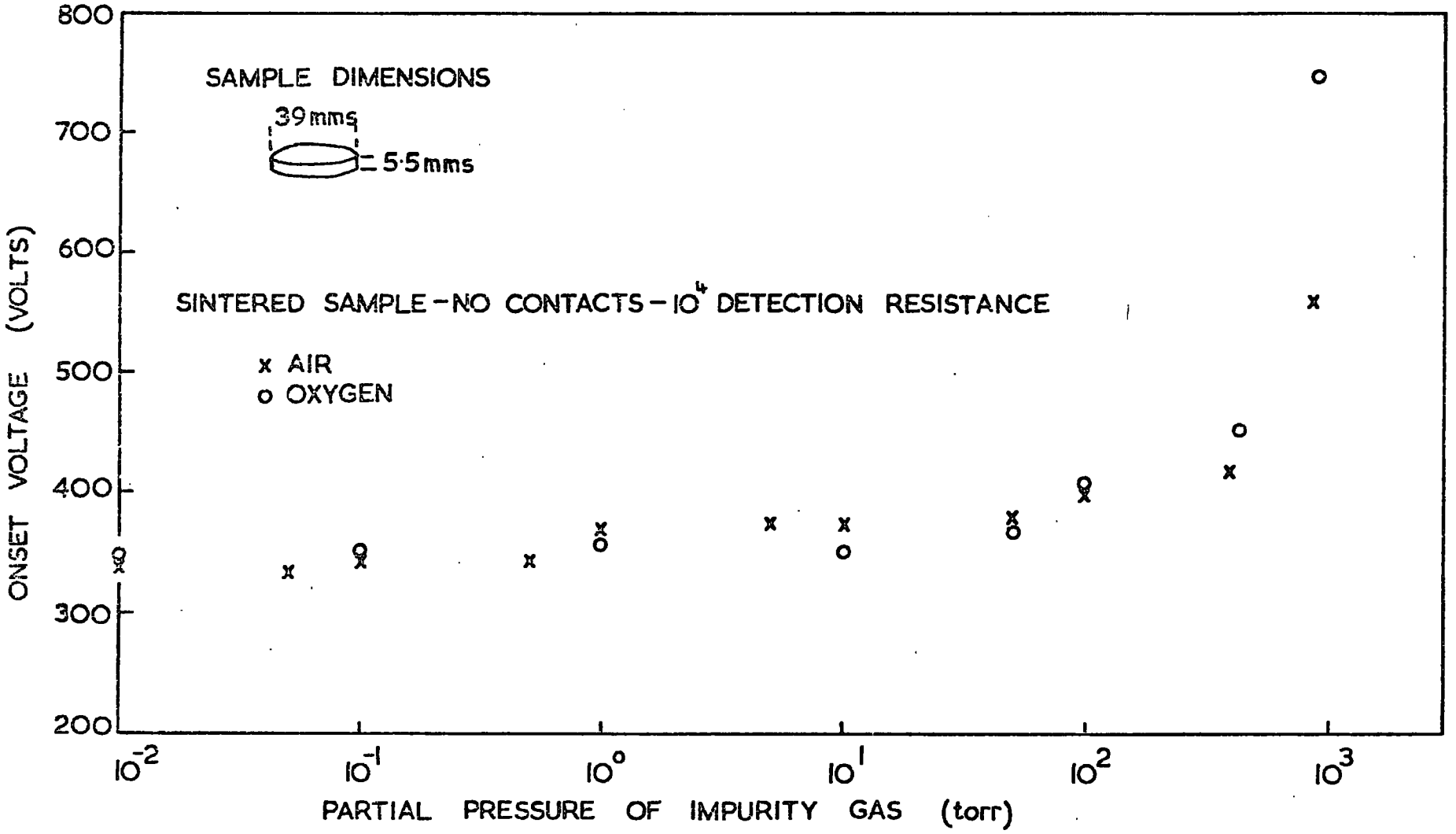

FIG. 6·11 EFFECT OF GAS IMPURITIES ON THE ONSET VOLTAGE OF PULSE BREAKDOWN IN NOMINALLY PURE ARGON AT 400°C.

initial measurement of the onset voltage on a 3.0 cm diameter sample gave a value of -700 volts for the onset voltage in dry argon. After evacuating and refilling the furnace chamber with an atmosphere of water-saturated argon the onset voltage was found to have dropped to -340 volts. The chamber was then evacuated to 10^{-2} torr and filled once again with dry argon. However the onset voltage on this occasion remained at -340 volts. During the next 24 hours the furnace was periodically evacuated and filled with dry argon. At the end of this time the onset voltage was found to have recovered to -650 volts.

The results of this experiment show that the onset voltage of pulse breakdown in argon is lowered by water vapour. They also show that the same onset voltage may be obtained in dry and wet argon ambients if the water-saturated argon has been introduced before the dry argon. This implies that the introduction of water vapour into the system does more than lower the breakdown strength of the gas. Consequently the variation of onset voltage between measurements is probably due to water vapour.

6.4 Pulse Height Distribution

A limited number of pulse height distributions (see Sec 4.6.1 for the experimental details) were taken during pulse count measurements. Most of these were recorded during the pulse count experiments reported in Section 6.2. The results of these measurements show that in most cases the pulse height distributions are linear, which is

consistent with gas discharges. In several measurements made at higher applied fields the distributions are distorted. This is thought to be due to two different pulse sources. The distributions are not sufficiently well resolved, the voltage increments used being too large, for detailed variations in the shape to be observed. This is unfortunate because it means that interesting second order effects, such as space charge distortion, cannot be detected. In view of this it must be realised that the double pulse source explanation of the distorted distributions is slightly speculative.

The pulse count rates for a sintered polycrystalline sample in nominally pure argon after different cleaning procedures have already been shown in Figures 6.7 and 6.8. Both these graphs show similar results, a high count immediately after cleaning and a lower one subsequently. Pulse height distributions were made in these experiments at various fixed voltages and the results are shown in Figures 6.12-6.15. The distributions for the first, second and third measurements of Figure 6.7 are given in Figures 6.12, 6.13a and 6.13b respectively. Similarly the distributions shown in Figures 6.14, 6.15a and 6.15b correspond to measurements 1, 2 and 3 in Figure 6.8. The pulse height distributions show that a linear relation exists between log ΔN and the pulse height at voltages up to 1.2 kV. The only exception to this rule is the 1.2 kV and 2.0 kV plots of Figure 6.12.

The same basic distribution of pulse height has been observed in experiments on single crystals. Figure 6.16 shows a pulse height distribution obtained on a 2.0 cm

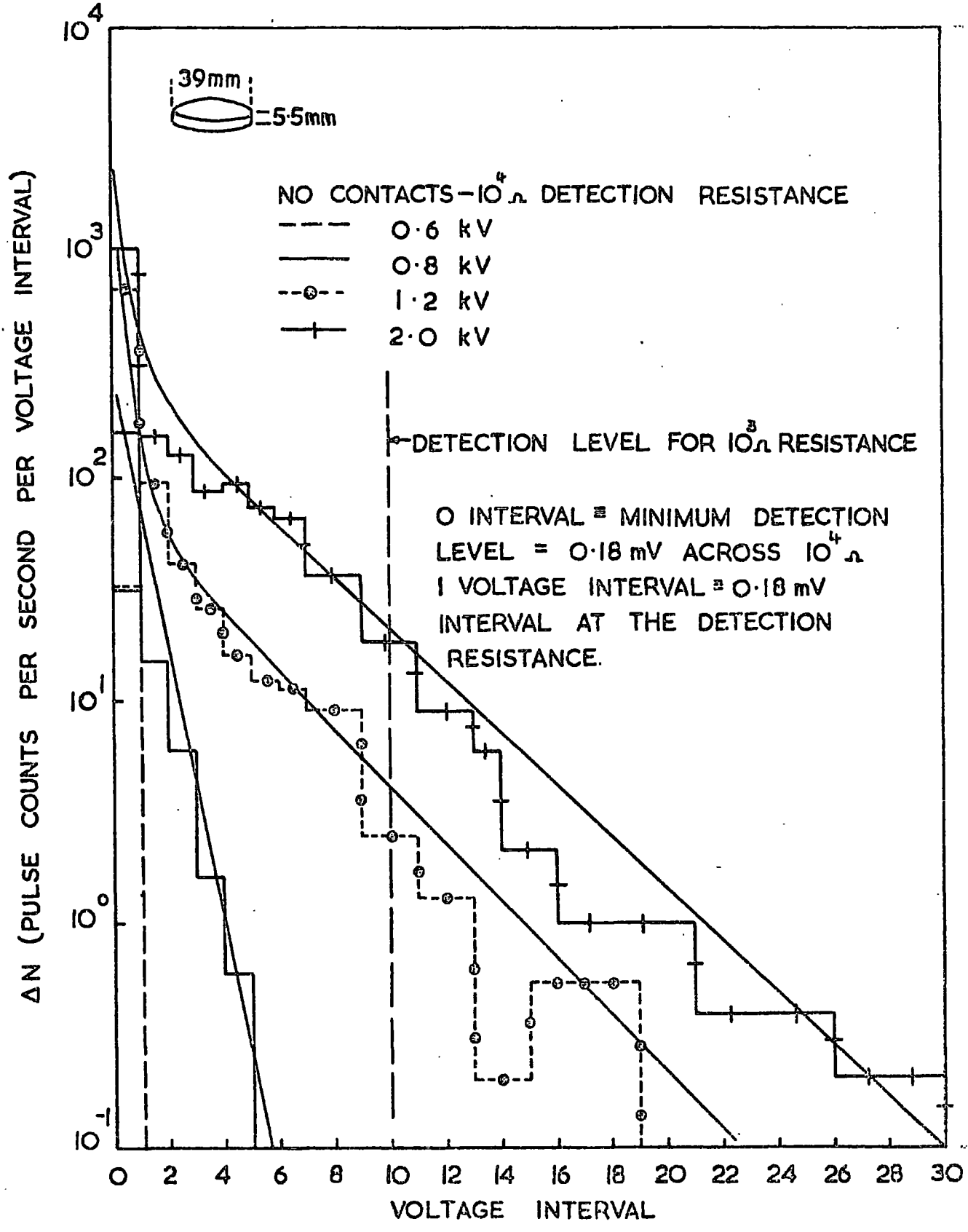

FIG. 6·12 PULSE HEIGHT DISTRIBUTION FOR SINTERED SAMPLE IN NOMINALLY PURE ARGON AT 400°C.

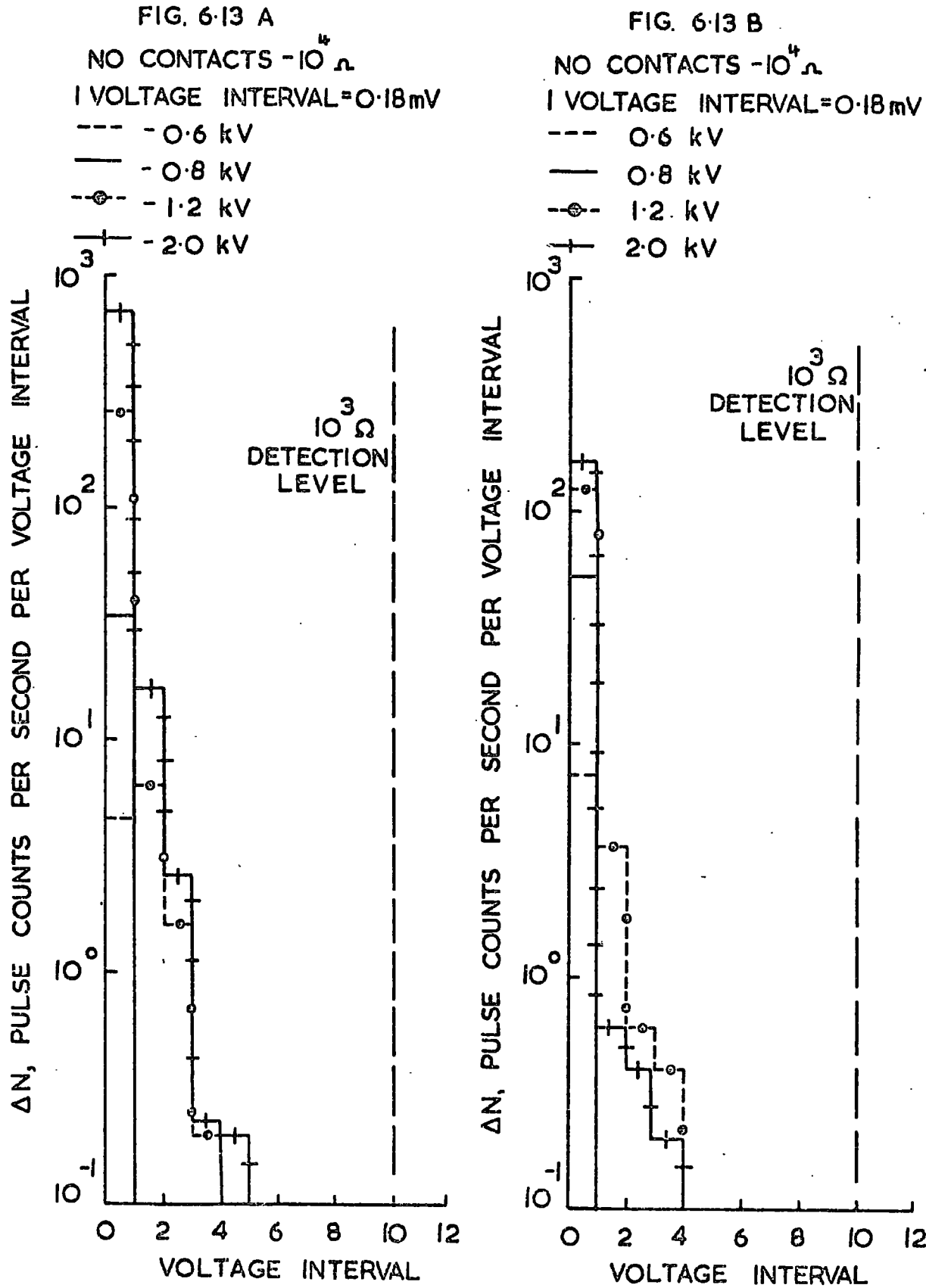

FIG. 6·13 PULSE HEIGHT DISTRIBUTIONS FOR SINTERED SAMPLE IN NOMINALLY PURE ARGON AT 400°C

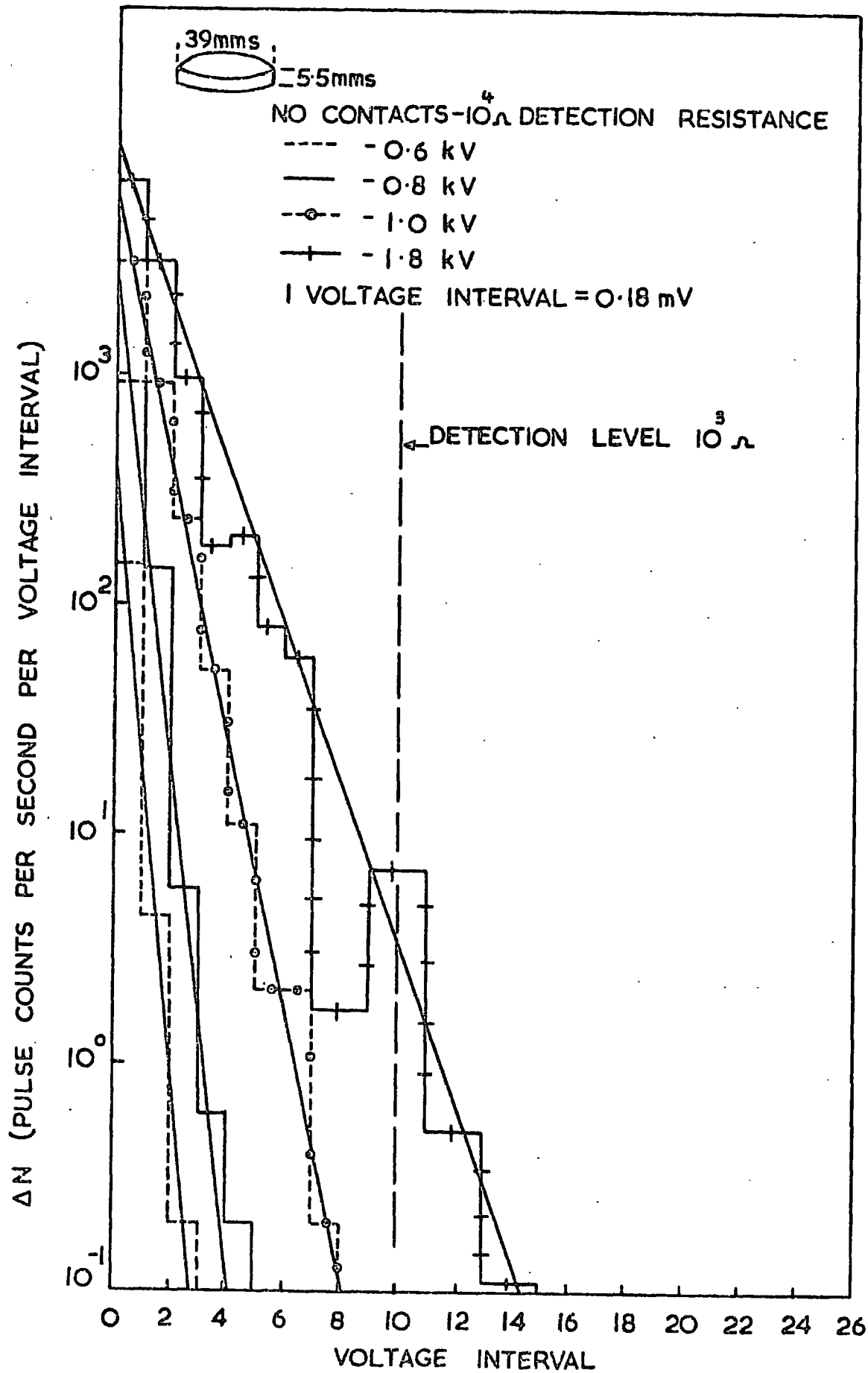

FIG. 6·14 PULSE HEIGHT DISTRIBUTION FOR SINTERED SAMPLE IN NOMINALLY PURE ARGON AT 400°C.

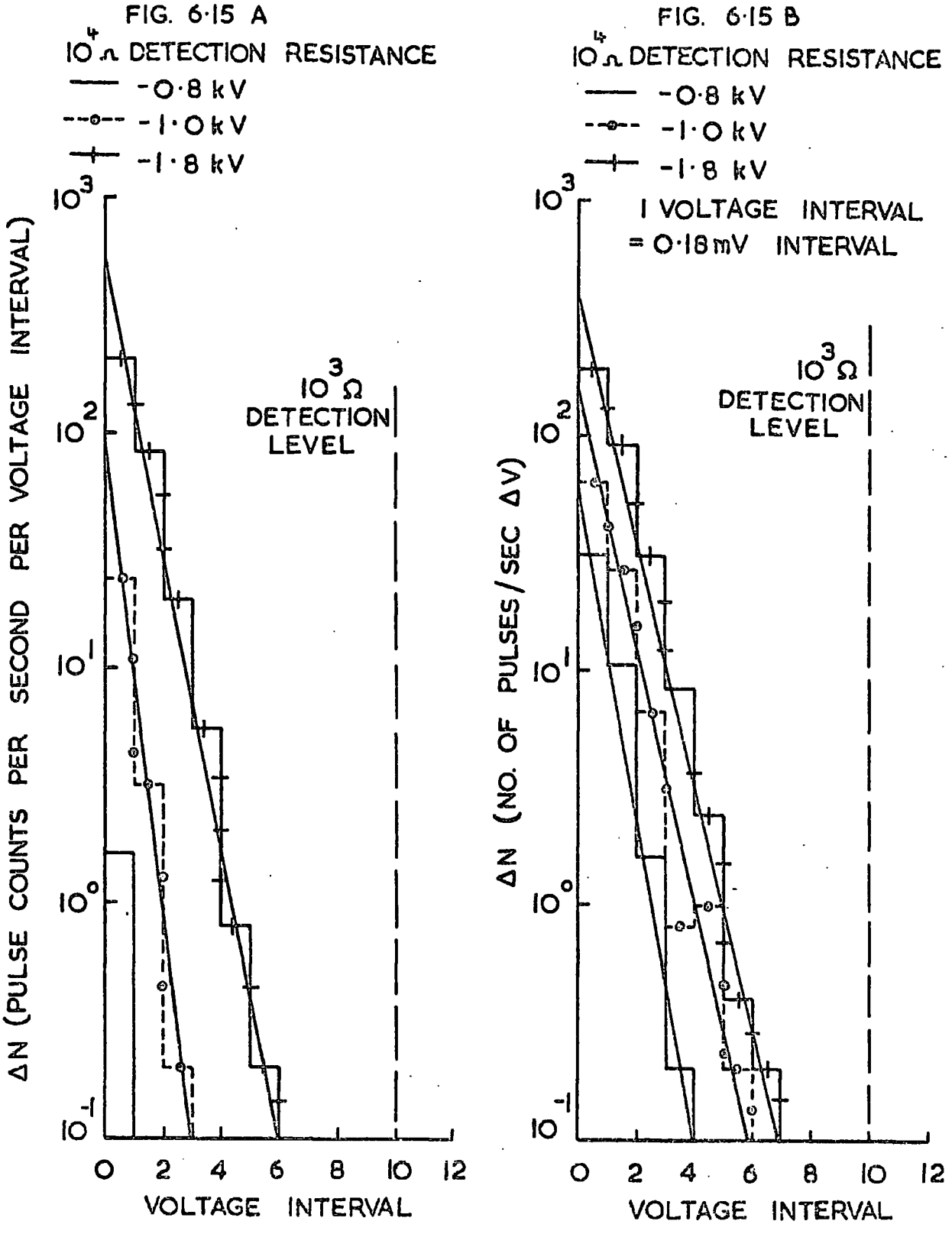

FIG. 6·15 PULSE HEIGHT DISTRIBUTION FOR SINTERED SAMPLE IN NOMINALLY PURE ARGON AT 400°C

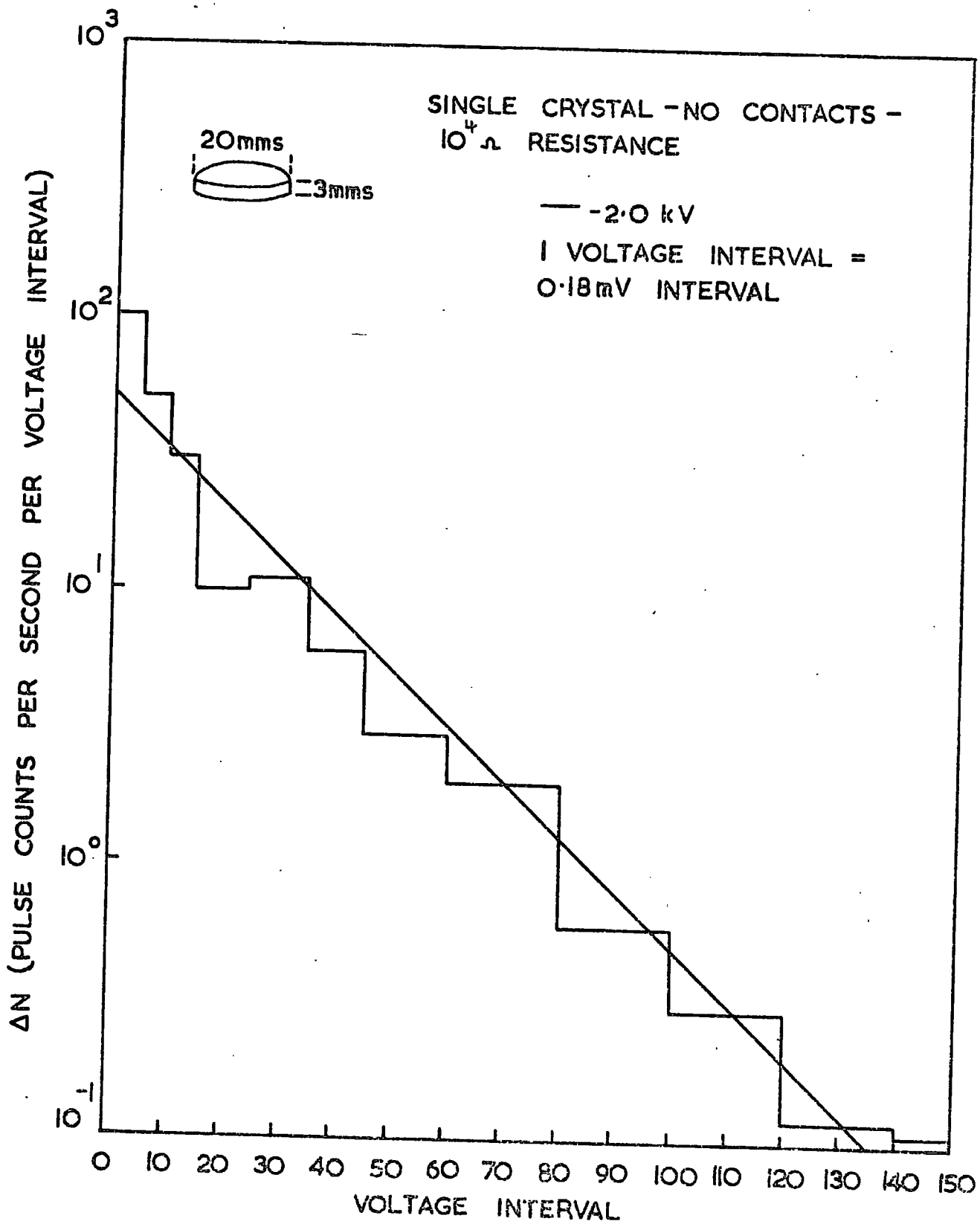

FIG. 6·16 PULSE HEIGHT DISTRIBUTION FOR SINGLE CRYSTAL SAMPLE IN NOMINALLY PURE ARGON AT 400°C

diameter single crystal in an atmosphere of nominally pure argon at 400°C. The slope of this distribution is very different to those obtained on sintered polycrystalline samples because of the very much larger size of the mean pulse charge. However although the slope of the distribution is different its basic shape is the same, i.e. the pulse height distribution is linear.

At higher voltages the pulse height distributions are often distorted by the presence of large pulses. In these cases the interpretation of the results are difficult because of the lack of reproducibility. As expected from pulse count measurements there is a large difference between the distributions recorded directly after cleaning of the sample and subsequent ones. The latter, i.e. results in Figures 6.13 and 6.15, all show similar distributions. Unfortunately there is also a difference between the two measurements directly after cleaning, i.e. Figures 6.12 and 6.14.

A distribution obtained in impure argon, i.e. impurity concentrations in the order of those calculated in Appendix C for 2 hours diffusion, directly after cleaning of the sample is shown in Figure 6.17. Although this was recorded with a detection resistance of 10^3 ohms it can be seen that the slopes of the pulse height distributions at each voltage are similar to those shown in Figure 6.14. This suggests that the difference between Figures 6.12 and 6.14 could be due to different impurities concentration in the argon.

In argon two distinct pulse shapes are observed which are characterised by their risetimes (see Sec.6.5). These

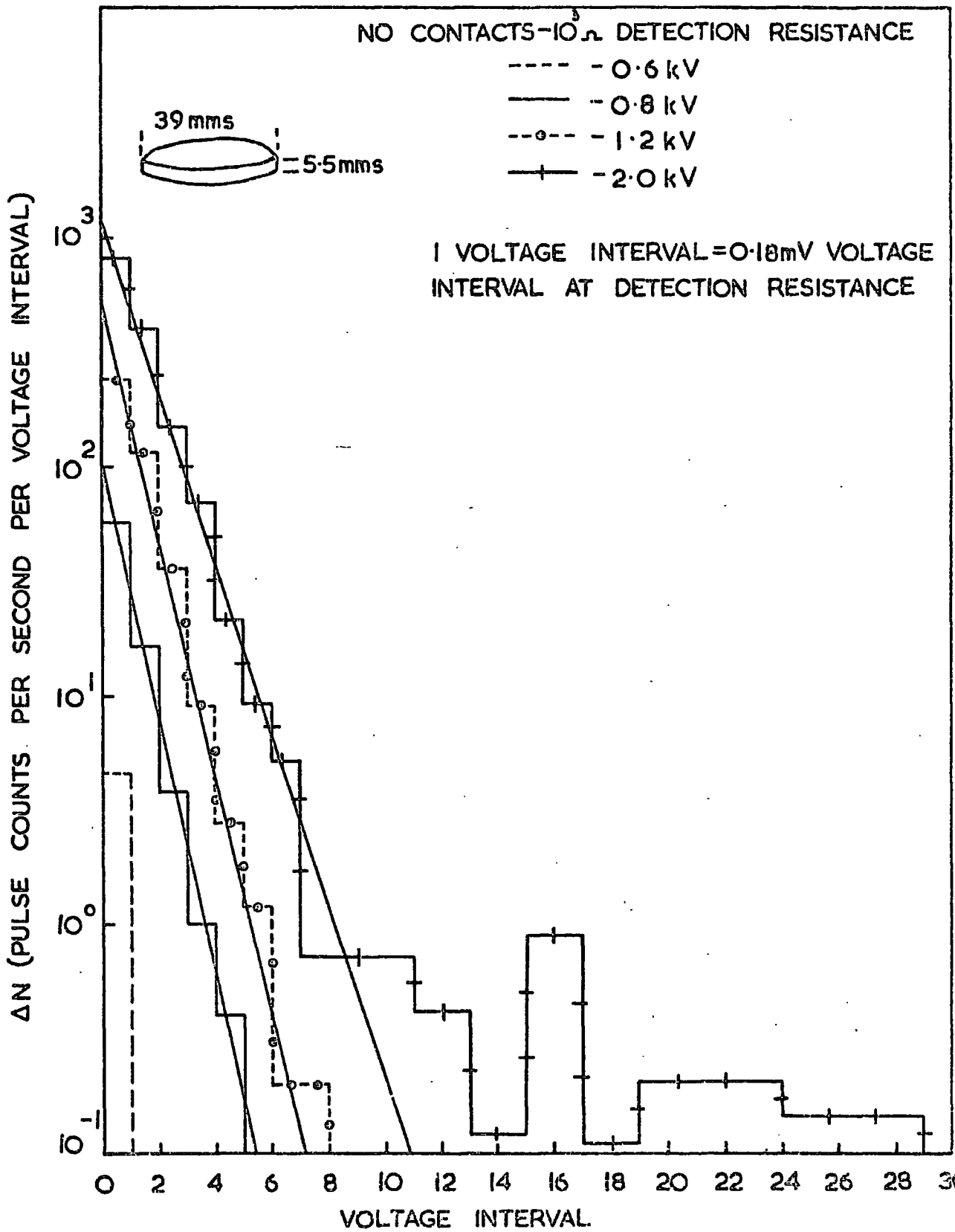

FIG. 6·17 PULSE HEIGHT DISTRIBUTION FOR SINTERED SAMPLE IN AIR CONTAMINATED ARGON AT 400°C.

two pulses appear at different applied voltages. The faster of the two pulses appears at voltages of approximately 1.2 kV and has a risetime which is limited by the detection circuit. Therefore the pulse charge, as measured from oscillograms, is proportional to the height of the impulse since the impulse equation is given by 2.1. Consequently, by measuring the pulse height and charge from oscillograms, the constant of proportionality can be found and the relation between pulse height and number of charge carriers per pulse, n, determined.

The shape of the larger pulse cannot be related to the equivalent circuit of the sample in this simple way as both the risetime of the pulse and decay are long compared with those expected for an instantaneous discharge. Hence the relation between the pulse height and the pulse charge is governed by the shape of the pulse. As a result the relationship between pulse height and charge is determined experimentally at each applied voltage directly from the oscillograms. It is found however that the pulse height is approximately proportional to the pulse charge. Hence the number of charge carriers per pulse is also proportional to the pulse height.

The pulse height distributions are consistent with discharges entirely in the ambient gas as studied extensively elsewhere (Wijsman,[19] Legler,[20] Davidson[21]). In gas discharges statistical fluctuations occur in the ionization process. These fluctuations, which produce a distribution in the size of the individual avalanches, may be observed if

n the number of primary electrons is small and the number of multiple avalanches are not too large. Under these conditions, statistical considerations show that a plot of log ΔN against n, the carrier number per avalanche, should be linear of slope $1/\bar{n}$, where $\bar{n}$ is the mean number of carriers per avalanche. ΔN is the number of avalanches with a carrier number between n and $n + \Delta n$, where Δn is the interval between the number of carriers. Consequently values of the mean carrier number can be calculated from the pulse height distribution if the relation between the pulse height and the carrier number is known.

The values obtained for the mean carrier number from the slopes of the pulse height distributions shown in Figures 6.12, 6.13, 6.14 and 6.15 are given in Table 6.1. Although the experimental error is large some definite conclusions can be drawn from these results. Firstly it can be seen that there is no significant increase in the mean carrier number above approximately 1.0 kV. This implies that the pulse charge is effectively independent of voltage. Secondly there is no significant difference in the carrier number between measurements directly after cleaning the sample and subsequent ones. Hence there must be a genuine difference in the pulse count rate between these measurements. Thirdly below approximately 1.0 kV the mean carrier number increases with increasing voltage.

TABLE 6.1

MEAN CARRIER NUMBER CALCULATED FROM PULSE HEIGHT DISTRIBUTIONS

APPLIED VOLTAGE	FIG. 6.12	FIG. 6.13a	FIG. 6.13b	FIG. 6.14	FIG. 6.15a	FIG. 6.15b
-600 volts	-	-	-	2.3×10^5	-	-
-800 "	2.5×10^5	-	-	6.2×10^5	-	1.4×10^6
-1000 "	-	-	-	7.8×10^5	1.4×10^6	1.1×10^6
-1200 "	9.4×10^5	4.8×10^5	8.3×10^5	-	-	-
-1800 "	-	-	-	7.6×10^5	1.0×10^6	1.1×10^6
-2000 "	9.2×10^5	3.0×10^5	1.0×10^6	-	-	-

6.5 The Shape of the Detected Impulse

6.5.1 Introduction

Three distinct pulse shapes have been observed at different times in experiments on the same sample in nominally pure argon. However of the three types of pulse not more than two have been seen in any single experiment. One of these pulses, designated Type 3, was only present in one experiment and has not been reproduced. This pulse, an example of which is given in Figure 8.5, appears to be a combination of the other two pulse types. Because of this and also because the pulse has not been reproduced, the results of this experiment will not be presented. In any case they do not differ significantly from the other results. Of the other two pulses, Type 2 has been observed in all experiments and Type 1 in most. The Type 2 pulse appears at lower voltages than the Type 1 pulse. This makes it possible to distinguish between the pulses at the lower voltages. At higher voltages however this is more difficult with the present experimental arrangement. Consequently the pulse shape measurements have been concentrated in the lower voltage range.

6.5.2. Type 1 Pulse

It has not been possible to resolve the Type 1 pulse with the present detection system, i.e. the rise and decay time of the pulse are faster than the detector. Because of this the shape of the detected impulse depends on the

detection impedance. Examples of the detected impulses are shown in Figure 6.18. The shape of these impulses are consistent with equation 2.1.

In experiments on sintered polycrystalline samples, the size and frequency of the pulse varied from one measurement to the next. For example, in one measurement, directly after chemical cleaning, the Type 1 pulse predominated only above 1.2 kV in contrast to the succeeding measurements. The effect of this on the pulse height distribution can be seen by comparing Figure 6.12 with Figure 6.13. At high voltages, that is slightly below spark breakdown, multiples of the Type 1 pulse were sometimes observed in a single oscillogram, an example of which is given in Figure 6.18. It has not been possible to make a quantitative study of the Type 1 pulse variation with applied voltage because of the presence of the Type 2 pulse. However oscillogram measurements indicate that both the charge and the height of the pulse increase with the applied voltage, see Figure 6.19.

The Type 1 pulse was not always seen in experiments on single crystals. For example in experiments where the pulse activity of single crystals was examined as a function of temperature (Sec 6.7.2) the Type 1 pulse was only observed on the 1.6 and 2.5 cm diameter samples, no pulses being observed on the 2.0 cm diameter sample. The size of the pulse on single crystals was generally found to be small, $< 4 \times 10^{-14}$ coulombs, and the minimum voltage at which they could be detected was not normally less than 2.0 kV. In contrast to sintered samples, multiples of the Type 1 pulse

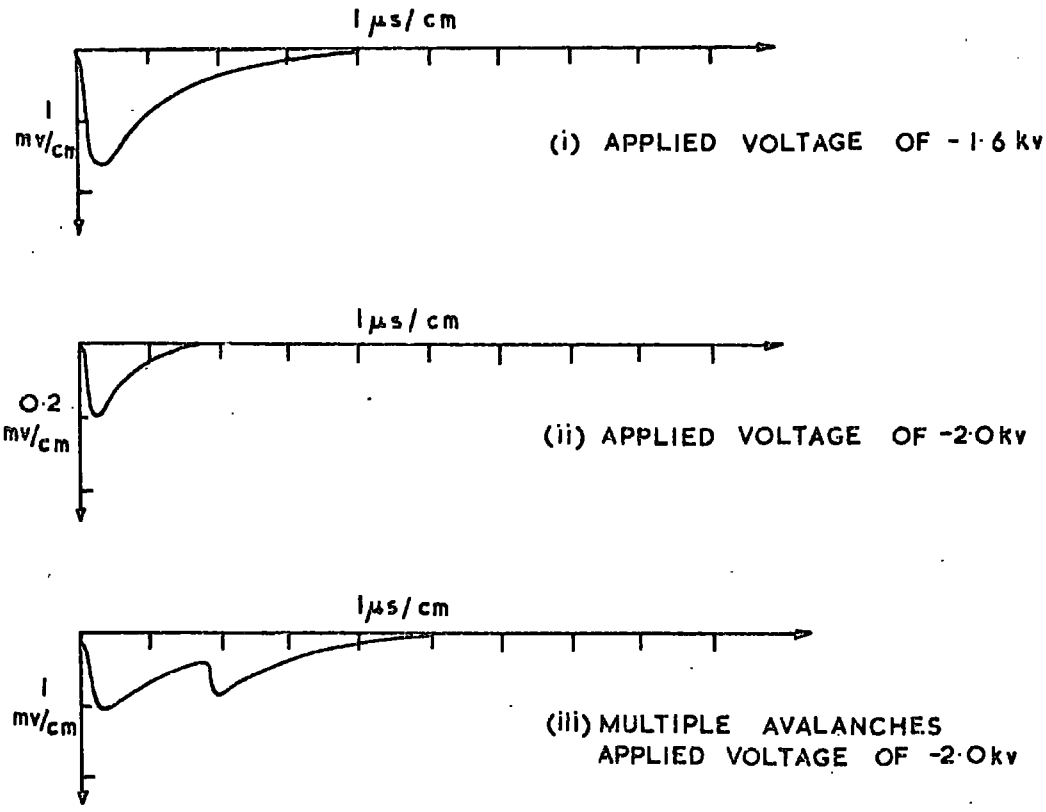

A. TYPICAL TYPE 1 PULSES (i) SINTERED POLYCRYSTALLINE (ii) SINGLE CRYSTAL ALUMINA
a(iii)

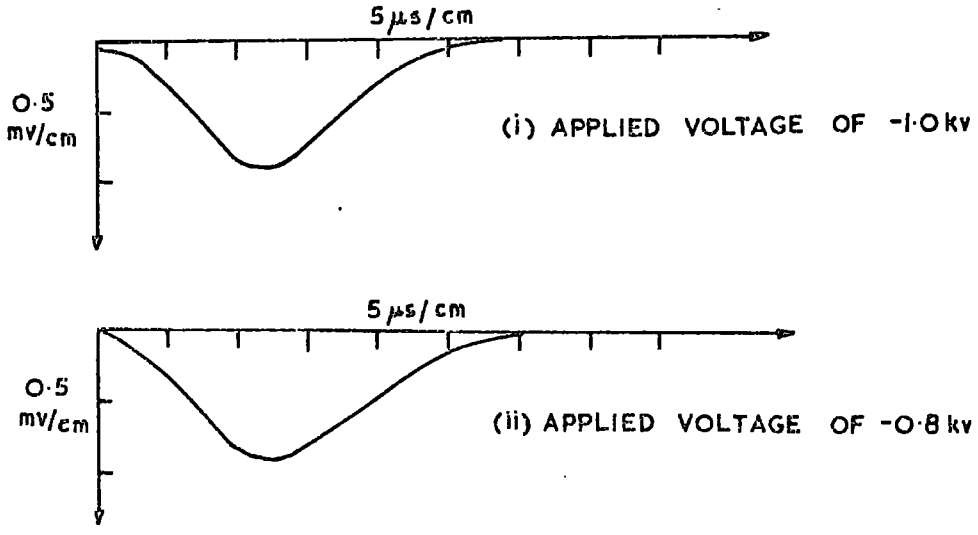

B. TYPICAL TYPE 2 PULSES (i) SINTERED POLYCRYSTALLINE (ii) SINGLE CRYSTAL ALUMINA

FIG. 6·18. IMPULSES RECORDED WITH A 10^4 Ω DETECTION RESISTANCE IN AN ARGON ATMOSPHERE OF 760 torr AT 400°C.

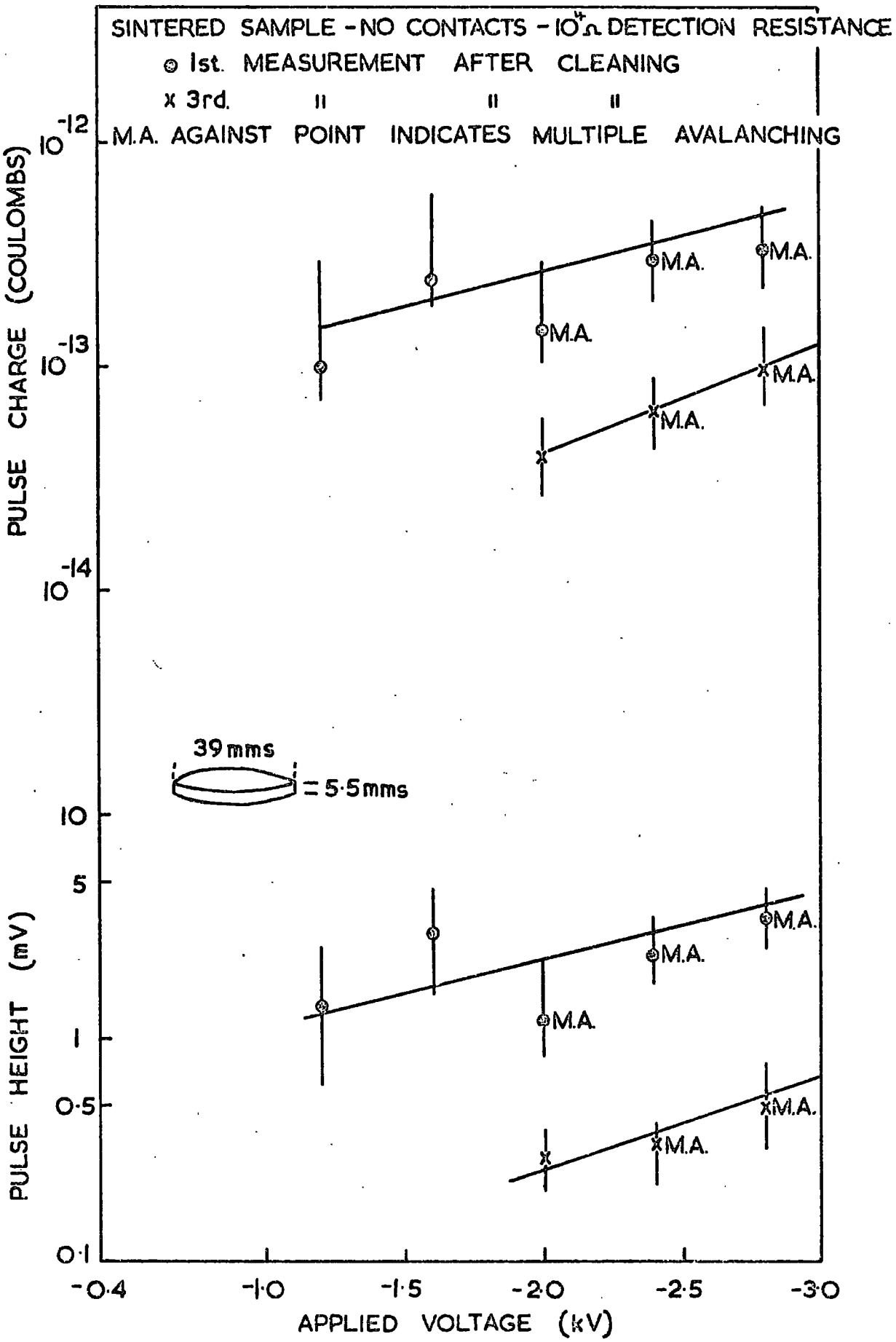

FIG. 6·19 CHARGE AND PEAK HEIGHT OF TYPE I PULSE OF SINTERED ALUMINA IN AN ATMOSPHERE OF ARGON AT 400°C – VARIATION WITH VOLTAGE.

in a single oscillogram were not recorded on single crystals. As in the case of sintered samples a quantitative study of the Type 1 pulse could not be made on single crystals.

A qualitative examination was made on both polycrystalline and single crystal samples of the effect of the ambient gas type and pressure on the height of the pulse. The results of the ambient gas type experiment, in which varying proportions of oxygen and argon were admitted to the chamber, were similar to those reported in Section 6.5.3.4 for the slower Type 2 pulse, i.e. the pulse height increased as the oxygen content of the ambient gas was raised. The height of the pulses was found to increase as the ambient gas pressure was reduced. However in contrast to the slower Type 2 pulse there was no decrease in pulse height at pressures below 100 torr, the pulse height continuing to increase until spark breakdown. At spark breakdown there was a sharp drop in pulse frequency to about 2 pulses per second and the generation of shock waves by the gas discharge. The impulses associated with spark breakdown were very large, between 10^{-8} and 10^{-9} coulombs.

6.5.3 Type 2 Pulse

6.5.3.1 Description of the Type 2 Pulse

In pure argon ambients the risetime of the Type 2 pulse was slower than the response of the detector, with the result that the pulse is undistorted. Typical examples of the pulses seen on single crystal and sintered polycrystalline samples are shown in Figure 6.18. From these it can be seen

that the rise and decay times of the pulses are of a similar length and that the pulse reaches a maximum in height at approximately half the duration time. It can also be seen that the current grows linearly with time rather than exponentially. Because of this the transit time of the pulses was measured in preference to the risetime.

6.5.3.2 The effect of voltage on the Type 2 Pulse

The results of oscillogram measurements on sintered polycrystalline samples are shown in Figures 6.20 and 6.21. These measurements were made in an atmosphere of nominally pure argon and undried air respectively. In both gases it can be seen that the pulse height is a maximum and the transit time a minimum at an applied voltage of approximately 2.0 kV. Similar variations in the shape of the pulse with applied voltage were seen at argon pressures of 300 and 120 torr, Figures 6.22 and 6.34 respectively. At both these pressures a maximum in the pulse height and a minimum in the transit time is observed as the voltage across the sample is raised. The voltage at which these maximum and minimum occur, hereafter called the maximum pulse height voltage, is pressure dependent, the voltage decreasing with pressure. The decrease in the pulse height, which occurs as the voltage is raised above the maximum pulse height voltage, is not accompanied by a corresponding decrease in pulse charge. The increase in the pulse height above 2.0 kV in Figure 6.22 is due to the Type 1 pulse.

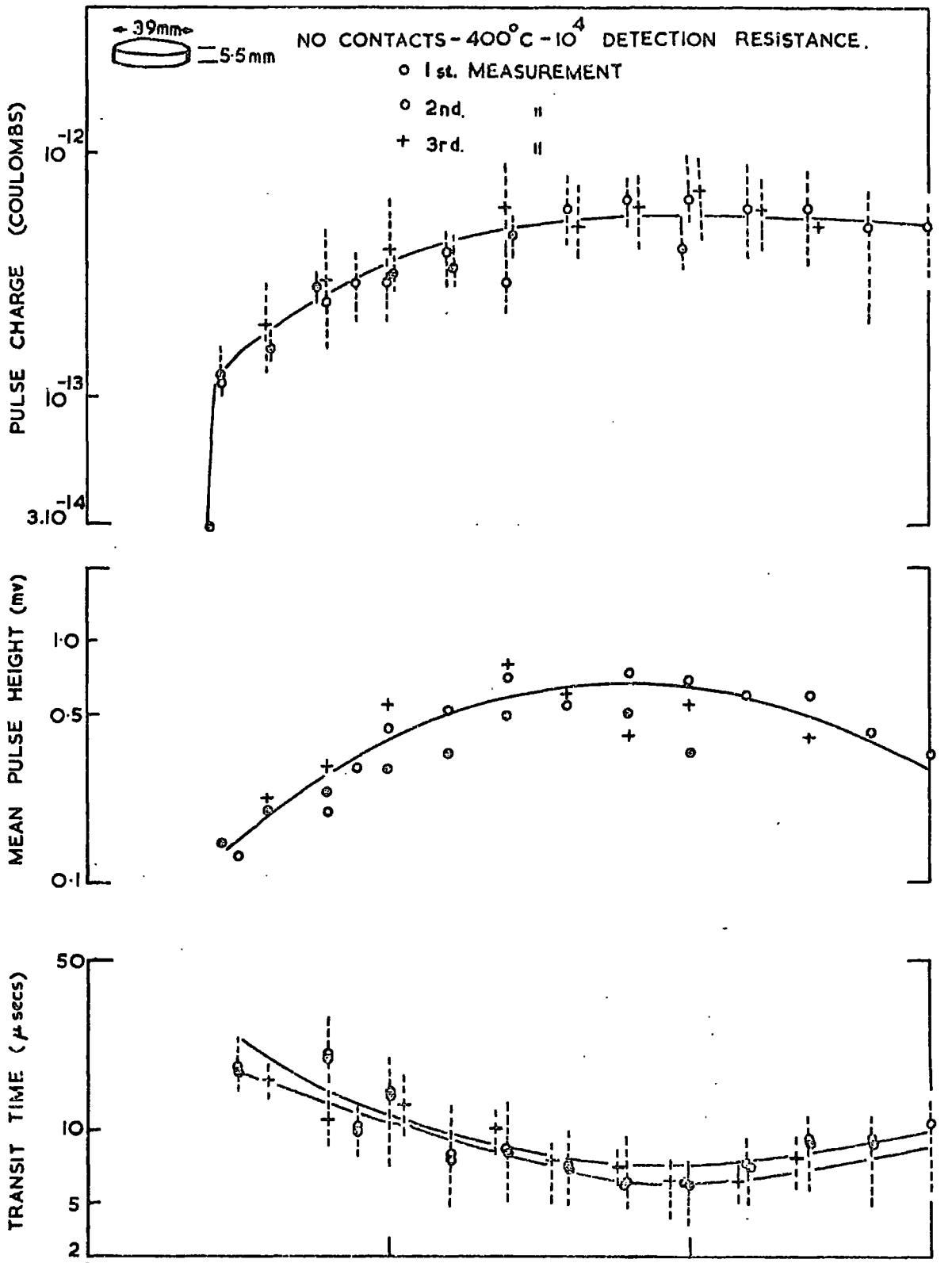

FIG. 6·20. PULSE PARAMETERS - v - APPLIED VOLTAGE SINTERED SAMPLE IN AN ATMOSPHERE OF NOMINALLY PURE ARGON AT 400°C.

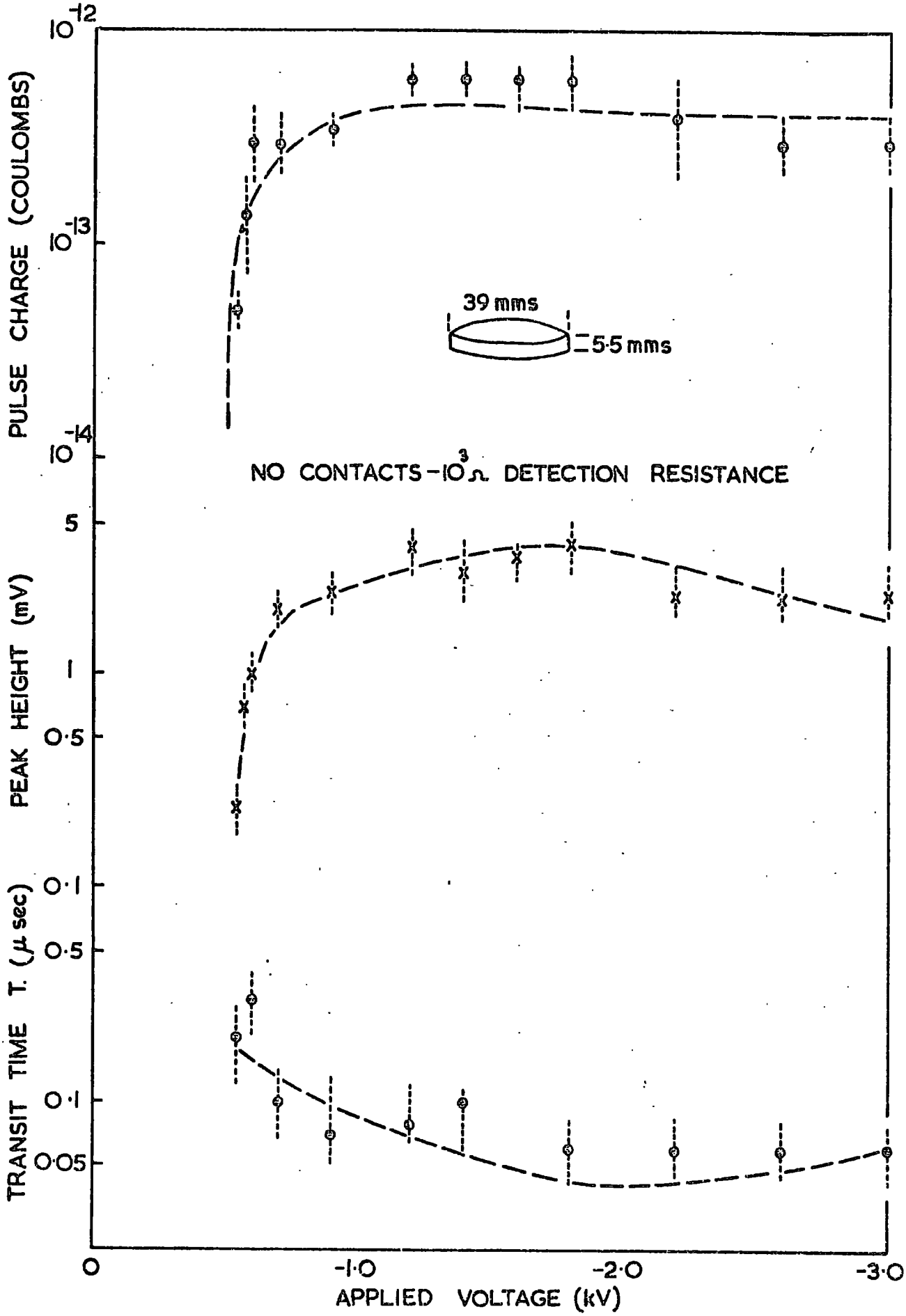

FIG. 6·21 PULSE PARAMETERS – APPLIED VOLTAGE FOR SINTERED SAMPLE IN AN ATMOSPHERE OF UNDRIED AIR AT 400°C

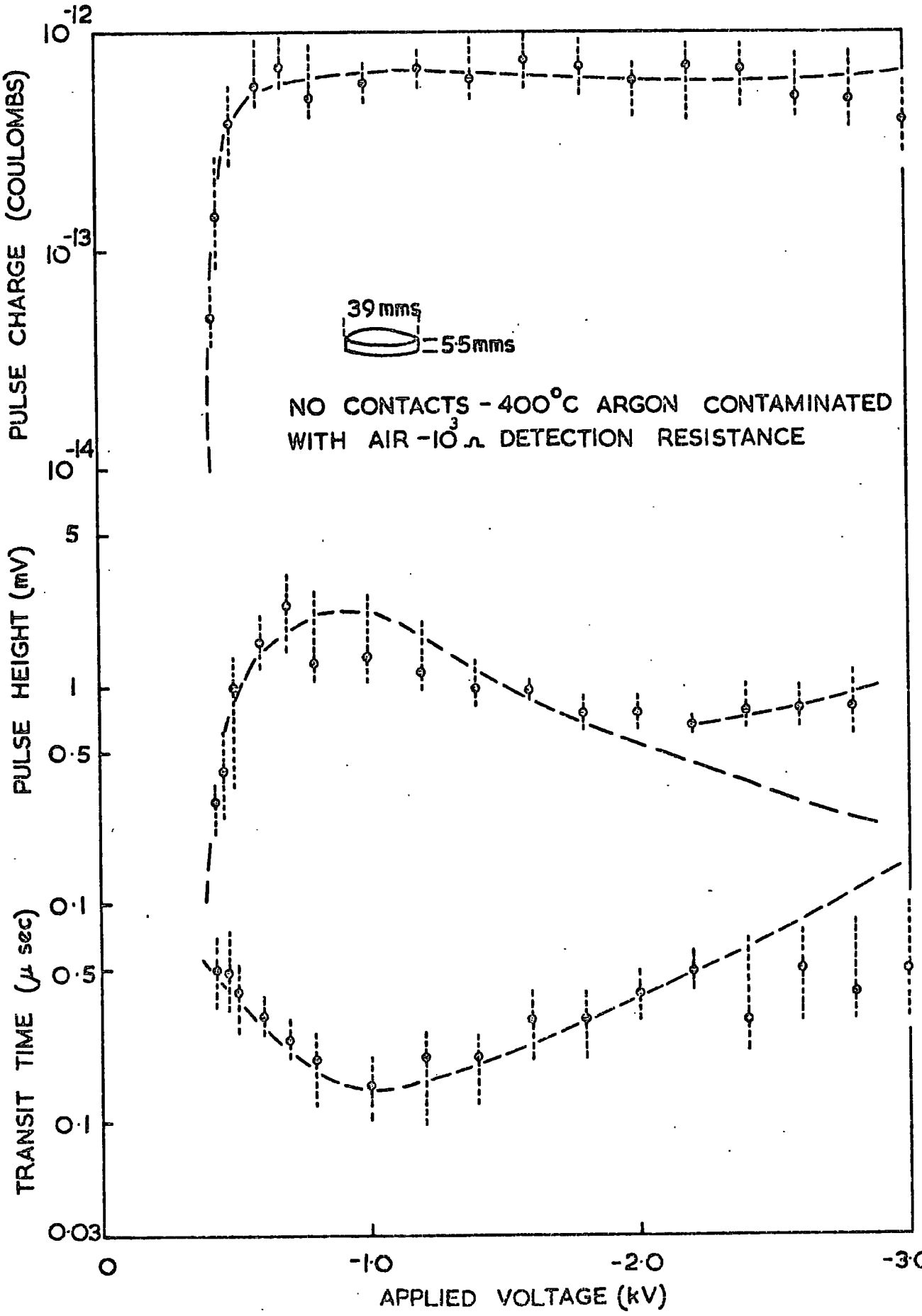

FIG. 6·22 PULSE PARAMETERS - vs - APPLIED VOLTAGE FOR SINTERED SAMPLE IN 300 torr OF ARGON AT 400°C

Similar results to the above were obtained in measurements on single crystals. Figure 6.23 shows the variation of pulse parameters with applied voltage in an atmosphere of nominally pure argon at 500°C. These measurements were made on the 2.0 cm diameter single crystal sample as it was heated to 900°C after being recontaminated, see Section 6.7.2 for the experimental details. These results, which again show the pulse height to be a maximum and the transit time a minimum at approximately 2.0 kV, are typical of pulse breakdown measurements on single crystals in an argon atmosphere. Although in most experiments on single crystals the maximum pulse charge was about 3×10^{-12} coulombs, a consistently large maximum pulse charge was observed in one experiment. This was in the first experiment in which the 2.0 cm diameter sample was heated to 900°C. On this occasion, the maximum pulse charge was approximately 1.0×10^{-11} coulombs at all temperatures.

6.5.3.3 The effect of pressure

The effect of pressure on the pulse breakdown of sintered polycrystalline samples was investigated in argon and nitrogen ambients. Similar results were obtained in both gases. Both ambients contained two hours diffused impurities, which probably explains why the results are so similar in the two gases. Pulse breakdown experiments on single crystals were limited to quantitative examination of pulse shape with pressure. These observations agreed with the results of the measurements on the sintered samples.

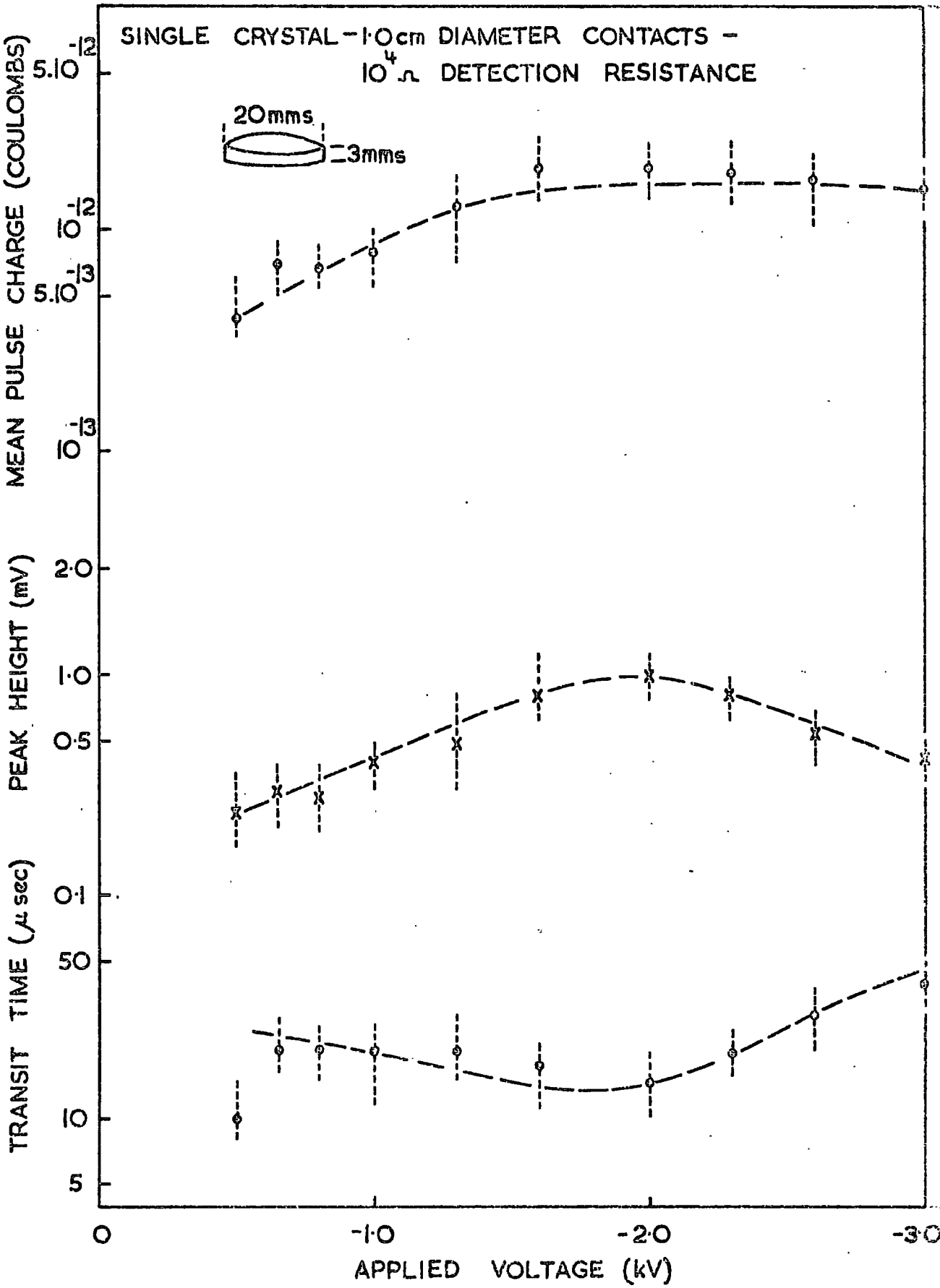

FIG. 6·23 PULSE PARAMETERS – vs – APPLIED VOLTAGE FOR SINGLE CRYSTAL IN AN ATMOSPHERE OF NOMINALLY PURE ARGON AT 500°C.

The variation of transit time and pulse height with pressure is shown in Figures 6.24 and 6.25 respectively. From these graphs it can be seen that the pulse height reaches a maximum and the transit time a minimum as the pressure is reduced from 760 to 300 torr. Hence it can be concluded that, at high ambient gas pressures, reducing the gas pressure has the same effect on the pulse parameters as increasing the voltage. The pressure at which this maximum in the pulse height and minimum in the transit time occur depends on the applied voltage. To a good approximation it can be seen that it occurs at a V/P ratio of 1.7 (where V is in volts and P is in torr). At lower pressures the transit time and the pulse height increase with decreasing pressure to a maximum at about 20 torr. Below this pressure the pulse height must decrease rapidly as it is not possible to detect pulses at 12 torr. In the case of the 1.0 kV curve in argon spark breakdown occurs at 80 torr.

The shape of pulse charge curve, which is shown in Figure 6.26, is very much as expected from the variation of the transit time and pulse height with pressure. At high pressures, where the transit time reaches a minimum and the pulse height a maximum, the pulse charge curve passes through a point of inflexion, while at lower pressures the pulse charge increases rapidly with decreasing pressure. The effect of pressure on pulse count rate is given in Figure 6.27, which shows that there is a fairly rapid increase in the count rate at lower pressures. In view of the increased pulse height at lower pressures, this effect may be

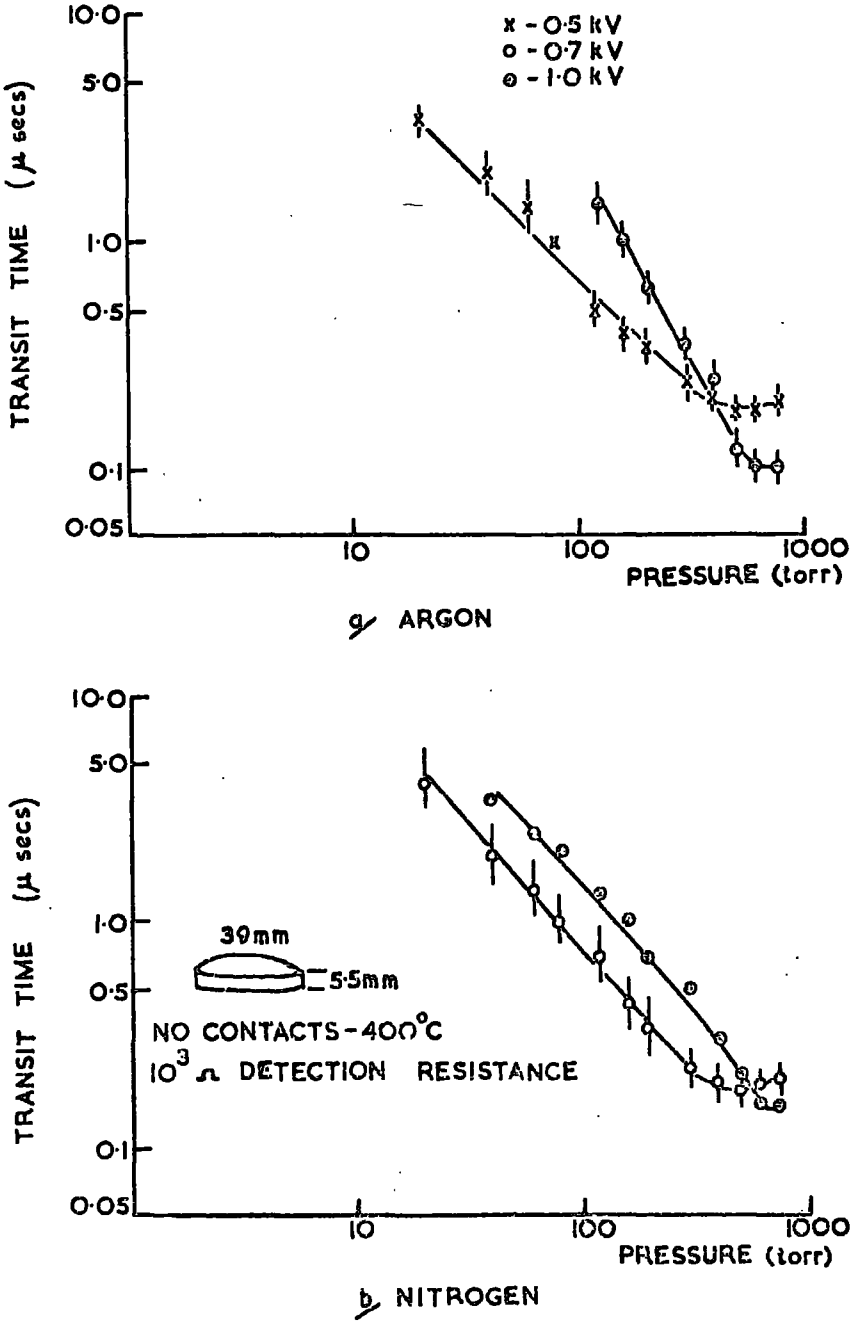

FIG. 6·24 VARIATION OF TRANSIT TIME WITH AMBIENT GAS PRESSURE FOR SINTERED ALUMINA AT 400°C.

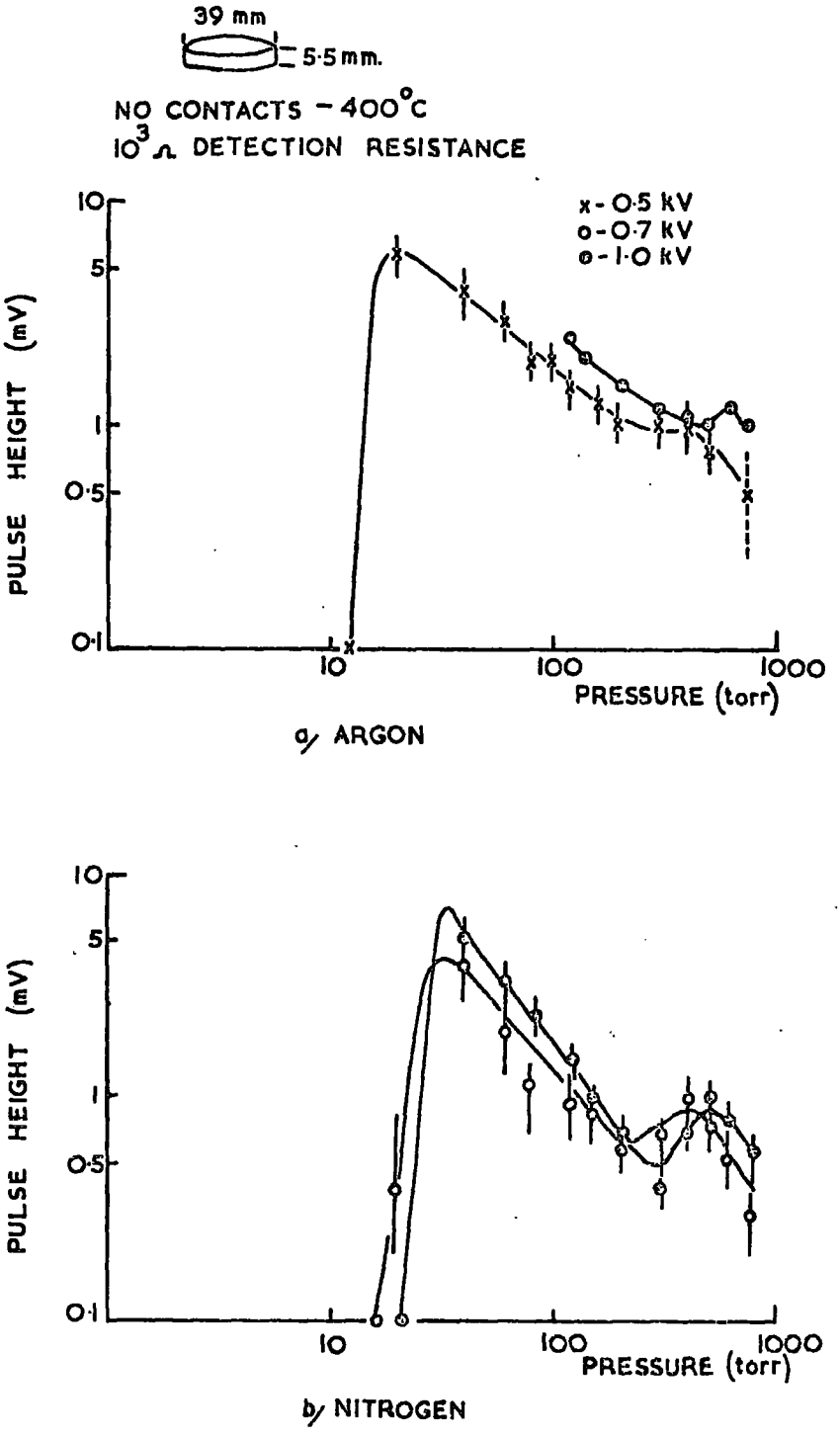

FIG. 6·25 VARIATION OF PULSE HEIGHT WITH AMBIENT GAS PRESSURE FOR SINTERED ALUMINA AT 400°C.

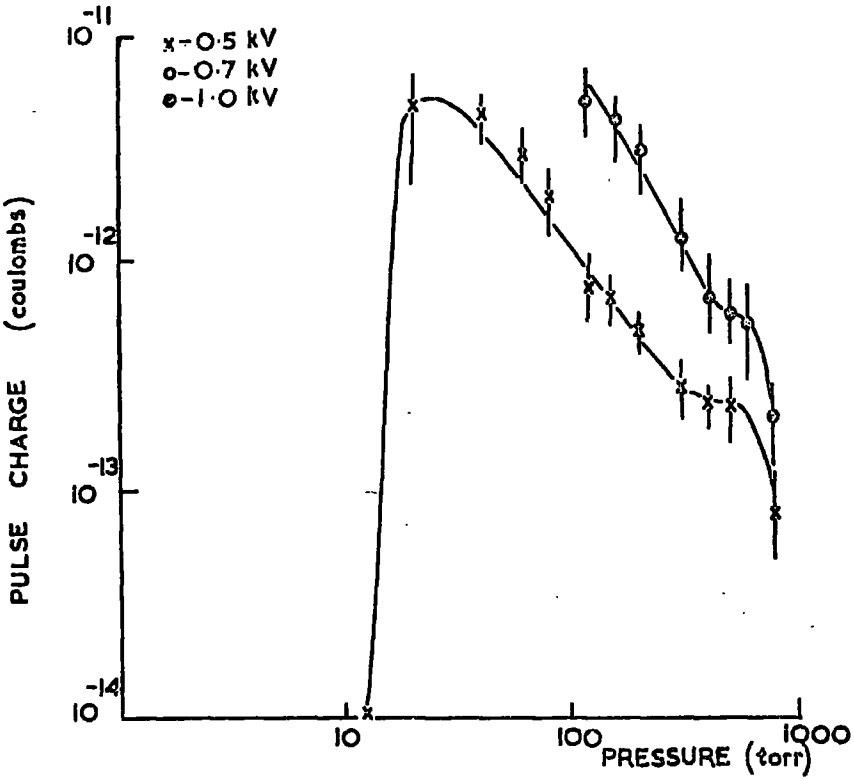

a/ ARGON

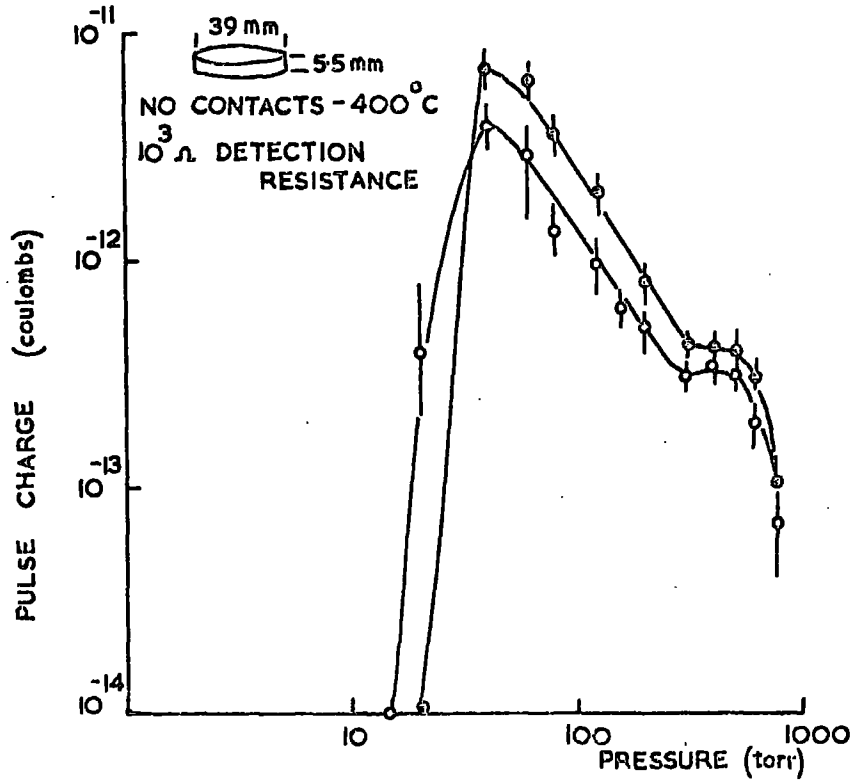

b/ NITROGEN

FIG. 6·26. VARIATION OF PULSE CHARGE WITH AMBIENT GAS PRESSURE FOR SINTERED ALUMINA AT 400°C.

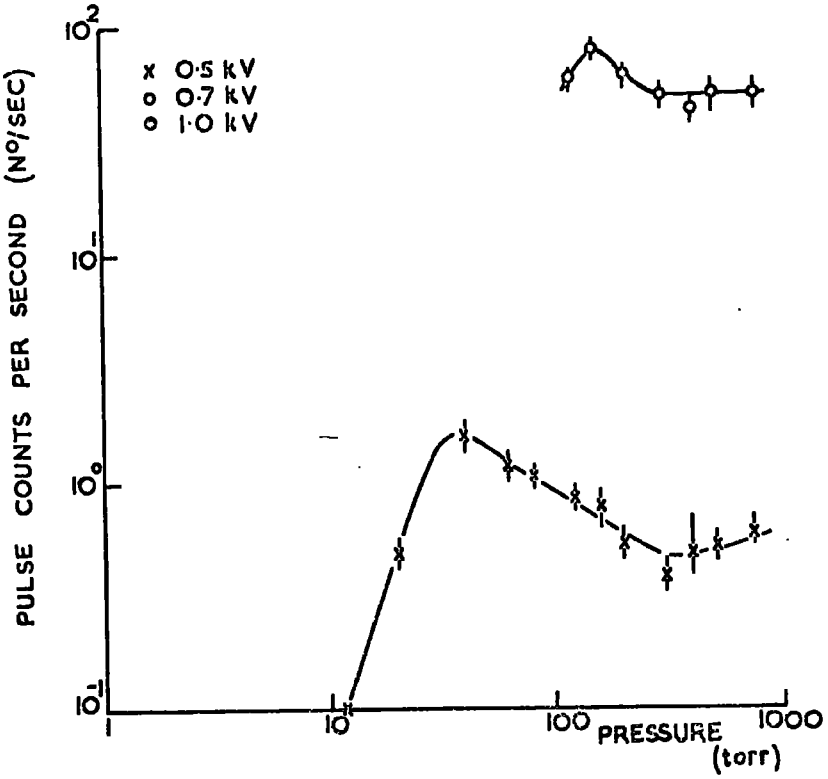

a/ ARGON

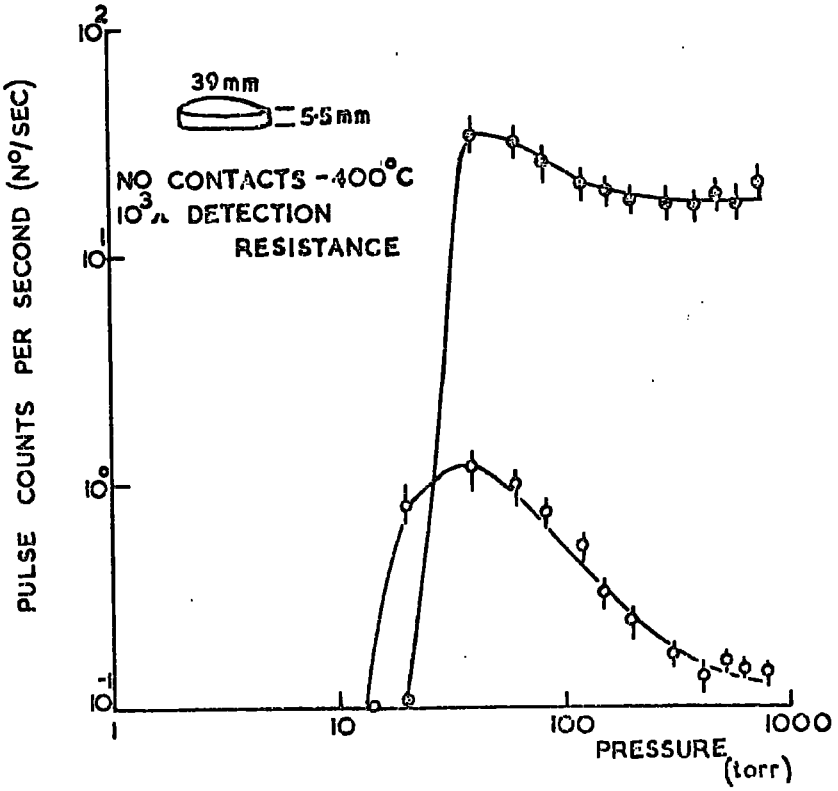

b/ NITROGEN

FIG. 6·27 VARIATION OF PULSE COUNT RATE WITH AMBIENT GAS PRESSURE FOR SINTERED ALUMINA AT 400°C.

attributed to an increase in the number of pulses above the detection level rather than to any increase in the absolute pulse count rate.

An approximate estimate may be made of the discharge path length from Figure 6.26. It can be seen from this that the pulses disappear at pressures between 10 and 30 torr, the exact value depending on the applied voltage. This disappearance of the pulses must be due to a fall in the ionization of the gas atoms. This is known to occur at high electron velocities and is the same effect as is seen in the Paschen breakdown curve of gases at Pd values below 10 torr mm. Equating this Pd value with the pressure at which the pulses disappear, i.e. about 4 torr when corrected to room temperature, gives a value for the discharge path of 0.25 cm. This estimate, which will be too large if the fields are non-uniform, sets an upper limit on the possible length of the breakdown path.

6.5.3.4 The effect of oxygen impurities in argon

Pulse count measurements on sintered samples show that the height of the pulse is affected by the concentration of oxygen impurities in the argon ambient gas. Figure 6.28 gives direct measurements of this variation of pulse height with oxygen partial pressure. The oxygen content in the nominally pure argon has been put at 0.01 torr and not the value estimated previously (0.05 torr). The effect of oxygen on the transit time and pulse charge is also shown in Figure 6.28. It can be seen that since the pulse height

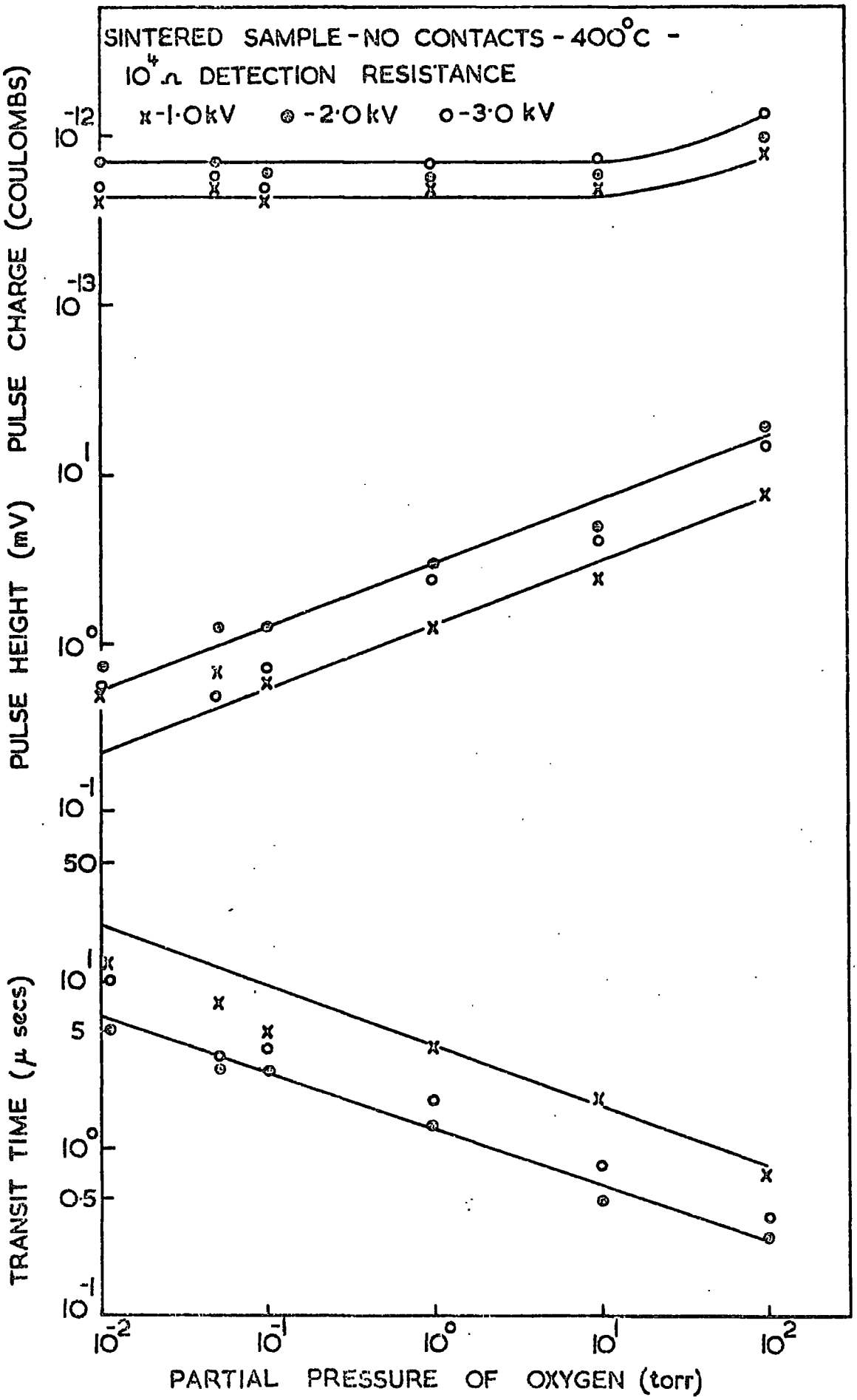

FIG. 6·28 VARIATION OF PULSE PARAMETERS WITH COMPOSITION OF THE AMBIENT GAS FOR AN OXYGEN - ARGON MIXTURE AT 760 torr.

increases with oxygen partial pressure there is a corresponding decrease in transit time. In contrast there is no very significant increase in the pulse charge with partial pressure of oxygen.

6.6 The Effect of Contacts and Electrode Geometry on Pulse Breakdown

6.6.1 Introduction

The effect on pulse breakdown of changing the electrode material, the electrode geometry and the contacts has been examined on a sintered polycrystalline sample. While most of the experiments have been concerned with altering the field distribution in the vicinity of the high voltage electrode a limited investigation has also been made of the effect of contacts at the low voltage electrode.

6.6.2 The effect of the high voltage electrode material

The effect of the high voltage electrode material on pulse breakdown was examined by replacing the normal Pt-40^{o}/o Rh electrode with a stainless steel one of similar geometry. Measurements of pulse breakdown were made at 400^{o}C in argon ambients of various pressures with both electrodes. Apart from the appearance of an occasional pulse below the onset voltage, no significant difference could be detected in pulse count rate or pulse shape between experiments conducted with this electrode and with the standard. With the plane stainless steel electrode, however, pulses were often recorded as much as 100 v below the genuine onset voltage. In this

voltage region, the pulse count rate was time dependent, decaying to zero within about three minutes of applying the voltage. However it should be noted that these effects were not observed with the spherical stainless steel electrode.

6.6.3 Contact experiments with a plane Pt-40°/o Rh high voltage electrode

Most pulse breakdown measurements have been made on polycrystalline samples with either no contacts or with small ones (i.e. less than the diameter of the electrodes). Early experiments (Young and Morant[22]) indicated that pulse breakdown was considerably affected by extending the contacts beyond the edge of the plane high voltage electrode. However more recent experiments in argon of very much greater purity have not substantiated these early results.

The later results of pulse count rate measurements with various contact arrangements are shown in Figure 6.29. These measurements were all made in an atmosphere of nominally pure argon on sample 2 at a temperature of 400°C. Because of the higher pulse count rate normally observed in the first measurement after cleaning of the sample, two pulse count measurements were made with each contact arrangement. Measurements 1 and 2 were made with no contacts on the sample while 3 and 4 were made with an 8 mm diameter contact at the high voltage electrode and a 4 mm diameter contact at the low voltage electrode. In subsequent measurements the diameter of the contact at the high

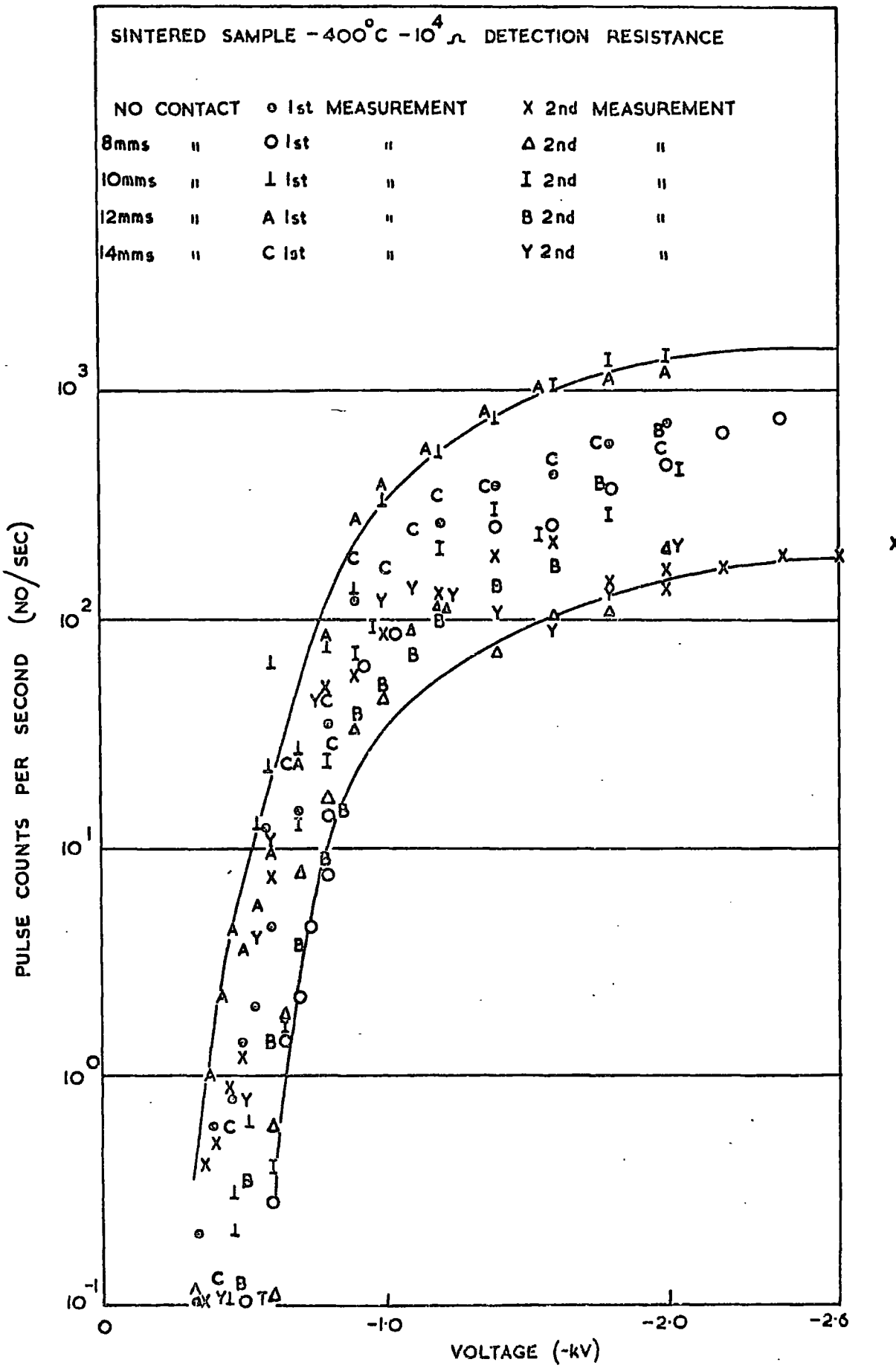

FIG. 6·29 EFFECT OF CONTACTS ON THE PULSE COUNT RATE OF SINTERED ALUMINA AT 400°C IN AN ATMOSPHERE OF NOMINALLY PURE ARGON.

voltage was increased, by depositing a fresh contact over the old one, while maintaining the size of the contact at the low voltage electrode constant. Statistical tests on these results show that there is no significant difference between the pulse count rates of these various contact arrangements. The technique used being to compare measurements 1, 3, 5, 7, and 9 and separately, measurements 2, 4, 6, 8 and 10.

During these pulse count rate measurements, pulse height distributions were recorded at various voltages. These also show no significant dependence on the contact arrangement. For example the pulse height distributions shown in Figure 6.32, which was recorded during measurement 10, is not significantly different from those shown in Figure 6.13, which were recorded during measurement 2. In addition there does not appear to be any significant difference in the pulse shapes observed in different measurements, both pulse types having a similar transit time and charge in each measurement. Consequently it can be concluded that provided the high voltage contact does not extend more than 2 mm beyond the edge of the electrode, pulse breakdown is not significantly affected by the presence of a high voltage contact.

The failure to observe a significant difference between measurements 1 and 3, and 2 and 4 shows that pulse breakdown is also not significantly affected by the low voltage contact provided that it is small. To investigate the effect of a large contact area at the low voltage

electrode, the sample was reversed after measurement 10, so that the contact extended 5 mm beyond the edge of the electrode. The effect of this reversal on the pulse count rate is shown in Figure 6.30. Measurement 1 is the pulse count rate immediately before the reversal, measurement 2 is the pulse count rate after reversal and measurement 3 the pulse count rate obtained after restoring the sample to its original position, i.e. 14 mm contact at the high voltage electrode.

To ensure that the results of this experiment were due to the contact reversal two precautions were taken; firstly the sample was only washed in deionized water and dried in alcohol between measurement (in an effort to reduce contamination effects) and secondly a rapid count rate measurement was made prior to the recording of measurement 2 (to eliminate the spuriously high pulse count rate sometimes recorded after chemical treatment of the sample). In view of the spread in the pulse count curves of Figure 6.29 it is obvious that nothing can be concluded from Figure 6.30.

In spite of this there does appear to be a difference in the pulse height distributions for the two cases. If Figure 6.31 is compared with Figure 6.32 it can be seen that there is a significant difference between the pulse height distribution with the 14 mm contact at the low voltage electrode, Figure 6.31, and that with the 14 mm contact at the high voltage electrode, Figure 6.32. This difference would not appear to be due to contamination since the repeated measurement (No 3) is very similar to the first (No 1)

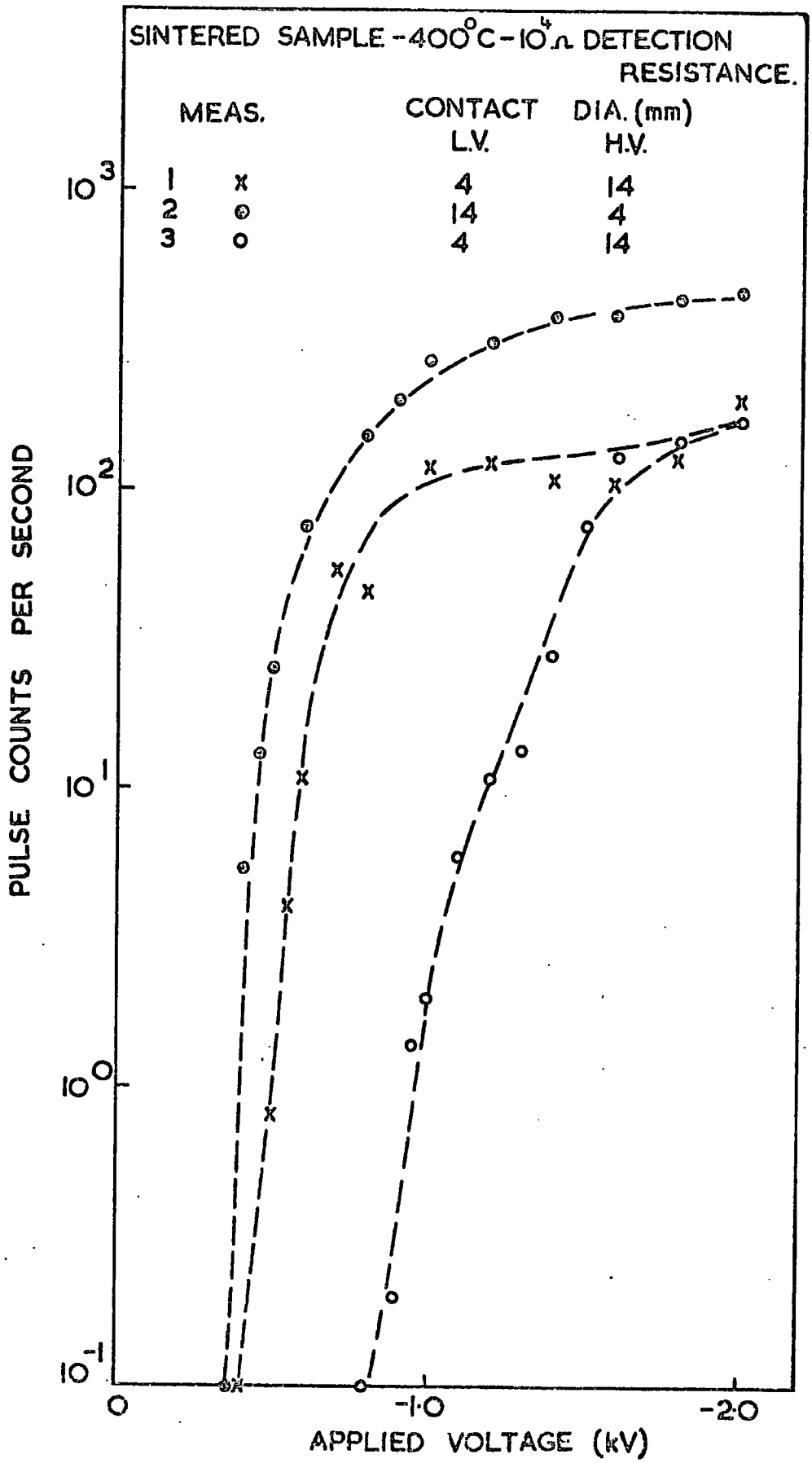

FIG. 6·30. EFFECT OF EXTENDING THE LOW VOLTAGE CONTACT BEYOND THE ELECTRODE ON THE PULSE COUNT RATE OF SINTERED ALUMINA IN ARGON AT 400°C.

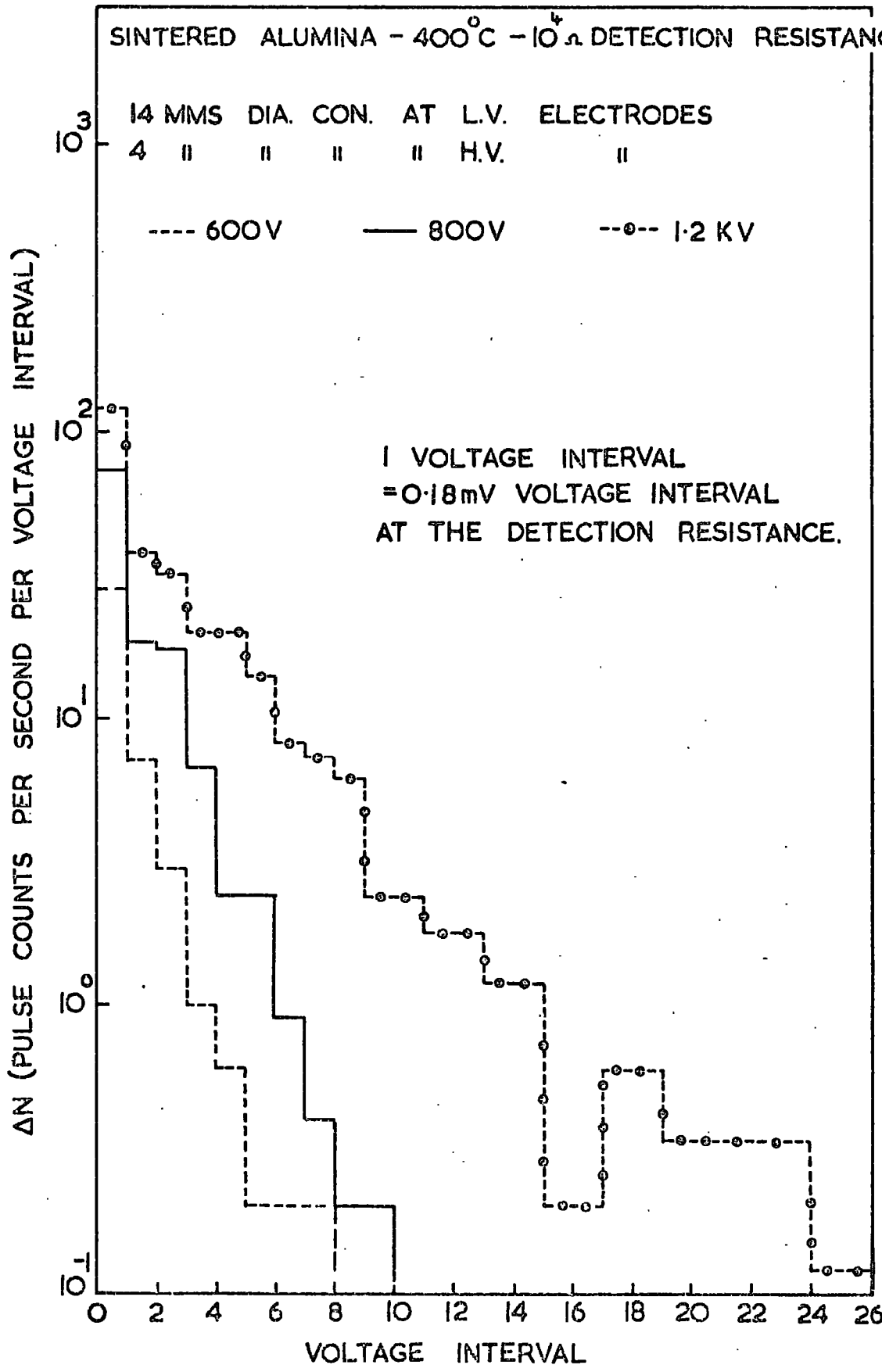

FIG. 6·31. PULSE HEIGHT DISTRIBUTION FOR SINTERED SAMPLE WITH LARGE AREA LOW VOLTAGE CONTACT IN ARGON AT 400°C.

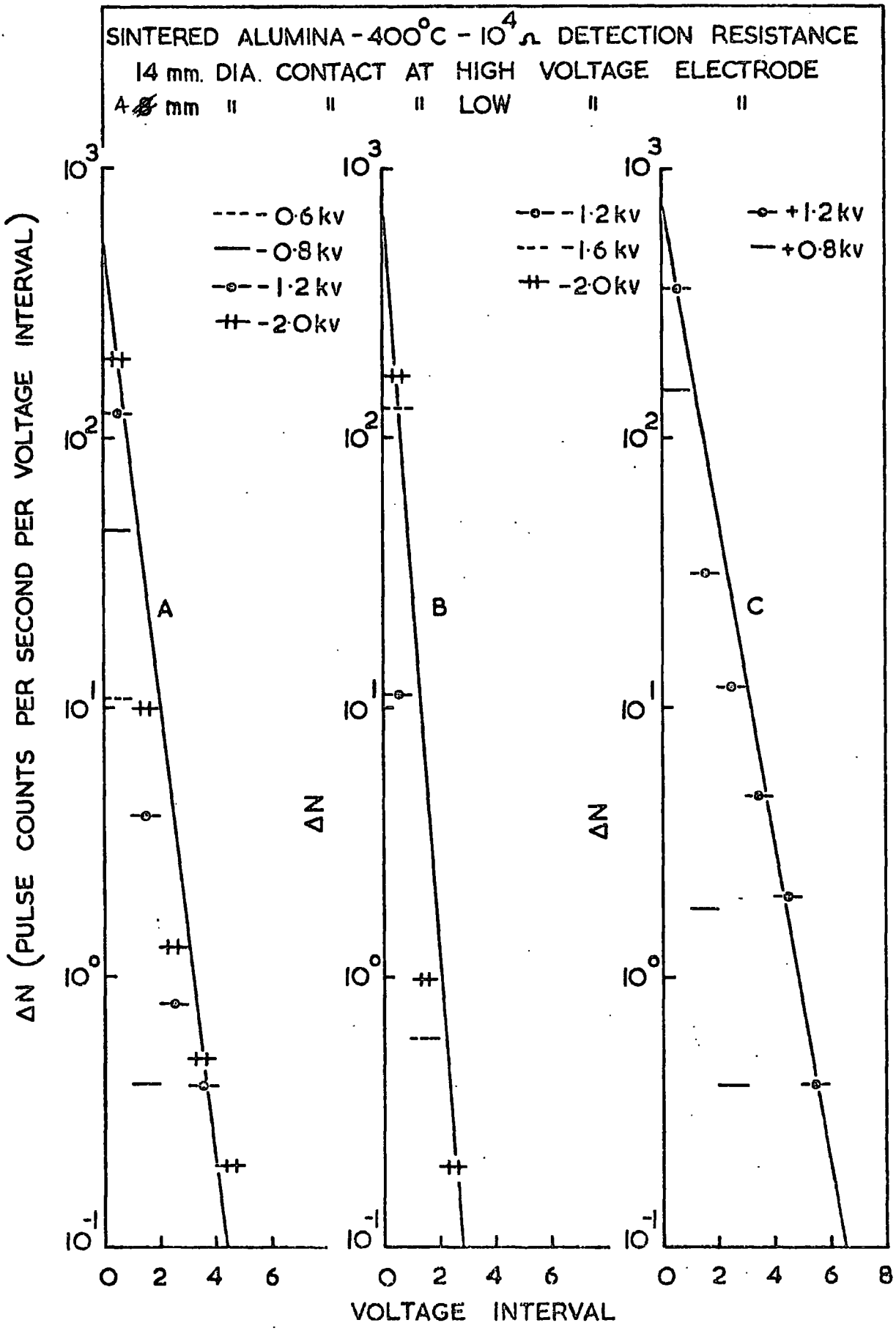

FIG. 6·32. PULSE HEIGHT DISTRIBUTIONS FOR SINTERED ALUMINA SAMPLE WITH CONTACTS AT 400°C IN AN ATMOSPHERE OF ARGON.

with the same conditions. The pulse height distribution shown in Figure 6.31 is characterized by the appearance of very large fast pulses of Type 1. In contrast to previous measurements without contacts these were observed at very low voltages, less than 600 volts. The effect of this on the pulse height distribution at 600 volts can be seen by comparing Figure 6.31 with 6.12, which shows the effect of fast pulses on a sample with no contacts. It is obvious from these results that the effect of extending the low voltage contact beyond the edge of the electrode is to increase the pulse activity associated with the fast pulses, thus indicating that these are being produced at the low voltage electrode, i.e. the anode in the present work.

The conclusion that the fast pulses are occurring at the anode is supported by experiments on reversing the polarity of the applied voltage. Two pulse height distributions were recorded at 800 and 1200 volts with a positive applied voltage. The contacts were reversed for these measurements, i.e. 14 mm contact at the low voltage electrode, which were made before the negative applied voltage measurements reported above. These results are shown in Figure 6.32C, and should be again compared with Figure 6.31. It is evident that when the high voltage electrode is positive, the number of fast pulses at 1.2 kV is so small that they do not significantly affect the pulse height distribution. In contrast a negative applied voltage causes the appearance of a significant number of fast pulses as low as 600 volts. This result would appear to indicate that the fast pulses

occur at the anode. The suggestion is that a higher onset voltage is required to initiate the fast pulses when they occur between insulator and electrode than when they occur between insulator and contact.

6.6.4 Contact experiments with a spherical stainless steel high voltage electrode

The experimental results presented in this subsection were obtained in impure argon ambients. The impurities in the argon are believed to result from the diffusion of air into the chamber in the 2 hour interval between filling of the chamber and the commencement of the measurements. Consequently the minimum partial pressures of air and water vapour in these experiments can be put at 4 torr and 0.1 torr respectively (see Appendix C). Unfortunately it has not been possible to repeat these experiments in nominally pure argon in the time available although a very rapid qualitative examination has been made. The observations confirm the results presented here for the sample without contacts, namely that there is no significant effect of the geometry of the high voltage electrode on pulse breakdown. Observations on a sample with a high voltage contact, 1.0 cm diameter, in nominally pure argon were not in complete agreement with the results presented below, the decrease in the pulse height with voltage being very much smaller than reported. However when the argon was not dried before being admitted to the chamber similar effects to those reported belowwere observed. It therefore appears likely

that the effects reported below are enhanced by the presence of water vapour in the ambient gas.

The results of pulse count measurements at pressures of 760 and 120 torr on sample 1 before the deposition of contacts are shown in Figure 6.33. The dotted line represents the pulse count curve obtained on the same sample without contacts with a plane high voltage electrode. The measurements were made at 400°C with a 10^3 ohms detection resistance. Statistical comparison of the pulse count curves obtained with plane and spherical electrode shows that they are not significantly different. The shapes of the pulses in the spherical electrode experiment were also not significantly different from those in experiments with plane electrodes. This can be seen from Figure 6.34, which shows the variation of pulse parameters with voltage in the 120 torr measurements on plane and spherical electrodes. From these results it can clearly be seen that there is no very significant effect of electrode shape on pulse breakdown.

An experiment was conducted on the same sample with a 1.0 cm diameter contact at the high voltage electrode. The results of pulse count rate measurements at various pressures with this arrangement are shown in Figure 6.35 and agree with similar measurements made by Wright (Private Communication) on magnesia. In this case the pulse count rate reaches a maximum at a voltage only slightly above the onset voltage. Once the maximum is reached the pulse count rate falls fairly rapidly as the voltage is increased. The

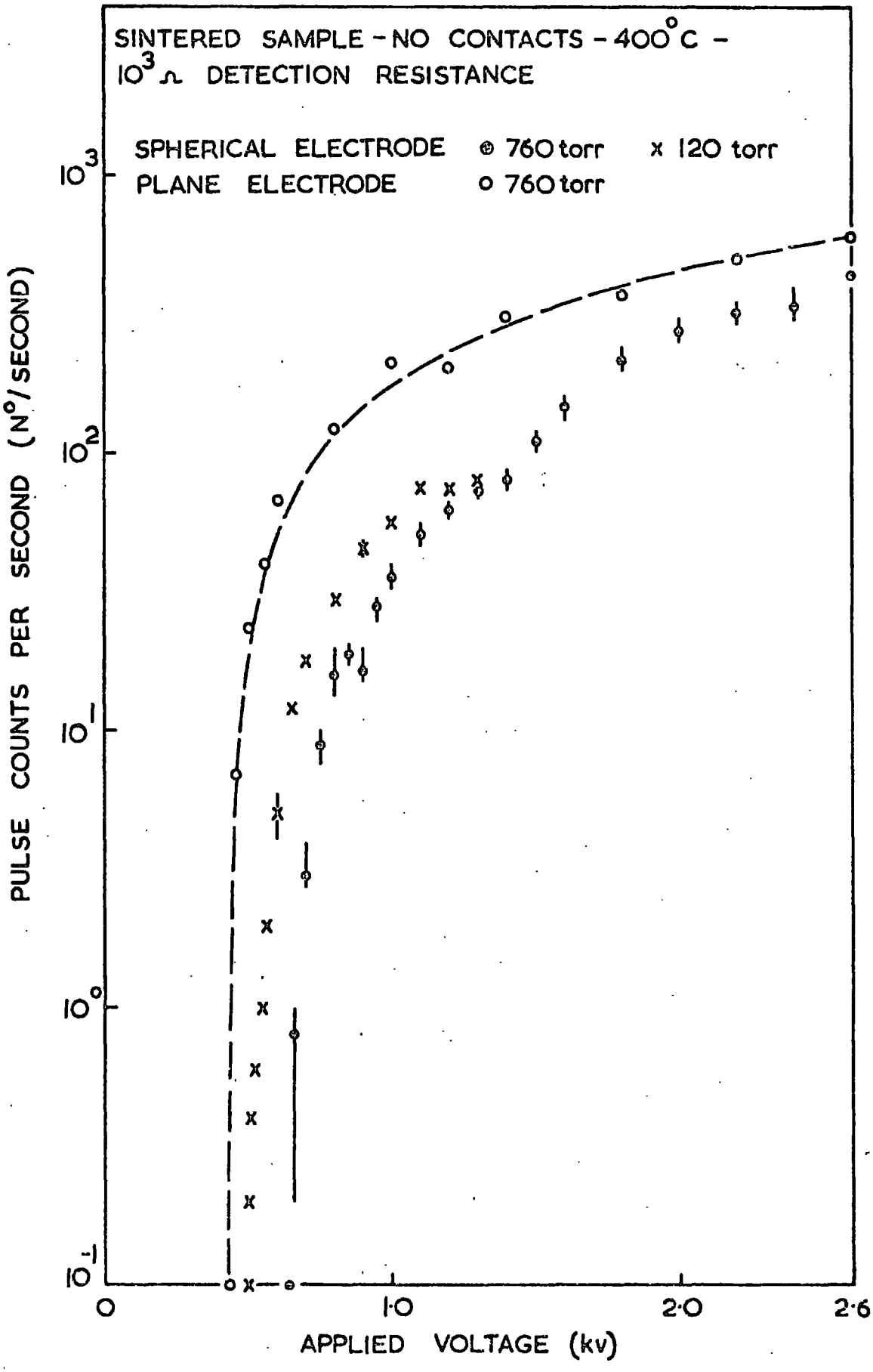

FIG. 6·33. EFFECT OF HIGH VOLTAGE ELECTRODE SHAPE ON THE PULSE COUNT RATE OF SINTERED ALUMINA IN AIR CONTAMINATED ARGON AT 400°C.

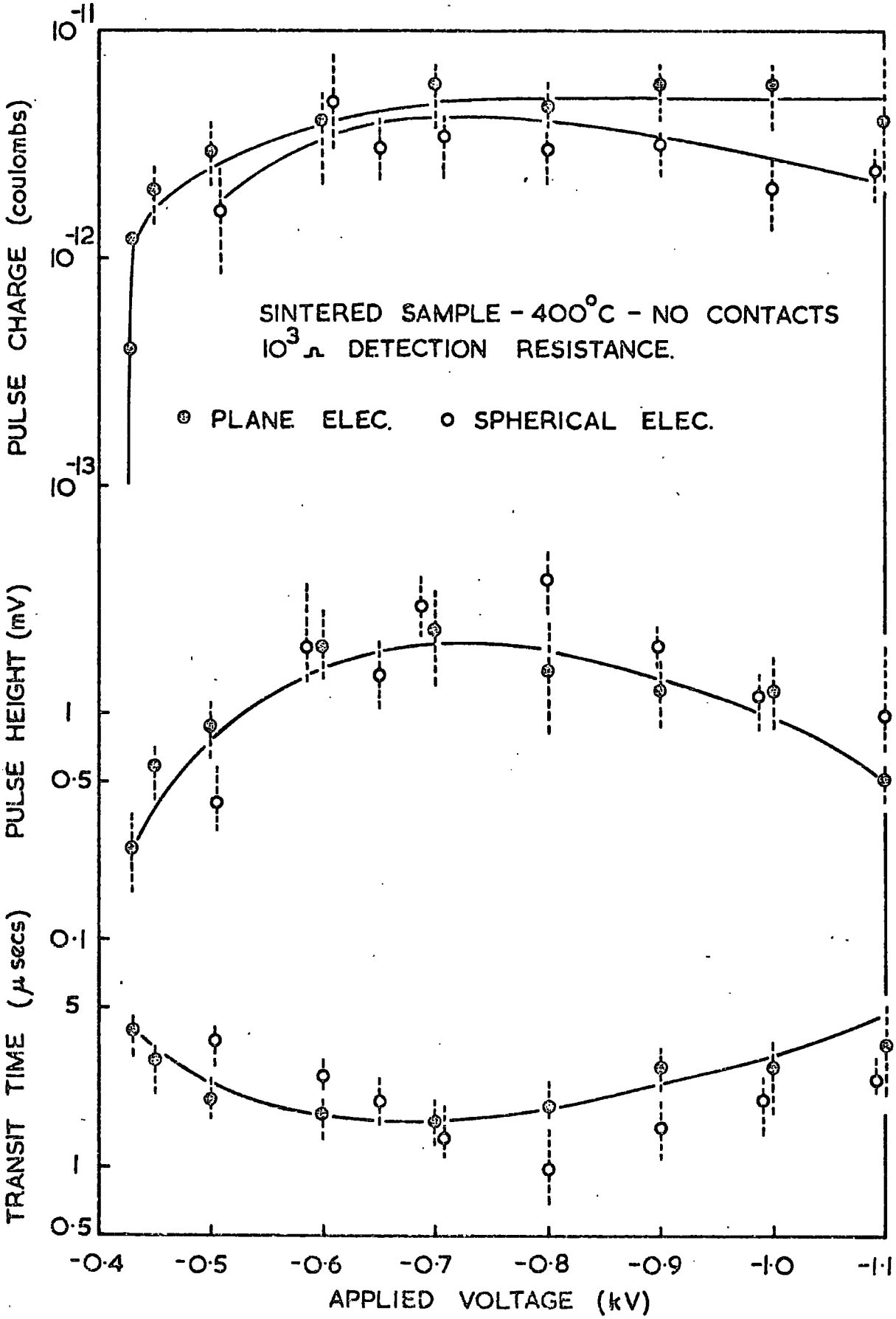

FIG. 6·34. EFFECT OF HIGH VOLTAGE ELECTRODE SHAPE ON THE PULSE PARAMETERS OF SINTERED ALUMINA IN AN AIR CONTAMINATED ARGON AMBIENT OF 120 torr AT 400°C.

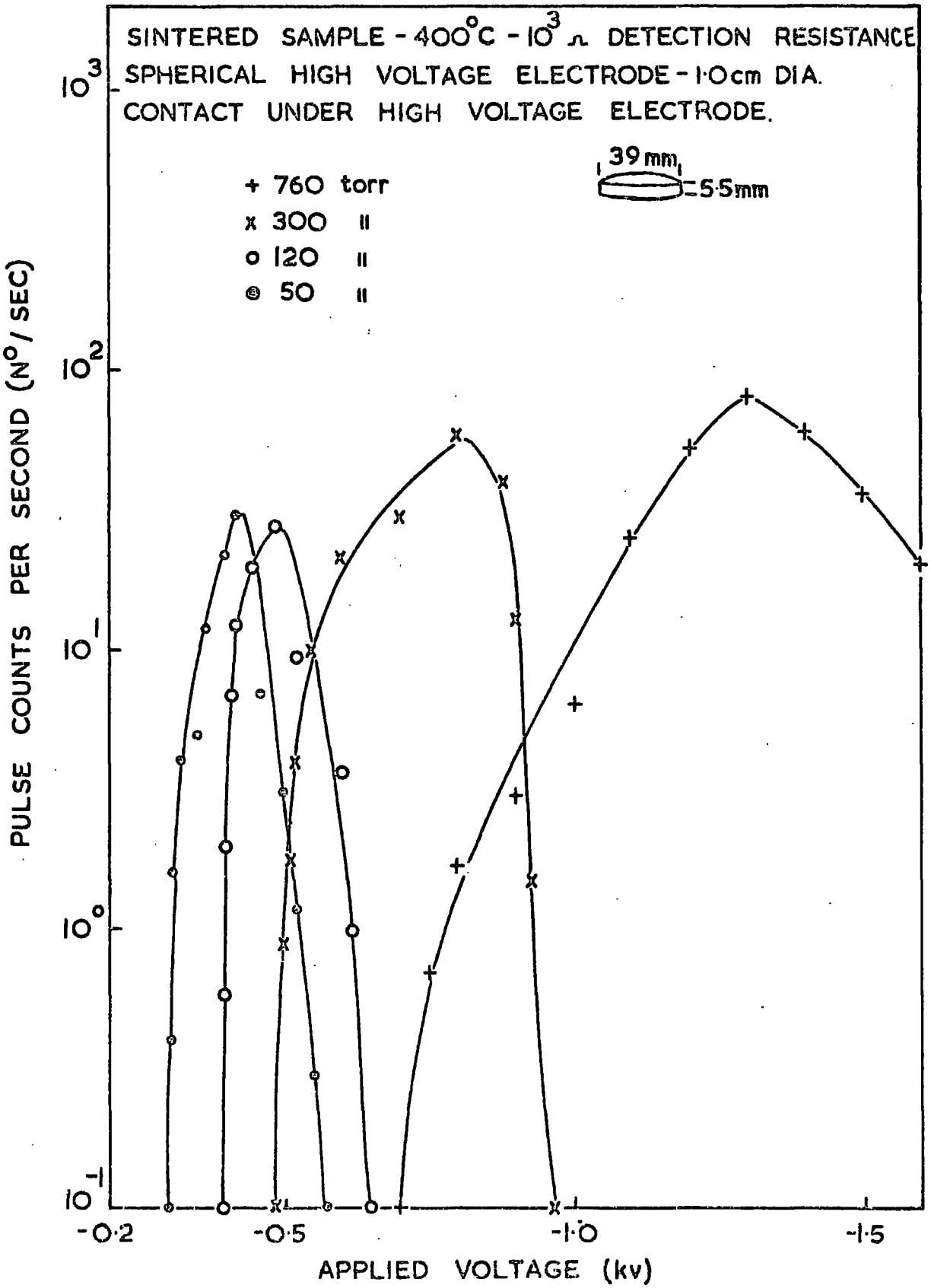

FIG. 6·35. EFFECT OF LARGE HIGH VOLTAGE CONTACT ON THE PULSE COUNT RATE OF SINTERED ALUMINA IN AIR CONTAMINATED ARGON AT 400°C.

effect is more pronounced at lower pressures. It can be seen that the voltage at which the maximum pulse count rate occurs falls as the pressure is reduced. At voltages above 2.0 kV the pulse count rate was found to increase again. These results, which were obtained at 400°C with a 10^3 ohms detection resistance were reproducible.

The reason for the unusual pulse count characteristic can be found from the pulse height distribution. The increase in the pulse count rate at the high voltages, i.e. above 2.0 kV, is due to the appearance of the fast Type 1 pulses, while the maximum in the pulse count rate at the lower voltages is associated with the slower Type 2 pulses. The reason for this maximum in pulse count rate can be seen from pulse shape measurements. The results of these, for the 120 torr measurements, are shown in Figure 6.36. It can be seen from this that the height of the pulses rapidly decreases as the voltage across the sample is increased. With a 10^3 ohms detection resistor, only current impulses above 1.8×10^{-7} amps can be detected and consequently pulse counts will only be detected between about 400 and 600 volts. If the value of the detection resistor is increased, the voltage range over which pulses can be counted also increases. Figure 6.37 shows the pulse count curves obtained at 120 torr with different resistors. While the count curve obtained with the 10^5 ohms resistor does show a slight minimum at 900 volts, this cannot be considered significant in view of the known distribution in the pulse heights. Consequently it can be concluded

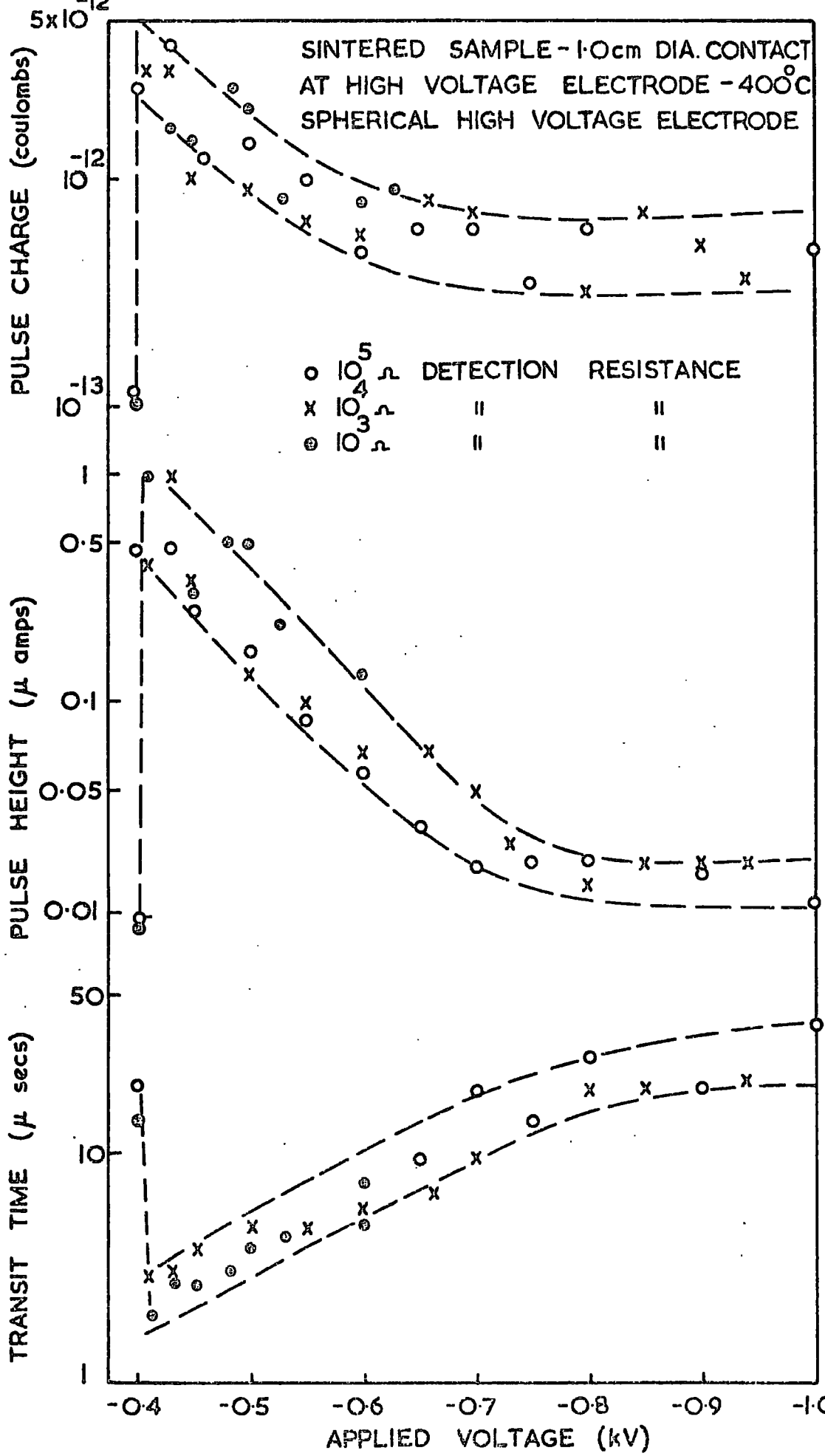

FIG. 6·36 EFFECT OF LARGE HIGH VOLTAGE CONTACT ON THE PULSE PARAMETERS OF SINTERED ALUMINA IN AN AIR CONTAMINATED ARGON AMBIENT OF 120 torr AT 400°C.

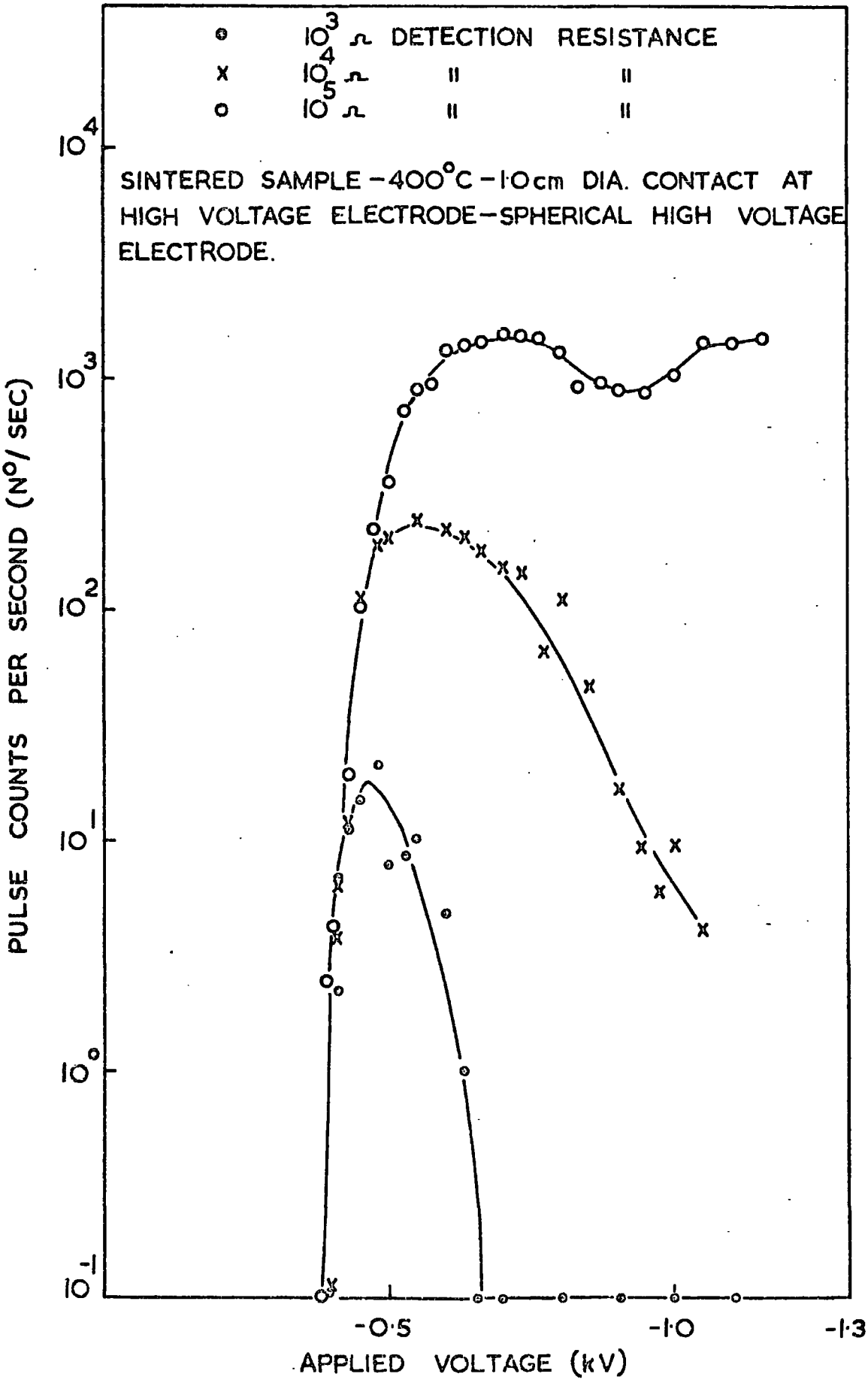

FIG. 6·37 VARIATION OF PULSE COUNT RATE (OF SINTERED ALUMINA AT 400°C IN AIR CONTAMINATED ARGON AMBIENT OF 120 torr) WITH DETECTION RESISTANCE.

that the variation of total pulse count rate with voltage is not significantly different in experiments with and without contacts although there is a large difference in the pulse shapes in these cases.

Comparison of Figures 6.34 and 6.36 shows that the variation of pulse parameters with applied voltage is significantly affected by the existence of a contact at the high voltage electrode. Since it has already been shown that pulse breakdown is unaffected by the geometry of the high voltage electrode and contacts, provided they do not extend very far beyond the edge of the electrode, the difference in the results must be due to the extent to which the contact extends. In other words it would appear that when the contact extends just beyond the edge of the electrode the change in the field distribution is not sufficiently large to significantly effect pulse breakdown, whereas if the contact is fairly well removed from the edge of the electrode the change in the field has a significant effect on pulse breakdown.

Although Figures 6.34 and 6.36 appear to be of very different forms this is not really the case. What happens in measurements with contacts at low pressure, i.e. 120 torr and below, is that the pulses reach a maximum in height at slightly above the onset voltage. Consequently the region in which the pulse height increases with voltage, which is easily observed on samples without contacts, is not seen in this case. In contact experiments at higher pressures however, the rise can be seen clearly as for example in

Figure 6.38, which shows the results of 300 torr measurements. Here the pulse height reaches a maximum and the transit time a minimum at about 500 volts. It can be seen by comparing Figures 6.38 and 6.22 which show results for a sample without contacts and a plane parallel electrode, that while the general shape of the curves are not affected by the contacts, the voltage at which the peak in the pulse height occurs is affected. It is also evident that there is a much more rapid decrease in the pulse height with voltage in measurements where a large contact is present. For this purpose a large contact is defined as one which extends at least 5 mm beyond the edge of the electrode.

6.7 The Effect of Temperature on Pulse Breakdown

6.7.1 Measurements on sintered polycrystalline samples

Two experiments have been conducted to investigate the effect of temperature on polycrystalline samples. In the first the sample was cleaned between successive measurements whereas in the second the sample was only cleaned at the beginning of the experiment. Different results were obtained in these two experiments. In the first experiment pulse breakdown was observed to increase with temperature over the range 100° to 800°C while in the second a minimum in pulse activity occurred at 600°C. Although the contact arrangements on the sample were different in the two experiments, it seems unlikely, in view of the results of Section 6.6, that the difference between the results was

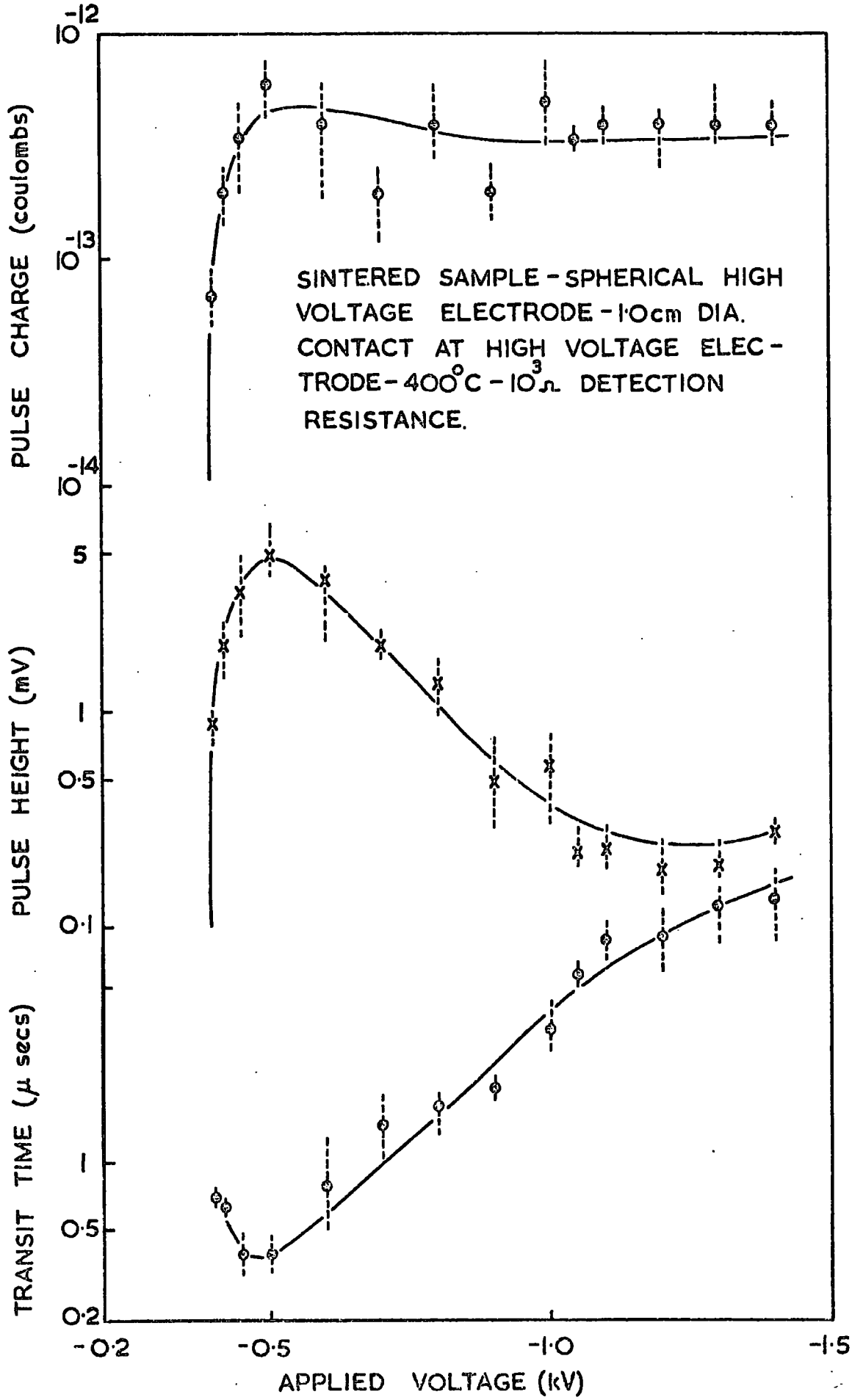

FIG. 6·38. PULSE PARAMETERS v APPLIED VOLTAGE FOR SINTERED SAMPLE WITH LARGE HIGH VOLTAGE CONTACT IN AIR CONTAMINATED ARGON AMBIENT OF 300 torr AT 400°C.

caused by this. Hence it appears that the variation of pulse breakdown with temperature is influenced by the chemical treatment given to the sample.

The variation of pulse count rate with temperature for these two experiments is shown in Figure 6.39. In the first experiment the measurements were made on sample 2, with no contacts, in an atmosphere of argon and with a 10^3 ohms detection resistor. In this experiment it can be seen that the pulse count rate increases rapidly with temperature to 600°C. At higher temperatures the pulse count rate approaches the resolution of the counter and further increases are not detected. Since the main amplifier was used in this experiment in the wideband condition, the resolving time of the detector was controlled by the pulse shape. Oscillograms show that the minimum resolving times at 700° and 800°C are 2.0 and 3.0 microseconds respectively, corresponding to pulse count rates of 5×10^5 and 3.3×10^5 counts per second.

In the second experiment the sample was used with a 1.4 cm diameter contact at the high voltage electrode and a 0.4 cm diameter contact at the low voltage electrode. The measurements were made in an atmosphere of nominally pure argon with a detection resistor of 10^4 ohms. From Figure 6.39 it can be seen that there is a minimum in the pulse count rate at 600°C. This minimum is due to the disappearance of the slow pulses at temperatures of 600°C and above. Below 600°C, few fast pulses were observed and hence most of the pulses were slow ones of Type 2. Above 600°C all the pulses were fast ones of Type 1 and no slow pulses could

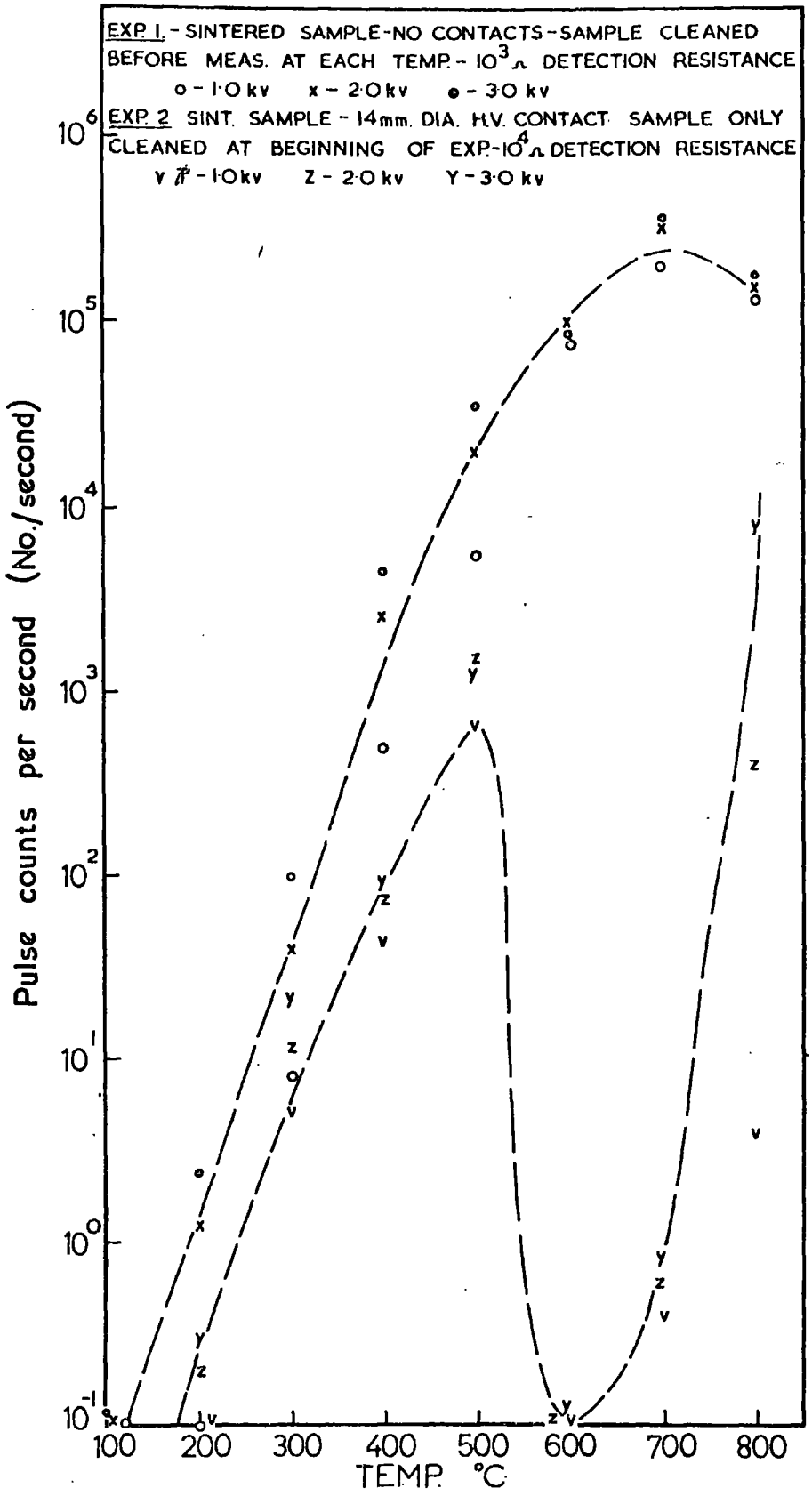

FIG. 6·39. Effect of temperature on the pulse count rate of sintered alumina in an atmosphere of argon.

be detected. It can be seen from the rapid increase in the pulse count rate above 600°C that the frequency of the fast pulses increases with temperature. In contrast the slow pulses reach a maximum in pulse count rate at 500°C. Above this temperature it appears that the pulse count rate falls very quickly as the temperature is raised, since the slow pulses become so infrequent that at 600°C they are not recorded at any applied voltage up to -3.0 kV. Similar results to these have been obtained on single crystal samples during the initial heating of the crystal. Since these measurements were also made on heating the sample after cleaning the results would appear to be in good agreement with single crystal observations.

In this second experiment, the d.c. resistance of the sample was measured in addition to pulse breakdown. The results of these measurements are given in Section 7.3.5. Because of the uneven contact diameters on this sample a further d.c. measurement was made of the resistance of polycrystalline alumina with contacts of the same diameter. Pulse breakdown measurements were also made during this experiment. However because of the large size of the low voltage contact, i.e. extending 4 mm beyond the edge of the electrode, the fast pulses predominated at all temperatures and the drop in pulse count rate, due to the disappearance of the slow pulses, was not seen.

In contrast to the second experiment, both types of pulse were evident in the first experiment above 600°C. This suggests that by recontaminating the sample between

measurements the slow pulses can be made to occur at higher temperatures. If this is the case the results may be influenced by other factors, such as the rate of heating or the impurity concentration in the ambient.

Neither of these experiments showed any very large variation of pulse shape with temperature. In the second experiment the shapes and sizes of the slow pulses were very similar at all the three temperatures examined. The results of pulse shape measurements in the first experiment at -1.0 kV are shown in Figure 6.40. Oscillograms taken during this experiment show that the transit time of the fast and slow pulses were not all that different at the lower temperature. For example at 300°C the transit time of the slow pulses was about twice that of the fast pulses. Consequently the argon used in this experiment must be very impure and hence the results must be treated with caution. However the results do indicate that the charge and transit time of the slow pulses increase with temperature while the height of the pulses remains constant.

6.7.2 Measurements on single crystals

Three 3 mm thick single crystal samples of different diameters, 1.6, 2.0 and 2.6 cm, were examined for pulse breakdown at the same time as the d.c. conductivity was measured as a function of temperature. On heating these samples to 900°C after chemical cleaning, pulse breakdown was observed over a range of temperatures. However once the samples had been heated to 900°C no significant pulse activity could

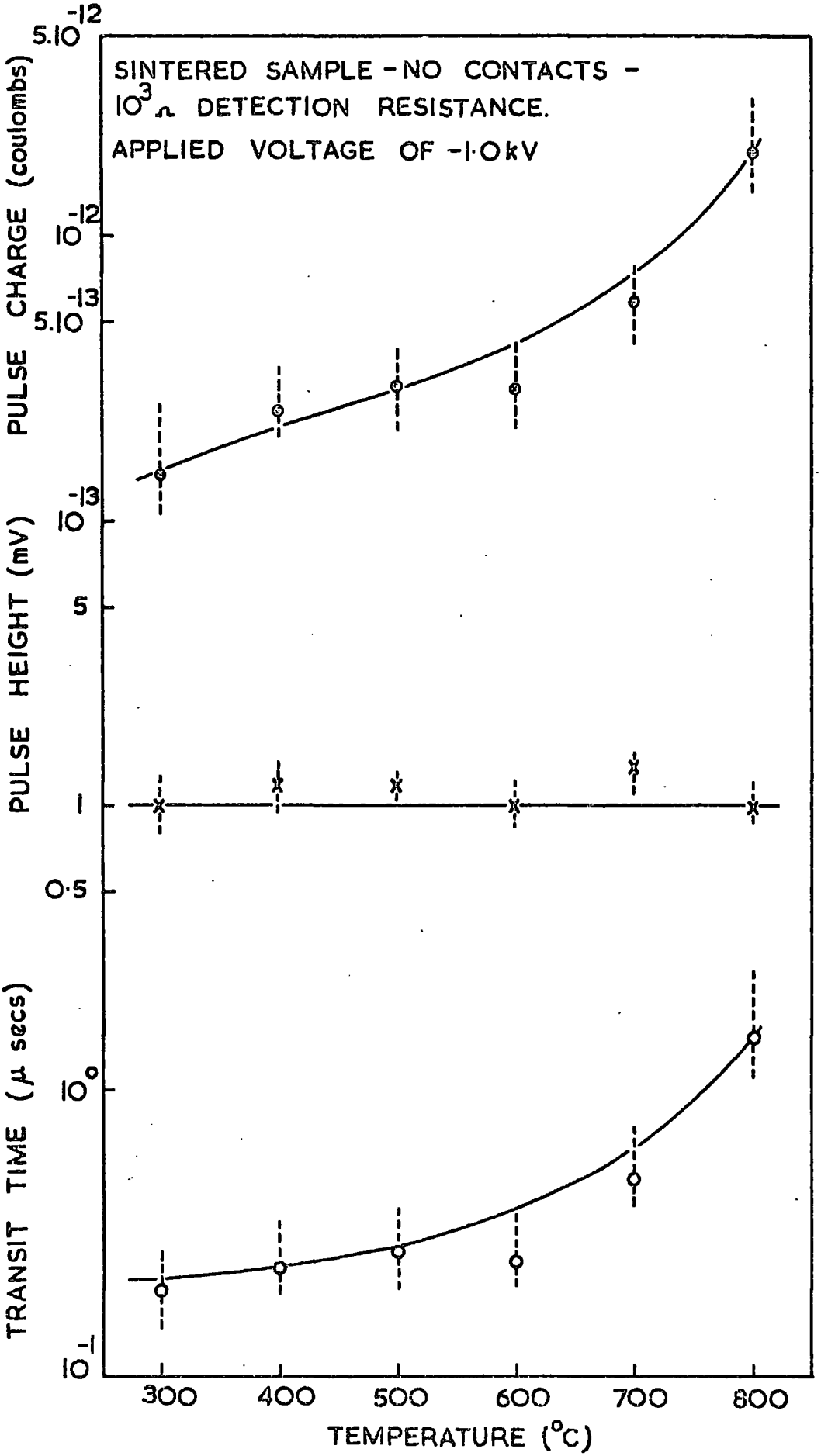

FIG. 6·40. PULSE PARAMETERS v TEMPERATURE FOR SINTERED ALUMINA IN ARGON AT ATMOSPHERIC PRESSURE.

be detected at any temperature within the range 0°C to 900°C, either on cooling or subsequent reheating of the sample. Pulse breakdown reappeared however if the sample was chemically cleaned before being heated. The appearance of pulse breakdown coincided with the measurement of an anomalously high d.c. conductivity (see Sec 7.3.4). The results of these pulse breakdown measurements on the 2.0 cm sample, i.e. the sample on which these effects have been most carefully studied, will be given in detail.

The variation of pulse count rate with temperature for the 2.0 cm diameter sample is shown in Figure 6.41. These results were obtained on heating the sample after chemical cleaning. From this figure it can be seen that no significant pulse breakdown occurs on cooling the sample from 900°C, only a very low pulse count rate being recorded at 600°C. It can also be seen from Figure 6.41 that the pulse count rate is a maximum at approximately 600°C. Comparison of this figure with Figure 7.4, the corresponding d.c. conductivity measurements, shows that the maximum in the pulse count rate occurs at the same temperature as the contamination peak in the conductivity curve.

After the results shown in Figure 6.41 had been obtained the sample was removed from the holder and fresh contacts were sputtered on the crystal. The only cleaning procedure given to the sample during this time was drying in alcohol immediately before replacing in the sample holder. On reheating the sample to 900°C no pulses were observed either on heating or cooling. The conductivity curve for this run

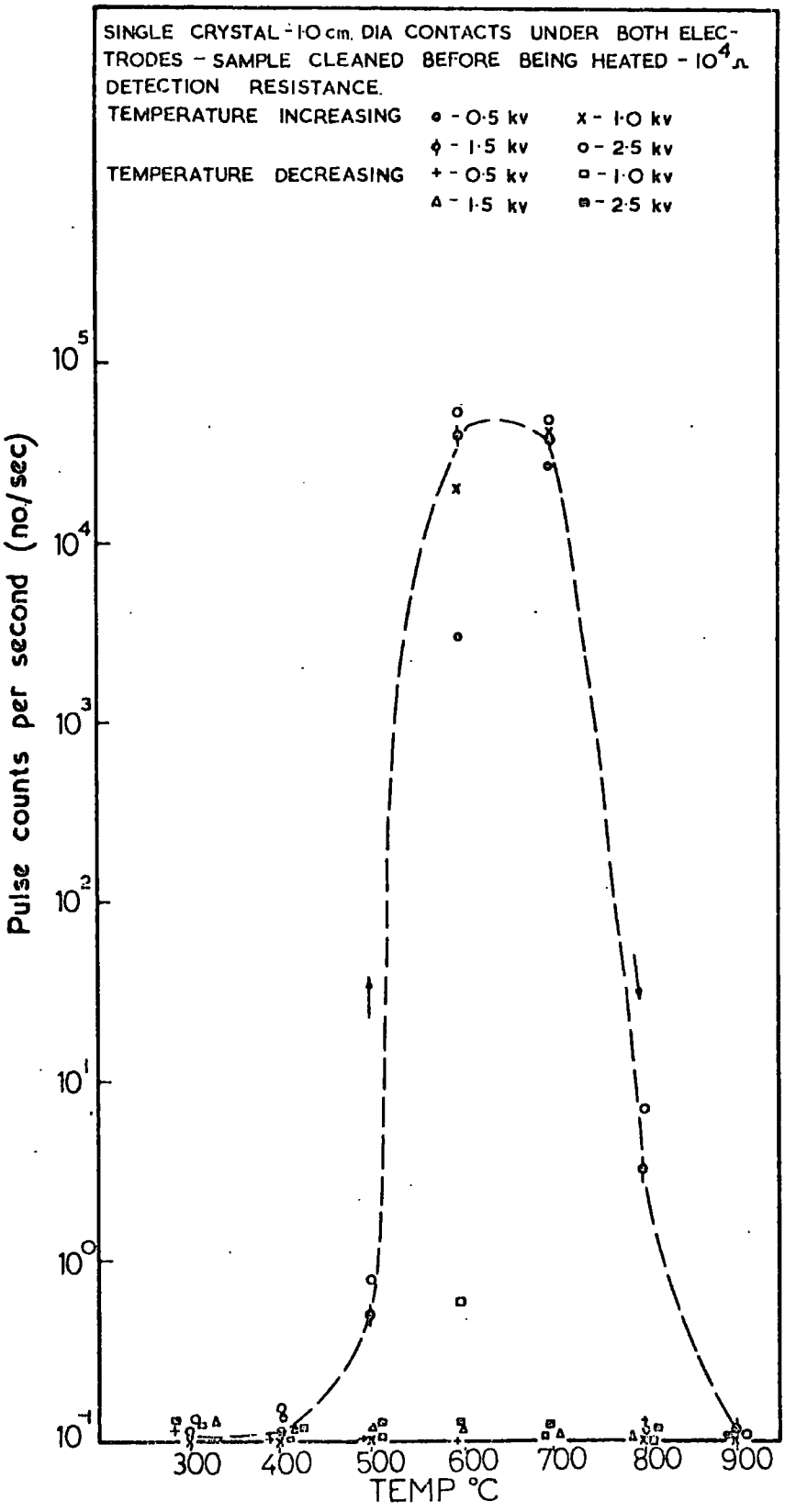

FIG. 6·41. Pulse count rate - v - temperature for 2·0 cm diam. single crystal sample in argon at 760 torr.

did not show any contamination effects. After this second temperature cycle the sample was cleaned normally and new contacts were deposited. Figure 6.42 shows the results of the pulse count rate measurements on the sample after this treatment. This shows that pulse breakdown again occurs on heating the sample to 900°C and that no significant pulse activity is observed on cooling. The conductivity curve on this run (see Fig. 7.5) again showed a contamination peak on heating.

Similar measurements were made on the two other single crystal samples. However in these experiments the third temperature cycle was omitted, i.e. the sample was not examined for pulse breakdown after it had been recleaned. The results of the pulse count rate measurements on these two other samples on the first temperature cycle after cleaning are shown in Figure 6.43. These results show that the pulse count rate on the 2.6 cm sample reaches a maximum at about 600°C and on the 1.6 cm sample at 500°C. The corresponding d.c. conductivity curves for these runs are shown in Figure 7.6. It can again be seen from this that the conductivity, on heating the sample after chemical cleaning, is anomalously high. On reheating these samples to 900°C after the deposition of fresh contacts, pulse breakdown was not detected on heating or cooling. The d.c. conductivity curves on this run also showed no contamination effects.

It has not been possible to detect any significant variation of pulse shape with temperature in these experiments on single crystals. That this was not seen indicates

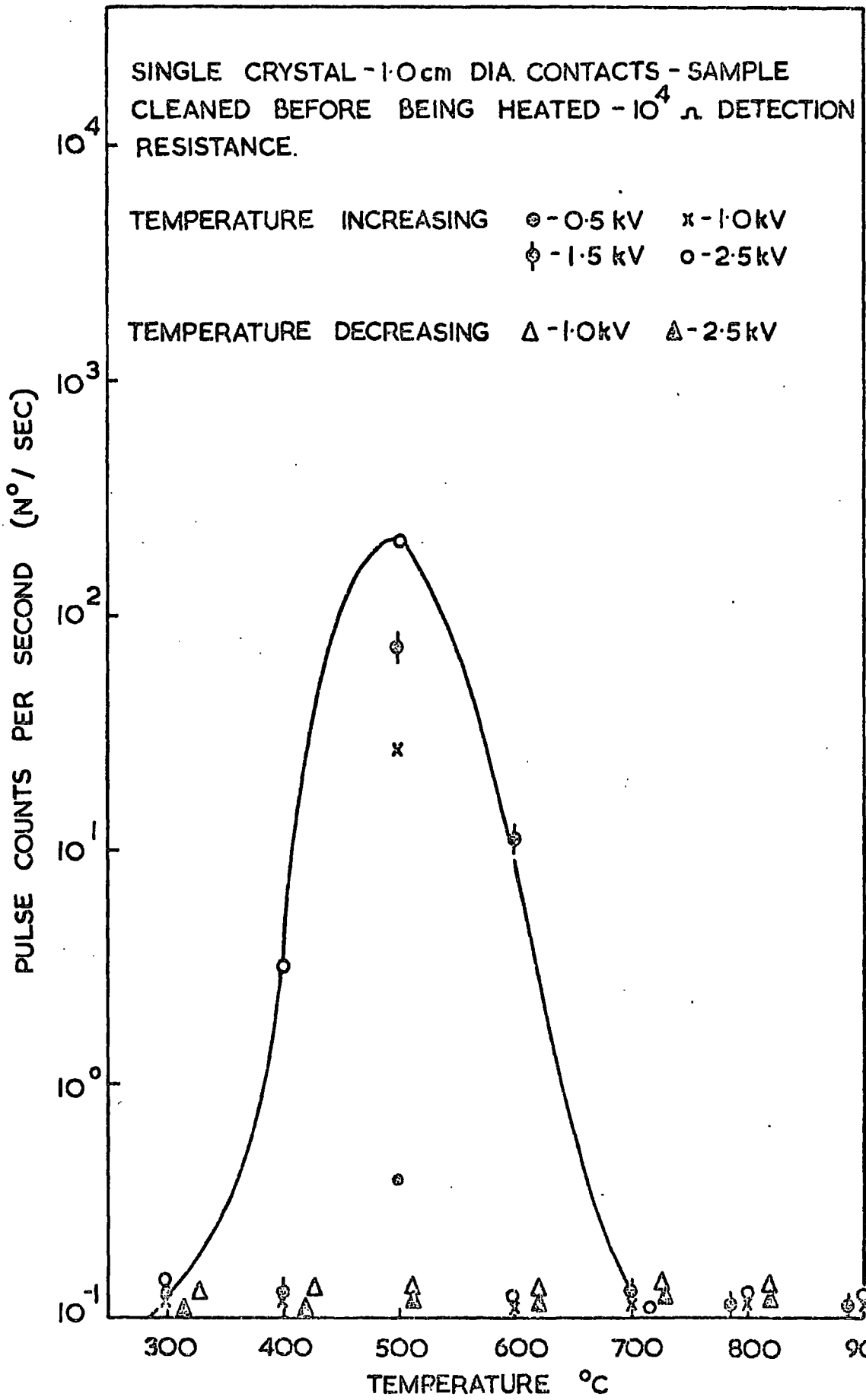

FIG. 6·42. PULSE COUNT RATE - v - TEMPERATURE FOR 2·0 cm DIAMETER SINGLE CRYSTAL SAMPLE IN ARGON AT 760 torr. (2nd. EXPERIMENT)

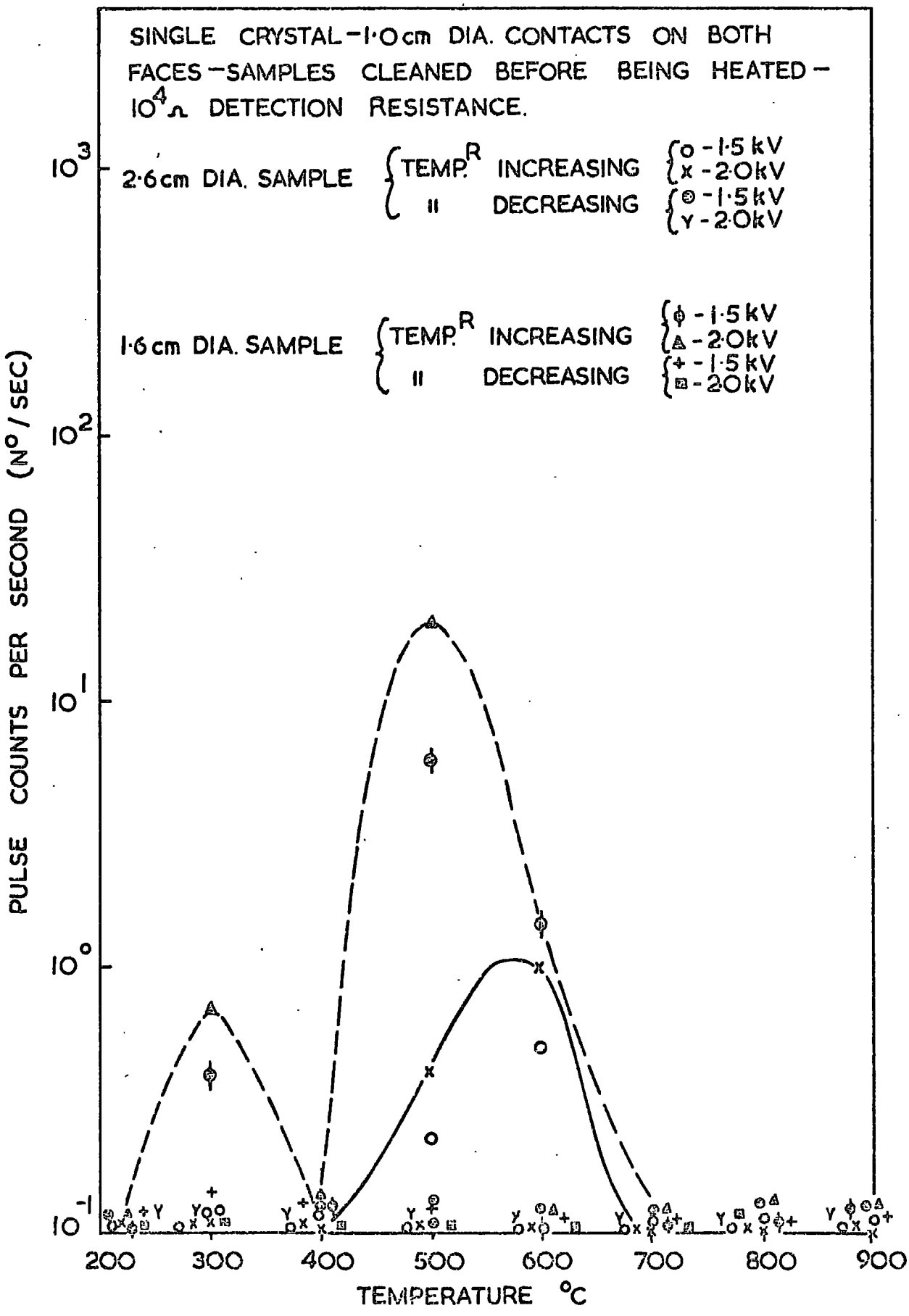

FIG. 6·43. PULSE COUNT RATE – v – TEMPERATURE FOR 2·6 cm AND 1·6 cm. DIAMETER SINGLE CRYSTAL SAMPLES IN ARGON AT 760 torr.

that the pulse shape does not vary much with temperature. However, due to the temperature dependence of the gas density, there is almost certain to be some effect of temperature on pulse shape. It is believed that, in the limited temperature range examined, this effect was obscured by the distribution of the pulse sizes and different levels of impurities in each measurement.

These results show clearly that pulse breakdown is only observed on single crystal alumina when the sample is chemically cleaned before being heated to 900°C. This means that pulse breakdown is induced by the cleaning process. The results also show that the cleaning process causes, in addition to pulse breakdown, the samples to have a higher d.c. conductivity on heating than on cooling.

CHAPTER 7

D.C. MEASUREMENTS ON ALUMINA

7.1 Introduction

D.C. conductivity measurements have been made on four single crystals and a sintered polycrystalline sample in the temperature range 200°C to 900°C in vacuum. The measurements on the single crystals, which were of a range of sizes, indicate that in this temperature region surface conduction is very important. The activation energy of the sample with the longest surface path, i.e. the sample on which surface conduction should be least important, is higher than previously reported for this temperature range and is in better agreement with the high temperature activation energies reported for electronic conduction than for ionic conduction, which has been predicted to predominate at these low temperatures. The conductivity of the sintered polycrystalline sample is some two orders of magnitude greater than those of the single crystals, and this is consistent with conduction along intergranular surface paths.

All four single crystals showed a higher conductivity on being heated to 900°C than on being cooled. This effect was only observed after samples had been chemically cleaned, in agreement with the work of Tucker and Gibbs,[3] and Champion.[4] Pulse breakdown, which is the same as the pulsing effect reported by the foregoing authors, was also only observed on heating samples to 900°C after chemical

cleaning (see Sec 6.7 for these results). D.C. measurements in argon pressures of 10^{-2} and 760 torr show that pulse breakdown can cause a significant increase in the measured d.c. current in single crystals. In contrast to single crystals, the sintered sample did not show a higher conductivity on being heated after chemical cleaning.

7.2 The D.C. Conduction of Alumina

There have been numerous measurements of the conductivity of alumina (see Cohen[23] for a review of the work prior to 1959). These measurements have been made over a wide range of temperatures, from 200°C to 1,700°C, and ambient conditions, from 1 atmosphere of air to 10^{-6} torr. Not only do the conductivity values and activation energies obtained by different authors show large differences (for example activation energies reported range from 0.25 to 4.6 eV), but also individual samples of the same author exhibit large variations. Because of this there has been a tendency to relate conductivity to sample purity, most authors explaining the results in terms of extrinsic electronic conduction in the bulk.

Prior to the work of Harrop and Creamer,[24] the basis for classifying alumina as an electronic conductor appears to be the work of Hartmann (1936),[25] who found that the conductivity of polycrystalline material was reversibly affected by heating in vacuum. The explanation offered by Hartmann being that alumina is an n-type semi-conductor which is reduced by heating in vacuum. However the temperature at

which Hartmann treated his samples, 450°C, appears to be too low for reduction of the bulk and consequently other explanations must be sought. Harrop and Creamer, who measured the electrical conductivity of single crystal alumina in the temperature range 800°C to 1,500°C, compared their results with the intrinsic ionic conductivity calculated from diffusion data. They found that ionic conduction was too small to account for the results and consequently concluded that alumina was predominantly an electronic conductor. Champion[4] drew a similar conclusion for the conductivity of single crystal alumina in the temperature range 250°C to 900°C.

More recently Matsumura[26] has measured the transport number of alumina by the galvanic-cell e.m.f. method in the temperature range 750°C to 1,500°C (see Davies[27] for a critical assessment of this method). This author's results, which are in agreement with other measurements by this method (Schmalzried[28]), indicate that alumina is predominantly electronic above 1,300°C and ionic below 800°C, while in between these two temperatures the conduction is mixed. In the temperature region where alumina is electronic, Pappis and Kingery[29] have investigated the effect of oxygen partial pressure on the thermoelectric e.m.f. They found the hot junction to be positive in high oxygen partial pressures, 10^{0}-10^{-10} atmospheres, and negative at low partial pressures, 10^{-10} atmospheres. Although this appears to indicate that alumina is n-type (Cusack[30]) at high oxygen pressures, Pappis and Kingery drew the opposite conclusion, namely that it was

p-type. It is not clear whether this discrepancy is due to an error on the part of the authors or the printers. At any rate the conclusion that alumina is a p-type semi-conductor at high oxygen pressures agrees with the observations of Matsumura.

In the temperature region which Matsumura predicts to be ionic, i.e. below 900°C, the situation is confusing, both positive and negative charge carriers being reported. Peters,[31] who measured a positive thermoelectric power over this range attempted to analyse his results in terms of simple semi-conductor theory. The analysis, which gave unrealistic values for carrier concentration and mobility, showed that the electrical properties of alumina at these temperatures could not be explained on a simple extrinsic semi-conductor model. Matsumura, in contrast to Peters, found the thermoelectric power of his crystals to be negative and suggested that alumina is an extrinsic ionic conductor at these low temperatures, the charge carrier proposed being aluminium ion vacancies. The only other published data on the thermoelectric power of single crystal alumina is the work of Dasgupta and Hart,[32] who found the sign of the thermoelectric power to change from negative to positive on heating crystals above 800°C. The conductivities of these samples, (separate publication by Dasgupta[33]), are rather high in comparison to most other published work suggesting extrinsic electronic conduction.

There does not appear to have been any specific investigation of surface conduction on single crystal

alumina. Tucker and Gibbs[3] examined the effects of chemical cleaning on conductivity and found it to be enhanced after cleaning. However apart from this work, which clearly demonstrates the importance of the surface, there has been no study of surface conduction on single crystal alumina. Heldt and Hasse[34] investigated the effect of humidity on the conductivity of sintered polycrystalline alumina and from this concluded that surface conduction predominated at low temperatures. Hensler and Henry[35] came to a similar conclusion from the dependence of conductivity on sample porosity. However since neither of these investigations were particularly systematic these conclusions are somewhat tentative.

7.3 Results

7.3.1 Effect of pulse breakdown on the d.c. current

Pulse breakdown produces an increase in the d.c. current of single crystals, the magnitude of which depends upon the count rate and the charge of the pulses. If pulse breakdown is particularly severe, the increase can be up to an order of magnitude. This contribution to the d.c. current from pulse breakdown can be seen in Figure 7.1, which shows the i-v curves for the 2.0 cm diameter sample at 700°C. The corresponding pulse breakdown measurements on this sample showed the pulse count rate to be 5×10^4 and 1×10^5 counts per second at 0.5 and 1.0 kV respectively. From oscillograms the mean pulse charge is approximately 1.0×10^{-11}

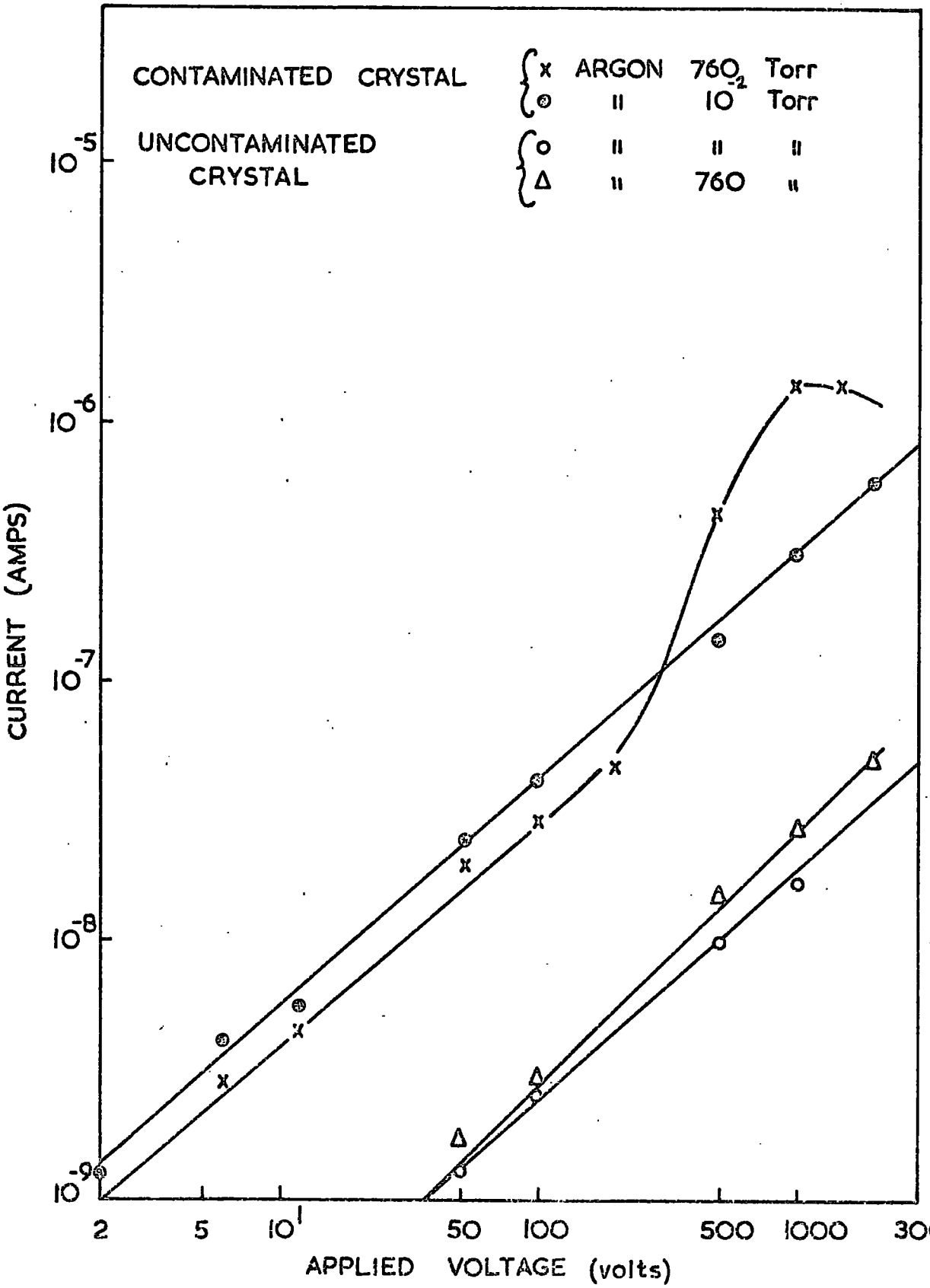

FIG. 7·1. I-V CURVES FOR 2·0 cm DIAMETER SINGLE CRYSTAL SAMPLE IN ARGON AMBIENTS AT 700°C.

coulombs, so that the mean pulse current from pulse breakdown measurements is 5×10^{-4} and 1.0×10^{-6} amps at 0.5 and 1.0 kV, which is in good agreement with the d.c. current.

When the pulse count rate has been very low, typically in the order of $^{1}/_{CR}$ where CR is the time constant of the d.c. measuring circuit, it has been possible to observe individual pulses with the pen recorder. Figure 7.2 shows an example of the trace seen. At high count rates, i.e. > 100 counts per sec, individual pulses cannot be distinguished and consequently the d.c. current through the sample shows an appreciable increase on the expected value. Between these two extremes lie the pulse count rates, typically 4 counts per sec, which cause the d.c. current level to fluctuate, see Figure 7.2. Tucker and Gibbs, because they were unaware of the effects of temperature on pulse count rate mistook the more irregular current traces observed at the higher temperatures for being more complex pulses, which they attributed to the complicated chemical treatment given to the sample. Oscillograms of the pulses show that this is not the case.

7.3.2 Variation of current with voltage

The i-v characteristics of the samples were measured at 100°C intervals on heating and cooling. When pulse breakdown did not occur, it was found that $I \alpha V^{K}$ on all samples, where k varied between 0.9 and 1.1 depending on the sample. Hence to a first approximation the samples obeyed Ohm' law. The effect of voltage polarity on resistance

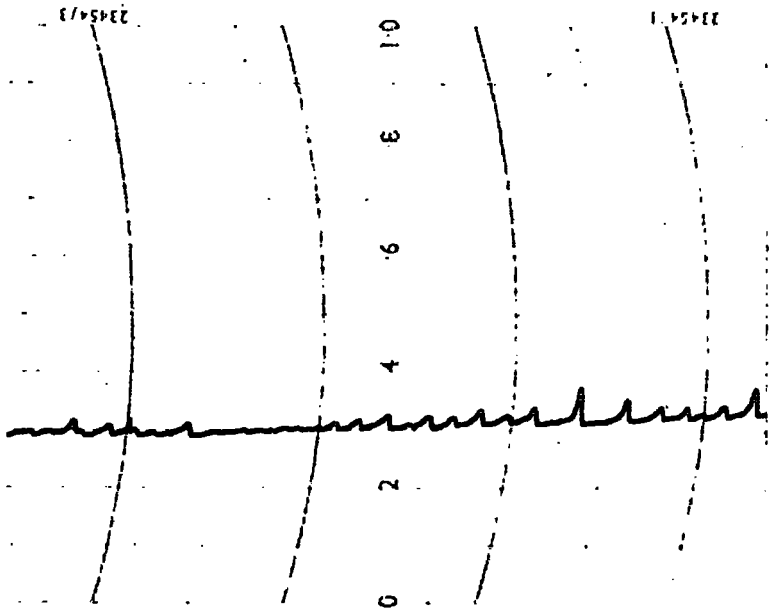

(i) Individual pulses resolved. Trace recorded at 500°C and -1.0 kV with $10^{10}\Omega$ detection resistor.
Scale; Abscissa 30 secs/inch. Ordinate 1 mV/division.

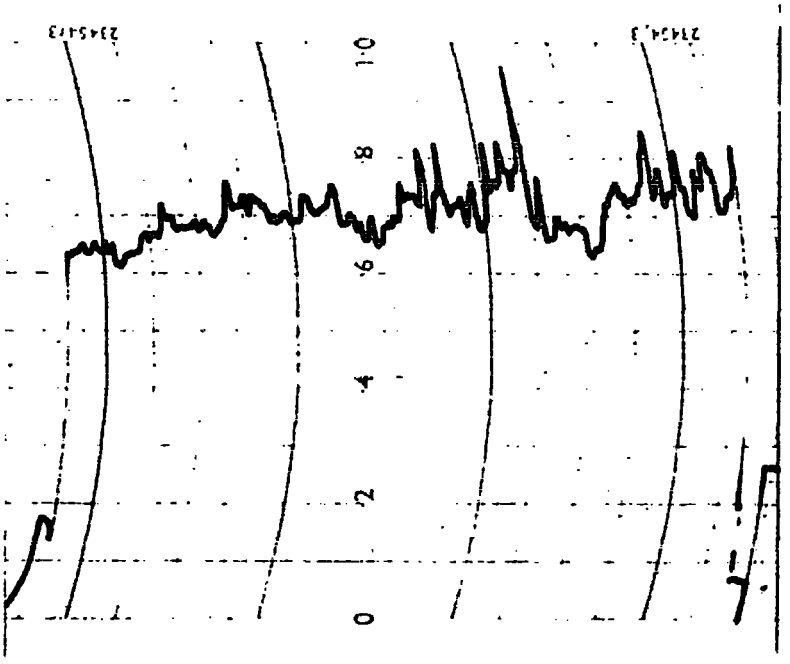

(ii) Individual pulses not resolved. Trace recorded at 700°C and -0.1 kV with $10^{7}\Omega$ detection resistor.
Scale; Abscissa 30 secs/inch. Ordinate 3 mV/division.

Fig. 7.2 Effect of pulse count rates of 0.2 counts/sec (i) and 4 counts/sec (ii) on the d.c. current of single crystal alumina.

was examined on all samples at 600°C. The I-V curves obtained at 600°C, on cooling samples from 900°C, are shown in Figure 7.3. It can be seen that the resistance of all five samples is independent of voltage polarity. No further examination of voltage polarity was made.

7.3.3 The effect of ambient gas pressure on d.c. measurements

No significant dependence of conductivity on argon pressure was detected. Figure 7.1 shows the effect of the argon gas pressure on typical i-v curves. From this it can be seen that, although a small increase in the resistance of the sample does occur as the pressure is reduced, the effect is not significant in view of the accuracy of the measurements.

The conductivity of the single crystals was measured at several temperatures as a function of ambient air pressure as well. The conductivity at an air pressure of 10^{-2} torr was not significantly different from that at the same pressure in argon. However the conductivity of all the crystals was found to increase as the ambient air pressure was raised. The increase was largest on the 1.0 cm diameter sample and smallest on the 2.5 cm one. Typically the conductivity of the 1.0 cm diameter sample increased by a factor of 2-3 on raising the ambient air pressure from 10^{-2} to 760 torr.

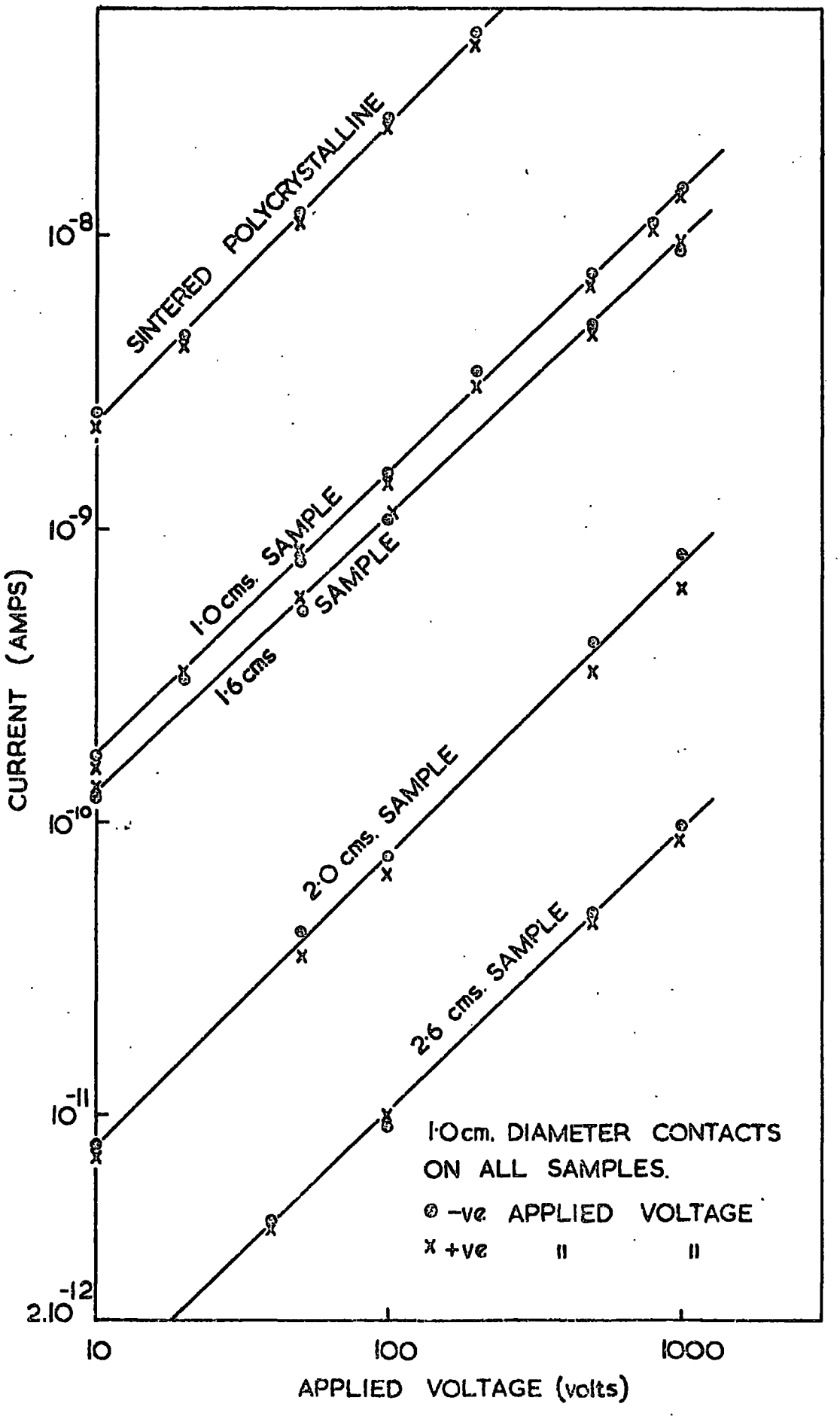

FIG. 7·3. I-V CURVES FOR POLYCRYSTALLINE AND SINGLE CRYSTAL ALUMINA SAMPLES IN AN ARGON AMBIENT OF 10^{-2} torr AT 600°C.

7.3.4 The effect of chemical cleaning on the variation of conductivity with temperature

A detailed study was made of the effect of sample cleaning on the conductivity of one of the single crystal samples, the 2.0 cm diameter one. The results obtained after the initial cleaning are shown in Figure 7.4. On heating the sample exhibited a peak in conductivity which was not seen on cooling. The temperature at which this peak occurs appears to be between 600°C and 700°C. The difference in conductivity between heating and cooling cycles also indicates the presence of a lower temperature peak at around 400°C, in agreement with the work of Tucker and Gibbs, who observed a similar peak at this temperature after HCl contamination of their sample.

After the first heating and cooling cycle the sample was removed from the holder and fresh contacts were sputtered on the faces. The only chemical treatment given to the sample during this time was drying in alcohol immediately before remounting in the sample holder. The conductivity curve obtained after this treatment can be seen to be in good agreement with the cooling curve of the previous run, see Figure 7.4. There is no peak in conductivity either on heating or cooling the sample. Below 550°C, the heating curve exhibits a slightly higher conductivity than the cooling curve, indicating that either the resputtering process or exposure to the atmosphere can affect the conductivity.

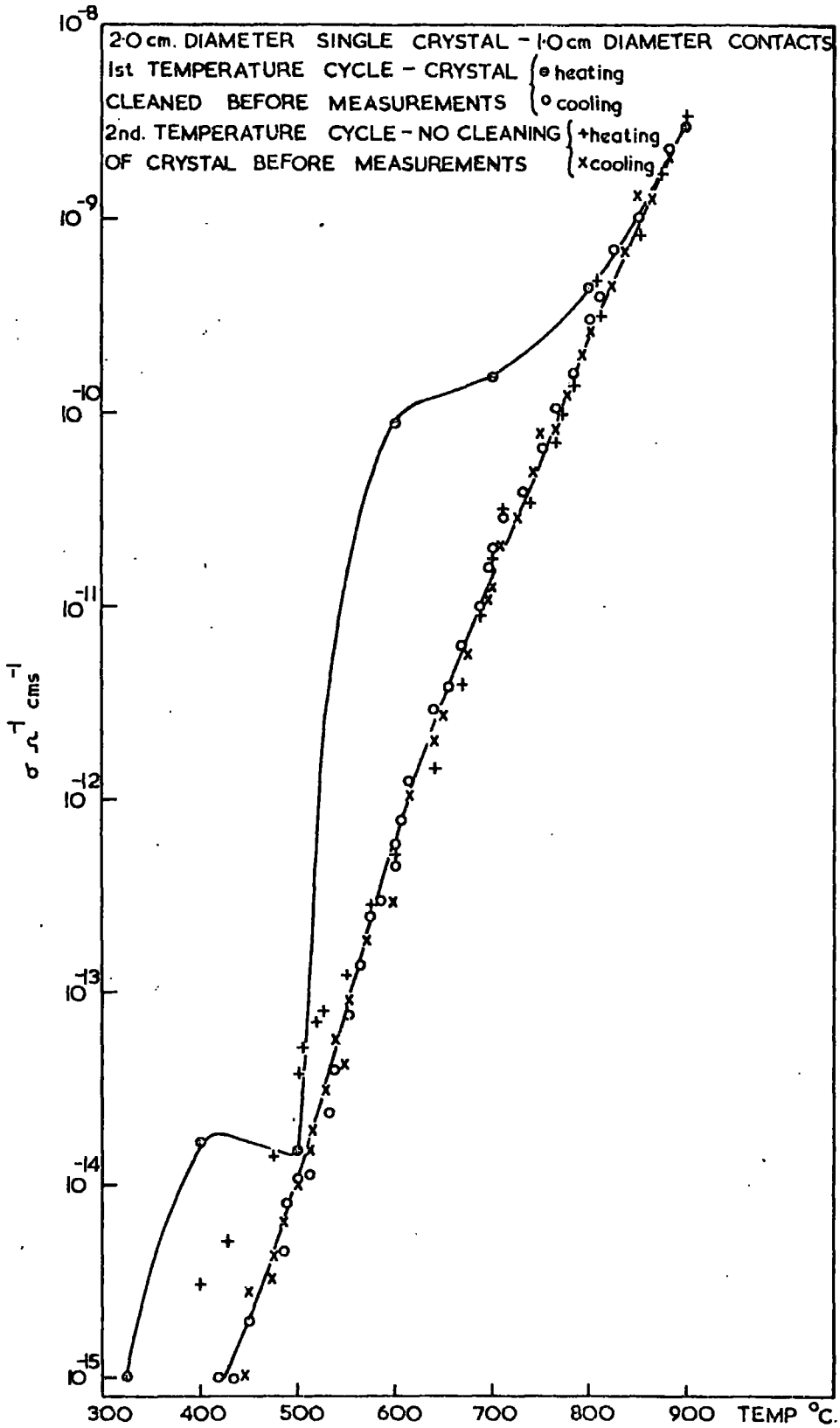

FIG. 7·4. VARIATION OF CONDUCTIVITY WITH TEMPERATURE OF 2·0 CM. DIAMETER SINGLE CRYSTAL SAMPLE IN ARGON AT 10^{-2} torr. (1st and 2nd TEMPERATURE CYCLES)

After this second temperature cycle the sample was cleaned normally and new contacts were deposited. The results obtained after this procedure are shown in Figure 7.5. A peak in conductivity is again seen on heating the sample. However the peak appears to occur at a lower temperature than previously, i.e. between 550°C and 600°C rather than 600°C and 700°C. Similar conductivity peaks have been observed on the other single crystal samples after chemical cleaning. These peaks show a similar spread in the temperature at which they occur; the temperatures being 700 $\pm$ 50°C and 550 $\pm$ 50°C for the 1.0 and 2.6 cm diameter samples respectively, see Figure 7.6. Although the 1.6 cm diameter sample does not exhibit any definite peak, see Figure 7.7, a higher conductivity is observed on heating the sample after cleaning. Tucker and Gibbs failed to observe a peak on their sample after the dislocation density had been increased from 10^6 to 10^7 per sq cm by bending. The absence of a peak on the 1.6 cm sample is probably due to a higher dislocation density.

It is not really possible to estimate activation energies for the contamination peaks from the limited data available, even assuming that $\log \sigma \propto {}^{1}/_{T}$ in the low temperature region before the peak. The best that can be said is that there does not appear to be a single activation energy in this temperature range. However without further work on this topic no definite conclusion can be drawn. It is interesting to note that the height of the conductivity peak appears to be related to the pulse count rate, the greater

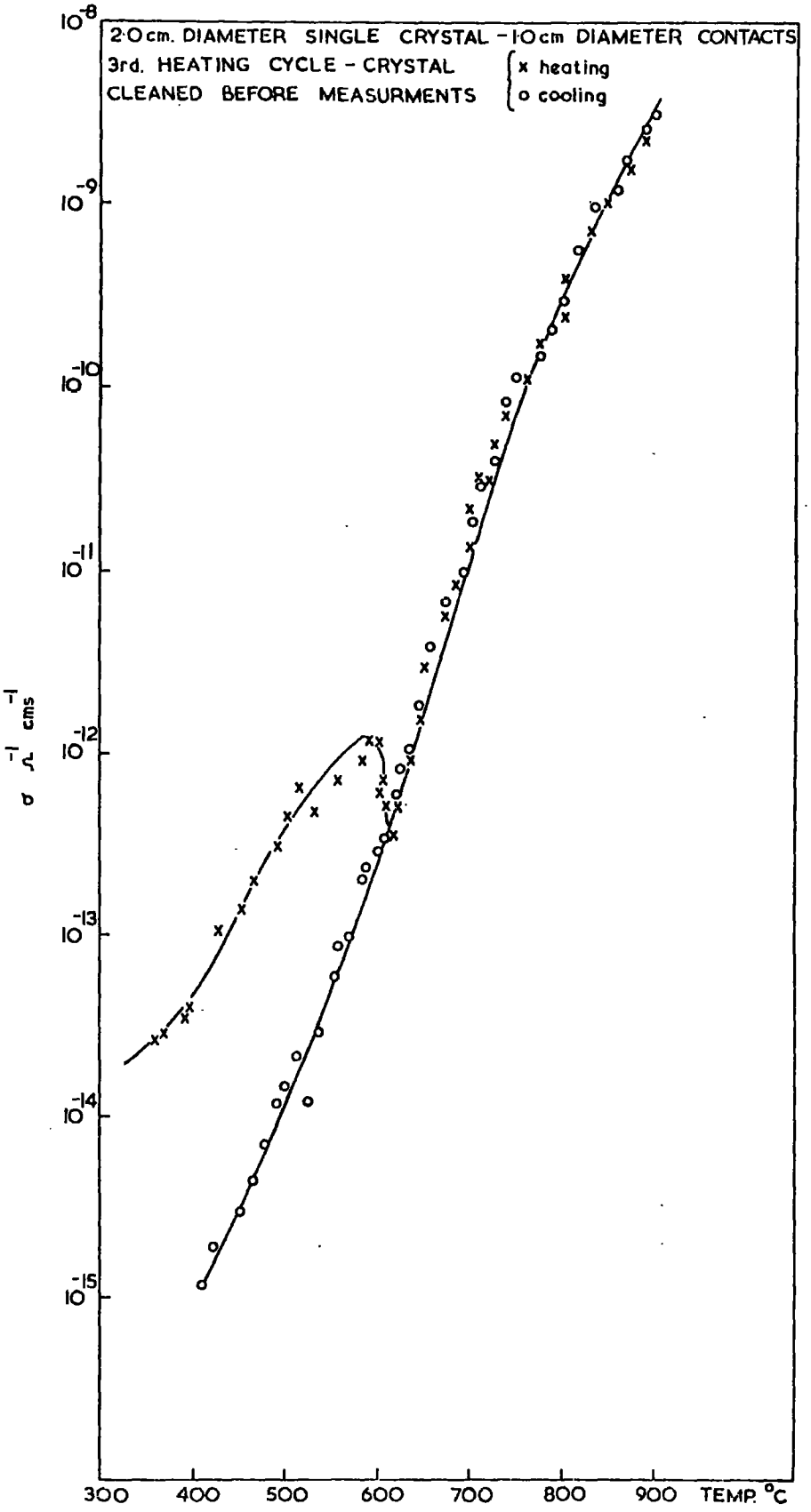

FIG. 7·5 VARIATION OF CONDUCTIVITY WITH TEMPERATURE OF 2·0 cm DIAMETER SINGLE CRYSTAL SAMPLE IN ARGON AT 10^{-2} torr. (3rd TEMPERATURE CYCLE)

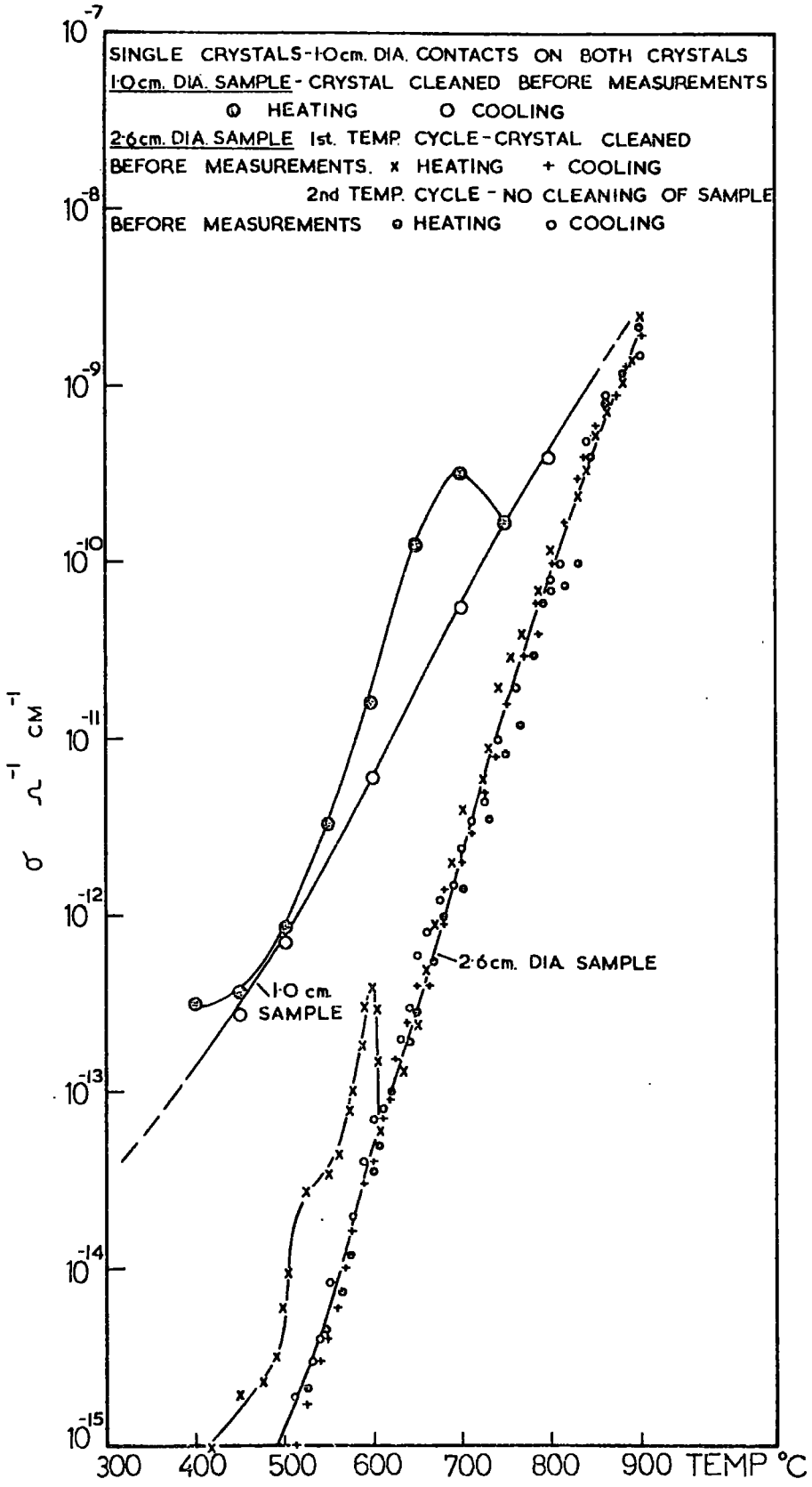

FIG. 7·6 Variation of conductivity with temperature of 1·0 and 2·6 cm. diameter single crystal samples in argon at 10^{-2} torr.

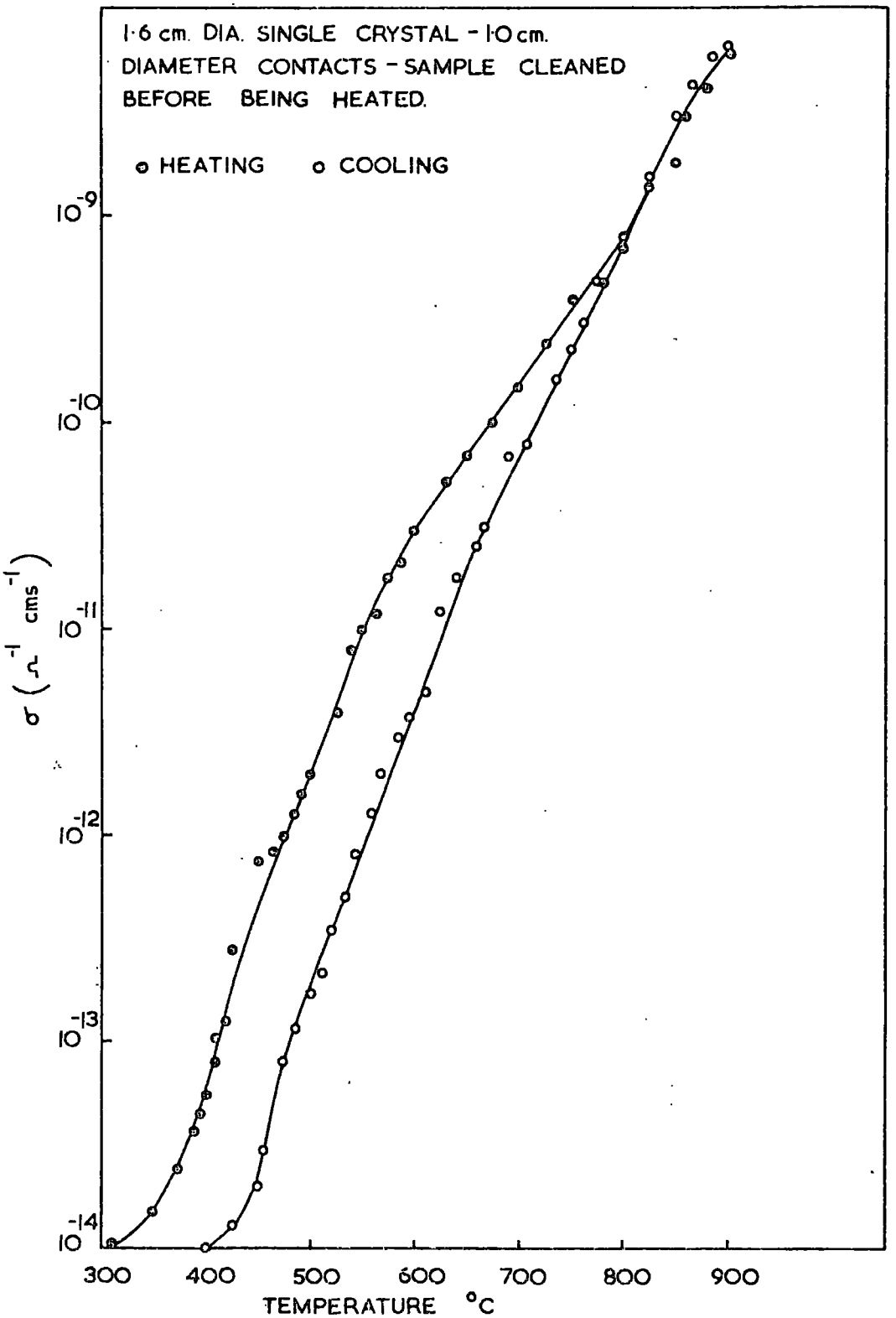

FIG. 7·7. VARIATION OF CONDUCTIVITY WITH TEMPERATURE OF 1·6 cm. DIAMETER SINGLE CRYSTAL SAMPLE IN ARGON AT 10^{-2} torr.

the conductivity of the contamination peak the greater the pulse count rate. This could explain why Champion observed pulsing at the comparatively low voltage of 100 v, since from the magnitude of his conductivity peaks his samples appear to be heavily contaminated.

7.3.5 Variation of conductivity with temperature

On both the 2.0 and 2.6 cm diameter single crystal samples reproducible results are obtained once the contamination peak is removed. Since Champion obtained similar results it seems reasonable to assume that the cooling curves of the 1.6 and 1.0 cm diameter samples represent the final conductivity values. Consequently these are compared with the conductivities of the other samples in Figure 7.8. In the higher temperature range, i.e. $^{1}/T \ll 1.1 \times 10^{-3}$ o K^{-1}, the conductivity can be represented by $\sigma = \sigma_o \exp {}^{-\varphi A}/_{KT}$ for all four samples. The activation energies for the samples in this region are 3.9, 3.1, 2.3 and 1.9 eV for the 2.6, 2.0, 1.6 and 1.0 cm diameter samples respectively. At lower temperatures, $\log \sigma \not\propto {}^{1}/T$ and hence the curves cannot be expressed in terms of a single activation energy. The results indicate a dependence of conductivity on sample diameter, the larger samples having a very much lower conductivity than the smaller ones. Consequently the results have been replotted in terms of surface conductance in Figure 7.9, along with the results of Champion. The spread in conductivities and activation energies between samples is very much lower in this case, the activation

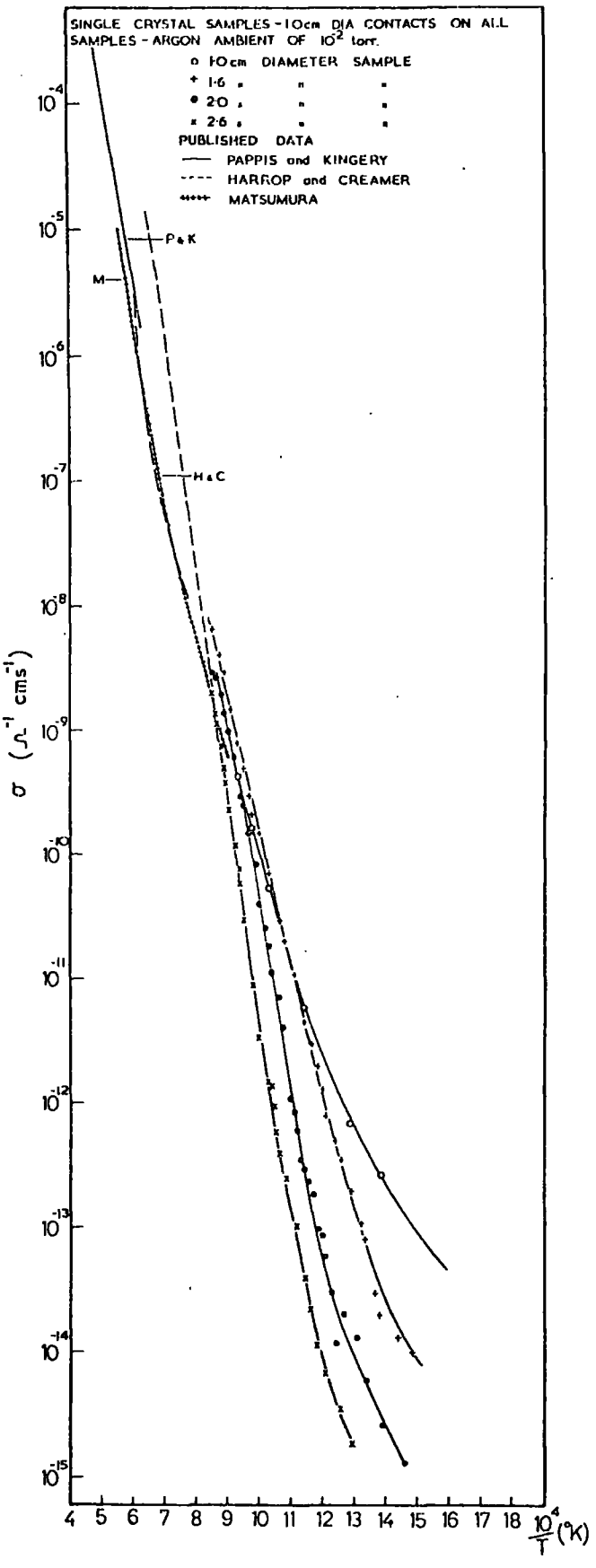

FIG. 7·8 Electrical conductivity of single crystal alumina samples in argon at 10^{-2} torr as a function of temperature.

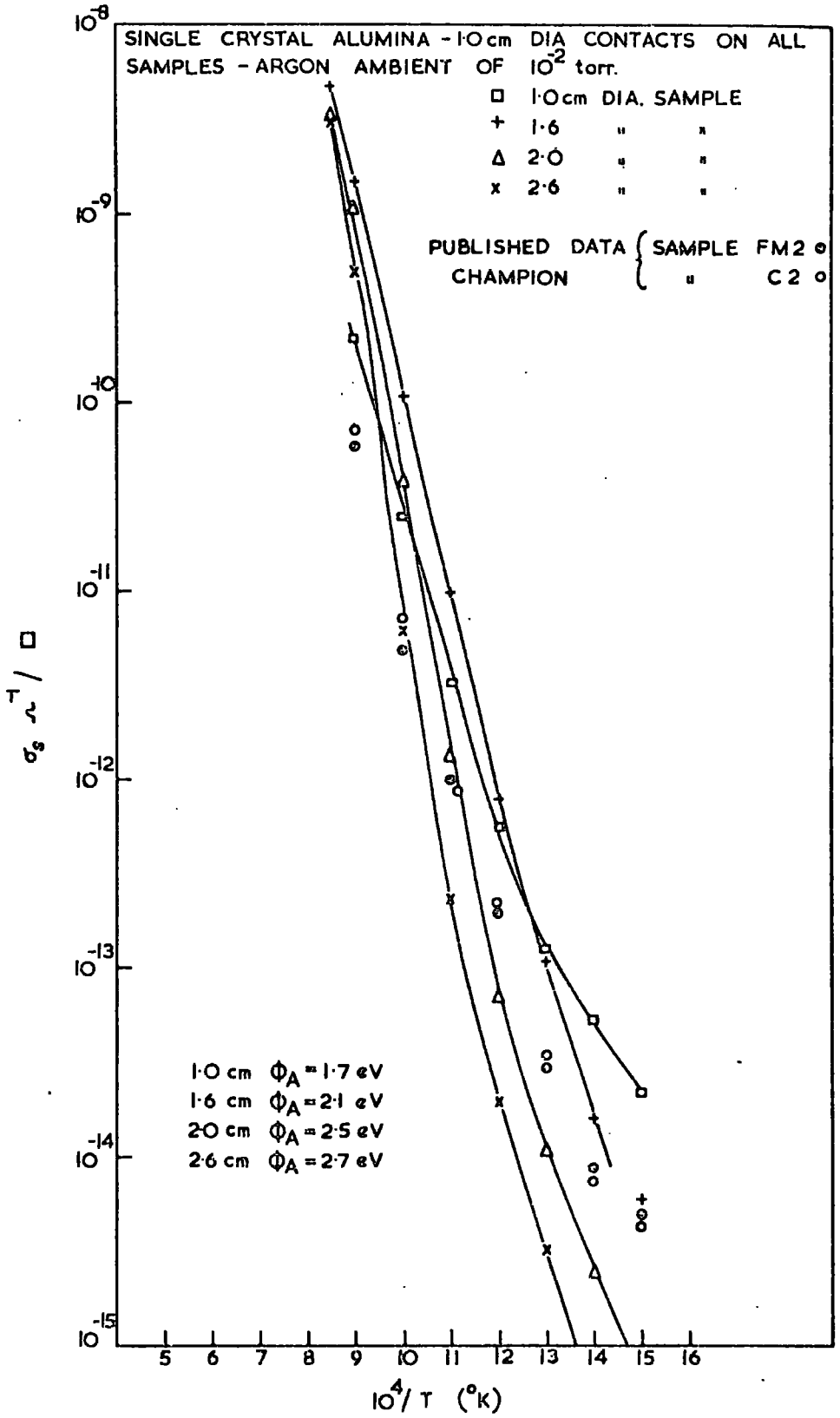

FIG. 7·9. BULK CONDUCTIVITY VALUES OF FIG. 7·8 REPLOTTED IN TERMS OF SURFACE CONDUCTANCE AND COMPARED WITH PUBLISHED DATA.

energies being 1.7, 2.1, 2.5 and 2.7 eV, (for samples of increasing diameter).

The results of the d.c. measurements on the sintered polycrystalline sample are shown in Figure 7.10. The lower of the two curves was recorded at the same time as one of the pulse count curve shown in Figure 6.39 while the upper curves were recorded on a separate occasion. The difference between the two curves is due to the contacts. The lower curve, which was recorded with different area contacts on the two faces of the sample has been converted to conductivity by multiplying by the geometry factor for the upper curve. Consequently the upper curve represents the true conductivity of the sample while the lower curve the comparative resistance. Both these measurements were made on heating the sample after chemical cleaning. The cooling curves, which have been omitted for the sake of clarity, were the same as the heating curves. From this it can be concluded that there is no significant effect of contamination on the conductivity of sintered polycrystalline alumina. The activation energy for the portion of the conductivity curve above 450^{o}C is the same as for the 1.0 cm diameter single crystal sample, i.e. 1.9 eV.

7.4 Discussion of the D.C. Measurements

The pulse breakdown results of Section 6 and the d.c. conductivity results of Section 7.3.4 show that both pulse breakdown and the d.c. contamination effects are caused by cleaning the sample chemically. This agrees with the

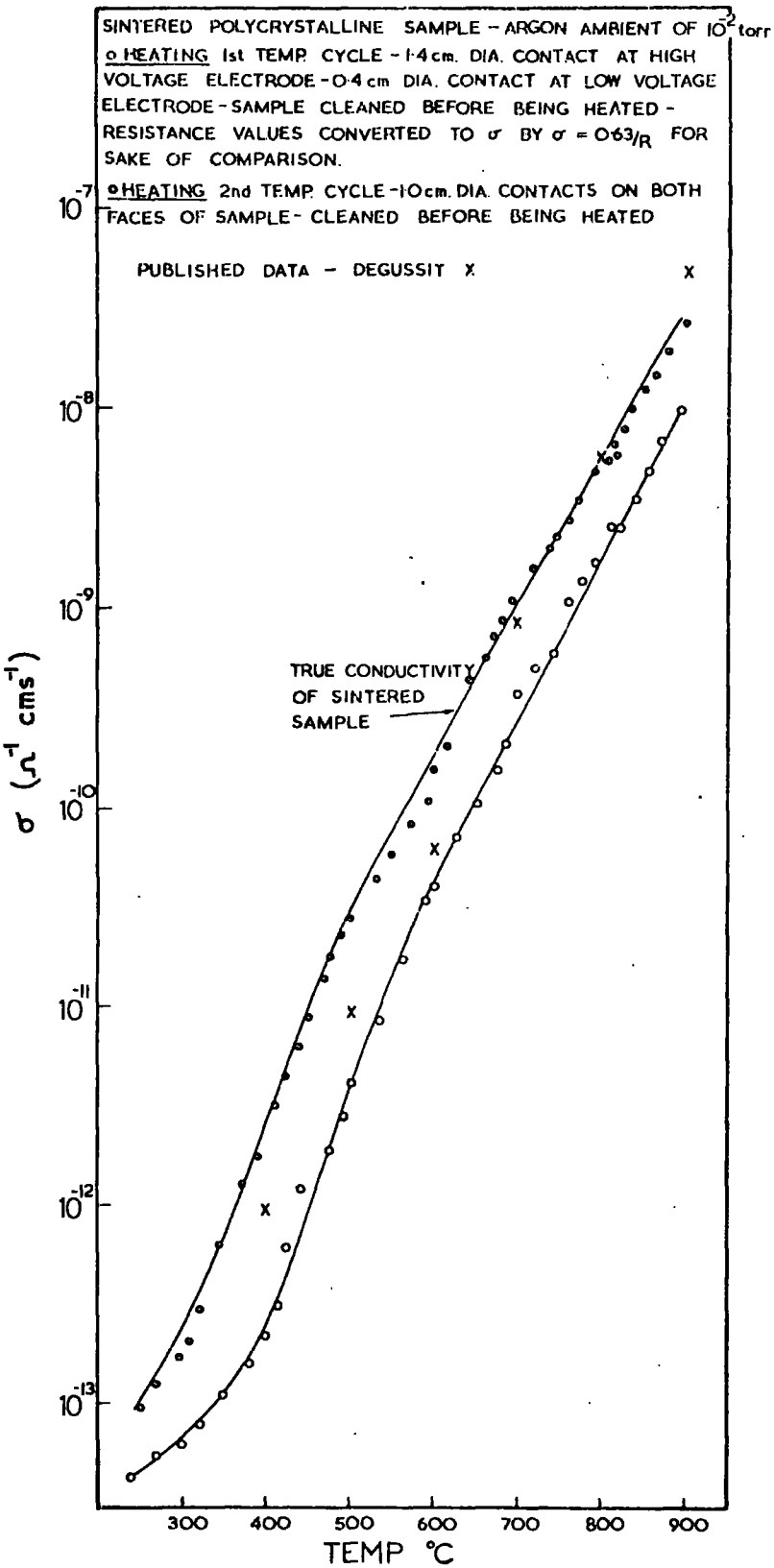

FIG. 7·10. Electrical conductivity of sintered poly-crystalline alumina as a function of temperature in argon at 10^{-2} torr.

results of other authors who have investigated the effect on the d.c. conductivity of chemical cleaning. Tucker and Gibbs, and Champion both observed peaks in the conductivity of alumina on heating after chemical cleaning. These authors also observed pulsing effects after chemically cleaning the alumina, Champion finding pulsing in the temperature region of the contamination peak and Tucker and Gibbs at slightly above the temperature region of the peak.

Tucker and Gibbs postulated an elaborate theory, based on the flow of impurity ions along dislocations, to explain their results. They suggested that ions were absorbed from the cleaning solution into a dislocation network at low temperatures and were subsequently expelled from the network at higher temperatures, the pulses being produced when the ions were suddenly 'drained' from the network. Champion felt that his results supported the mechanism proposed by Tucker and Gibbs because of variations in the pulse activity of samples with different dislocation densities. However since Champion did not examine the reproducibility of the contamination effects this interpretation must be treated with reserve, particularly so in view of the present work, which shows variations in pulse activity between successive measurements on the same sample.

The model proposed by Tucker and Gibbs does not explain how the ions are able to diffuse into the dislocation network. Since the ions diffuse into the dislocations during the cleaning process the activation energy associated with this diffusion must be small for any appreciable amount of

absorption. This would seem to eliminate the possibility of the ions diffusing substitutionally, since the activation energies for cation and anion vacancy diffusion along a dislocation are unlikely to be very much less than 2.2 and 2.5 eV respectively, the bulk values, and imply diffusion via interstitial sites. From the crystal structure of oxides however interstitial anions are unlikely because of their size (Kroger[36]), so that the possibility of either oxygen or chlorine ions diffusing interstitially may be excluded. Hence the only ion from the cleaning solution which could diffuse into the dislocation network is hydrogen, which has apparently been suggested by Gibbs.[37] However, since free hydrogen ions do not exist in solution (Glasstone[38]), it is difficult to see how this could occur, unless of course a surface reaction is involved.

From the above it seems unlikely that any of the ions from the solution diffuse into dislocations during the cleaning process. If the ions do not diffuse into the crystal they must become absorbed on the crystal surface. Tucker and Gibbs used several cleaning solutions and found that the temperature at which the contamination peak occurred was different for each solution. They attributed this to the absorption of different ions from each solution. However from the variations in the temperature of the contamination peak observed in this work with one standard cleaning solution, it appears that factors other than the cleaning solution govern the temperature at which the peak occurs, for example the rate of heating, orientation of

crystal, etc. Hence it seems probable that the same ions or molecules were absorbed on the crystal surface in the various cleaning solutions used by different workers. Since water molecules are the only ones common to all solutions it seems reasonable to assume that, on a desiccant as good as alumina, these are the contaminating molecules.

Recent surface studies by Brennan and Pask[39] and Webster et al[40] show that hydroxyl ions are present on the surface of the ionic crystals, alumina and magnesia, at temperatures up to 900°C. These hydroxyl ions appear to be OH^- (Peri and Hannan[41]). If these ions are formed by the thermal dissociation of absorbed water molecules, then at low temperatures the alumina surface will be covered by absorbed water molecules and at high temperatures by a layer of hydroxyl ions. Hence the two contamination peaks which are observed on heating alumina could be due to these absorbed molecules, the low temperature peak between 150°C and 400°C being caused by the absorbed water molecules and the high temperature one between 400°C and 800°C by the hydroxyl ions.

Hence an alternative to Tucker and Gibbs' explanation may be proposed. On cleaning alumina in dilute aqueous solutions water molecules become absorbed on the surface. These water molecules dissociate on heating, forming a surface layer of OH^- ions. These hydroxyl ions, probably because they are chemisorbed, cause the main contamination peak in the conductivity. By a temperature of 900°C the hydroxyl ions are desorbed with the result that the conductivity of the alumina falls to the normal value. The

pulsing effects, which the results of Chapter 6 show to be gas discharges, are caused by the desorption of the hydroxyl ions. The possible ways by which this can occur are discussed in Chapter 8.

The way in which the hydroxyl ions affect the d.c. conductivity will now be considered. Tallan and Detwiler[42] have pointed out that the surface of alumina could be more conducting than the bulk because of the tendency of space charges to form at the surface of ionic crystals. These space charges build up at the surface of crystals, in which the energy to form a cation vacancy is different to that to form an anion vacancy, to maintain equal numbers of defects in the crystals. Hence if the energy to form a cation vacancy is less than that to form an anion vacancy, which it is in alumina, the interior of the crystal will contain an excess of cation vacancies and the surface an excess of anion vacancies and cations. This favours the formation of further anion vacancies and maintains an equilibrium concentration of defects in the crystal. The surface of the crystal, which will contain an excess of metal ions, can therefore behave like an n-type semi-conductor because of the energy states of the anion vacancies acting as donor centres within the forbidden gap. Below this n-type region will be a p-type region due to the cation vacancies.

The presence of chemisorbed or absorbed ions on the surface will alter the concentration of defects in the space charge layer because of the extra charge. Hence the effect of chemisorption will be to reduce the number of energy

states due to the defects while introducing additional states within the forbidden gap due to the chemisorbed impurities themselves. If the concentration of the energy states due to the chemisorbed impurities is greater than those due to the defects, and the activation energy associated with the impurities is not too large, a change in the activation energy of the conduction process could be observed as the hydroxyl ions are formed, by the dissociation of the water molecules, on the alumina surface. At low temperatures the activation energy of the conduction process could also be affected by the absorption of gas molecules, as has been observed.

Tallan and Detwiler suggested that these space charges could be responsible for the dielectric loss effects which occur in alumina. They examined these effects at temperature between -160°C and 400°C and found them to be affected by the type and pressure of the ambient gas and also chemical cleaning. They found that the results of these dielectric loss measurements were explained by interfacial polarisation rather than by dipolar relaxation, suggesting the presence of surface charges. A dielectric loss peak was also found by Tallan and Graham[43] in measurements on single crystal over the temperature range 700°C to 1,200°C. These authors observed that the activation energy of the loss peak was affected by the heat treatment given to the samples, the activation energies being lower on heating than on cooling. They suggested that this could be due to reduction of the crystal surface. Tallan and Graham also interpreted their

results in terms of interfacial polarisation, although they felt that the results on the undoped crystals, in contrast to the deliberately doped crystals, indicated a high resistivity surface layer rather than a low one.

On this space charge model the activation energies of the dielectric loss peaks should represent the activation energy for surface conduction, hence if alumina does conduct via a surface layer the activation energies determined from d.c. conductivity and dielectric loss measurements should be the same. Tallan and Detwiler found the activation energies of the dielectric loss peak at low temperatures to be 0.5 eV in oxygen and hydrogen atmospheres and 0.25 eV in vacuum. This agrees very well with the activation energies determined from conductivity measurements at these low temperatures, Champion, whose measurements were made in air, observing the same activation energy, 0.5 eV, and Hartmann finding similar values, 0.4 eV and 0.25 eV in air and vacuum respectively. In the higher temperature region in which Tallan and Graham made their measurements there is a similar agreement between the activation energies determined by the two methods. Tallan and Graham finding the activation energies of the undoped samples to be 1.6 ± 0.2 eV and 2.4 ± 0.1 eV before and after reduction of the alumina respectively. These values are in good agreement with the reproducible activation energies measured by Peters and Champion below 900°C, 1.7 eV being measured by both authors, and by Stulova and Shalabutov[44] at higher temperatures, 2.5 eV. Similar activation energies to those determined by

dielectric loss measurements have also been measured by Dasgupta, Harrop and Creamer, and Matsumura. Hence the good agreement between the d.c. conductivity and dielectric loss measurements support the surface space charge model.

The higher activation energy observed by Tallan and Graham on cooling appears to be due to reduction of the surface of the alumina. However, whereas Tallan and Graham thought it was due to the surface becoming highly non-stoichiometric, recent work indicates that it is associated with a change in surface structure. L.E.E.D. studies by Charrig[45,46] and Chang[47] show that at temperatures of about 1,000°C a change in the surface structure of the 0001 face of alumina occurs. Both these authors found this change in structure to be consistent with the formation of a layer of AlO, in agreement with the oxygen deficient surface layer proposed by Brennan and Pask. This change in surface structure may explain a number of electrical effects observed at these temperatures, in particular the change in the sign of the thermoelectric power observed by Matsumura, Dasgupta and Champion. That this is a surface effect is supported by the pressure dependence of the temperature at which the change in carrier sign occurs (Dasgupta).

From the above it can be seen that many of the low temperature electrical properties of alumina can be explained by a surface space charge model. These include the increased conductivity after cleaning, the changes in activation energy on heating and the pressure dependence of the conductivity. The present d.c. conductivity measurements can also be

explained by this model if it is assumed that the conductivity of the space charge layer is not too different from the bulk. Figures 7.8 and 7.9 show that the results of measurements on the single crystal samples are not in very good agreement when plotted in either bulk conductivity or surface conductance. This suggests that a mixture of bulk and surface conduction is being measured on these samples, particularly in view of the increase in activation energy with surface path. Hence, if the surface and bulk conductances are not too different, surface conduction may be expected to predominate on the smallest sample and bulk conduction on the largest. On this basis it seems reasonable to compare the activation energy of the smallest sample with other low temperature values and the activation energy of the largest crystal with the high temperature bulk values.

The activation energy of the 1.0 cm diameter single crystal sample, 1.9 ± 0.4 eV, compares favourably with Champion's high temperature value of 1.7 eV. If this is the activation energy of the surface layer, as previously suggested, Champion's results should be considered in terms of surface conductance. There is a considerable spread in the conductivity values obtained by Champion on different samples. Of his four samples, three have the same surface area and one has a smaller surface area. This latter sample also has the highest conductivity. The spread in Champion's results is therefore reduced by replotting his conductivity values in surface conductance, as can be seen from Figure 7.9. The activation energies of the samples are also in better

agreement when plotted in surface conductance, Champion's samples having a surface activation energy of 1.6 eV compared with 1.7 eV for the 1.0 cm diameter sample. Thus both Champion's and the present work indicate that surface conduction is important on alumina below 900°C.

The results of the measurements on the sintered polycrystalline sample are in agreement with the surface conduction model. Because the sintered sample consists of a large number of compressed granules, the current will pass through the bulk of the sample along the surface of the grains, as suggested by Henry and Hensler. Hence because of the very large effective surface area of the sample the conductivity of the sintered sample will be very much greater than the single crystal. However, although the conductivity will be greater, the activation energy will be similar to that of the single crystals on which surface conduction predominates, i.e. the 1.0 cm diameter sample, which it is. The fact that the contamination effects were not detected on the sintered sample, even though they are present, shows that the conduction along the real surface of the sample is insignificant compared with the conduction along the surfaces of the grains in the bulk, as expected from the higher conductivity of this sample.

The sample with the largest surface area should exhibit the smallest surface conduction. Consequently it seems reasonable to compare the activation energy of this sample 3.9 ± 0.8 eV with the known bulk values. Since Matsumura's work indicates that alumina should be predominantly ionic in the temperature range studied, the measured activation data

may be compared with established diffusion data. Oiski and Kingery[48] measurements of intrinsic and extrinsic oxygen diffusion gives values for the activation energies of 6.6 ± 1.1 eV and 2.5 ± 0.4 eV respectively. Since neither of these agree with the measured value it is unlikely that oxygen diffusion is responsible for the observed conductivity. Intrinsic or extrinsic aluminium ion conduction does also not appear likely. Paladino and Kingery[49] measuring an activation energy of 4.9 ± 0.7 eV for intrinsic diffusion and estimating the activation energy for extrinsic diffusion as 2.2 eV (the error being ± 1.3 eV). Comparison of the activation energy with the higher temperature measurements of extrinsic electronic conduction is in better agreement, Pappis and Kingery and Matsumura reporting an activation energy of 3.0 eV and Harrop and Creamer 4.26 eV. None of these authors give any values for the error of their measurements but since all these values fall almost within the error of the present work this is not important. Hence the activation energy of this sample is in better agreement with the activation energies of electronic rather than ionic conduction. If the conductivity of the bulk is electronic it seems likely that the surface will be also and so that the activation energy of 1.8 eV may be ascribed to the electronic conduction in the surface.

It is interesting to compare the activation energy for the 2.5 cm diameter sample with that for intrinsic conduction. Harrop[50] has estimated the temperature dependence of the forbidden gap, from the optical work of Gilles[51] and

Loh,[52] as Ei = 10.7 - 0.0024 T (K) eV. On this basis one may estimate the forbidden gap at 800°C as 8.1 eV and hence the activation energy for intrinsic conduction at this temperature is 5.35 eV, which is not in agreement with the activation energy of 3.9 eV for the largest sample. Hence if the conductivity of this sample is extrapolated to higher temperatures, a comparison with Harrop and Creamer and Pappis and Kingery shows that the conductivity of the sample is too high to be intrinsic. Thus if bulk conductivity is being measured it must be extrinsic.

For a normal extrinsic semi-conductor which is uncompensated the activation energy of conduction is half the energy level of the impurity. In this sample this would mean that the impurity level is close to the band edge, if a donor level then just above the valence band, which is very unlikely. Hence it appears that the normal extrinsic semiconductor model cannot be applied to alumina, as found by Peters. This result would seem to support Harrop's contention that polaron 'hopping' theory is a more appropriate model for conduction in alumina. Consequently if a jump energy of 2.5 eV is used (Harrop) the depth of the impurity level is 2.8 $\pm$ 0.6 eV, a value similar to the activation energies for surface conduction. This suggests that the difference between the bulk and surface activation energies may be due to the different mechanisms of conduction, polaron hopping in the bulk and extrinsic semi-conduction in the surface.

7.5 Conclusion

The d.c. conductivity of single crystal alumina in the temperature range 300°C to 800°C is increased by cleaning samples in a dilute solution of HCl. The conductivity returns to the normal reproducible value after samples are heated to 900°C, showing that the contaminating agent is removed by thermal treatment. The effect is attributed to absorption of water molecules from the cleaning solution and it is thought that at elevated temperatures the water molecules dissociate to hydroxyl ions. The presence of these ions is considered to modify the electrical properties of the surface and cause the increase in the conductivity.

The normal d.c. conductivity of single crystal alumina in the temperature range 300°C to 900°C indicates a dependence of conductivity on sample dimensions. It is suggested that this is due to the surface of alumina being more conducting than the bulk as a result of the formation of space charges at the surface. The good agreement between the activation energies of the smallest single crystal and the sintered polycrystalline sample supports this model. The lack of increase in the d.c. conductivity of sintered polycrystalline alumina after chemical contamination also agrees with this model since in this case it seems likely that the current passes through the bulk of the sample along the surface of the grains.

The activation energy for surface conduction is 1.7 eV and that for bulk conduction, 3.9 eV. This latter value does not agree with the expected activation energy for either

intrinsic or extrinsic ionic conduction, so that it is unlikely that single crystal alumina is an ionic conductor below 900°C. The relatively high value of the bulk activation energy also makes it unlikely that alumina is a simple extrinsic electronic conductor. Hence it seems that conduction in alumina at these low temperatures could be due to polarons, as suggested by Harrop.

Pulse breakdown produces an increase in the measured d.c. current, with the result that the sample is no longer ohmic. This increase is due to the d.c. measuring circuit integrating the pulses.

CHAPTER 8

DISCUSSION

In Chapter 6 a large number of results on pulse production were presented. These results are summarized in Section 8.1 before discussing them in detail and relating them to the d.c. conduction measurements of Chapter 7.

8.1 Summary of Pulse Breakdown Results

Two distinct types of pulse have been observed in pulse breakdown studies on alumina. The first, the Type 1 pulse, is faster than the response of the detector circuit whereas the other, Type 2, is relatively slow and can be faithfully reproduced. The Type 1 pulse has the shape expected from the impulse equation 2.1 while the Type 2 pulse has a shape which is altogether different with a long transit time and a pulse height which is a maximum at half the duration. The two pulse types vary in different ways with the experimental parameters and it therefore appears that they are not related.

In most conditions the Type 2 pulses predominate, particularly at the lower voltages and at temperatures below 600°C. The incidence of Type 1 pulses is very variable, depending critically on the sample, and they are most frequent immediately after cleaning. The Type 1 pulses have a high onset voltage which depends on the anode dimensions so that they are probably associated with this electrode.

Multiples of Type 1 pulses can be seen just before spark breakdown occurs.

The 'pulse breakdown voltage' is usually the onset voltage for the Type 2 pulses and this can vary from 300 to 1200 volts (except in conditions in which there is no pulse activity at all corresponding to a breakdown voltage of greater than 3 kV). The frequency of the Type 2 pulses rises rapidly with voltage just above the threshold and it tends to saturate at higher voltages. In certain conditions the pulse frequency passes through a maximum and decreases again at voltages above 1.5 - 2.0 kV.

On single crystal samples the Type 2 pulses are only seen on the first heating following chemical cleaning. The pulse count rate then passes through a maximum at between 400 and 600°C when heated to 900°C. The temperature at which the maximum occurs coincides with a peak in the d.c. conductivity. With polycrystalline samples there is also evidence of a maximum in the pulse count rate when samples are heated to 900°C, but, in contrast to single crystal, there is no corresponding peak in the d.c. conductivity.

The shape of the Type 2 pulses varies with the applied voltage. As the voltage is increased, the pulse height passes through a maximum and the voltage at which this occurs depends on the cathode arrangement and the gas pressure. This suggests that the Type 2 pulses occur in the vicinity of the cathode. This variation in pulse height also accounts for the fall of pulse frequency with voltage described previously. In conditions in which the height

decreases rapidly, only the larger pulses are counted so that the frequency appears to fall as the mean height approaches the detection limit.

The mean height of the Type 2 pulses at constant applied voltage reaches a peak at pressures of between 20 and 40 torr, and it decreases rapidly at lower pressures so that at 10 torr the pulses are not detectable. The pulse height also increases rapidly with the impurity content of the argon, for which oxygen and water vapour are thought to be equally responsible. Thus, if the detection limit is high, pulse breakdown may not be observed at all up to 3 kV in very pure argon in some circumstances.

With fixed conditions the distribution of the pulse heights is of the Poisson form as expected from gas avalanche statistics and this leads to values of between 10^5 and 10^6 for the mean number of electronic charges per pulse. The mean pulse charge varies with pressure in much the same way as the pulse height, reaching a peak at between 20 and 40 torr and decreasing rapidly at lower pressures.

8.2 Surface Discharge Model of Pulse Breakdown

The preliminary work described in Chapter 5 showed conclusively that pulse breakdown is associated with both the alumina surface and the ambient gas. This means that any explanation of pulse breakdown must account for the critical dependence of pulse production on both the ambient gas and the alumina sample. In this section the outline of a model is given which explains both factors as well as the majority of the detailed results of Chapter 6. The

model proposed is that surface discharges occur at each of the two electrodes and that these produce the two impulse shapes observed in the external circuit. The faster of the two impulses (Type 1) is thought to be produced by surface discharges at the anode and the slower (Type 2) by surface discharges at the cathode.

The large amount of information on the Type 2 pulse allows a detailed explanation of the gas mechanism associated with this pulse. On the other hand the very limited information on the Type 1 pulse allows no more than a tentative suggestion as to its origin. Consequently most of the discussion in this chapter is concentrated on the Type 2 pulse. The justification for this is the high onset voltage of the Type 1 pulse (which makes its occurrence unlikely in a nuclear fission chamber operating under normal conditions) and also the absence of this pulse in similar studies on magnesia (A. Wright, private communication). This latter fact indicates that the pulse may be associated with the unusual electrode arrangement used in the present work, thus making the pulse unique to this investigation.

A surface discharge will occur between points on an insulator and an electrode surface when the electric field in the gas between them exceeds the breakdown field of the gas. Therefore, for the model shown in Figure 8.1 a surface discharge will occur between the points A and B whenever the field in the gas is in excess of the breakdown field Eb. Hence if Vb is the voltage between the points at which the electrical stress in the gas equals Eb, and Vi is the voltage between the electrodes at which this occurs

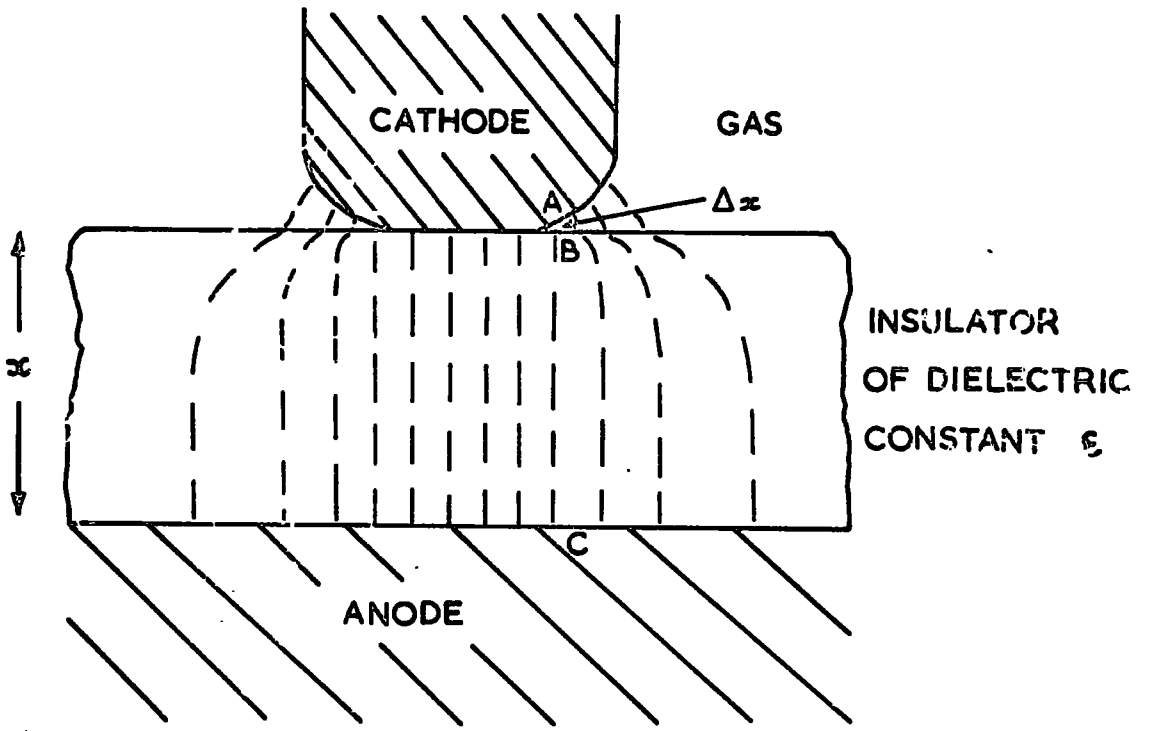

FIG. 8·1 SIMPLE MODEL FOR SURFACE DISCHARGES, SHOWING FIELD DISTRIBUTION IN INSULATOR.

(termed the inception voltage) then

$$Vi = Vb + V_{BC}$$

where V_{BC} is the voltage between points B and C in Fig. 8.1. Provided the field is normal to the surface of the insulator at the discharge point, the field in the gas, Eg, will be related to the field in the dielectric by $Eg = \epsilon E$. Hence whenever a discharge occurs the field in the gas, Eg, reaches the breakdown value Eb. The discharge inception voltage, Vi, with this assumption is

$$Vi = Eb.\Delta x + Eb.\ x/\epsilon$$

where Δx is the discharge distance in the gas and x the thickness of the sample. Hence, on a simple surface discharge model, the inception voltage, and therefore the measured onset voltage, will vary linearly with sample thickness, as has been found experimentally for the Type 2 pulses (see Figure 8.2).

If the experimental results of the Type 2 pulse are interpreted on the above surface breakdown model, values of 2.4 kV/cm and 0.1 cm are obtained for the breakdown field and path length of the discharge respectively. Assuming this estimate of the path length, we find that the field required for Paschen breakdown under similar conditions

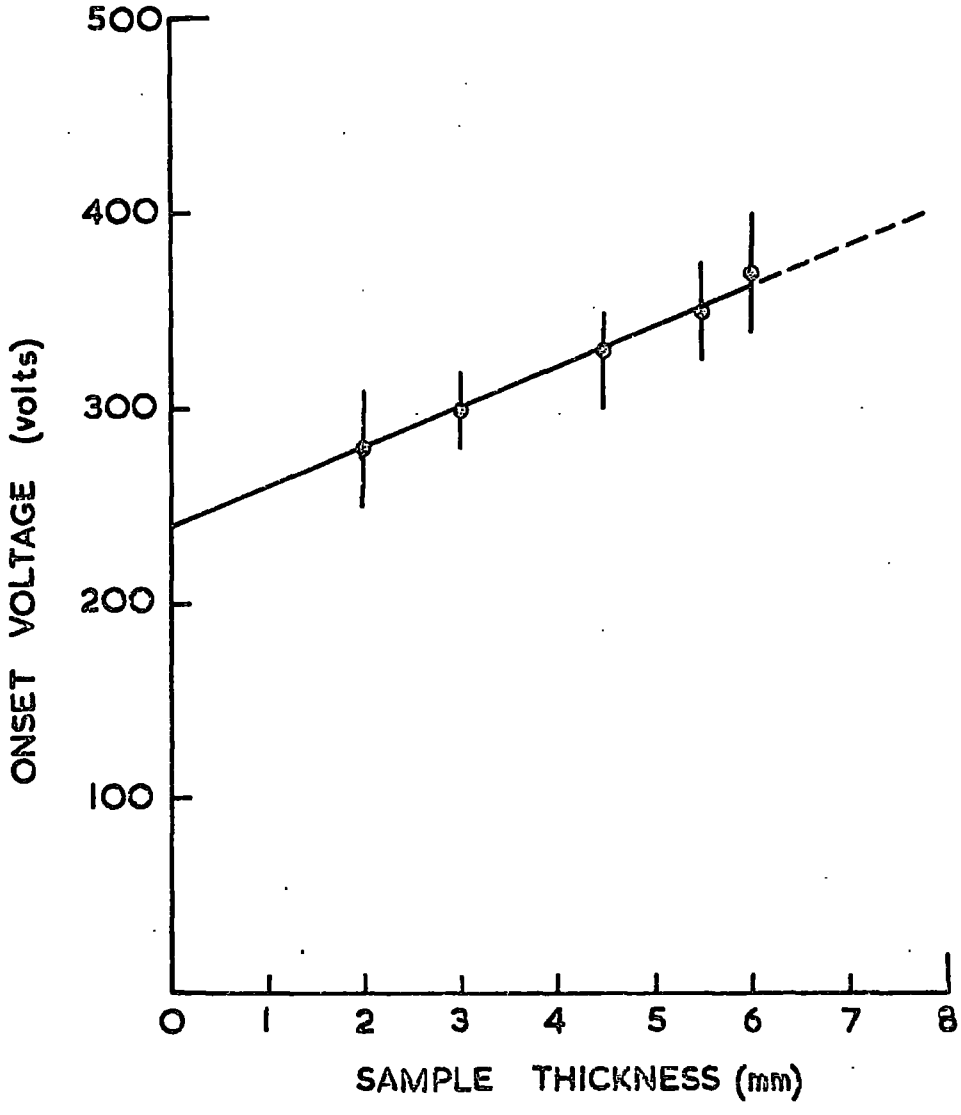

FIG. 8·2. DEPENDENCE OF ONSET VOLTAGE ON SAMPLE THICKNESS FOR POLYCRYSTALLINE ALUMINA IN NOMINALLY PURE ARGON AT 400°C.

(i.e. a 0.1 cm discharge in an atmosphere of argon at 400°C) is about a factor of four larger than the value of the field estimated above. This difference could be due to the non-uniform field distribution at the edge of the electrode giving a low value for the estimated field. However if, as seems likely over such small distances, the divergence of the field can be neglected this difference must be due to the Type 2 pulses occurring below the Paschen breakdown voltage.

On the model of Figure 8.1 a surface discharge occurs whenever the voltage V_{AB} becomes equal to Vb. The first discharge therefore occurs at the applied voltage Vi and further discharges occur as the voltage is raised above this level. For discharges occurring below the Paschen breakdown voltage the pulse frequency is likely to be governed by the rate at which primary electrons are generated in the gas. Hence, in the event of this generation rate being below the time constant of the discharge circuit, the rate of production of primary electrons will govern the frequency of the external impulses whereas when it is above the circuit time constant the frequency will be controlled by the rate at which the charge builds up across the gap. The frequency of the discharges in this latter case will be given by

$$f = \frac{R_{ab} + R_{bc}}{R_{ab} R_{bc} (C_{ab} + C_{bc})} \cdot \left\{ \log_e \frac{V}{V - V_i} \right\}^{-1} \qquad 8.3$$

(See Appendix D)

where V is the applied voltage, Rab and Cab the resistance and capacitance of the gas between the points A and B, and Rbc and Cbc the resistance and capacitance of the insulator between B and C. If Rab $\simeq$ Rbc and Cab $\simeq$ Cbc the expression

reduces to

$$f = \frac{1}{R_{bc} C_{ab}} \left\{ \log_e \frac{V}{V - V_i} \right\}^{-1} \qquad 8.4$$

This is the expected relationship between f and V for cases in which the generation rate is high, for example in a polycrystalline sample at 400°C.

The constant Cab in equation 8.4 may be estimated from

$$Cab = \pi \times e/V_b$$

where π is the mean number of carriers per discharge, e the electronic charge and Vb the breakdown voltage. Hence, for a polycrystalline sample in an atmosphere of argon at 400°C, Cab $\simeq 7 \times 10^{-16}$ farads since Vb $\simeq$ 240 volts and n 1 x 10^6 electrons at voltages above 1.2 kV (see Table 6.1). Thus, assuming Rab = $k\rho \simeq 2 \times 10^{12}$ ohms at 400°C (i.e. k is assumed to be 1) we obtain

$$f \simeq 700 \left\{ \log_e \frac{V}{V - V_i} \right\}^{-1}$$

which is shown plotted in Figure 6.2. It can be seen from this figure that above 1.2 kV the shape of the theoretical and experimental curves agree while below this voltage they do not. It is obvious that in this low voltage range some form of discharge expansion occurs which affects the values of the circuit components (and also possibly the breakdown voltage). To allow for this the product Cab x Rbc may be rather arbitrarily allowed to decrease linearly over the voltage range from Vi to 1.2 kV and then the two curves can be made to agree over the whole range (Fig. 6.2).

On a surface discharge model the temperature as well as the voltage will affect the pulse frequency. Therefore when the generation rate of primary electrons is high the pulse frequency, as given by equation 8.4, will be proportional to the conductivity of the insulator, since $Rbc = k\rho = k/\sigma$. Hence if the effect of temperature on Cab and Vi is small, the temperature variation of the pulse frequency, at constant voltage, will be governed by the sample conductivity. In cases where the generation rate of primary electrons has been kept high by cleaning the surface of the insulator between measurements, the variation of frequency with temperature is in good agreement with this model, i.e. $f \alpha \sigma$. However where the sample has not been cleaned between measurements the variation of frequency with temperature does not agree with this model. In the latter case the generation rate is believed to be below the circuit response time, with the result that at higher temperatures the pulse frequency is controlled by the generation rate.

The diagram shown in Figure 8.1 is a simplified model of the field distribution at the electrodes. A more realistic model of the field distribution is given in Figure 8.3, from which it can be seen that the field at the anode is greater than that at the cathode. Hence on the model of surface discharges at each electrode the anode discharge should occur at a lower inception voltage than the cathode discharge if both discharges are caused by Paschen breakdown of the gas. The reason that this does not occur is believed to be due to the cathode discharge occurring below the Paschen breakdown

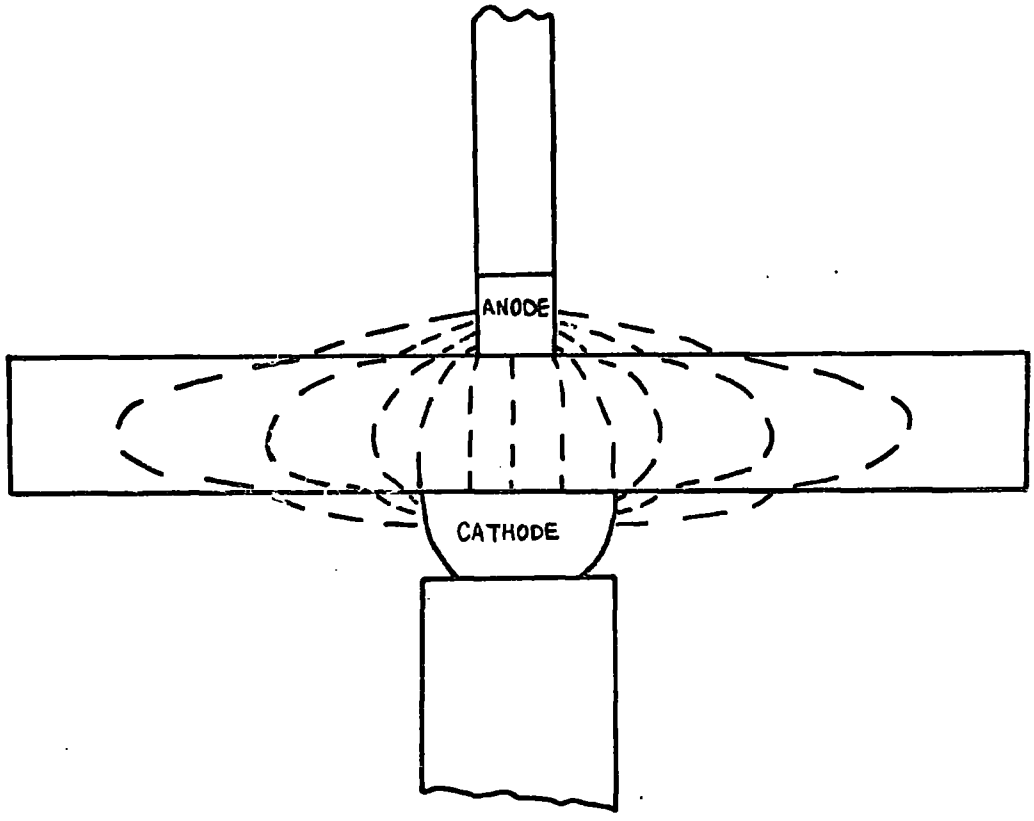

FIG. 83 FIELD DISTRIBUTION IN INSULATOR IN TWO TERMINAL MEASUREMENTS.

voltage, as previously suggested. The origin of the Type 2 pulse at the cathode and not the anode was shown by exposing a single crystal sample to a prolonged period of pulse activity from the Type 2 pulse alone and observing the resultant discoloration of the insulator surface around the cathode (see Figure 8.4).

In addition to the visual evidence mentioned above, there is also evidence that the Type 2 pulse originates at the cathode from contact experiments. In cases in which the field at the edge of the cathode has been significantly increased without altering the field at the anode (as, for example, in the experiment where the plane electrode was replaced with a spherical one while maintaining a sputtered contact at the cathode) only the Type 2 pulse has been affected. Where, however, the field at the anode has been altered by extending the contact beyond the edge of the electrode, it has been found that only the Type 1 pulse has been affected. This agrees with the model of surface discharge at the two electrodes since extending the contact beyond the electrode increases the tangential stress component of the field at the alumina surface and increases the divergence of the field in which the discharges occur. The contact experiments are therefore in agreement with the model of surface discharges at both electrodes.

8.3 The Shape of the Pulses

Before discussing the shape of the Type 1 and 2 pulses in detail mention must be made of a third pulse which has

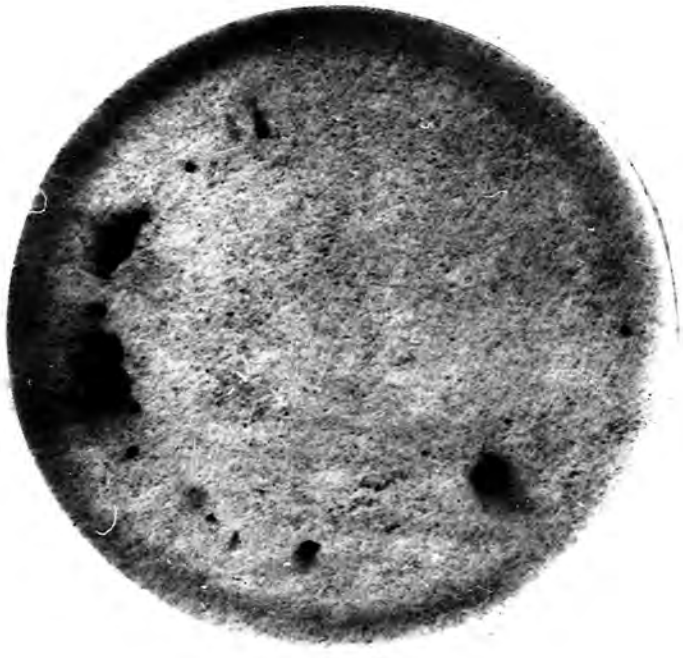

FIG. 8.4. SURFACE OF SINGLE CRYSTAL AFTER 40 HOURS OF TYPE 2 PULSE ACTIVITY, SHOWING DISCOLORATION AROUND CATHODE.

been observed in the pulse breakdown studies. This pulse, an example of which is given in Figure 8.5, appears to be a combination of the other two pulse types, having a fast and slow component. The pulse was only observed on polycrystalline samples at voltages above 1.5 kV when the pulse frequency was high, with the result that it is likely to be caused by the superposition of the other two pulse types. This could happen if the discharging at the two electrodes is particularly severe as then the supply voltage drops momentarily and when it recovers discharges occur simultaneously at each electrode. Although this explanation for the third type of pulse seems to be the most likely one the possibility that it comes from a single discharge has also been considered since this might have helped to explain the other two pulse types. Unfortunately, however, no consistent model could be proposed for a single discharge source to cover all three pulse types.

From the simplified equivalent circuit given in Appendix E it can be seen that the time constants of the equivalent circuit must be known before the rate of rise of current in the discharge can be deduced from the external pulse shape. However if the two extremes of an integrated and differentiated pulse are considered and the expected results compared with the experimental ones, some conclusions may be drawn about the effect of the circuit on the pulses.

In the case of an integrated pulse the total current in the external circuit is the sum of the conduction current and the displacement current. Hence the equivalent circuit

PULSE RECORDED IN AN ATMOSPHERE OF NOMINALLY PURE ARGON AT 400°C AND AN APPLIED VOLTAGE OF -2·0 kV WITH A 10^4 Ω DETECTION RESISTOR.

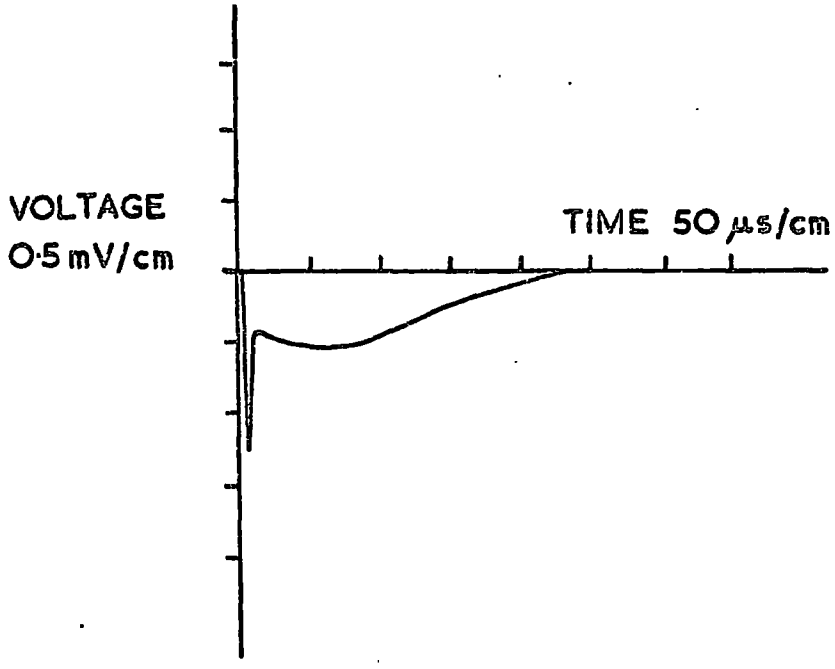

FIG. 8·5. THIRD PULSE TYPE - BELIEVED TO RESULT FROM SUPERIMPOSITION OF OTHER TWO PULSES.

must be known in order to deduce the conduction current from the pulse shape accurately. The height of an integrated impulse will continue to rise until all the charged particles created in the discharge are collected by the electrodes, with the result that the duration of the pulse depends on the velocity of the ions. In the case of a differentiated pulse, on the other hand, the shape is governed by the current growth of the discharge since the displacement current is small. The shape of the impulse is therefore largely controlled by the growth of the electron component of the discharge in this case since the ion current is small because of the relatively low ionic velocity. Hence for a differentiated pulse the duration will depend on the drift velocity of the electrons rather than that of the ions.

As already mentioned the shape of the Type 1 pulse depends on the resistance of the detector circuit. This means that the pulse is faster than the response of the detector and that it is not resolved. It is not therefore possible to decide whether the pulse is integrated or differentiated by the circuit. However the former appears to be more likely in view of the speed of the pulse. Positive burst corona or single electron avalanches in gases would, in general, produce fast electron pulses similar to the Type 1 pulse. If these were the source of the Type 1 pulses then the multiple pulse shown in Figure 6.18 could be due to multiple electron avalanches. This would mean that the time interval between the pulses (1-5 μsec) is the time taken by the positive ions in traversing the gap assuming

that the secondary electrons are produced by positive ions. On this basis, the transit time of the electron avalanche may be put at 10 - 50 nanosecond, since the electron velocity is about 100 times greater than the ion velocity, and this is faster than the circuit could detect.

The shape of the Type 2 pulse can be explained in detail if it is assumed that the growth of the electron component of the discharge controls the pulse shape. This assumption is justified from the effect of adding impurities to argon. For a pulse produced by the electron component of an avalanche, the peak height will be inversely proportional to the transit time of the electrons. Hence if the transit time decreases, due to an increase in the electron velocity, the peak height will also increase. In argon it is well known (see, for example, Massey and Burhop[53]) that small concentrations of molecular impurities reduce the thermal velocities of the electrons. This in turn reduces the elastic collision cross section of the electrons and increases the mean free path between collisions, causing an increase in the electron drift velocity. In contrast, the drift velocities of the positive ions are virtually independent of the impurity concentration in argon because of the different elastic collision cross section (McDaniel and Crane[54]). Hence the variation of the shape of the Type 2 pulse with the oxygen content of the argon indicates that the pulses are produced by the electron component of the discharge.

The variation of pulse shape with oxygen impurity is therefore consistent with the duration of the pulse being

inversely proportional to the velocity of the electrons. If the pulse shape was at all dependent on the velocity of the positive ions it is unlikely that such a large change in duration could be induced by the addition of oxygen impurities. This result therefore appears to indicate that the pulses are not being integrated by the circuit. This view is supported by the changes of the height and of the duration of the pulse with applied voltage and pressure, since the pulse height is proportional to the charge and inversely proportional to the length of the pulse to a good approximation. If the pulse was being integrated the pulse height, Vo, would be proportional to the charge and inversely proportional to the circuit capacitance. The height would also be independent of the transit time, unlike the case of a differentiated pulse where $Vo \propto Q/T$. It would therefore appear reasonable to assume that the distortion of the Type 2 pulse by the total equivalent circuit is small.

To relate the current growth of the discharge to the fundamental parameters of the gas process, i.e. the ionization coefficients, requires a detailed knowledge of the field distribution. Since this is unknown it is impossible to give a detailed description of the pulse shape. Nevertheless there are two prominent features of the pulse, namely the linear growth of the current with time and the attainment of the full pulse height in about half the pulse length, which can be explained.

It is well established that in argon at high pressures, i.e. low E/P values, secondary electrons are produced by

a photoeffect at the cathode (Colli and Facchini[55]). With this secondary mechanism the individual avalanches of a series cannot be distinguished in the total current impulse. This merging will also occur if the number of secondary electrons is large, irrespective of the secondary mechanism. To a first approximation the mean current per avalanche for a series of this type is given by

$$\bar{i} = K\bar{Q}/T_g$$

where K is a constant, $\bar{Q}$ the mean charge per avalanche and Tg the mean time between successive generations. The shape of the current impulse can then be expressed as

$$i(t) = K\bar{Q}/T_g \cdot M(t)$$

where M(t) is the mean number of avalanches per generation as a function of time. For a long series of avalanches Raether[56] has shown that when t is very much less than the total duration of the discharge, T

$$M(t) = 2t/T_g - 1$$

and the maximum of the series is reached at a time T/2. For shorter series the maximum occurs at slightly longer times than T/2 and the current growth deviates slightly from linearity, i.e. i is proportional to $t^{3/4}$ rather than t^1.

At low pressures, where the transit time of the Type 2 pulse is long and the pulse charge large, the observed pulse shape is in excellent agreement with that expected theoretically for a long series of individual avalanches. However

under such conditions the ion current of the discharge must also be considered since a large number of ions may accumulate in the gap during the series. However this does not affect the basic characteristics of the current growth so that i is still found to be proportional to t and the peak height still occurs at T/2.

Legler (20) has shown that the probability for the occurrence of a series of avalanches of K generations depends on the value of the function μ, where

$$\mu = \gamma (\exp \alpha d - 1)$$

and α is the first Townsend ionization coefficient, d the discharge distance and γ the coefficient of secondary emission. If no space charge amplification of the series occurs and $\mu = 1$, the probability is zero for an infinite series and 0.5 for a single avalanche. Hence with no space charge amplification there is an equal probability of observing either a single or a multiple avalanche. There is no evidence of single electron avalanches associated with the Type 2 pulses in this work so that either $\mu \gg 1$ (in which case the probability of a single electron avalanche decreases) or there is space charge amplification of the discharge. For both these conditions the theoretical probability of an infinite series occurring becomes finite. The results show that even at low pressures, where the series may be very large, an infinite series is seldom seen so that there must be a restraining effect which stops the discharge from continuing indefinitely. This restraining

effect is believed to be the formation of space charge in the gas. Charges accumulate in the low field regions of a discharge as a result of the attachment of electrons to neutral molecules and atoms. Hence non-uniform fields and electronegative impurities are necessary for the formation of space charges and both of these occur in the present work. Discharges of this type are known as corona pulses and are of the type first observed by Trichel. The mechanism of these 'Trichel pulses' is discussed in detail in the following section.

8.4 Corona Discharges, a Possible Explanation of Pulse Breakdown

8.4.1 Introduction to corona discharges

The subject of corona discharges is well reviewed in the recent book by Loeb.[57] This gives a detailed account of the mechanism of corona discharges between point to plane electrodes in pure gases. In the present work we are concerned with corona pulses over a wide range of conditions including varying gas pressure and purity, irregular electrode geometries, insulating electrodes and unconditioned electrode surfaces. We are also concerned with discharges in gases at high temperatures which have seldom been investigated in the past. Most of the present work is on argon and previous work on corona in this gas is also limited. A detailed study of corona processes in argon has been made by Das[58] but, as Loeb points out, the interpretation of much of this work is uncertain. For

this reason the present discussion, which must inevitably be somewhat speculative, is confined to a qualitative description of corona discharges.

Trichel pulses are usually supposed to be avalanches which are quenched by their own space charge. They occur in divergent fields with the result that ionization is restricted to the high field region of the gap. Negative ions are formed during the discharge. These accumulate in the low field region and form space charges which quench the discharge. As the field is increased the ionization region gradually extends until, at high E/P values, it covers the whole of the gap. Under these conditions there is no region in which space charges can accumulate and infinite series of avalanches occur which lead to sparking.

At voltages below the threshold for Trichel pulsing, pre-onset corona have been observed in point to plane corona studies (Loeb et al[59]). These pre-onset corona are long series of avalanches produced by photoeffect at the cathode. The generation rate of negative ions in these discharges is low because only a small number of electrons have sufficient energy to form negative ions. Consequently the recombination rate of the ions exceeds the generation rate and negative space charges do not occur. There is some positive space charge enhancement of the field at the cathode but this is small. Hence to a good approximation pre-onset corona can be considered as multiple avalanches in which there are no space charge effects. The voltage at which the rate of ion generation exceeds the recombination rate and leads to the formation of negative ion

space charge therefore defines the threshold for Trichel pulsing.

In air at room temperature, pre-onset corona are found to occur at voltages of about 100 volts below the Trichel pulse threshold. If the processes are similar in the present work, the lower voltage pulses could be pre-onset corona. Assuming that these pre-onset corona are initiated by a small number of primary electrons then avalanche statistics will apply, so that the pulse height distributions obtained at low voltages could be interpreted in this way. At higher voltages the pre-onset corona are transformed into Trichel pulses by the negative space charge and this would explain why long series of multiple avalanches have been observed without sparking.

8.4.2 The effect of voltage on corona discharges

The effect on corona discharges of increasing the field can be considered in three regions viz low, intermediate and high fields. In each region different mechanism control the discharge growth. Although the variation of all the mechanisms with voltage should be considered for a full description, only the dominant mechanism in each region will be discussed here.

(i) The low field region, where the pulse charge increases with field

In this region we are concerned with the transition from the pre-onset corona to the Trichel pulse and the development of the Trichel pulse itself.

The effect of increasing the field on the pre-onset corona is to increase the charge of the pulse. This is because increasing the field increases the ionization rate in the gas so that larger avalanches are formed with more avalanches per generation. However as the ionization rate increases, the field of the positive space charge also increases. This increases the drift velocity of the electrons with the result that the transit time of the pulse decreases.

Once the field is high enough for the generation rate of negative ions to exceed the recombination rate, negative space charges form. The rate at which the positive and negative space charges build up is controlled by the ionization rate of the electrons. Hence as the ionization rate increases the rate of space charge formation increases and the time taken for the discharge to be quenched is reduced.

(ii) The intermediate field region, where the pulse charge is independent of field.

Once the transition to the Trichel pulse is complete, further increase in the field does not significantly affect the pulse size. This is because increasing the field increases the probability of negative ion formation.

To form negative ions by disassociative attachment of oxygen molecules, which is the most likely mechanism in these conditions, requires an electron energy of 3.6 eV. It follows that the greater the mean electron energy the greater is the probability of negative ion formation

because the mean electron energy will be much less that 3.6 eV in corona discharges. Thus increasing the field produces a rise in the number of ions formed per avalanche and results in an increase in the charge density of the negative space charge layer. Thus there is a rapid build up of the negative space charge layer at the beginning of the discharge and this results in the increased field being transferred to the region between the negative space charge and the anode. The effect of this on the discharge is to maintain constant ionizing conditions at the cathode.

(iii) The high field region where the pulse charge decreases with field

In this region the predominant effect is the expansion of the discharge. Increasing the field causes an extension of the ionization region into the gap. The negative space charge region is thus formed further from the cathode. It follows that an increasing number of positive ions will arrive at the cathode before the discharge is quenched and these will have greater velocities the further the negative space charge region is from the cathode. Because of the increased distance of the glow region beyond the negative space charge from the cathode, photons are lost to the cathode by diffusion. Consequently secondary photoemission diminishes while electron emission due to positive ions increases. Because of this the discharge contracts radially and lengthens along the axis. Fewer negative ions are needed to quench the discharge in this case because of the concentrated space charge density. The pulse charge therefore decreases with field in this region.

The transition from photoemission to positive ion emission also affects the electron velocities. With photoemission the positive ions may be considered stationary since their velocities are relatively low. However when the emission is due to positive ion bombardment the ions must move into the cathode to produce the secondaries and this will influence the electron velocities. The effect is to reduce the space charge enhancement of the field near the cathode because of the smaller number of positive ions. The electrons are therefore accelerated through a reduced field so that their velocities fall. This decrease in the electron velocities causes the duration of the pulses to increase.

8.4.3 The effect of the cathode on corona discharges

According to Loeb[57] the applied voltage at which the expansion of the corona discharge occurs depends on both the field and the area of the cathode surface available to the discharge. Loeb suggests that as the voltage is raised a point is reached at which the maximum avalanche proliferation over the limited surface available cannot be exceeded, so that increasing the field beyond this point causes a more rapid expansion of the discharge along the axis than previously. This suggestion would explain the dependence of pulse shape on cathode arrangement in the present work.

When the contact extends well beyond the edge of the electrode the discharge is transferred from the electrode to the contact. Under these conditions the highly

divergent fields restrict the discharge to the contact edge with the result that the surface area of the cathode available to the discharge is much reduced. Thus the only way the discharge can expand, once it has spread along the circumference of the contact, is along the discharge axis. In all other experiments, where the discharge occurs at the electrode, little axial expansion occurs because the large surface area of the contact leads to radial expansion of the discharge.

It can be seen from Figure 8.4 that material is deposited at several points around the edge of the electrode after pulse breakdown. Although this may indicate that discharges are occurring simultaneously at several points around the circumference there is another more likely explanation for this distribution. It is well known that on dirty surfaces corona discharges wander to points of lowest work function. A corona discharge, which is localised at a point on the electrode, will gradually clean up the surface at this point and then move to a point of greater photoemissive yield. Consequently the corona will flicker around the surface of the electrode. This wandering of the discharge does not necessarily involve the actual movement of the corona over the surface. The corona can start at a dirty point and die away as the point is cleaned up; a new corona then appears at another point often at a slightly higher applied voltage.

The movement of the corona is also believed to be responsible for the irregularities which are sometimes

observed in the pulse count curves (as shown, for example, in the lower curve in Figure 6.7) where a drop in the pulse count rate may occur as the corona at one point dies away and that at another builds up. The effect of the movement of the Trichel pulse on the discharge current in air has been investigated by English[60] who found that the effect caused the current to fluctuate as the field was increased. This would correspond to fluctuations in the pulse count rate since the measurements were made in the region where the pulse charge is independent of voltage.

8.4.4 The effect of pressure on corona discharges

The experimental variation of pulse shape with pressure is also similar to that expected for Trichel pulses. At high pressures the mean free path of the electrons is small so that there is considerable excitation of the gas atoms. Thus there is large multiplication of the avalanches by photoemission. The negative space charge is formed within a short distance of the cathode because of the high gas density and the corona is rapidly quenched. The length of the pulse is therefore relatively small.

At low pressures the mean free paths are greater than at high pressures and the electron energies are higher. This causes the cathode glow area of the discharge, i.e. the region of positive space charge, to be further from the cathode and very much more diffuse. The same applies to the negative space charge region. Also the rate of generation of the avalanches by photoemission is reduced as the discharge expands. Hence at low pressures the

generation of secondaries by positive ions becomes important. As before this causes the discharge to expand more rapidly along the axis. However, as the negative space charge is more diffuse and further from the cathode, more negative ions are needed to quench the discharge at low pressures than are required at high fields so that the pulse charge increases as the pressure is lowered.

As the pressure is reduced further a point is eventually reached at which the electron velocities become so high that the effective ionization coefficient is reduced. Thus the rate of ion generation falls (although the coefficient of negative ion formation itself increases) and more generations are needed to quench the discharge. The pulse length therefore increases as its charge decreases. This effect only occurs when the ionization region does not approach the anode too closely, i.e. at relatively low fields. At higher fields the ionization region extends almost to the anode with the result that sparking occurs before the field becomes high enough to cause a decrease in the ionization coefficient.

8.5 The Effect of the Alumina Surface on Pulse Breakdown

Two explanations, both of which seem to be equally probable, are offered for the dependence of pulse breakdown on the chemical treatment of the alumina. These explanations depend on impurities being desorbed from the alumina surface on heating the samples after chemical cleaning. In the first explanation the desorbed impurities contaminate

the ambient gas and lower its breakdown potential while in the second the desorbed impurities themselves eject the initiating primary electrons of the discharge from the cathode. The first explanation only explains the absence of pulse breakdown in the inert gases while the second is independent of the gas.

(i) The Trichel pulse explanation

Weissler[61] has investigated the effects of various impurities on the action of point-to-plane corona discharges in argon at room temperature. He found that in pure argon ambients neither Trichel pulses nor continuous corona discharges occurred before sparking. He also found that small quantities of oxygen impurities ($0.1^{o}/o$) in the argon caused the appearance of Trichel pulses. These pulses occurred well below the sparking potential of the pure argon, which in itself was well below the sparking potential of the impure gas. The reason for this effect, which is confined to the inert gases, is the metastable states of the argon atoms. In the pure gas, avalanches do not occur because of the very low generation rate of secondary electrons at the cathode, the metastable states delaying and diffusing the photons. The introduction of oxygen into the argon quenches the metastable states and causes a rapid increase in photoemission from the cathode, with the result that long series of avalanches appear. However as oxygen is an electronegative gas, Trichel pulses occur (because of the negative space charges) rather than the steady corona which occurs in argon containing impurities other than oxygen (e.g. nitrogen).

The concentration of impurities in the nominally pure argon used in this work has been estimated at 0.01°/o (see Section 6.2). This impurity concentration is too low to significantly affect the metastable states of the argon atoms. Thus when there is no additional impurity in the system the voltage at the electrode edge has to be raised to the sparking potential of the gap before a discharge occurs. If the voltage necessary for sparking is larger than that of the supply, pulse breakdown will only be observed in the system when the impurity concentration in the gas exceeds 0.1°/o. This is believed to occur when samples are heated after cleaning as the desorption then increases the concentration of electronegative impurities in the gas to the required level.

The desorption of OH and H_2O molecules from the surface of alumina on heating has already been discussed in Section 7.4. These molecules will, even if not desorbed as negative ions, readily form negative ions during the discharge because of their high electron affinity (McDaniel[62]). Consequently if sufficient impurities of these types are desorbed during heating the gas will become contaminated and Trichel pulsing will occur. Hence pulse breakdown will only be observed in a pure argon ambient on heating crystals after chemical cleaning.

The above model does not seem able to explain why Tucker and Gibbs[3] and Champion[4] found similar effects in air, i.e. the disappearance of pulse breakdown on cooling. However, these authors did not investigate the effects of

voltage on the pulse production and moreover they both made measurements at relatively low applied voltages, Tucker and Gibbs at 300 volts and Champion at 100 volts. If H_2O molecules are desorbed during the heating cycle as well as OH ions, then pulse breakdown will be occurring in relatively damp air on the heating cycle and dry air on cooling. The effect of water vapour on the onset voltage of pulse breakdown in argon has been described in Section 6.3. If water vapour has a similar effect on the onset voltage in air, which seems likely in view of the known effects of water vapour on the formation of negative ions (Pack et al[63]), then the pulses will occur at a lower onset voltage on heating than on cooling in air. Hence it may be that if Tucker and Gibbs and Champion had used higher voltages they would have observed pulse breakdown on both heating and cooling cycles.

(ii) The positive ion emission explanation

Trichel pulses occur regularly if there is a plentiful supply of primary electrons. If the supply is not plentiful then the pulses will occur at irregular intervals depending on the source of primaries. For example, Loeb et al[59] found the pulses to occur in bursts due to the irregular emission of electrons from dirty spots on the electrode. Of the possible sources of primary electrons at an electrode, thermionic and field emission are the most common. Calculations of the thermionic emission current from the electrode, even allowing for a Schottky reduction of the potential barrier, show that these currents are much too small to be the source of primaries. Similar calculations for field

emission from the edges of the contact show that this source is probably too small also. However field emitted electrons could be the source of primaries if enhanced emission occurs, as a result of the Malter effect, at points where the cathode touches the alumina surface. This could possibly explain why pulse breakdown is found with magnesia as well as alumina, since these two materials have the highest secondary emission coefficients.

There are two other possible mechanisms for the emission of primary electron from the cathode apart from those mentioned above namely photoemission and positive ion bombardment. The first of these is unlikely to occur, since there is no obvious source of photons, so that the second would appear the only alternative source of a regular supply of electrons. Cohen[23] mentions that positive ions have been detected on heating alumina although he does not give the species. However provided these ions have an ionization energy greater than twice the work function of the metal, i.e. $>$ 10 eV (the work functions of Pt and Rh being about 5 eV), electrons will almost certainly be emitted from the cathode on the incidence of an ion (Llewellyn-Jones[64]). Hence if positive ions are only emitted by alumina after it has been chemically cleaned, the absence of pulse breakdown on cooling would be explained since, once the alumina surface has been cleaned up, there will be no positive ions to initiate the discharges.

Hill[67] has recently shown that protons are incorporated interstitially into the lattice of rutile single crystals

grown by the Verneuil process. He suggests that above 400°C these protons combine with chemisorbed OH ions to cause the observed desorption of H_2O molecules from rutile above this temperature. If, by analogy, it is supposed that protons are incorporated into alumina crystals grown by the Verneuil process then a similar mechanism could be responsible for the emission of the positive ions. For example the hydrogen could combine with water on the surface to produce OH_3^+, an ion which would almost certainly produce electron emission from the cathode on impact. Such a mechanism would explain why Dasgupta[33] failed to observe any contamination effects in his work, since his crystals were pulled from the melt, and Champion[4] observed smaller contamination effects on his flux melt crystal than his Verneuil ones. Hence it would seem that the desorption of positive ions is a very feasible explanation for the dependence of pulse breakdown on chemical treatment.

It is concluded that either of the above explanations could account for the dependence of the pulse production on the chemical treatment of the alumina and that there is insufficient evidence to choose either of them.

CHAPTER 9

CONCLUSION

9.1 The Source of Pulse Breakdown

The preliminary investigation of pulse breakdown reported in Chapter 5 showed that both the ambient gas and the alumina sample were necessary for pulse breakdown to be observed. This fact eliminated several possible causes of pulse breakdown, including sources in the bulk of the insulation, sources entirely in the gas and sources in voids or cavities within the insulation. From this preliminary study it was therefore concluded that pulse breakdown is due to some sort of surface discharge involving both the alumina and the ambient gas.

The detailed study of pulse breakdown reported in Chapter 6 showed that pulse breakdown was critically dependent on the pressure, type and purity of the ambient gas. It also showed that pulse breakdown was affected by the geometry of the electrodes and the size of the contacts on the alumina. From these and other results it was concluded that pulse breakdown is produced by discharges in the ambient gas between the edges of the electrodes and the alumina surface. This explanation is supported by the good agreement between experiment and a simple surface discharge model.

The detailed study revealed that pulse breakdown in argon produced two different pulse shapes in the external circuit, a fast Type 1 pulse and a slow Type 2 pulse. The fast pulse was not accurately resolved by the detection

circuit and its occurrence was variable, normally being detected only at high voltages on polycrystalline samples. Because of this it has not been possible to study this pulse in detail and only a tentative suggestion can be made as to the origin. The slower of the two pulses on the other hand, was fully resolved and could be reliably reproduced. This allowed a detailed study to be made of the effects of a wide range of experimental parameters on the pulse shape.

In Chapter 8 it was shown that distortion of the Type 2 pulse is likely to be small and that its shape is dominated by the electronic component of the discharge. It was also shown that the shape of the pulse is consistent with a long series of avalanches formed by a photoelectric secondary mechanism. The absence of very long series however suggests that a restraining mechanism exists to prevent the avalanches from continuing indefinitely. The most likely mechanism is the formation of space charges in the gas which quench the discharge. This is similar to the mechanism of Trichel pulses and it is therefore suggested that the Type 2 pulses are produced by negative corona discharges of the Trichel pulse type.

The Trichel pulse explanation accounts for the variation of the shape of the Type 2 pulse with all the experimental parameters. As the voltage is raised the pulse charge passes through a maximum and the duration a minimum. The voltage at which this occurs depends on both the field distribution and the surface area of the electrode available to the discharge. This voltage will be lower when the

discharge is to a contact on the alumina surface than when it is to the electrode directly. The effect of pressure is also explained since both the charge and the duration of the pulse increase as the pressure is reduced.

The combined pulse breakdown and d.c. conductivity measurements on single crystals showed that the appearance of pulse breakdown in argon coincides with a peak in the d.c. conductivity. Pulse breakdown and the conductivity peak were only observed on the single crystals after samples had been chemically cleaned and as they were heated to 900°C. Neither pulse breakdown nor the conductivity peak were observed on cooling the crystals from 900°C or on subsequent reheating. This showed that these effects are produced by chemical contamination of the alumina surface.

In Chapter 7 it was shown that the peak in the d.c. conductivity could be related to the desorption of impurities from the alumina surface. In Chapter 8 it was further shown that this same effect, i.e. the desorption of impurities, could be responsible for pulse breakdown. Two explanations were considered, both of which appeared equally likely. In the first explanation it was suggested that negative ions or neutral molecules desorbed by the alumina raised the impurity level in the argon sufficiently for Trichel pulsing to occur. In the second explanation it was suggested that positive ions were desorbed by the alumina surface and that these initiated the Trichel pulses on impact with the cathode.

9.2 The d.c. Conductivity of Alumina

It was shown in Chapter 7 that chemical cleaning of single crystal alumina samples caused the appearance of a peak in the conductivity curve of alumina on heating, in agreement with published work. The temperature at which this conductivity peak occurred was very variable and probably depended on the cleaning procedure, the concentration of the cleaning solution and the rate of heating of the samples. This suggests that previous work, in which the position of the peak was correlated with the use of different acid solutions, may be in error. In contrast to the result with the single crystal samples, the polycrystalline alumina did not have a peak in the conductivity curve on heating to 900°C after chemical cleaning.

The d.c. conductivity of single crystal alumina was found to be different for samples of different diameters. The sample with the largest diameter had the lowest apparent bulk conductivity and the highest activation energy, and the sample with the smallest diameter the highest apparent conductivity and the lowest activation energy. This indicates a dependence of conductivity on sample diameter and hence a significant contribution from surface conduction. The difference between the samples was reduced by plotting the results in terms of surface rather than bulk conductance. The conductance of polycrystalline alumina was found to be about an order of magnitude greater than the most conducting single crystal although it had an activation energy similar to that sample.

It was concluded in Chapter 7 that the contamination peak results from chemisorbed ions modifying the electrical properties of the alumina surface, in agreement with recent studies of the effect of chemisorption on the electrical properties of powdered alumina (Khoobiar et al[66]). These chemisorbed ions are believed to be formed by the thermal dissociation of molecules adsorbed from the cleaning solution. Since water molecules will be adsorbed on the alumina surface during cleaning, these ions are most likely to be OH^-. The absence of a contamination peak on polycrystalline alumina is explained by the high conductivity of the sample, since in this case the current passes through the bulk of the sample along the surface of the individual grains.

The d.c. conductivity of the single crystal samples was finally interpreted in terms of a mixture of bulk and surface conduction. The activation energy for surface conduction was estimated, from measurements on both single crystal and polycrystalline alumina, at 1.7 eV and that for bulk conduction at 3.9 eV. The low activation energy for the surface was shown to be consistent with electronic conduction in the non-stoichiometric surface layer. The bulk activation energy does not agree with that expected for either intrinsic or extrinsic ionic conduction and it is therefore unlikely that single crystal alumina is an ionic conductor below 900°C.

9.3 Implications for Discharge-Free High Temperature Insulation

From this work it can be seen that there are several

possible ways of improving the pulse breakdown properties of alumina insulators.

(i) Pulse breakdown can be eliminated by reducing the gas pressure around alumina insulation to better than 10^{-1} torr. However, if leakage increases the pressure to just above this, there will be intense pulse activity and sputtering of metals which will eventually destroy the insulation.

(ii) Pulse breakdown can be reduced by heating the sapphire to at least 900°C in pure argon to remove contamination from the surface. Cleaning of the surface by ion bombardment may also help. The surface may become recontaminated by exposure to air.

(iii) Polycrystalline alumina may continually desorb impurities at high temperatures due to diffusion from the bulk. This applies to a lesser extent to single crystals. Czochralski-grown crystals may be superior in this respect, although they have not been used in the present work.

(iv) Pulse breakdown may be eliminated by using argon of exceptional purity. To achieve this, it is necessary to purify 99.995°/o argon further and to ensure that it is not contaminated subsequently by desorption from metal and insulator surfaces. Parts to be insulated will also require to be leak-free to a very high degree.

(v) Pulse breakdown may be reduced by decreasing the local high fields due to irregularities on the electrode surfaces and at the electrode-sapphire interface. Field concentrations may be reduced by polishing or by making part of the insulation of a material such as silica which has a lower dielectric constant.

(vi) Single crystal sapphire has a much higher insulation resistance than polycrystalline alumina.

9.4 Suggestions for Further Work

This study has shown that pulse breakdown is caused by surface discharges which are very sensitive to the purity of the ambient gas and the state of the alumina surface. The dependence of pulse breakdown on these two distinct impurity processes has made the investigation and study of this phenomenon difficult. Consequently these should be investigated separately in future work to avoid the difficulties encountered in the direct measurements made here. Further research to this end should be concentrated on the following aspects, which are also of fundamental interest in their own right.

(i) A study of the desorption characteristics of alumina using an ultra-high vacuum furnace and mass spectrometer to identify the ions produced. Measurements to be made as a function of surface cleaning procedure for polycrystalline and single crystal samples. With the latter there is

likelihood of hydrogen diffusion from Verneuil-grown material and this may be associated with the OH or H_2O ions that probably give pulse breakdown. Czochralski-grown crystals may contain much less hydrogen and they should be compared with Verneuil crystals obtained from various sources. This is of general interest for the solid state study of sapphire.

(ii) The study and control of impurities in nominally pure argon in the pulse breakdown measuring furnace using the mass spectrometer. This would show the influence of the desorption of oxygen and water vapour on the present results as required for improvements in the furnace conditions and for the eventual production of pulse-free devices.

(iii) A systematic study of corona pulses in high temperature gases using point-plane metallic electrodes. With high-speed circuitry the electronic and ionic pulses can be studied separately and compared with the present pulse behaviour. The electrical measurements can be correlated with optical observations of the growth of corona discharges at up to 500°C using a photomultiplier. The aim of this work would be:

a) to confirm the dependence of pulse production on gas purity in order to find the acceptable impurity limits and optimum gas type

and b) to examine the influence of different electrode materials to find the best metals to use for the reduction of pulse breakdown. As far as is known there has been no previous work on corona at high temperatures.

(iv) A study of the influence of an insulating surface on corona pulses using simple geometry such as a metal point just above a plane alumina surface. This topic is of great importance for insulation studies in general but it does not seem to have been seriously investigated previously. The work would be extended to more complex geometries, such as that used previously, and to practical alumina insulators.

(v) Continued study of surface conduction in alumina single crystals in order to explain the conduction mechanism and how it is affected by impurities and by desorption from the surface.

Each item of the programme outlined above will extend our knowledge of part of the pulse breakdown process and show the conditions needed to minimise its occurrence. On the present hypothesis there appears to be no fundamental

reason why it should not eventually be possible to produce discharge-free gas filled insulation for use up to at least 3 kV and 600°C.

APPENDIX A

COMPUTER PROGRAMME FOR ANALYSING OSCILLOGRAMS

The oscillograms were analysed by an Elliot 803 computer. The computer language used was Algol and the computer programme is given overleaf. For this programme to be used the oscillograms had to be expressed in cartesian co-ordinates and this was done with a digital plotter. The computer reads off information from the data tape until the instruction to stop is given. The signal for this is the number 9999 on the data tape. This signal was given between each oscillogram. The oscillogram scale was put onto the data tape after each stop signal to give the computed values in the appropriate units.

```
SAPPHIRE PULSE ANALYSIS;
BEGIN REAL AREA,ARISE,BRISE,RTIME,ADEC,BDEC,DTIME,YA,YB;
INTEGER N,K,Q,L,J,P,TMAX,YMAX,XMAX;
INTEGER ARRAY X(1:200),Y(1:200);
SWITCH S:=AGAIN;
PRINT £AREA   YMAX   XMAX   RTIME   DTIME;
AGAIN:  YMAX:=9999; AREA:=0;
FOR K:=1,K+1 WHILE X(K-1) NOTEQ 9999 DO
BEGIN READ X(K),Y(K);
      IF Y(K) LESS YMAX THEN
      BEGIN
      YMAX:=Y(K);XMAX:=X(K);TMAX:=K;YA:=0.9×YMAX+0.1Y(1);
      YB:=0.1×YMAX+0.9×Y(1);
      END;
END; CHECKS(£A);
FOR N:=1,N+1 WHILE X(N+1) NOTEQ 9999 DO
BEGIN N:=CHECKI(N);
      AREA:=AREA+((2×Y(1)-Y(N)-Y(N+1))×(X(N+1)-X(N))÷2);
END; CHECKS(£B);
FOR L:=1 STEP 1 UNTIL TMAX DO
BEGIN L:=CHECKI(L);
IF Y(L) GR YB AND Y(L) NOTEQ Y(L+1) THEN
      BRISE:=X(L)+((YB-Y(L))×(X(L+1)-X(L))÷(Y(L+1)-Y(L)))
ELSE IF Y(L) GR YA AND Y(L) NOTEQ Y(L+1) THEN
      ARISE:=X(L)+((YA-Y(L))×(X(L+1)-X(L))÷(Y(L+1)-Y(L)));
END; CHECKS(£C);
FOR Q:=TMAX,Q+1 WHILE X(Q+1) NOTEQ 9999 DO
BEGIN Q:=CHECKI(Q);
IF Y(Q) LESS YA AND Y(Q) NOTEQ Y(Q+1) THEN
      BDEC:=X(Q)+((YB-Y(Q+1))×(X(Q+1)-X(Q))÷(Y(Q)-Y(Q+1)));
END; CHECKS(£D);
      RTIME:=ARISE-BRISE;
      DTIME:=BDEC-ADEC;
READ J,P;
      AREA:=(AREA×J×P)÷(92↑2);
      YMAX:=YMAX÷92;
      XMAX:=XMAX÷92;
      RTIME:=(RTIME×P)÷92;
      DTIME:=(DTIME×P)÷92;
PRINT
     ££L2,AREA,PREFIX(£,£S4),YMAX,XMAX,RTIME,DTIME;
GO TO AGAIN;
END;
```

APPENDIX B

AIR LEAKAGE INTO THE FURNACE CHAMBER DURING FILLING WITH THE AMBIENT GAS

During the filling of the furnace chamber with the ambient gas air will leak into the system and cause contamination. An estimate of the amount of contamination can be made from the leak rate of the system.

If W is the total quantity of air which leaks into the chamber during filling, the partial pressure of air in the chamber after filling due to leaks is W/V, V being the volume of the chamber in litres. Now if Q is the rate of flow of air into the system through the leaks,

$$W = Q.dt$$

The leaks in the system may be represented by a small pipe of conductance U connected to the outside ambient. If Pa is the pressure of the outer end of the pipe (atmospheric end) and P is the pressure at the inner end (system end), then

$$Q = U.\ (Pa - P)$$

and

$$W = U.\ (Pa - P).\ dt \qquad -1/.$$

The pressure in the chamber t seconds after the tap between the gas reservoir and the evacuated chamber has been opened can be expressed as

$$P = Pr\ (1 - \exp\ (-\ t/T)) \qquad -2/.$$

provided that Po, the pressure in the chamber at t = 0, is very much less than Pr.

In this equation T is the time constant of filling which is equal to V/Ur (Ur being the conductance of the pipe to the reservoir) and Pr is the gas pressure at the reservoir. Substituting for P in equation 1 and integrating between the limits 0 and t gives

$$W = U.(Pa - Pr)t + Pr.T(1-\exp -t/T) \quad -3/.$$

Since the pressure at the reservoir was set at 1.5 atmospheres, the time taken to fill the chamber to 1 atmosphere is approximately equal to the time constant of filling. Hence, substituting t = T in equation 3 gives

$$W = U.(PaT - PrT.\exp - 1) \quad -4/.$$

Using a value of 10^{-6} litres per second for the conductance of the pipe, U, and a time of 300 seconds for T (determined by measuring the time constant for filling the chamber) in equation 4 gives a value of 0.1 torr litres for W. Therefore since the volume of the chamber is 3 litres, the partial pressure of air in the chamber due to leakage while filling is approximately 0.03 torr.

APPENDIX C

DIFFUSION OF AIR INTO THE FURNACE CHAMBER

Air was found to be diffusing into the furnace chamber through leaks in the vacuum system during the time interval between the filling of the chamber with the ambient gas and the making of the pulse count measurements. By measuring the leak rate of the vacuum system it has been possible to determine the effective size of the leakage paths and hence make an estimate of the partial pressure of air which will diffuse from the outside into the filling gas.

The argon in the furnace chamber can be effectively considered as connected to the outside atmosphere by a small pipe of conductance U. Air will leak through this pipe at a rate, $Q = U.(Pa - PO) \simeq U.Pa$ for $Pa \gg Po$. Hence by measuring the leak rate of the vacuum system, i.e. by using $Q = V.\, dP/dT$, the conductance of the pipe can be determined. The problem now is to express the conductance of the pipe in terms of its dimensions. This will depend on whether the gas flow is viscous or molecular. Considering the relatively high pressures involved in this gas flow, Poiseuille's equation will be used for the conductance of the pipe. Hence for viscous flow

$$U = (r.d^4/128\eta L).\bar{P}$$

where d and L are the diameter and length of the pipe respectively, η the viscosity of the gas and $\bar{P}$ the mean pressure between the ends of the pipe.

For air at room temperature

$$U = (182.d^4/L)\ \bar{P} \text{ litres per second.}$$

If it is assumed that the length of the pipe is unity, i.e. 1.0 cms, and the mean pressure $\bar{P}$ is 380 torr, we have

$$d = 0.1\ (U/6.9.)^{1/4} \text{ cms}$$

or $$d = 0.01\ (Q/0.52)^{1/4}$$ after substitution of $U = Q/Pa.$

The quantity of gas diffusing through the pipe in time T is obtained by solving the diffusion equation for one dimensional flow,

$$dN/dt = - D.dc/dx.A \qquad - 1/.$$

in which D is the diffusion constant, A the cross section of the pipe, dN/dt the rate of diffusion, and dc/dx the concentration gradient in the direction of diffusion. In the case of a linear concentration gradient along the pipe,

$$dc/dx = N/L$$

if N is the difference in the concentration between the two ends of the pipe and L is the length. For diffusion into the furnace chamber from the atmosphere, we have $N = n_o$, the molecular density of the atmosphere, at $t = 0$ and $N = n_o - n$, n being the molecular density at the chamber end of the pipe, at $t = T$.

Integrating equation 1 between $t = 0$ and $t = T$ gives, for a linear gradient,

$$n = n_o(1 - \exp(-DAT/L)) \qquad - 2/.$$

Substituting into this equation the value for A derived from the leak rate by assuming L = 1 allows equation 2 to be evaluated and an estimate made of the air impurities in the ambient gas from diffusion.

Two cases will be considered:-

(i) When the time interval between filling the chamber and making the pulse count measurements is 2 hours and the leak rate of the chamber is 8×10^{-4} torr litres sec^{-1}, i.e. the conditions in the early pulse count experiments. The effective diameter of the pipe, in the case of a leak rate of 8×10^{-4} torr litres sec^{-1}, is

$$D = 0.002 \text{ cms}$$

i.e. $$A = \pi \times 10^{-6} \text{ cms}^2$$

The diffusion coefficient for air into argon can be taken as the same as that for nitrogen and oxygen into argon, the diffusion coefficients being 0.20 cm sec in both cases. Substituting D = 0.20, $A = \pi \times 10^{-6}$ cm, T = 2 x 3600 sec, and L = 1 cm into equation 2 gives

$$n = n_o (1 - \exp 0.0015) = 0.005\, n_o$$

hence $P_{AIR} = 0.005\, P_o = 4$ torr.

A similar calculation may be made for the diffusion of water vapour into the system. Using the above values of A, T and L and known values for D and Po [D = 0.24 cm sec for H_2O into A and Po = 17.5 torr (S.V.P. of H_2O at 20°C)]

gives, after substitution in equation 2, a value of 0.1 torr for the diffused pressure of water vapour in the system.

(ii) When the measurements are made directly after the chamber has been filled with the ambient argon. In this case impurities are diffusing into the chamber while the pulse count measurements are being made. The leak rate of the chamber in this type of measurement was 3×10^{-4} torr litres per second and the diffusion time was approximately 30 minutes, i.e. the diffused impurities at the end of the measurements are being estimated.

For a leak rate of 3×10^{-4} torr litres per second

$$D = 0.0015 \text{ cm}$$

and

$$A = 1.89 \times 10^{-6} \text{ cm}^2.$$

Using the above value for A, a value of 30 x 60 seconds for T and the values previously quoted for the diffusion coefficient of air into argon and water vapour into argon gives, after evaluation of equation 2, values for the diffused impurities in this case of

$$Pd \text{ (air)} = 0.5 \text{ torr} \quad \text{and}$$

$$Pd \text{ (water)} = 0.01 \text{ torr.}$$

APPENDIX D

VARIATION OF DISCHARGE FREQUENCY WITH APPLIED VOLTAGE

Figure A shows an equivalent circuit for the sample and external leads. The discharge across AB is represented by instantaneously short circuiting the capacitor C_{AB}. This will occur when the voltage across AB reaches the gas breakdown voltage V_b. The time interval between discharges is therefore the time taken for the capacitor to recharge to the breakdown voltage V_b after a discharge. The charging current through C_{AB} at any time t is given by

$$i_c = \frac{V_{BC}}{R_{BC}} + C_{BC}\frac{dV_{BC}}{dt} - \frac{V_{AB}}{R_{AB}}$$

$$= \frac{V - V_{AB}}{R_{BC}} - C_{BC}\frac{dV_{AB}}{dt} - \frac{V_{AB}}{R_{AB}} \qquad 1/.$$

since the applied voltage, V, is constant.

Also $$i_c = C_{AB}\frac{dV_{AB}}{dt} \qquad 2/.$$

Hence equating 1/ and 2/ gives

$$(C_{AB} + C_{BC})\frac{dV_{AB}}{dt} + \left(\frac{1}{R_{BC}} + \frac{1}{R_{AB}}\right)V_{AB} - \frac{V}{R_{BC}} = 0 \qquad 3/.$$

Solving 3/ and applying the boundary condition $V_{AB} = 0$ at $t = 0$ gives

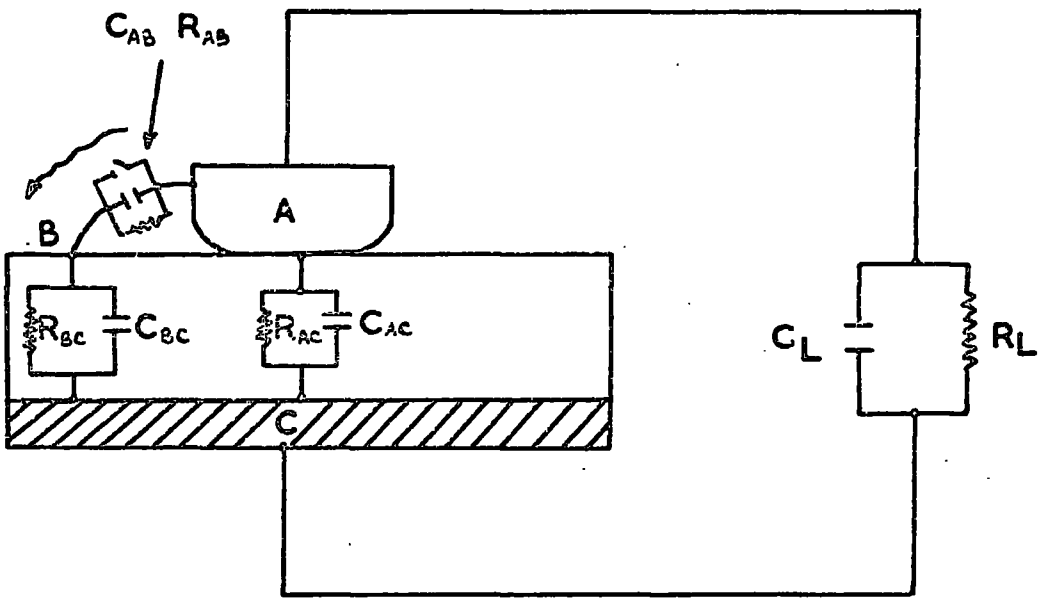

FIGURE A

$$V_{AB} = \frac{R_{AB}}{R_{BC} + R_{AB}} V \left\{1 - \exp\left(\frac{-t \cdot R_{AB} + R_{BC}}{R_{AB} R_{BC}(C_{AB} + C_{BC})}\right)\right\}$$

At $t = T$ $V_{AB} = V_b$ and we have

$$V_b \frac{R_{BC} \pm R_{AB}}{R_{AB}} = V \left\{1 - \exp\left(\frac{-T \cdot R_{AB} + R_{BC}}{R_{AB} R_{BC}(C_{AB} + C_{BC})}\right)\right\}$$

$$= V_i$$

$$\text{i.e. } T = \frac{R_{AB} R_{BC}(C_{AB} + C_{BC})}{R_{AB} + R_{BC}} \log_e \frac{V}{V - V_i}$$

Hence the discharge frequency f for this model is given by

$$f = \frac{1}{T} = \frac{R_{AB} + R_{BC}}{R_{AB} R_{BC}(C_{AB} + C_{BC})} \left\{\log_e \frac{V}{V - V_i}\right\}^{-1}$$

APPENDIX E

ANALYSIS OF SIMPLIFIED EQUIVALENT CIRCUIT

The complete equivalent circuit for the sample and associated leads in two terminal measurements will be similar to that shown in Figure E.1. An analysis of this circuit to find the relation between the discharge current and the external impulse is somewhat difficult. Because of this an analysis has been made of the simplified circuit shown in Figure E.2. This circuit neglects the inductive elements in the leads, the resistive, capacitive and inductive elements in the earth screen and all coupling between the earth screen and the leads. With the possible exception of the inductance of the E.H.T. lead, $\simeq 50$ μH, these assumptions are justified by the small values of the circuit components.

The circuit of Fig. E.2. may be analysed by matrix algebra. If this is done it can be shown that for a unit impulse function of magnitude I_o across AB the voltage across R_M is given by

$$v_M(t) = R_M I_o \left\{ 1 - \exp\left(-t/\gamma_1\right) - \frac{R_{BC}\, C_{AB}}{\gamma_2 - \gamma_1} \exp\left(-t/\gamma_2\right) \right\}$$

where $$\gamma_1 = R_M(C_{AC} + C_M + C_{AB})$$

$$\gamma_2 = R_{BC}(C_{BC} + C_{AB})$$

provided that $C_E \gg C_A$ at $R_{AC} \gg R_S$ or R_E which holds for the equipment and sample used.

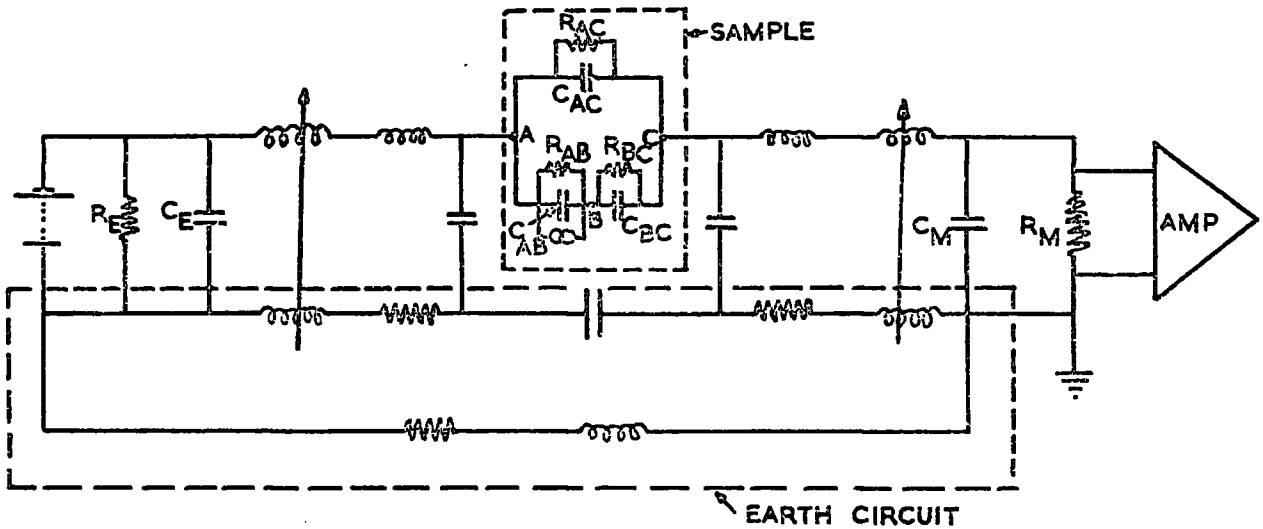
SAMPLE
R_{AC}
C_{AC}
A
R_{AB}
R_{BC}
C
B
C_{AB}
C_{BC}
R_E
C_E
C_M
R_M
AMP
EARTH CIRCUIT

FIG. E. 1.

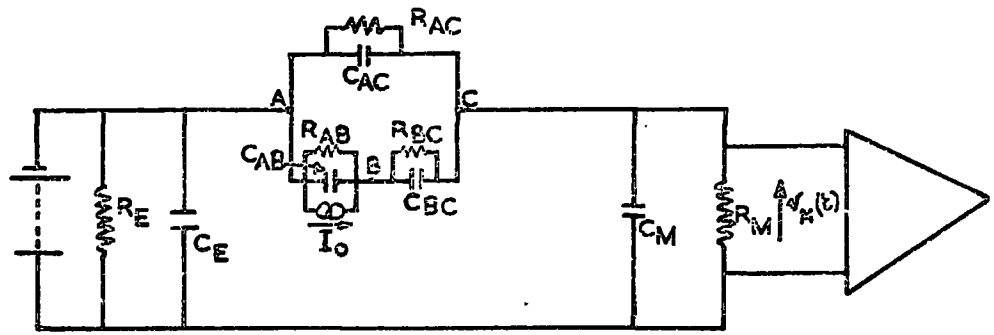
R_{AC}
C_{AC}
A
C
R_{AB}
R_{BC}
C_{AB}
B
C_{BC}
I_o
R_E
C_E
C_M
R_M
$V_R(t)$

FIG. E. 2.

REFERENCES

(1) ABSON, W., SALMON, P.G., and PYRAH, S., 1958, Proc. IEE, 105 (B), 349.

(2) DUBOIS, E., and GOODINGS, A., 1963, U.K.A.E.A. Reactor Group Research Report No. M402.

(3) TUCKER, R.N., and GIBBS, P., 1958, J. Appl. Phys., 29, 1375.

(4) CHAMPION, J.A., 1964, Brit. J. Appl. Phys., 15, 633.

(5) LOUP, J.P., and ANTHONY, A.M., 1964, Revue des Hautes Temperatures et des Refractaires, 1, 15.

(6) PETERS, D.W., FEINSTEIN, L., and PELTZER, C., 1965, J. Chem. Phys., 42, 2345.

(7) WRIGHT, A.J., 1968, Ph.D. Thesis, University of London.

(8) MASON, J.H., 1965, Proc. IEE, 112(7), 1407.

(9) HASHIMOTO, H., 1960, J. Inst. Elect. Eng. Japan, 5, 85.

(10) KREUGER, F.H., 1964, Discharge Detection in High Voltage Equipment (London: Heywood).

(11) DAKIN, T.W., and LIM, J., 1957, Trans. Amer. Inst. Elect. Eng., 76, 1059.

(12) GILLESPIE, A.B., 1953, Signal, Noise and Resolution in Nuclear Counter Amplifiers (London: Pergammon).

(13) HARRISON, D., 1965, J. Radio and Electronic Engineer, 29, 149.

(14) CURTIS, D.A., 1961, Ph. D. Thesis, University of Durham.

(15) BROWNLEE, K.A., 1949, Industrial Experimentation (London: H.M.S.O.).

(16) REES, A.L.G., 1954, Chemistry of the Defect Solid State (London: Methuen).

(17) MEEK, J.M., and CRAGGS, J.D., 1953, Electrical Breakdown of Gases (Oxford: O.U.P.)
(a) Page 86, (b) Page 62, Table 1.23.

(18) HORNBECK, J.A., 1951, Phys. Rev., 83, 375.

(19) WIJSMAN, R.A., 1949, Phys. Rev., 75, 833.

(20) LEGLER, W., 1955, Z. Phys., 140, 221.

(21) DAVIDSON, P.M., 1964, Proc. Phys. Soc., 83, 259.

(22) YOUNG, M.L., and MORANT, M.J., 1967, Fourth Technical Progress Report on Contract No. CON/WIN/EMR/ 138. University of Durham.

(23) COHEN, J., 1959, Bull. Amer. Ceram. Soc., 38, 441.

(24) HARROP, P.J. and CREAMER, R.H., 1963, Brit. J. Appl. Phys., 14, 335.

(25) HARTMANN, W., 1936, Z. Physik., 102, 709.

(26) MATSUMURA, T., 1966, Canad. J. Phys., 44, 1685.

(27) DAVIES, M.O., 1963, J. Chem. Phys., 38, 2047.

(28) SCHMALZRIED, H., 1963, Z. Physik. Chem., 38, 87.

(29) PAPPIS, J. and KINGERY, W.D., 1961, J. Amer. Ceram. Soc., 44, 459.

(30) CUSACK, N., 1958, Electrical and Magnetic Properties of Solids (London: Longmans).

(31) PETERS, D.W., 1966, J. Phys. Chem. Solids, 27, 1560.

(32) DASGUPTA, S. and HART, J., 1965, Brit. J. Appl. Phys., 16, 725.

(33) DASGUPTA. A., 1966, Brit. J. Appl. Phys., 17, 267.

(34) HELDT, K. and HAASE, G., 1954, Z. Angew. Phys. 6, 157.

(35) HENSLER, J.R. and HENRY, E.C., 1953, J. Amer. Ceram. Soc., 36, 76.

(36) KROGER, F.A., 1964, Chemistry of Imperfect Crystals (Amsterdam: N.H.P.)

(37) GIBBS, P., 1958, Office of Naval Research Tech. Report No. IX, Contract N-ONR-1288(03).

(38) GLASSTONE, S., 1956, Textbook of Physical Chemistry (London: Macmillan).

(39) BRENNAN, J.J. and PASK, J.A., 1968, J. Amer. Ceram. Soc., 51, 569.

(40) WEBSTER, R.K., JONES, T.L., and ANDERSON, P.J., 1965, Proc. Brit. Ceram. Soc., 5, 153.

(41) PERI, J.B., and HANNAN, R.B. 1960, J. Phys. Chem., 64, 1526.

(42) TALLAN, N.M.Z. and DETWILER, D.P., 1963, J. Appl. Phys., 34, 1650.

(43) TALLAN, N.M. and GRAHAM, H.C., 1965, J. Amer. Ceram. Soc., 48, 512.

(44) STULOVA, G.M. and SHALABUTOV, Yu.K., 1968, Soviet Phys. Semiconductors, 1, 996.

(45) CHARRIG, J.M., 1967, Appl. Phys. Lett., 10, 139.

(46) CHARRIG, J.M. and SKINNER, D.K., 1969, Proc. Fourth Int. Materials Symp. (New York: Wiley).

(47) CHANG, C.C., 1968, J. Appl. Phys., 39, 5570.

(48) OISHI, Y. and KINGERY, W.D., 1960, J. Chem. Phys., 33, 481.

(49) PALADINO, A.E. and KINGERY, W.D., 1962, J. Chem. Phys., 37, 957.

(50) HARROP, P.J., 1965, Brit. J. Appl. Phys., 16, 729.

(51) GILLES, A., 1952, J. Phys. Radium., 13, 247.

(52) LOH, E., 1964, Solid State Commn., 2, 269.

(53) MASSEY, H.S.W. and BURHOP, E.H.S., 1952, Electronic and Ionic Impact Phenomena (Oxford: O.U.P.).

(54) McDANIEL, E.W., and CRANE, H.R., 1957, Rev. Sci. Inst., 28, 684.

(55) COLLI, L. and FACCHINI, U., 1954, Phys. Rev., 96, 1.

(56) RAETHER, H., 1964, Electron Avalanches and Breakdown in Gases (London: Butterworths).

(57) LOEB, L.B., 1965, Electrical Coronas, their basic physical mechanisms (Berkeley: U.C.P.).

(58) DAS, M.K., 1961, Z. Angew. Physik, 13, 410.
" 1960, Ph.D. Thesis, Tech. Univ. Karlsruhe.

(59) LOEB, L.B., KIP, A.F., HUDSON, G.C., and BENNET, W.H., 1941, Phys. Rev., 60, 715.

(60) ENGLISH, W.N., 1950, Phys. Rev., 77, 850.

(61) WEISSLER, G.L., 1943, Phys. Rev., 63, 101.

(62) McDANIEL, E.W., 1964, Collision Phenomena in Ionized Gases (New York: Wiley).

(63) PACK, J.L., VORSHALL, R.E., and PHELPS, A.V., 1962, Phys. Rev., 127, 2084.

(64) LLEWELLYN-JONES, F., 1957, Ionization and Breakdown in Gases (London: Methuen).

(65) HILL, G.J., 1968, Brit. J. Appl. Phys., 1, 1151.

(66) KHOOBAR, S., CARTER, J.L., and LUCCHES, P.J., 1968, J. Phys. Chem., 72, 1682.